Fatigue Behaviour of Coke Drum Materials and Its Application to Extend the Service Lives of Coke Drums

by

Jie Chen

A thesis submitted in partial fulfillment of the requirements for the degree of

Doctor of Philosophy

Department of Mechanical Engineering
University of Alberta

Abstract

Coke drums are vertical pressure vessels used in the delayed coking process in petroleum refineries. They are normally constructed of carbon or low carbon alloy steels internally clad with stainless steel to protect the coke drums from corrosion during operations. Significant temperature variation during the delayed coking process causes damage in coke drums in the form of bulging and cracking. Hundred thousands of dollars are spent to repair the units and the loss from the disruption of the production could be even much higher. There are studies on the fatigue life estimation for coke drums, but these are based on uniaxial strain-fatigue life curves at various constant temperatures, which do not consider cyclic temperature conditions. There are relatively few investigations involving experiments to simulate and predict the damage and fatigue life of coke drums. To more accurately analyze the fatigue damage mechanism of coke drums, a systemic-experimental investigation on fatigue behaviours of coke drum materials has been carried out in this study. A thermal-mechanical fatigue (TMF) testing system has been successfully designed and developed to perform the complex TMF tests. The developed system can successfully simulate cyclic thermal-mechanical loading conditions experienced by coke drums. In addition, an alternative strain control and measurement technique is developed for strain-controlled fatigue tests at elevated temperature. The fatigue lives of the candidate materials are first investigated under isothermal condition. More complex TMF tests are then performed on these candidate materials. Two coke drum base materials (C-½Mo and 2¼Cr-1Mo) are investigated and compared under isothermal and thermal-mechanical cyclic loadings. Based on the current experimental study and, in combination with the API survey data, it is concluded that C-

½Mo is a better base material than 2¼Cr-Mo from the standpoints of fatigue resistance. Since the coke drums are constructed by welding a number of shell plates, the fatigue behaviours of weld and heat affected zone (HAZ) material are also studied. A modified four-point correlation (FPC) method has been developed to predict the fatigue lives of weld and HAZ material based on their tensile properties. Finally, based on the TMF data of the coke drum materials obtained through this study, along with a new statistical fatigue life prediction method developed in our group, the fatigue lives of coke drums can be more reasonably predicted.

This study leads to better understanding of damage mechanisms occurring in coke drums. The comprehensive coke drum material data obtained through this study are valuable for designers and operators of coke drums. More important, a number of useful guidelines including optimal selection of materials, more accurate analysis method and reliable life prediction method for coke drums are summarized. Application of these guidelines will be beneficial for designing and manufacturing of more robust new coke drums, as well as for extending service lives of the existing coke drums from the operational and maintenance point of view.

Preface

This thesis is an original work by Jie Chen. Some of the research conducted for this thesis forms part of an Collaborative Research Projects with Suncor Energy, Husky Energy, and Sumitomo Heavy Industries, Ltd., Japan, and it is also funded by Natural Sciences and Engineering Research Council of Canada.

The technical apparatus referred to in chapter 2 was designed and developed by myself, with the assistance of B. Faulkner. The new developed strain control technique for high temperature fatigue tests in chapter 3, a comparative study on fatigue lives of 2¼Cr-1Mo and C-½Mo base materials used for the construction of delayed coke drums in chapter 4, a proposed fatigue life prediction method for coke drum base, weld, and HAZ materials from tensile properties in chapter 5, a temperature dependent fatigue life prediction model for coke drum materials in chapter 6, as well as an experimental evaluation of fatigue life of coke drum materials with weld and clad materials in chapter 7 and 8 are my original work. Statistical method for the fatigue life estimation of coke drums in chapter 9 is the work collaborated in our research group with Dr. Z. Yan and Y. Zhang.

Part of chapter 2 of this thesis has been published as J. Chen and Z. Xia, "Fatigue behaviour of coke drum materials under thermal mechanical cyclic loading," *Theoretical Applied Mechanical Letters* 2014, 4(4):6-041006. Chapter 5 of this thesis has been published as J. Chen and Z. Xia, "A fatigue life prediction method for coke drum base, weld, and HAZ materials from tensile properties," *Materials & Design* Vol. 63, 575-583,

2014. I was responsible for the development of the technical apparatus, experimental investigation and analysis as well as the manuscript composition. Dr. Z. Xia assisted with the manuscript edits and was the corresponding author. Chapter 7 of this thesis has been published as J. Chen, T. Yamamoto, Z. Xia and K. Esaki, "Experimental Evaluation of Fatigue Life of Coke Drum Materials with Weld Sections," in the proceeding of ASME 2013 Pressure Vessels and Piping Conference, Vol. 3: Design and Analysis, Paris, France, July 14-18, 2013. I was responsible for the experimental investigation and analysis as well as the manuscript composition. T. Yamamoto and K. Esaki were involved with project initiation and manuscript revision. Dr. Z. Xia assisted with the manuscript edit and was the supervisory author. The permission for inclusion of this conference paper in this dissertation is granted by ASME.

Acknowledgements

The author wishes to express his sincere appreciation to Dr. Zihui Xia for his guidance and patience throughout this endeavour. Without his guidance and persistent help this dissertation would not have been possible.

My deepest gratitude is extended to Mr. Bernie Faulkner, who gives me great help and invaluable suggestion on developing the experimental facility and manufacturing the test specimens. It would not be possible to successfully develop the unique testing system without him.

I also would like to take this opportunity to express my thanks to Mr. John Aumuller and other members of coke drum research team and ACME group, for offering great support and discussions. It was a great pleasure to be among them. Furthermore, I would like to thank Mr. Li Liu and Mr. Edward Wang, who provides me enormous help during their summer research.

I am especially grateful to my wife, Shuo Tong, for being so patient and supportive throughout my PhD study. I would like to express my deep gratitude to her for standing right behind me with all her warmth, sensitivity, and understanding.

And last of all, I would like to thank both of our parents for their spiritual care and amazing love and support.

Table of Contents

List of Tables

List of Figures

Nomenclature

$C_{inst.}$ – Coefficient of strain correlation between gauge length and dimple length

ε_{gauge} – Strain measured at gauge length

ε_{dimple} – Strain measured at dimple length

$\varepsilon_{thermal}$ – Thermal strain

ε_{mech} – Mechanical strain

ε_{hoop} – Hoop strain

ε_{axial} – Axial strain

ε_{tot} – Total strain

$\Delta\varepsilon_{dimple}$ Strain range measured between two dimples

$\Delta\varepsilon_{gauge}$ Correlated strain range at gauge length

$\Delta\varepsilon$– Strain range

E – Young's modulus

K' – Cyclic strength coefficient

n' – Cyclic strain hardening exponent

$\Delta\sigma$ – Stress range

δ – Displacement

σ_{hoop} – Hoop stress

σ_{axial} – axial stress

$\Delta\sigma/2$ – stress amplitude

$\Delta\varepsilon/2$ – Strain amplitude

$\Delta\varepsilon_p/2$ – Plastic strain amplitude

$\Delta\varepsilon_e/2$ – Elastic strain amplitude

$2N_f$ – Reversals to failure

N_f – Number of cycles to failure

σ'_f – Fatigue strength coefficient

b – Fatigue strength exponent

ε'_f – Fatigue ductility coefficient

c – Fatigue ductility exponent

$\sigma_{0.2\%}$ – Yield Strength at 0.2% offset parallel line

σ_{ult}– Ultimate tensile strength

ε_f– Elongation at fracture

σ_f – True fracture strength

$R_{plastic}$ – Reduction factor for plastic line

$R_{elastic}$ – Reduction factor for elastic line

S_w/S_b Yield strength ratio between weld and base materials

S_{cw}/S_c Yield strength ratio between clad-weld and clad materials

T_{max} – Maximum temperature in a thermal cycle

T_{min} – Minimum temperature in a thermal cycle

API – American Petroleum Institute

CSSC – Cyclic stress strain curve

CTE – Coefficient of Thermal Expansion

FEA – Finite Element Analysis

FPCM – Four-Point Correlation Method

HAZ Heat affected zone

ILCF – Isothermal Low Cycle Fatigue

LCF – Low Cycle Fatigue

MC - Manson-Coffin Relation

MPS – Method Proposed by Socie

MFPCM – Modified Four-Point Correlation Method

MM – Median Method

MSSC – Monotonic Stress Strain Curve

MUSM – Modified Universal Slope Method

PCGL – Parallel Cylindrical Gauge Length

RA – Reduction of Area

R.T. – Room temperature (20°C)

TC – Thermocouple

TDFPCM – Temperature Dependent Four Point Correlation Method

TMF – Thermal-Mechanical Fatigue

UMLM – Uniform Material Law Method

USE – Universal Slopes Equation

CHAPTER 1 Overall Introduction

1.1 Background of Coke Drums and Its Operation

Coke drums are vertical pressure vessels used in the delayed coking process in petroleum refineries. They are normally constructed of carbon or low carbon alloy steels internally clad with AISI 410S or AISI 405 stainless steel to protect the coke drums from corrosion during operations [1]. They range from 4 to 9 meters in diameter and around 25 meters in height. The maximum shell thickness varies from 0.014 to 0.042 meters. The pressure ranges from 100 to 500 kPa, and the maximum operation temperature ranges from 427 to 482°C.

A typical coke drum cycle in term of temperature is shown in Fig. 1.1. First, heavy residual is imported into a coker heater and heated to approximately 482°C. Before direct the heavy oil into the coke drum, the drum is preheated by flowing vapour from the bottom of the drum to the top (Temperature rises from approximate 150 °C to 360 °C). Then, the hot heavy oil is directed into the coke drum to begin the fill cycle. The fill cycle usually takes 14-18 hours. When the filling is complete, light hydrocarbon from the coke produced during the thermal cracking process is removed by steam stripping (Temperature drops from 450 °C to 250 °C approximately). After that, high rate of quench water is injected into the coke drum cooling the vessel and possibly extracting the solid coke. After soaking, the solid coke is cut by applying the high-pressure water steams. After all the coke is removed from the drum, the coke drum is checked and reheated in order to prepare for a new operation cycle [1].

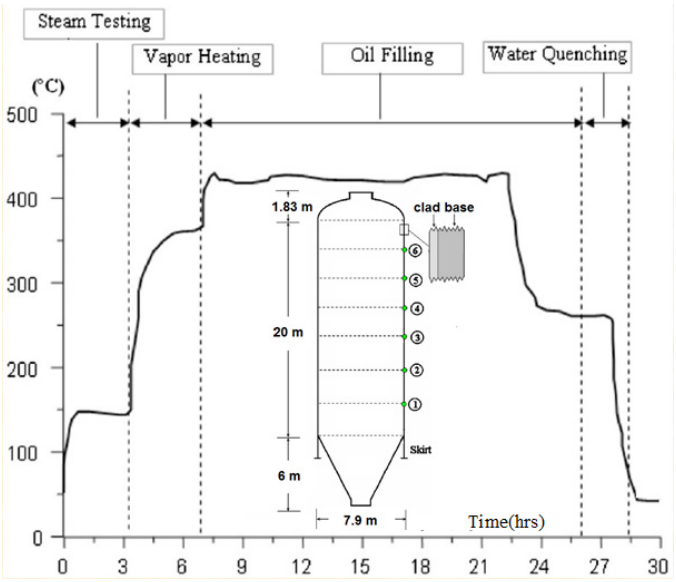

Figure 1.1 Typical coke drum thermal cycle

The average operation life of coke drums is above ten years [1]. However, there are several kinds of service related damages of coke drum components reported. Damages of coke drums in the form of bulging deformation or cracking have been reported from time to time. Every year millions of dollars are spent on repairs and even more are lost due to interruption of the production. It is therefore critical for this equipment to maintain long-term reliability to meet the challenges of today's economic and labour environments.

1.2 Problems and Studies Related with Coke Drum

Coke drums have historically been designed according as ASME Section VIII Division 1 [2]. Even though it is commonly agreed that coke drums are subjected to cyclic thermal and mechanical loads, they are initially not designed for cyclic loads. Thus, their operational life is much shorter than other pressure equipment in refineries [3]. The significant temperature variation during the delayed coking process, such as heating and quenching, causes the useful life of coke drums to be shortened comparing with other pressure vessels under non-cyclic thermal condition. The severe cyclic thermal-mechanical load makes coke drums susceptible to damage. In the past decades, to speed

up the production, the frequency and severity of these cycles significantly increased. Some of the plants reduced the cycle time from 24 to 12 hours or even shorter. As a result, it becomes more often and earlier to have through-wall cracking in the shell and/or skirt region of coke drums because they were not designed for the more brutal fatigue service in which they currently operate [4].

It is also found that shell bulging is one of the causes leading to cracking and failure in the vessel shell of coke drums. Radial bulging is identified as a "reoccurring difficulty" that existed in essentially all operating coke drums of the time [5]. After some years of operation under the cyclic thermal-mechanical load, the coke drums tend to start developing circumferential bands of bulging in the shell, and cracks initiate in the base metal primarily near the welds and heat affected zones [6]. The root cause of the shell bulging is the intense thermal cycling during the operation of the filling-quenching cycle [7]. The bulges are normally found near the circumferential weld seams which normally have higher yield strength, and the base material finally tend to become thin and fails via cracking as the result of the restraint caused by the weld seams [8-10]. Oka et al. [11] also investigated the root causes of bulging. They agreed that bulging is caused by thermal stresses due to the presence of hot and cold spots in the coke drum wall. The maximum equivalent stress in the shell can reach the yield point of the coke drum material. In addition, the presence of hot and cold spots during the cooling stage introduces significant thermal stresses that can initiate permanent deformation or bulges in the coke drum wall. Ju et al. [12] also studied the elastic-plastic behaviour of a coke drum under both thermal and mechanical loadings as well as with considering the hot and cold spots. It is found that clad layer yields at the very early stage in an operating cycle and permanent deformation is caused in the first operating cycle. It is also found that both hot and cold spots will cause shell distortion or bulging of the shell and the cold spot can cause more severe deformation than the hot spot. Several cold and hot spot effects taking place at the same location can form bulging progressively.

There have been several measuring techniques involved to identify the bulging and cracking problems of coke drums. The traditional inspection method of

characterizing the coke drum distortion is performed with an internal visual and dimensional inspection. However, this type of inspection is only performed during major unit turnarounds that occurred once every four years [13]. There are also new inspection methodologies including laser bulging inspection [14], high temperature strain gauge monitoring [15], and finite element analysis, etc. The FEM analysis carried by Rutt and Clark [13] shows a local doubling of axial stress in the area of the weld crack, which would significantly reduce the fatigue life of the material in that region.

There is also agreement that low cycle thermal fatigue is considered the failure mode for coke drums. There are several researches related to study the fatigue life of coke drums. Oka et al. [16, 17] performed FEA study on the shell to skirt junction area. The thermal fatigue life is calculated based on low cycle fatigue properties of the base material (SA 387 Gr. 11 Cl. 2) at 500°C. Sasaki et al. [18] conducted a fatigue life evaluation on skirt to shell attachments. They also compared fatigue strength of three metals: base metal, weld metal and heat affected zone of base material (SA 387 Gr. 11 Cl. 2) by conducting low cycle fatigue tests at room temperature. Li et al. [19] performed a FEA study on the welding area between the drum body and the skirt. The service life of the coke drum is estimated through the calculated strain and the fatigue test results of base weld at 500°C. Ramos et al. [20] used FEA results and the fatigue life of two base and weld materials (SA 387 Gr. 11 Cl. 2 and SA 387 Gr. 12 Cl. 2) at 454°C to estimate the fatigue life of coke drums.

References [16, 18, 19, 20-22] performed the fatigue life estimation for coke drums by conducting low cycle fatigue tests. However, these low cycle fatigue tests were only conducted on base material under uniaxial fully-reversed isothermal condition. Xia et al. [23] conducted a finite element study on the heat transfer and stress analysis of coke drum for a complete operating cycle. It was found that significant stress and strain values are observed in the clad of the coke drum, which exceeds the yield limit of the material. The noticeable difference in the thermal expansion coefficients (CTE) of the clad and base and the relative small thickness of the clad comparing to that of the base material are the main causes of the high stress in the clad layer. Ju et al. [12] carried out a global

elastic-plastic stress analysis of coke drum under thermal-mechanical loadings. It is also found that the clad experiences yielding in the loading cycle. In addition, it is observed that the stress and strain states of clad materials under each operational cycle are non-fully-reversed, multi-axial and temperature-dependent. Therefore, the coke drum fatigue life evaluation based only on base material is not sufficient. A more accurate evaluation of the fatigue life behaviour should be carried out under loading conditions similar to the operational condition, such as under thermal-mechanical cyclic loading. References [9, 24, and 25] investigated the fatigue life assessment for coke drums, and the fatigue life curve is obtained from either ASME code [26] or API 579 [27]. In addition, fatigue life curves provided by these codes are design curves, and it is recommended for using as reference at the maximum temperature of 371 °C. However, the temperature of the coke drum wall can experience as high as 482°C in operation. Furthermore, the fatigue life from the code does not specify the loading condition for the life curves. Therefore, it is inappropriate and inaccurate to evaluate the fatigue life of in-service coke drums from the design fatigue life curves. It is also realized that the design should at least consider two fatigue processes in coke drums: one is the global cyclic stresses/strains experienced by the coke drum under operational temperature and mechanical (pressure, dead weight, etc.) loads; the other is the local stress/strain extremes caused by the hot/cold spot effect. The latter case is more complicated since the location, temperature difference and frequency of the affected areas are most possibly in a random nature. In this regard, a stochastic fatigue life analysis method instead of a deterministic one might be more appropriate.

Coke drums were constructed from carbon steel in early years to low alloys steels such as Carbon-½ Moly, 1 ¼ Cr or even higher alloys in more recent years. New drum material selection has been towards increasing Chrome Moly alloy content [10]. API survey [10] data shows that 13 out of 22 coke drums installed between 1950 and 1969 were made of C-Mo steels, but only 2 of 22 drums that were installed between 1980 and 1997. However, in those two periods, 2 out of 22 coke drums were made of Cr-Mo steels between 1950 and 1969 while 19 of 22 were installed between 1980 and 1997. Steels with higher Cr and Mo contents are presumed to have better thermal cycling resistance because of their higher yield strength and better creep resistance. However, there is little

evidence to demonstrate the improved fatigue endurance of these materials. The coke drums constructed from these materials still experience the same type of damage and failure in sometimes notably shorter exposure times. Milan et al. [28] performed the comparative study on alternative selections of coke drum materials through FEA with input material properties taken from ASME Boil & Pressure Vessel Code, Section II [29]. They recommended materials based on the better matching of the coefficients of thermal expansion between clad and base materials and lowering the stress level in the clad layer. However, there is no study related to the fatigue properties of these materials.

Coke drums are initially not designed considering cyclic loads. It has not been usual practice to give serious consideration to the possibility of fatigue failure. However, due to the severe cyclic thermal and mechanical loads, their operational life is normally much shorter than other pressure equipment in refineries. Furthermore, weld seam locations are shown to be especially susceptible to failure since pressure vessel codes of construction allow the presence of limited defects which can be shown to contribute to initiation and propagation of crack failure. It becomes necessary to calculate pressure stresses and thermal stresses in detail and to determine whether or not fatigue failure is possible in the early stage of the operation. Therefore, reliable fatigue life curves are essential in this evaluation process. Even though there were fatigue tests conducted for coke drum materials [16, 18, 19, 20-22]. They are either for base material at single temperature, or not provided in the literatures. There are even fewer resources available for fatigue life curves of weld or heat affect zone materials of coke drums.

Most of the coke drum studies mentioned above is only focused on base materials. There are very few investigations on the influence of yield strength ratio between the weld and the base on the fatigue lives of coke drums. It is a common consideration that the yield strength of the weld should be close to that of base material in order to keep strength uniformity throughout the drum shell sections. However, this effect of the yield strength matching on the shell durability is not yet clarified quantitatively [30]. Moreover, due to the difficulty of designing a fatigue specimen for the entire coke drum wall, to the

best of author's knowledge, there has not been a study considered the clad section (clad and clad-weld) of the actual clad wall structure of the coke drum.

The above new findings clearly indicate that a more reliable thermal-mechanical fatigue life and design methodology needs to be developed for the coke drums. A comparative study of coke drum materials from fatigue life point of view is necessary. A method that can accurately estimate the fatigue lives of coke drum materials including weld and HAZ with minimum input data is demanding. In addition, quantitative evaluation of the effect of the yield strength matching on the shell durability needs to be explained. This will help not only in constructing more robust new coke drums, but also in improving performances and extending lives of the existing equipments (Many existing coke drums are at replacement age.).

1.3 Objectives of the Study

The overall objective of the proposed research is to obtain a more reliable thermal-mechanical fatigue life and design methodology for the construction of robust and longer life coke drums and to propose realistic strategies for improving performance and extending service lives of existing coke drums. This main objective will be reached by the completion of the following goals:

1. To experimentally investigate fatigue lives of coke drum materials under thermal-mechanical cyclic loading;
2. To confirm whether the trend of material selection to Chrome Moly alloy content is beneficial to enhance the reliability of coke drums;
3. To develop a temperature dependent fatigue life prediction model for coke drum materials;
4. To investigate the fatigue life relations of base, weld and HAZ and develop a unified prediction model for these materials;
5. To study effect of the yield strength matching between weld and base materials on the shell durability;

6. To more accurately estimate the service life of coke drums based on stochastic fatigue life analysis with the help of the obtained test results;
7. To provide some guidelines for the design, manufacturing, operation and maintenance of coke drums to improve their long term reliability.

To reach the above goals, a systemic-experimental investigation of fatigue lives of coke drums is carried out in this study. Three coke drum materials are selected to be tested under different temperature and loading conditions. A thermal-mechanical fatigue (TMF) testing system has been designed and developed to perform the complex TMF tests. The fatigue lives of the candidate materials are first investigated under isothermal condition. More complex TMF tests are then performed on these materials. Based on the comprehensive experimental studies, more accurate isothermal low cycle fatigue (LCF) and TMF data of coke drum materials will be achieved, and more reliable fatigue life prediction models will be developed for these materials. Subsequently, two coke drum base materials (C-½Mo and 2¼Cr-1Mo) are investigated and compared under isothermal and thermal-mechanical cyclic loadings. In addition, a comparative study between isothermal and thermal mechanical fatigue lives of these materials is conducted. A new temperature-dependent method is proposed based on several different coke drum materials. It only uses Young's modulus, ultimate tensile strength, elongation at fracture and temperature as input data to estimate the strain-life relations. Low cycle fatigue tests at elevated temperature of 250°C are carried out on base, weld and HAZ materials. Based on the test results, a unified method for predicting fatigue lives of these materials from their tensile properties is developed. Furthermore, structural specimens have been designed and manufactured based on the cross sectional structure of the coke drum wall. It consists of four different materials: base, base-weld, clad, and clad-weld. Additionally, three groups of the structural specimens with different yield strength ratios of base-weld to base are prepared. Low cycle fatigue tests at elevated temperature of 250°C are carried out on these specimens. Furthermore, finite element analyses based on the actual specimen's geometry and material properties are conducted to help in understanding the experimental observations. Finally, by using the stochastic fatigue life analysis method, which considers global loading and random thermal loading from hot/cold spots,

developed in our group with the TMF life curves, more reliable service life of coke drums is estimated.

Successful completion of this study will lead to better understanding of damage mechanisms occurring in coke drums, to provide useful guidelines in optimal selection of materials, design and manufacturing of more robust new coke drums, as well as for extending service lives of the existing coke drums from the operational and maintenance point of view. The benefit of the successful completion of this research to industrial users is to design and construct new equipment that is more robust and to improve service life of existing equipment.

1.4 Outline of the Thesis

The thesis is arranged in the following sequence: The first chapter gives a brief background of the problems and scope of this research. In chapter 2, a developed biaxial thermal mechanical fatigue testing system and its application on clad material is introduced. In chapter 3, a new strain control and measurement technique for high temperature fatigue tests is developed. In chapter 4, a comparative study on fatigue lives of 2¼Cr-1Mo and C-½Mo base materials used for the construction of delayed coke drums is performed. In chapter 5, a fatigue life prediction method for coke drum base, weld, and HAZ materials from tensile properties is introduced. In chapter 6, a temperature dependent fatigue life prediction model for coke drum materials is proposed. In chapter 7, an experimental evaluation of fatigue life of coke drum materials with weld sections is discussed. In chapter 8, an investigation on the effect of weld yield strength on the fatigue life of clad shell structure of coke drums is presented. In chapter 9, a statistical method for the fatigue life estimation of coke drums is introduced. Finally, in chapter 10, the content of the thesis is summarized.

References

[1] Penso, J. A., Lattarulo, Y. M., Seijas, A. J., Torres, J., Howden, D., and Tsai, C. L., "Understanding Failure Mechanisms to Improve Reliability of Coke Drum," PVP ASME, 395, pp. 243–253. (1999)

[2] ASME, ASME Boiler & Pressure Vessel Code, Section VIII, Division I, Rules for Construction of Pressure Vessels, ASME, New York, (2007).

[3] Oka, M, et al. "Study On The Effects Of Switching Temperature On The Thermal Fatigue Life Of The Shell-To-Skirt Junction Of Coke Drum." Journal Of Pressure Vessel Technology-Transactions of ASME 133- 6 (2011)

[4] Boswell, R. S., and Wright, B. "State-of-The-Art Improvements in Coke Drum Design and Life Extension Practices." Proceedings of ASME Pressure Vessels And Piping Conference (2008): CREEP2007-26254.

[5] Weil, N.A. and Rapasky, F.S., "Experience with vessels of Delayed – Coking Units", API 23rd Midyear Meeting, (1958)

[6] Shargay, C., Singh, A., Munsterman, T., Antalffy, L., "Coke Drum Design and Fabrication Issues", Proceedings of ASME Pressure Vessels And Piping Conference(2010): PVP2010-25765

[7] Pieper, C.J., Shockley, L.R. and Stewart, C.W., "Coke Drum Design-Longer Life through Innovation", AIChE 2000 Spring National Meeting, Atlanta, GA, March 5-9, (2000)

[8] Boswell, R., "Coke Drum Bulges", Stress Engineering Services, May, (2001)

[9] Boswell R.S., Ferraro T., “Remaining Life Evaluation of Coke Drums”, Plant Engineering, Design and Responsibility Symposium, Energy Engineering Conference, (1997)

[10] API Proceedings “1996 APE Coke Drum Survey-Final Report”, American Petroleum Institute, Washington, DC, (1996)

[11] Oka, M., Himsar A., Masashi D., and Hiroyuki F.. "Initiation of Bulges in a Coke Drum Subjected to Cyclic Heating and Cooling, also Cyclic Mechanical Loads" Journal of Thermal Stresses 33-10 (2010)

[12] Ju, F., Aummuler, J., Xia, Z. and Plessis, P. D., “Global and Local Elastic-Plastic Stress Analysis of Coke Drum Under Thermal-Mechanical Loadings”, Journal of Pressure vessel technology, 133 (2011)

[13] Rutt, D.K., Clark, R.D., “Stress Analysis Using Actual Coke Drum Bulge Profiles a Case Study”, AIChE 2000 Spring National Meeting, Atlanta, GA, March 5-9, (2000)

[14] Samman, M. and DuPlessis, P., “The Bulging Intensity Factor (BIF), A technique for assessing the bulging severity of coke drums”, RMC-07-100 NPRA Reliability & Maintenance Conference, NPRA Houston, TX, (2007)

[15] Clark, R. D., Rytt, D. K., et al., “Coke Drum Life Improvement – A Combined Approach”, AIChE 2002 Spring National Meeting, New Orleans, Louisiana, March 10-14, (2002)

[16] Oka, M, et al. "Study On The Effects Of Switching Temperature On The Thermal Fatigue Life Of The Shell-To-Skirt Junction Of Coke Drum." Journal of Pressure Vessel Technology-Transactions of ASME 133-6 (2011)

[17] Oka, M., Ambarita, H., Kawashima, K. and Daimaruya, M. "Effect of hot feed injection time on thermal fatigue life of shell to skirt junction area of coke drums" Proceedings of ASME Pressure Vessels And Piping Conference (2010): PVP2010-25183

[18] Sasaki, Y., and S. Niimoto. " Study on Skirt-to-Shell Attachment of Coke Drum by Evaluation of Fatigue Strength of Weld Metal." Proceedings of ASME Pressure Vessels and Piping Conference (2012): PVP2011-57314

[19] Li, Z., Zhou X., Xu W., and Fenkun L., "Safe Life Estimation of Coke Drum in Service Environment." Journal of Pressure Vessel Technology134-3 (2012)

[20] Ramos, A., Rios, C. and Vargas, J., "Mechanical Integrity Evaluation of Delayed Coke Drums", PVP-Vol.359, Fitness for Adverse Environments in Petroleum and Power Equipment, ASME (1997)

[21] Ramos, A., Rios, C., etc., "Delayed Coke Drum Assessment Using Field Measurements and FEM", PVP-Vol.368, Analysis and Design of Composite, Process, and Power Piping and Vessels, ASME (1999)

[22] Ramos, A. J., Rios, C. and Vargas, J.A.R., "Fatigue Life Prediction of Delayed Coke Drums", Vision Techenologica, Vol.6, 93-100,(1999)

[23] Xia, Z., Ju, F. and Plessis, P. D., "Heat Transfer and Stress Analysis of Coke Drum for a Complete Operating Cycle", Journal of Pressure vessel technology, 132 (2010)

[24] Sohel, M., Panwala, M., Srinviasan, K. N., and Mehta, S. L., "Creep-fatigue interaction in coke drums: An approach based on API 579-1/ASME FFS-1 2007", Proceeding of ASME Pressure Vessels and Piping Conference (2009): PVP2009-77483

[25] Penso, J. A., Hazime, R., “Comparison of thermo-mechanical fatigue life assessment methods for coke drums”, Proceeding of ASME Pressure Vessels and Piping Division conference (2010): PVP2010-25810

[26] ASME Boiler and Pressure Vessel Code (BPVC) Section VIII Division 2, New York, N.Y., American Society of Mechanical Engineers, (2007)

[27] API 579-1/ASME FFS, 2007

[28] Nikic, M., and Z. Xia. "Alternative Selections of Delayed Coke Drum Materials Based on ASME Material Property Data." Proceedings of The ASME Pressure Vessels and Piping Conference (2012): PVP2012-78548

[29] ASME Boiler and Pressure Vessel Code (BPVC) Section II, New York, N.Y., American Society of Mechanical Engineers, (2007)

[30] Chen, J., Yamatomo, T., Xia, Z., and Esaki, K., “Experimental Evaluation of Fatigue Life of Coke Drum Materials with Weld Sections”, Proceeding of ASME Pressure Vessel and Piping Conference (2013): PVP2013-97095

CHAPTER 2 Development of Biaxial Thermal-Mechanical Fatigue Testing System and Its Application[1]

To simulate complex thermal mechanical loading condition, an independent strain and temperature controlling with computer-controlled laboratory equipment was successfully designed and developed. The developed thermal mechanical fatigue (TMF) testing system is capable of generating simultaneous thermal and mechanical loading. It has been fully tested and verified to satisfy the requirement of simulating the thermal mechanical loading which is similar as the load experienced by coke drums. An investigation was successfully carried out on a clad material of coke drums with the developed system. From the test results, the TMF life of TP 410S cycling between 100°C and 480°C is slightly shorter than isothermal low cycle fatigue (ILCF) at 480 °C. Furthermore, from the investigation of biaxial TMF tests, the internal pressure causes mean strain in hoop direction, the strain-life relation from uniaxial TMF can give very good prediction on bi-axial case with the consideration of mean stress.

[1] Part of this chapter is published in *Theoretical Applied Mechanical Letters*, 2014, 4(4): 6-041006
Part of this chapter presented in 13th International Conference on Fracture, June 2013, Beijing, China

2.1 Introduction

To experimentally investigate the fatigue life of coke drum materials under thermal-mechanical cyclic loading especially under bi-axial cyclic loading conditions, a thermal-mechanical fatigue (TMF) testing system is required. In order to simulate this complex loading condition, an independent strain and temperature control using computer-controlled laboratory equipment is necessitated. As a result, the cost of TMF testing is usually very expensive and conducting this type of test is more difficult and very time-consuming. There are several existing house-built and commercial TMF testing systems available for different experimental purposes. In 1986, Warren and Cowles [1] introduced a simplified thermal mechanical fatigue test method to study fatigue life of gas turbine engine airfoils under TMF loading. A load-controlled TMF is used instead of typical strain-controlled test. By using this method, a less complicated parameter is used to control the machine during the thermal cycling. However, a prerequisite of knowledge of the stress endpoints corresponding to the strain during loading cycle is essential. This relation can be either obtained from a strain-controlled TMF testing or cyclic stress-strain hysteresis loop from corresponding temperature interval. This simplified method is limited to these test cycles which do not introduce large plastic strain, and also prerequisite of stress-strain relation is needed. Therefore, for low cycle fatigue which is mainly dominated by plastic deformation, a strain-controlled TMF testing system is more accurate and appropriate. Jin et al. in 1989 [2] successfully implemented a TMF testing system to study fatigue life of Ni-base superalloy under uni-axial thermal-mechanical loading. A high frequency induction heater is used, and the temperature in TMF varies from 571 to 823°C at rate of 400 seconds per cycle. A axial strain signal and a temperature signal are generated by the computer to simulate the in-phase and out of phase loading conditions. Even though this study investigates the fatigue life limited up to extreme low cycle fatigue regime (<1000 cycles), the duration of conducting each test at rate of 400 seconds per cycle is still time-consuming. Bartsch et al. [3] used a special designed TMF testing system to study failure behaviour of a material used in gas turbine blades under thermal-mechanical cycling. A hollow specimen is heated outside and cooled inside to generate thermal gradient over the cross section of the

specimen and at the same time a controlled uni-axial tensile mechanical load is applied to simulate a bi-axial stress state. The thermal load with radiation furnace is powered by quartz lamps. However, by using this method, it is very difficult to control the stress state along the gauge length by introducing the thermal gradient, especially, when large plastic deformation occurs. In addition, it is impossible to generate a uniform deformation along the gauge length for thin-walled tubular specimen.

Therefore, a TMF testing system design that is capable of generating simultaneous thermal and mechanical loading as well as bi-axial loading condition on the thin-walled tubular specimen is an essential prerequisite to study the fatigue behaviour of the coke drum materials under the complex thermal-mechanical loadings. Furthermore, a study of SA 204 TP 410S, a clad material for coke drums, has carried out by the developed biaxial TMF testing system. A strain-life relation for TP 410S under thermal mechanical fatigue loading is obtained.

2.2 Design Strategy for the Biaxial TMF Test System

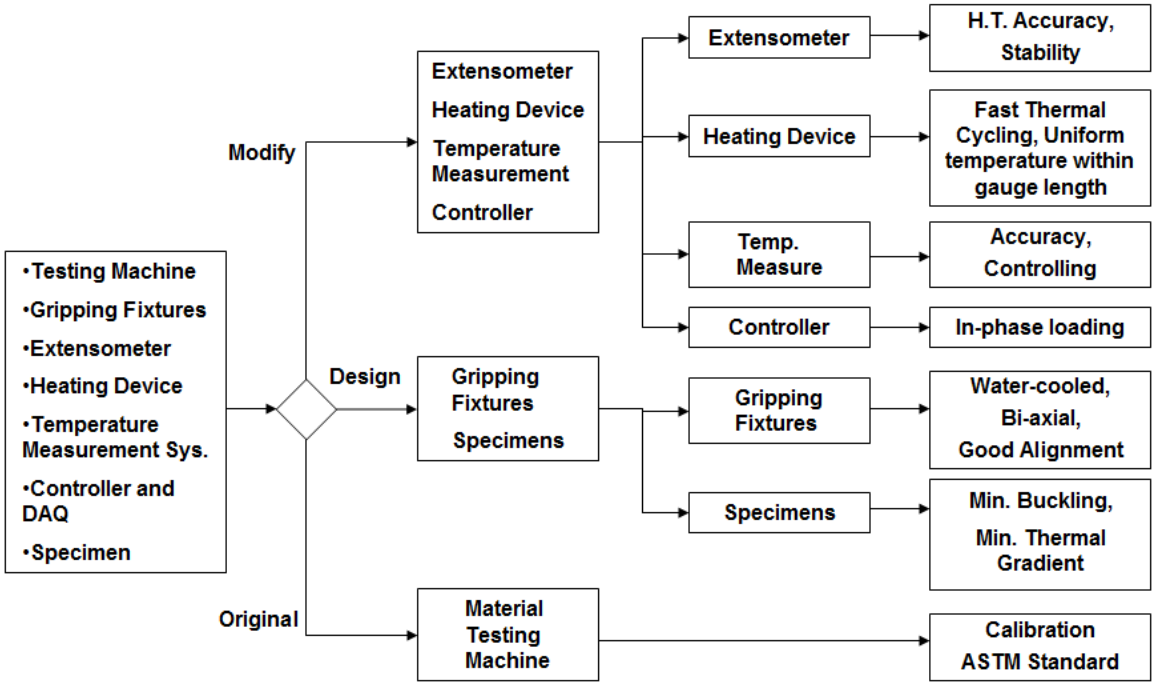

Figure 2.1 Flowchart of bi-axial TMF testing system development

A schematic of the development bi-axial TMF testing system is shown in Fig. 2.1. It consists of three major development phases: Original phase, Modification phase, and Design phase. In the Original phase, a closed-loop servo-controlled hydraulic MTS testing machine is used as a principal uni-axial loading frame. It has loading capacity of 89 kN in either tension or compression. The load cell is carefully calibrated with an elastic calibration device, as seen in Fig. 2.2, with accuracy of ±0.009 kN. The overall test system is verified in accordance with ASTM E4 [4] and E467 [5].

Figure 2.2 Picture of load cell calibration

The second and third phases, Modification and Design, involve six components: extensometer, heating device, temperature measurement, controller, gripping fixtures and specimens. In these two development phases, modification and design are required on these devices to meet the testing requirement as shown in Fig. 2.1.

2.2.1 High Temperature Extensometer

A non-contact extensometer was first selected as a candidate for measuring strain in the TMF system. Tao and Xia [6] developed a non-contact strain measurement and control system for fatigue test of polymer materials by digital image correlation with reference marks on the specimen. It was successfully implemented in ambient temperature tests. However, by carrying out several experiments, it was found very difficult to use in high temperature strain-controlled test. The reference marks gradually disappeared throughout the long-term test, and the convection and radiation on the surface of the polished specimen during the fast temperature cycling causes very unstable strain signals. In addition, due to limited speed of strain signal correlation and feedback, it is difficult and risky to implement this approach to control the strain for the high temperature TMF test. The second candidate is using a uniaxial MTS extensometer (Model 634.11). However, a conventional room temperature extensometer uses clamp-on knife-edge to mount on the specimen. It is impossible to use it at high temperature environment. Therefore, a modification on the MTS extensometer is necessary for high temperature testing. As shown in Fig. 2.3, knife-edge is replaced by a pair of quartz legs with conical tips, and the length of the legs is about 100 mm which can provide sufficient sensitivity to the strain gauge as well as keep the unit distant from the heating source. A pair of adapters is used to securely fix the quartz legs on the extensometer as shown in Fig. 2.3. A pair of punched dimples is also required on the specimen to securely and precisely position the tips of the extensometer. The modified extensometer is carefully calibrated before test.

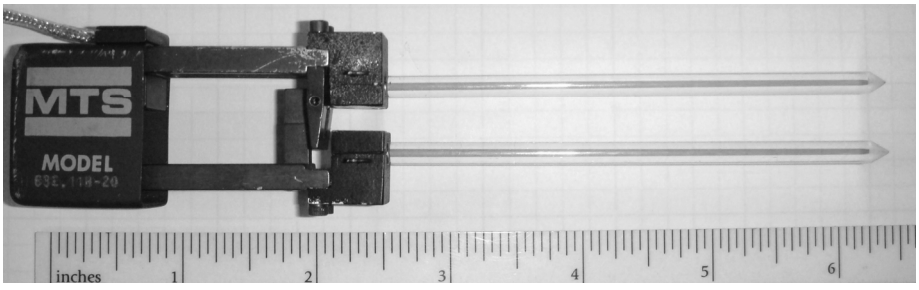

Figure 2.3 Picture of modified MTS extensometer

There are three different methods to fix the extensometer on the specimens. The first method invented is to use fibre-glass strings with springs, as shown in Fig. 2.4 (a). The advantage of this method is to easily and quickly setup the extensometers. However, it is found that, after a few thermal cycles, the strings are hardened and shaped. The strings are not longer capable of holding the weight of the extensometer. The second approach is to build a fixture frame and use loop spring to apply the compressive load, as seen in Fig. 2.4 (b). The advantage of this method is that the extensometer can be positioned on the specimen securely. However, due to the constraint of the loop spring, it is very difficult to initially locate the precise position on the specimen for the conical tips. Furthermore, induction heating is used as a heating device (will be introduced in the following section). There is signal interference associated with strain reading during heating phase from the induction unit. The induction unit causes serious strain shifting and noise during the unit on and off. Therefore, it is impossible to perform the test with strain-controlled mode under this circumstance, which could induce severe load shock by the shifted strain signal. After spending huge amount of time on experimentation, it is found that the shifted and noisy strain signal can be eliminated by completely insulating all wires and connectors of the extensometer from the MTS frame electrically. On the other hand, this fixture is directly attached on the MTS column. Consequently, this method is also eliminated from the final design. The third technique is to use four rubber bands to apply the compressive load, as shown in Fig. 2.4 (c). This method not only provides the easiness and security of installing the extensometer, but also it helps to entirely insulate the extensometer electrically from the load frame. Therefore, the third design is selected as the final method for installing the extensometer.

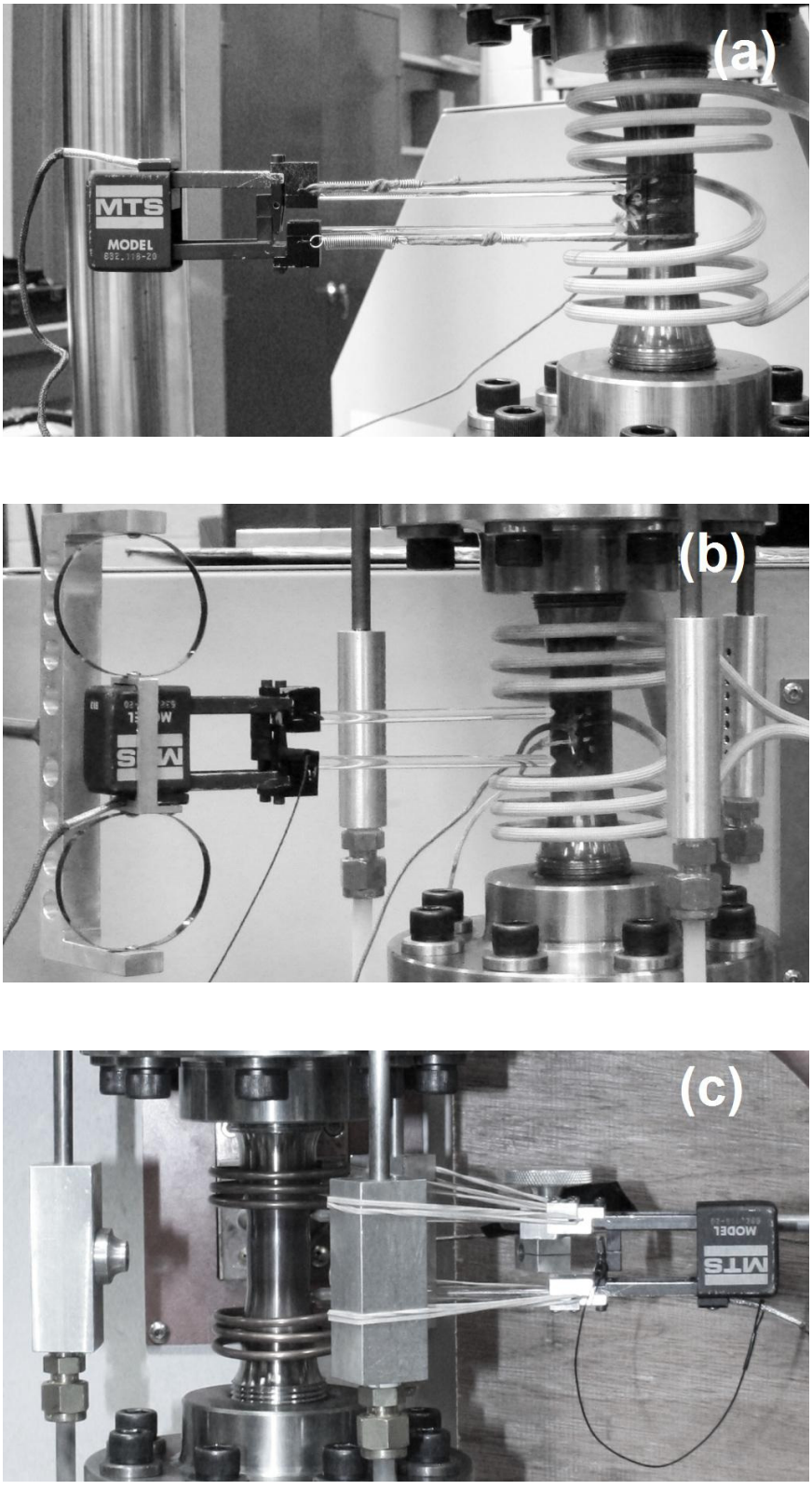

Figure 2.4 Pictures of extensometer fixtures

2.2.2 Heating Device

The TMF testing involves a temperature cycling. Therefore, a relatively fast heating and cooling is essential for conducting a fatigue test. There are various techniques including induction, direct resistance, radiant, or forced air heating. By evaluating the scope of this research and the interested regime of fatigue life, an induction heating with power rated at 5 kW is selected as effective heating source. The unit with high frequency (135~400 kHz) can provide relatively rapid heating rate to feed the purpose. The induction unit mainly consists of a power unit, a working coil, and a cooling system. By positioning the conductive material such as metal specimen inside the working coil, the specimen can be heated up at adjustable rates. Because the working coil provides an open environment, this approach also offers an opportunity to install active specimen cooling (for example, forced air) to achieve a desired cooling rate.

One of the difficulties using this system is to minimize the dynamic thermal gradient along the axial-direction of the specimen. The configuration of working coil plays an important rule affecting the thermal gradient along the axial direction. Variables such as number of coil turns and patterns can have significant effect on the thermal gradients. There are several researchers [7-10] investigated the effect of working coil configuration on the thermal gradient of the specimen. In [7] it was found that by using ten-turns one direction helical configuration of the working coil, the thermal gradient along the gauge length of a solid cylindrical specimen could be within ±10°C at 800°C. In [9] an investigation on the effect of working coil configuration on solid flat specimen was carried out. It concludes that an elliptical coil with its centre axis perpendicular to the middle axis of the specimen gives a smallest thermal gradient on the solid flat specimen. In addition, it was recommended in [10] that a longitudinal opposite direction working coil is for better axial temperature gradients. An experimental investigation of effect of working coil configurations on thermal gradient along a flat specimen was first carried out, as shown in Fig. 2.5.

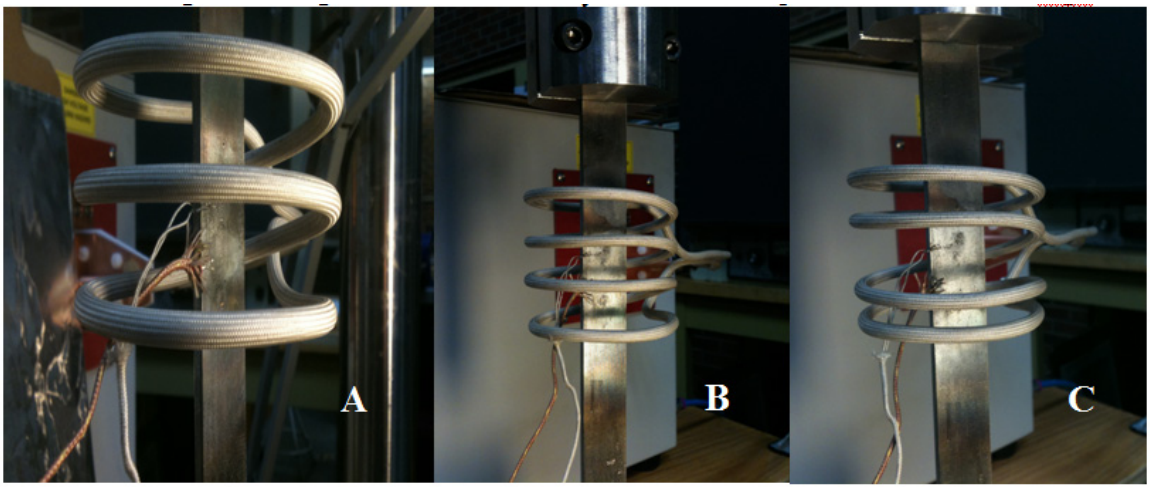

Figure 2.5 Configuration of working coil on flat specimen

Fig. 2.5 A-C shows the one direction longitudinal configuration with different turns. Two thermocouples are welded on the specimen, one in the middle of the working coil and the other one is 12.7 mm away (half of the gauge length) from the center. The temperature is increased up to 500°C, and the dynamic temperature is recorded. The results showed that the working coil configuration C (4 turns with 25 mm gap in the middle) gives the minimal thermal gradients (10°C) at 500°C.

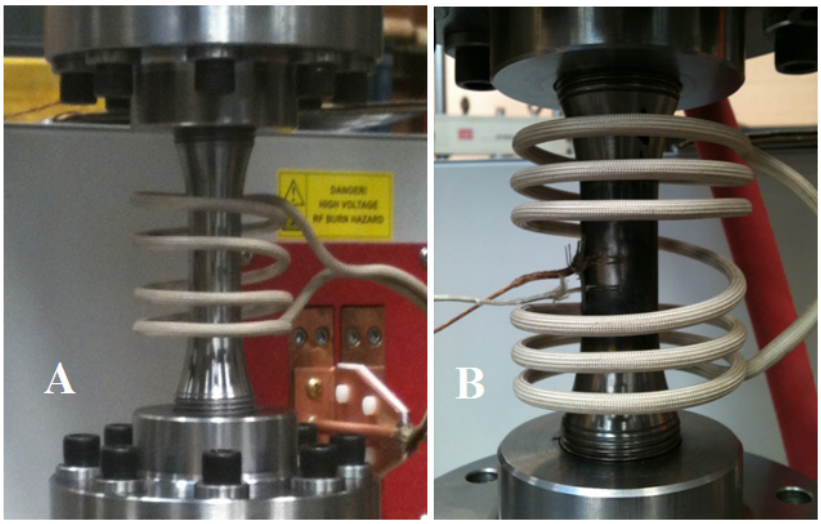

Figure 2.6 Configuration of working coil on thin-walled tubular specimen

Figure 2.6 shows the two different working coil configurations on thin-walled tubular specimen. Two thermocouples were welded on the surface of the specimen, one in the middle of the gauge length and the other one 12.7 mm away from the center. The temperature increases up to 500°C, and the temperature time path is recorded accordingly. The results showed that the working coil configuration A (4 turns with gap in the middle) gives larger thermal gradients (50°C) at 500°C. If the number of turns increases to 6 with gap in the middle, the thermal gradients greatly reduced to 10°C at 500°C.

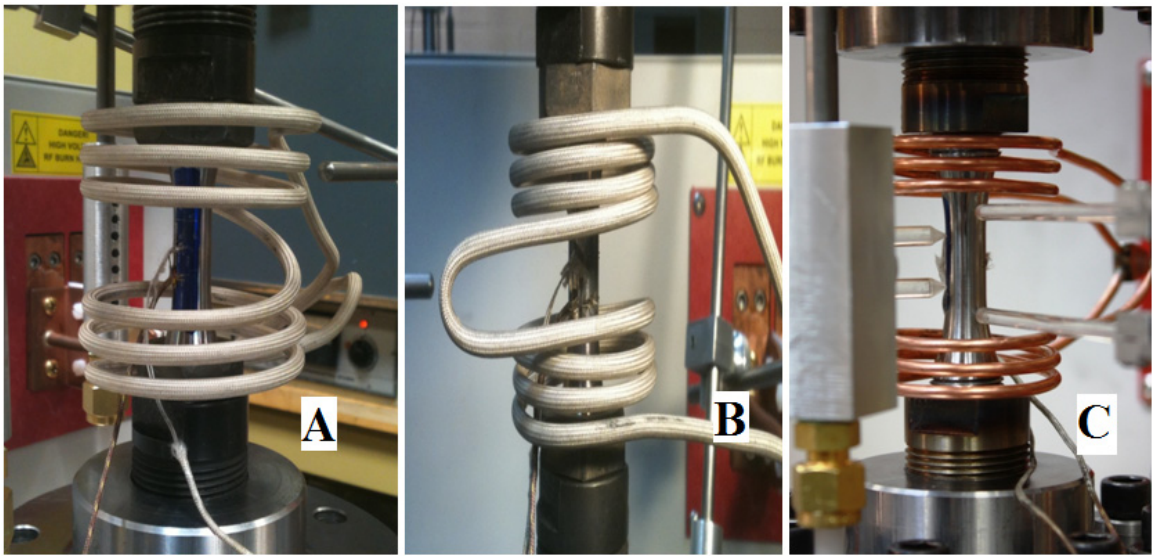

Figure 2.7 Configuration of working coil on cylindrical solid specimen

Figure 2.7 shows the three different working coil configurations on cylindrical solid specimen. Two thermocouples are welded on the surface of the specimen, one in the middle of the gauge length and the other one is 12.7 mm away from the center. The temperature increases up to 500°C, and the dynamic temperature is recorded. The results showed that the working coil configuration A (6 turns with gap in the middle) gives larger thermal gradients (30~40°C) at 500°C. A configuration of longitudinal opposite-direction working coil (Fig. 2.7 B) is then tested, the result showed oppose thermal gradient (500°C in the center, 520~530°C at 12.7 mm away from the center). After several trial and error experimentations, the third configuration C is designed. Two separate working coils are attached on the power unit, and each with three turns. From the experimental result of this configuration, the dynamic thermal gradient almost

disappears (within 5~10°C) along the axial direction at 500°C. Therefore, through this series of experimentations of working coil configuration, two separate working coil gives the minimal thermal gradient in axial direction.

2.2.3 Temperature Measurement of Test Specimen

There are several ways of measuring the temperature on the specimen such as thermocouples, non-contacting sensors, and so on. In [11], it suggests that the specimen temperature shall be measured using thermocouples in contact with the specimen surface in conjunction with an appropriate temperature indicating device. In this study, a OMEGA programmable temperature controller is selected, and it has high accuracy ±0.1°C of temperature reading. It also has the capability of communicating with the main controller of the testing machine to output the temperature data and control the heating device.

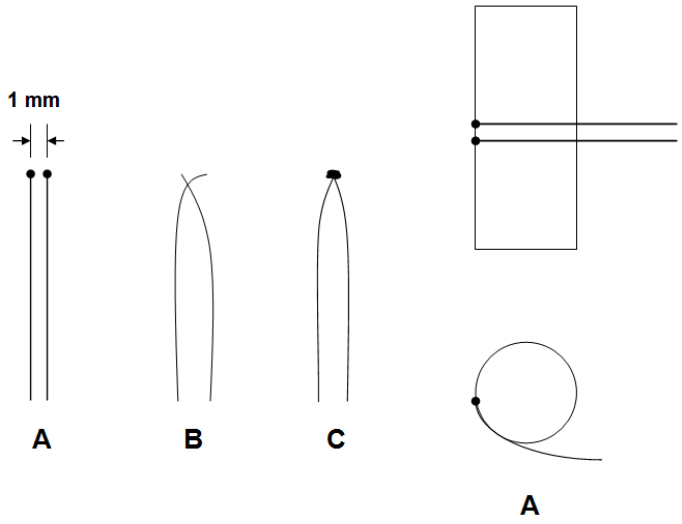

Figure 2.8 Thermocouples welding and wrapping

The non-contact temperature measurements such as pyrometry are not recommended because oxidation induced alterations of the specimen surface may affect the accuracy of measurement [10,12]. Spot welded, ribbon type and coaxial thermocouples may be applied for the dynamic temperature-measurement and control during TMF tests. Figure 2.8 shows the common thermocouples welding, and method-A

is recommended. The thermocouple wires should be individually spot-welded on the specimen surface and wrapping around the specimen surface over a length of at least 10 times the wire diameter. The thermocouple wires shall not contact each other at the welding point. The separation of the thermocouple wires at the welding point shall not exceed 1 mm. Method B and C in Fig. 2.8 are not suggested. Beck and Rau [12] found all three thermocouple fixing methods, spot welded, ribbon type, and coaxial thermocouples, are applicable and give an identical T-t path in the dynamic temperature measurement if certain requirements met. In addition, spot-welded thermocouples can be used for temperature measurement and control in TMF testing with temperature rated up to 50°C/s if a sufficient contacting length applied. They also recommended K and N type thermocouples for maximum temperature up to 850°C because of their higher thermo-voltage. In this study, a K-type spot-welded thermocouple is adopted (Fig. 2.9). By comparing with ribbon type thermocouples under temperature cycling between 100 and 480°C, it is found that these two methods give almost identical dynamic temperature measurement.

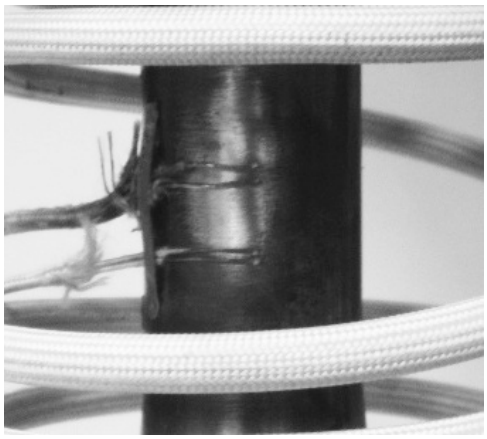

Figure 2.9 Thermocouples spot welded on tubular specimen

2.2.4 Control System

To conduct in-phase strain-controlled TMF test, a program is written in the control system to accurately manage all the components. There are two different

controlling modes designed to conduct in-phase TMF test: time-dependent (Fig. 2.10) and temperature-dependent (Fig. 2.11) strain-controlled.

The dynamic temperature of the specimen is measured by the spot-welded thermocouple, and the temperature controller sends the measurement to the signal controller synchronistically. There are six signal channels, which include heat, cooling jet, hydraulic, strain and load, temperature and nitrogen, installed on the signal control module. The signal controller sends the commands to the heater and air jet during the heating and cooling phases, and it also controls the axial strain to feedback the hydraulic piston to apply the load. Meanwhile, it also sends back all signals to the data acquisition (DAQ) system to display all dynamic readings. All the data is stored by the data acquisition on timed-basis.

2.2.4.1 Time-dependent strain-controlled mode

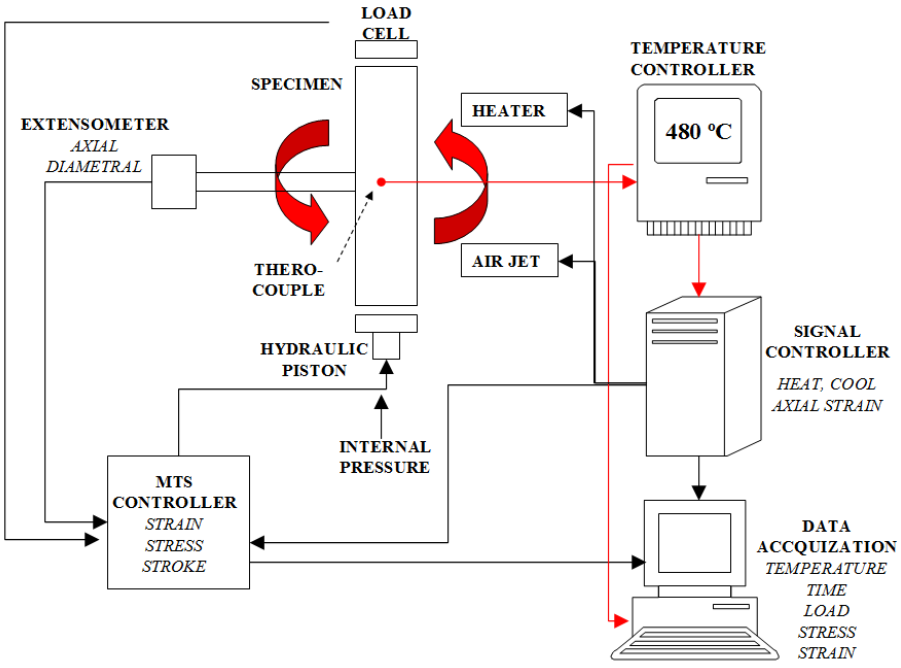

Figure 2.10 Demonstration of time-dependent strain-controlled mode

The thermal cycling is carried out at beginning of each test, and thermal strains at T_{max} and T_{min} are recorded. The stabilized durations of heating and cooling are also traced. The total strains at T_{max} and T_{min} are calculated as:

$$\varepsilon_{Tot}^{T_{\max}} = \varepsilon_{Thermal}^{T_{\max}} + \varepsilon_{mech} \tag{2.1}$$

$$\varepsilon_{Tot}^{T_{\min}} = \varepsilon_{Thermal}^{T\min} + (-\varepsilon_{mech}) \tag{2.2}$$

The durations of heating and cooling and the corresponding total strains are entered into the controlling program. The strain-controlled test can run under cyclically in-phase between temperature and its corresponding calculated total strain. After the test, thermal strain is fitted as a function of temperature in a polynomial equation. The mechanical strain can be obtained by subtracting the thermal strain from the recorded total strain.

2.2.4.2 Temperature-dependent strain-controlled mode

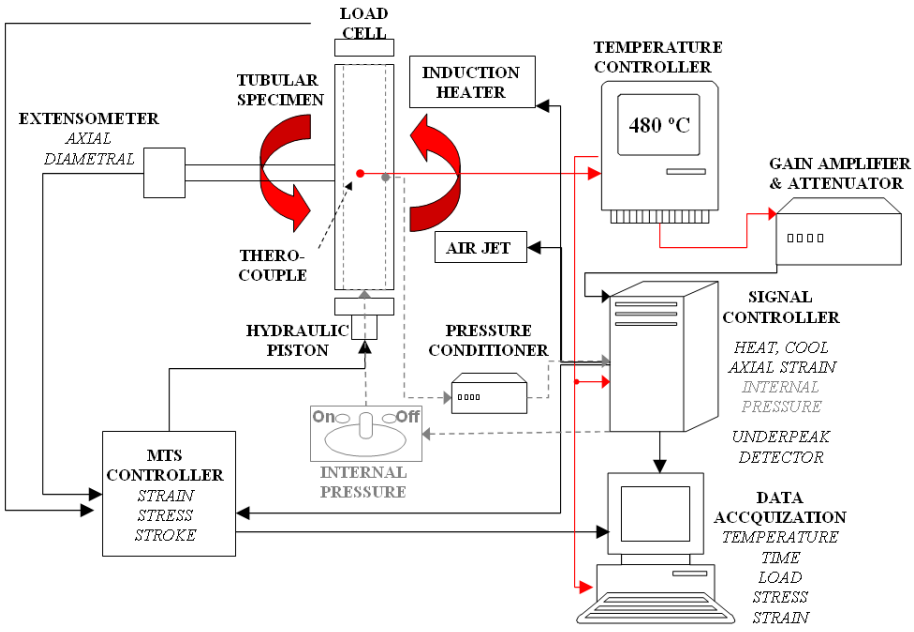

Figure 2.11 Demonstration of temperature-dependent strain-controlled mode

The thermal cycling is carried out at beginning of each test, and thermal strains at T_{max} and T_{min} are recorded. The total strains at T_{max} and T_{min} are first calculated according to Eq. 2.1 and 2.2, and then the strain-temperature range ratio φ is defined as:

$$\varphi = \frac{\Delta\varepsilon}{\Delta T} = \frac{\left(\varepsilon_{Tot}^{T_{\max}} - \varepsilon_{Tot}^{T_{\min}}\right)}{\left(T_{\max} - T_{\min}\right)} \tag{2.3}$$

both ε and T in voltage.

The ratio of input to output voltages of the gain amplifier and attenuator is then adjusted to the ratio φ. The mechanical and temperature cycling between T_{max} and T_{min} will generate a voltage which is equal to total strain at the corresponding temperature. After the test, thermal strain is fitted as a function of temperature in a polynomial equation. The mechanical strain can be obtained by subtracting the thermal strain from the total strain.

The advantage of the time-dependent strain-controlled mode is easy to setup and start the test. However, due to the unsteady period of heating and cooling (such as change of environmental condition), the controlled-total strain can be either advanced or delayed within a cycle. It is not uncommon to have mismatched durations between strain up/down and temperature up/down. The advantage of the temperature-dependent strain-controlled mode is more accurate in controlling total strain. The controlled strain is independent of heating and cooling time, and it is directly controlled by the dynamic temperature signal. Therefore, the controlled-strain is assured to cycle in between the preset strain range. The only drawback of this control mode is time-consuming to setup. In this TMF testing system, the temperature-dependent strain-controlled mode is preferred.

2.2.5 High Temperature Gripping Fixtures

The primary purpose of the gripping fixtures is to directly transfer the load to the specimen, and also it can provide good alignment. Since TMF test involves both thermal and mechanical load cycling, it is important to maintain the stable thermal cycling and

uniformly dynamic temperature along the gauge length as well as protect the load cell from overheating. In order to avoid long-term drift of the temperature cycle realized within the gauge length, it was suggested that additional water cooling at the specimen ends may be required [10,12].

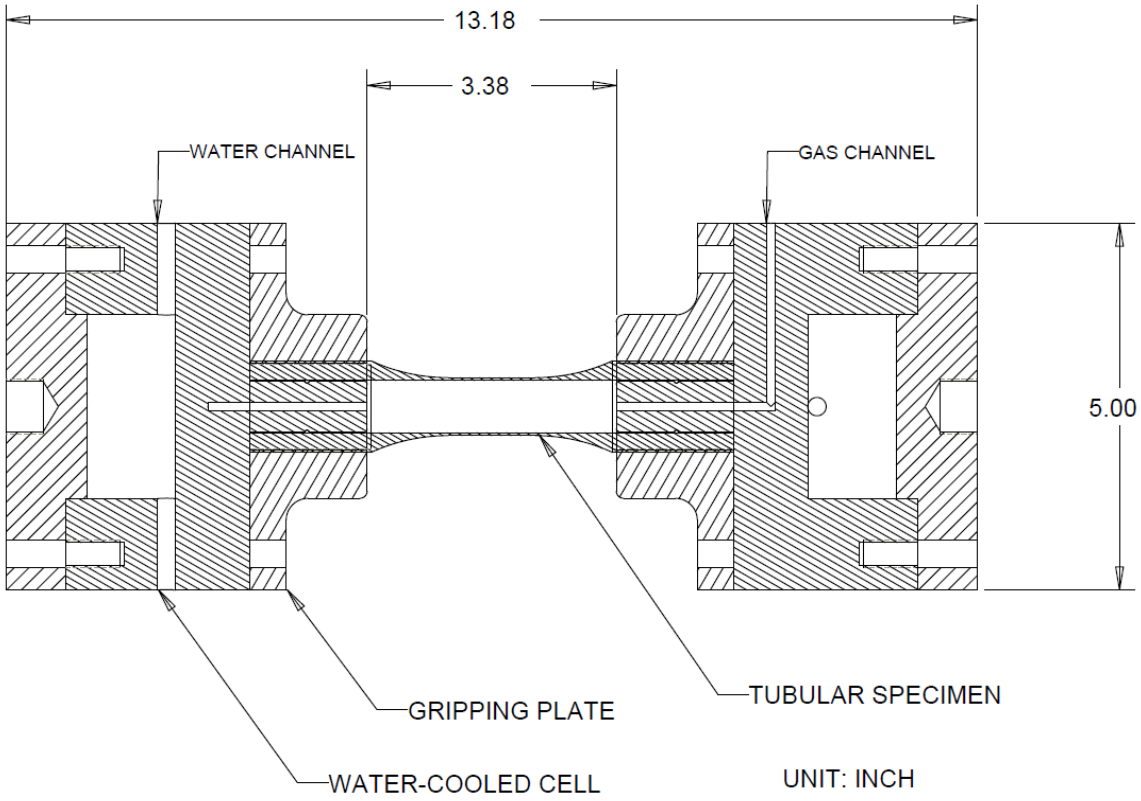

Figure 2.12 Drawing of TMF gripping fixture

Figure 2.12 shows the designed TMF gripping fixture. It includes a pair of gripping plates, a pair of water-cooled cells, and two gas channels. The specimen ends can be threaded in both gripping plates, and the plates are attached to the water-cooled cells with eight bolts on each side. The flow rate of cooling water can be adjusted to adapt different heating rate. Two gas channels with sealing O-rings can direct pressurized nitrogen into tubular specimen to generate internal pressure. Another advantage of this design is that the length of the load train is minimized, and then it can ensure better alignment of the specimen under compressive loading. The specimen alignment under tensile and compressive axial force is verified according to ASTM E1012-05 [13]. Figure

2.13 shows a specimen for the alignment test installed on the load train. The thin-walled tubular specimen is employed, and the thickness and gauge length of the specimen is 1 mm and 30 mm, respectively. There are total eight strain gauges (two sets of four with each set mounted on one of the two strain measurement planes) installed on the specimen. The gauges are equally spaced at 90 degrees to one another around the circumference of the specimen. The tensile and compressive axial forces are applied within the elastic region of the specimen. The strains are recorded from the eight strain gauges after the load applied. The bending strain is calculated according to ASTM E1012-05 [13] and found to be within 2% of the minimum axial strain range imposed for repeated trials, which is less than the ASTM E606 [14] required minimum value 5% for fatigue test.

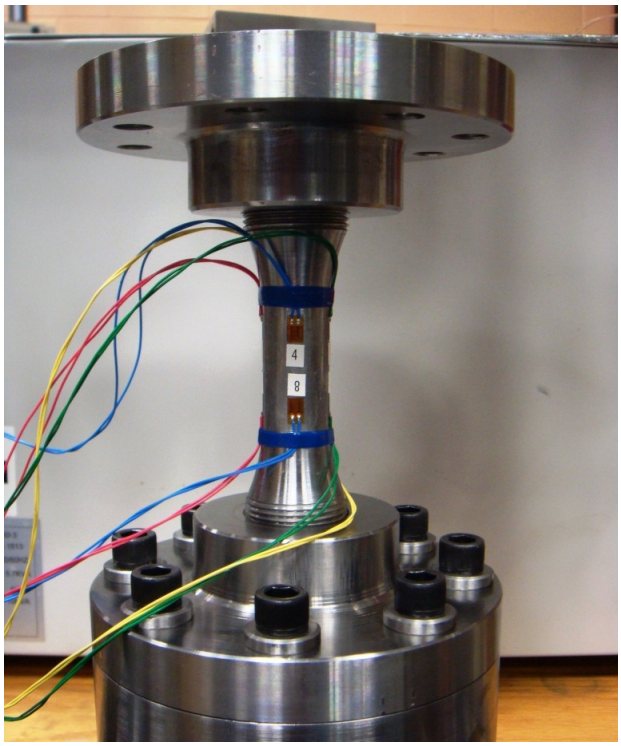

Figure 2.13 Picture of verification of test frame and specimen alignment

2.2.6 Internal Pressure

To simulate bi-axial loading, thin-walled tubular specimen is internally pressurized by nitrogen gas. As shown in Fig. 2.14 (left), a pressure gauge with an

automatic pressure relief valve and a needle pressure relief valve is installed on the upper gripping fixture. The internal pressure inside a specimen can be altered manually to a preset value by adjusting the needle valve. The automatic pressure relief valve can be set to a predetermined value, and the gas will be automatically released when the internal pressure of the specimen exceeds this preset value. A pressure control valve is installed on the lower cooling cell, as seen in Fig. 2.14 (right). In addition to that, a needle valve is also implemented to adjust the inlet gas flow, and it allows the pressurized nitrogen to continuously run into the specimen during testing. The pressure valve is directly controlled by a pressure conditioner and signal controller (refer Fig. 2.11). When through-wall crack presents on the shell of the specimen, the internal pressure will drop depending on the inlet valve opening. Therefore, from the experimentation, it is found that when the needle valve has one-turn opening, it will allow the internal pressure apparently dropping, which can be detected by the pressure conditioner. When pressure drops to 80% of the initial preset value, the program will shut off the pressure valve, which the internal pressure will no longer supply to the tubular specimen. Additionally, the sensitivity of the crack detection can be directly related to the magnification of pressure alteration which can be adjusted by the inlet needle valve attached to the pressure valve.

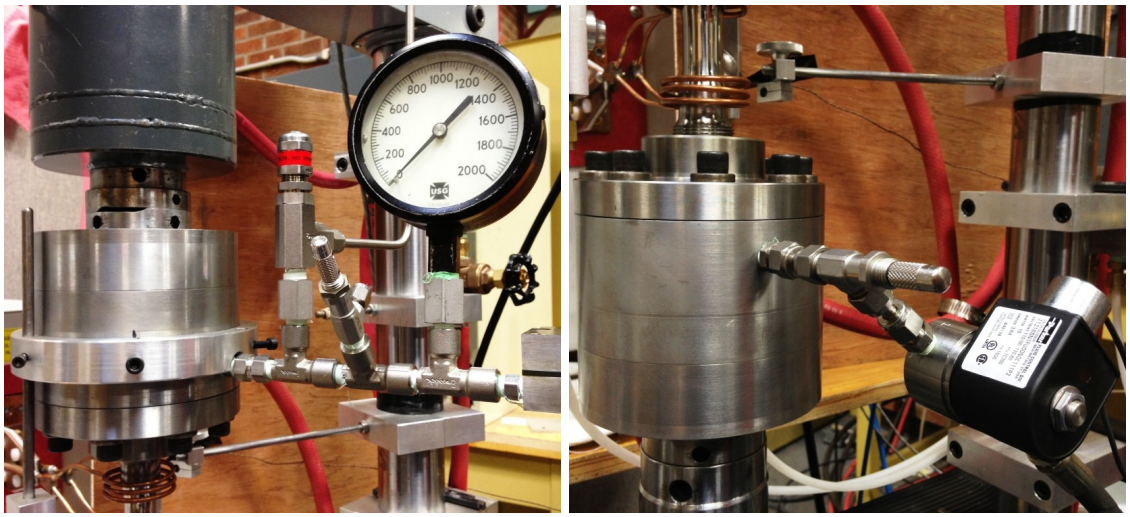

Figure 2.14 Pictures of pressure gauge (left) and pressure control valve (right)

2.2.7 Design of TMF Specimens

There are two different geometries of TMF fatigue specimens designed. The first one is for uniaxial TMF test. The new specimen geometry, as shown in Fig. 2.15, is designed by modifying the solid cylindrical specimen geometry according to ASTM E606-04 [14]. However, instability of specimen under cyclic loading at high temperature is noticed. The gauge length is then slightly shortened to 0.6" (15.24mm), and gauge diameter is 0.4" (10.16mm). The both ends of the specimen have 1.89" (48 mm) long thread, and the total length of the specimen is 6" (152.4mm). It is confirmed that the new geometry minimizes the instability of the specimen under cyclic loading at high temperature through several careful experimentations. The diameter of the hole is 0.25" (6.35mm), and the inner surface of the hole is polished to the same roughness as the outer surface of the gauge section to maintain consistency. The gauge section of the specimens is carefully polished by 3M sandpaper gradually to a grit size of 600 (average particle diameter 16 μm).There are several advantages of using this geometry for TMF test: first, it minimizes the thermal gradient in radial direction during dynamic thermal cycling. Secondly, the material reduction in the gauge length can increase both heating and cooling rates which will shorten the cycling time. Furthermore, it can further improve the stability of the specimen during intensive thermal mechanical loading.

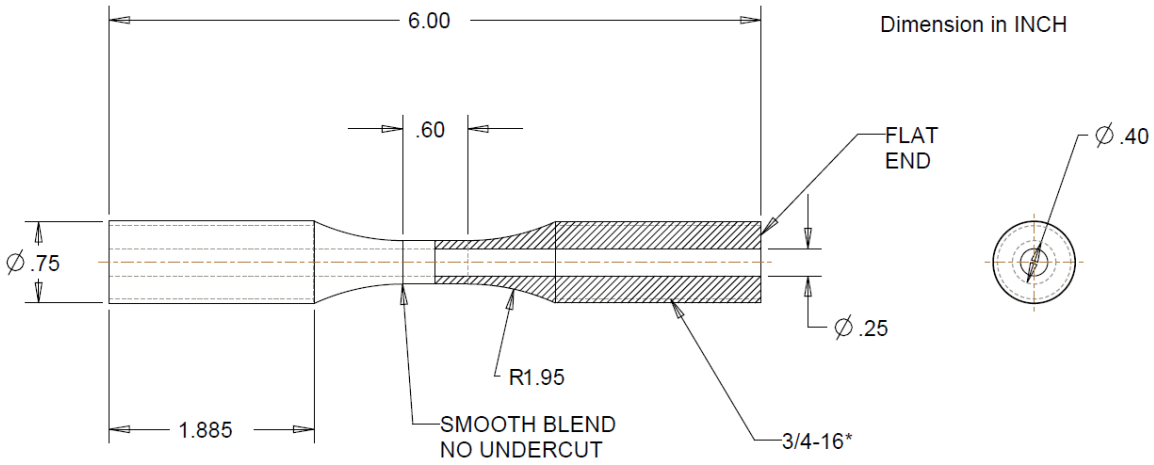

Figure 2.15 Specimen drawing for uniaxial TMF test

The second geometry is for bi-axial TMF test as shown in Fig. 2.16. The thin-walled tubular specimen is designed based on the axial-torsional fatigue specimen according to ASTM E2207-08 [15]. The mean diameter of gauge length is 0.75" (19.05mm), and the wall thickness is 0.04" (1 mm). The ratio of mean diameter to wall thickness is 18.75:1 which is greater than thin-walled tube criterion (10:1). To avoid buckling and minimize thermal gradient along the axial direction of the specimen, two-stepped diameter is employed, which reduces noticeable amount of material in the heating zone as well as minimizes the gauge length. The gauge length is 0.6" (15.24mm), and the total length of the specimen is 6.6" (167.6mm). This designed geometry is experimentally proven for good stability and satisfactory thermal gradient under fast thermal mechanical cyclic loading.

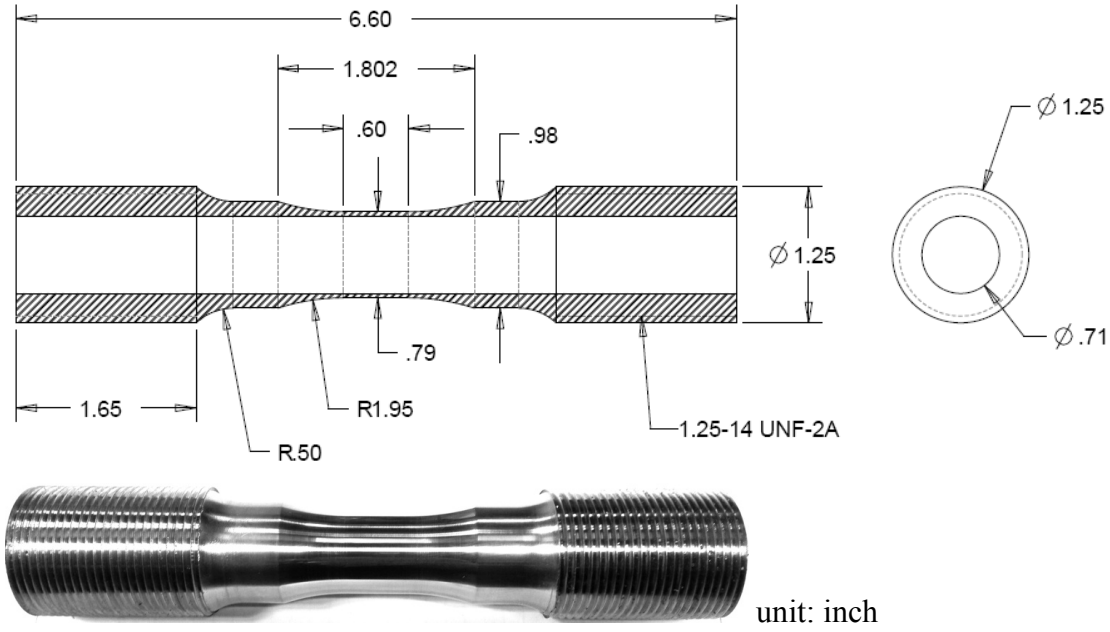

Figure 2.16 Specimen for bi-axial TMF test

2.2.8 Overview of the Completed System

The complete biaxial TMF testing system is shown in Fig. 2.17. It includes the induction heating system, main test frame, control module, nitrogen supply and data acquisition system (induction cooling system is not shown). The entire system and its

components are validated and verified through tons of experimentation according to ASTM standards [4, 5, 11, 13, and 14]. The picture of the main load frame is shown in Fig. 2.18. It primarily includes a load cell, a pair of cooling cells, three air cooling jets, induction coil, pressure valve and gauge, and an extensometer. It has been entirely tested to satisfy the requirement of simulating the thermal mechanical loading which is similar to the loading experienced by coke drums.

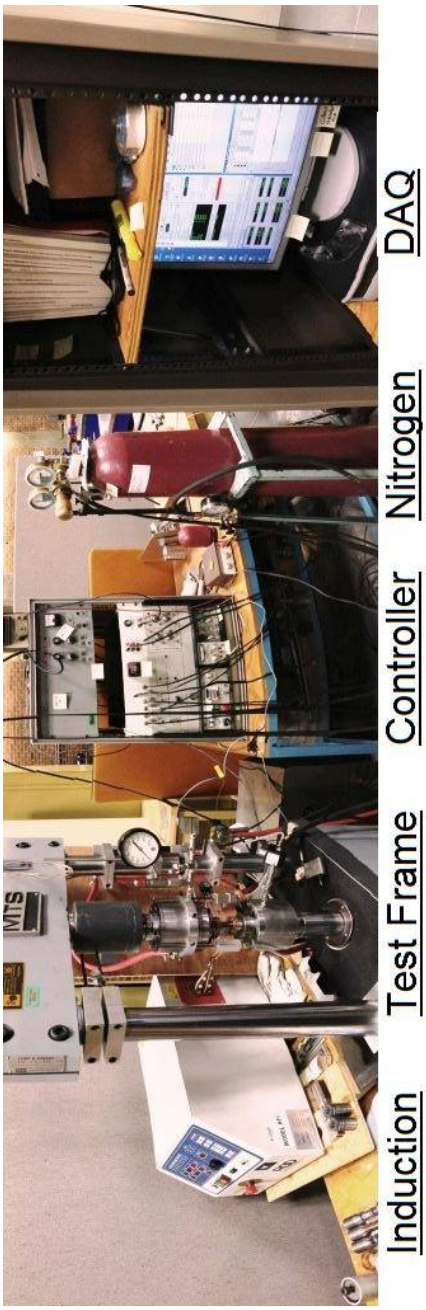

Figure 2.17 Picture of the complete TMF testing system

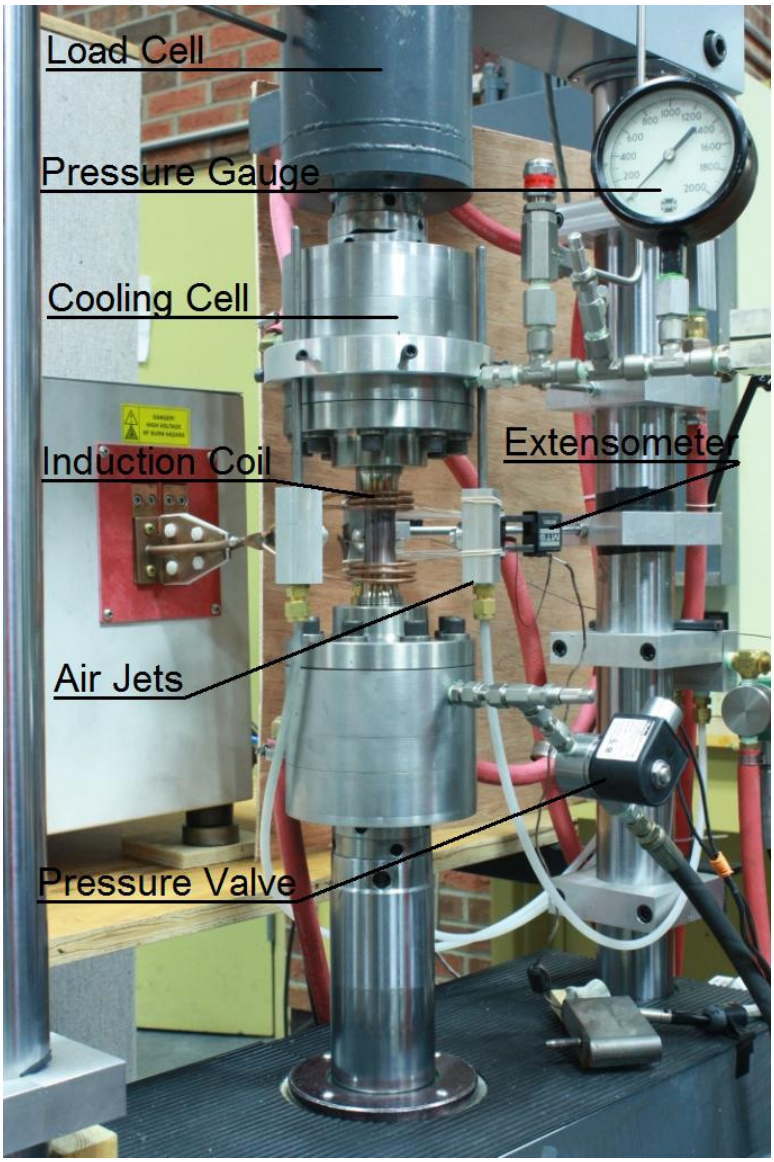

Figure 2.18 Picture of main test frame

2.3 Application of the TMF System on SA204 TP410S

A clad material (SA 204 TP 410S) of coke drums is investigated under the thermal-mechanical cyclic loadings. In addition, a comparative study between isothermal and thermal mechanical fatigue lives of this clad material is conducted.

2.3.1 Test Program

Isothermal low cycle fatigue (ILCF) tests are first conducted at 100°C and 480°C for clad material by using high temperature isothermal fatigue testing system [16]. A solid specimen which has identical profile dimension as uniaxial TMF specimen (Figure 2.15) is used. The selected test temperature of 480°C represents the upper bound of typical operational temperature for coke drums. The uni-axial ILCF tests are carried out as benchmark tests for comparison. The ILCF tests are performed under strain-controlled condition at a strain rate of 0.005/sec throughout all tests. The tests are conducted for fully-reversed cyclic loading ($R = \varepsilon_{\min}^{mech} / \varepsilon_{\max}^{mech} = -1$) at both temperatures. Afterwards, TMF tests are carried out on the developed system. The tests are performed under temperature-dependent strain-controlled condition, and in-phase thermal-mechanical loading is applied at a cycle rate of 0.02Hz. The temperature is cycled between 100°C and 480°C throughout the test. At each strain level, there are at least two tests conducted to insure the repeatability and accuracy of the data. Each fatigue test stops when the maximum load decreases to 6 *kN* for the ILCF solid specimens and 3.7 *kN* for the TMF tubular specimens. The reasons for this failure criteria are: (1) to protect the equipment from the sudden rupture of the specimen; (2) the set failure point is very close to the final separation, and it covers over 95% of the entire life; (3) the intact specimen provides ease in disassembling of the tested specimen.

2.3.2 Test Results and Comparison of ILCF and TMF of 410S

Table 2.1 lists the ILCF test results for the clad steel at 100°C and 480°C as well as TMF tests.

Table 2.1 Fatigue test results of SA 204 TP410S

ILCF 100 °C			ILCF 480 °C			TMF 100~480 °C		
Δε/2	Δσ/2	$2N_f$	Δε/2	Δσ/2	$2N_f$	Δε/2	Δσ/2	$2N_f$
mm/mm	MPa	Reversals	mm/mm	MPa	Reversals	mm/mm	MPa	Reversals
0.0027	258	46,020	0.0023	182	30,800	0.0023	206	23,094
0.0027	256	50,440	0.0023	181	42,240	0.0023	206	28,884
0.0044	293	12,240	0.0033	194	15,040	0.0028	209	12,054
0.0044	291	18,360	0.0033	197	11,760	0.0028	208	13,402
0.0068	317	5,902	0.0044	209	8,860	0.0035	220	7,176
0.0068	320	5,420	0.0044	210	6,840	0.0035	226	7,866
0.0092	331	1,824	0.0068	226	3,288	0.0047	237	3,096
0.0092	328	1,702	0.0068	227	1,514	0.0046	239	4,156
~	~	~	~	~	~	0.0074	267	1,228
~	~	~	~	~	~	0.0075	266	1,000

In 1910, Basquin [17] observed stress-life data could be fitted by

$$\frac{\Delta\sigma}{2} = \sigma'_f (2N_f)^b \tag{2.4}$$

where Δσ/2 is the true stress amplitude, $2N_f$ is reversals to failure (2*cycles to failure), σ'_f is fatigue strength coefficient, and b is fatigue strength exponent.

In the 1950s, Coffin [18] and Manson [19] found that plastic strain-life (ε_p-N) data can be related by a similar power law function

$$\frac{\Delta\varepsilon_p}{2} = \varepsilon'_f (2N_f)^c \tag{2.5}$$

where $\Delta\varepsilon_p/2$ is the plastic strain amplitude, ε'_f is the fatigue ductility coefficient, and c is the fatigue ductility exponent. From the above relations and expression of total strain:

$$\frac{\Delta\varepsilon}{2} = \frac{\Delta\varepsilon_e}{2} + \frac{\Delta\varepsilon_p}{2} \tag{2.6}$$

Then, the elastic strain amplitude ($\Delta\varepsilon_e/2$) can be related to Basquin's function by

$$\frac{\Delta\varepsilon_e}{2} = \frac{\Delta\sigma}{2E} = \frac{\sigma'_f}{E}(2N_f)^b \tag{2.7}$$

In combining Coffin-Manson-Basquin's relation, the total strain verse fatigue life can be rewritten as

$$\frac{\Delta\varepsilon}{2} = \frac{\Delta\varepsilon_e}{2} + \frac{\Delta\varepsilon_p}{2} = \frac{\sigma'_f}{E}(2N_f)^b + \varepsilon'_f(2N_f)^c \tag{2.8}$$

The detailed decomposition of total strain into plastic and elastic portions versus reversals for 100°C ILCF, 480°C ILCF and TMF are shown in Fig. 2.19 (a)~(c). It can be seen that the data is well fitted by linear regression as the form of Eq. 2.5 and Eq. 2.7 for plastic and elastic portions correspondingly. The parameters obtained from this procedure are summarized in Table 2.2. The data for mechanical strain amplitude versus reversals, in Fig. 2.20, are fitted by the Coffin-Manson-Basquin relation (Eq. 2.8). It can be seen that as the test temperature increases the fatigue life of 410S decreases evidently.

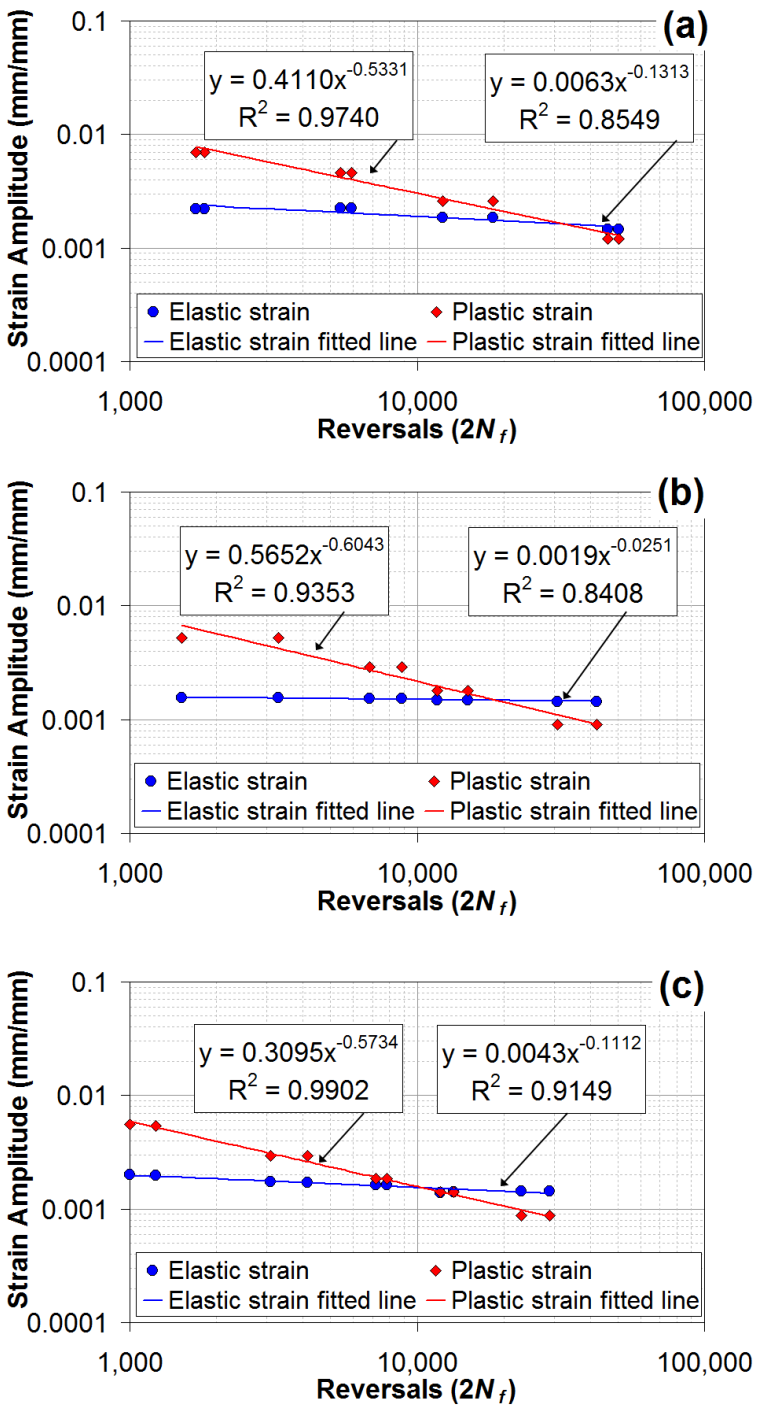

Figure 2.19 Summary of elastic amplitudes and plastic amplitudes vs. $2N_f$

(a) 100°C ILCF (b) 480°C ILCF (c) TMF 100°C~480°C

Table 2.2 Summary of fatigue parameters for TP410S

	100°C	480°C	TMF
Young's Modulus (GPa) - E	185	167	185
Fatigue strength coefficient (MPa) - σ'_f	1165.5	317.3	795.5
Fatigue strength exponent - b	-0.1313	-0.0251	-0.1112
Fatigue ductility coefficient - ε'_f	0.411	0.5652	0.3095
fatigue ductility exponent - c	-0.5331	-0.6043	-0.5734

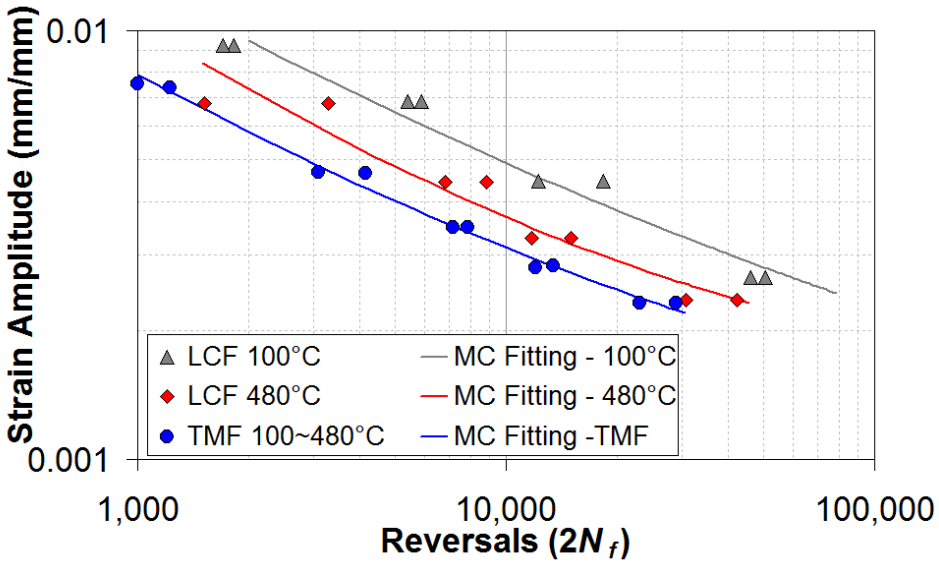

Figure 2.20 Comparisons of ILCF and TMF for TP410S

The TMF life of TP 410S is evidently shorter than ILCF at 480 °C by a factor of 1.5, see Fig. 2.20. To investigate this phenomenon, a microstructure exam is carried out on tested ILCF and TMF specimens. As shown in Fig. 2.21 (a) the transgranular crack is observed on ILCF specimen. However, for specimen under thermal mechanical loading, an intergranular crack is observed as seen in Fig. 2.21 (b). In the meantime, multi-microcracks are spotted on the TMF specimen in Fig. 2.21 (C). Therefore, creep damage has more influence on the fatigue life of TP 410S under thermal mechanical loading.

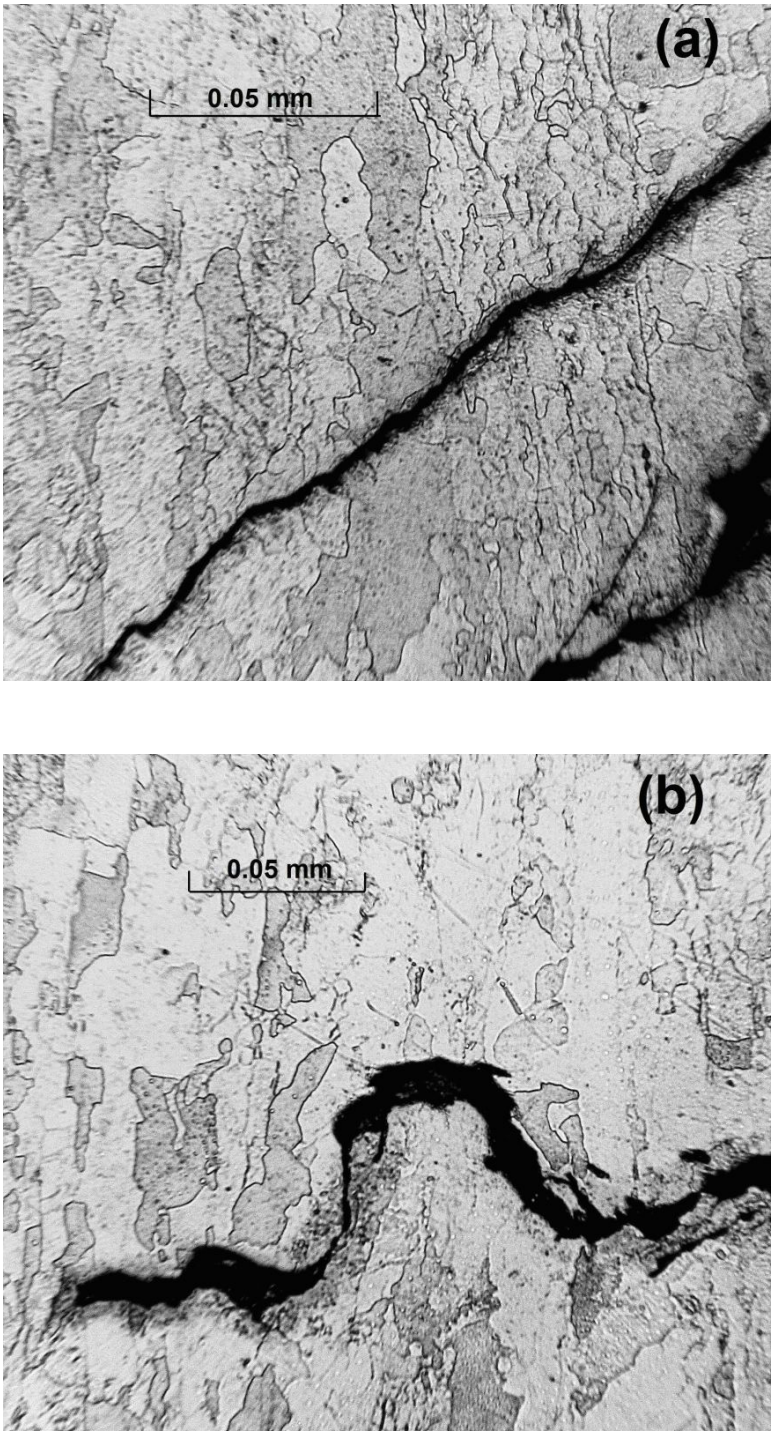
(a)
0.05 mm
(b)
0.05 mm

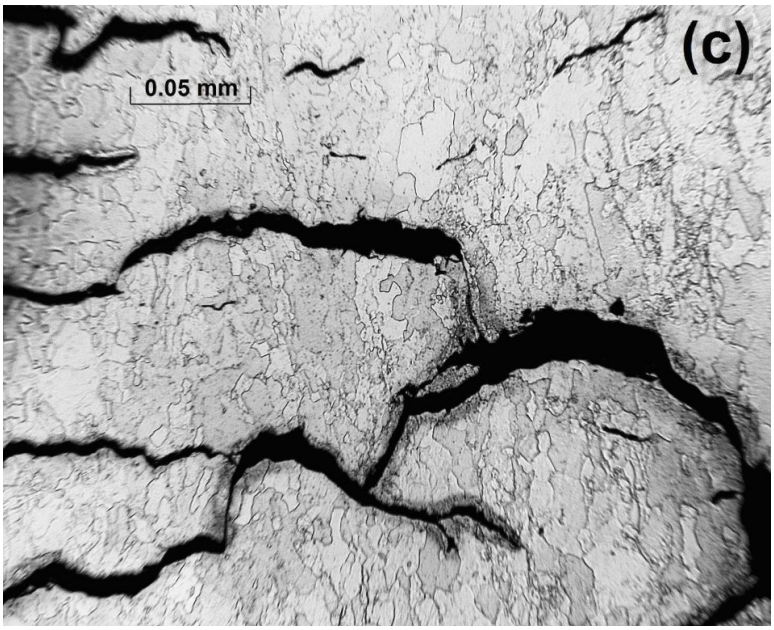

Figure 2.21 Microstructures of tested ILCF and TMF 410S
(a) ILCF 480 °C 0.33% strain (b) and (c) TMF 0.35%

2.3.3 Comparison of Time and Temperature Based TMF Tests

To confirm the consistence of the TMF test, two sets of TMF tests, nine time-based and 10 temperature-based TMF tests, are performed. The strain-life results are shown in Fig. 2.22, and a power function is fitted through linear-regression for each set of test respectively. From the statistical factor R square, it indicates that the temperature-based TMF tests results in more consistent fatigue data than time-based TMF tests. This is mainly due to that time-based test is significantly sensitive to its surrounding environment. Any temperature variation could cause the temperature-load mismatch within a loading cycle. It is also observed that the maximum loads at corresponding maximum temperatures sometimes fluctuate throughout a complete test. From the experience, a closed test environment is recommended to eliminate the temperature variation if time-based TMF testing was used. Therefore, more reliable temperature-based TMF test is adopted in this investigation. Furthermore, from the comparison of the two different testing methods, it is found that the strain-life relations from the two

methods are greatly agreed with each other. Therefore, it is also confirmed that the developed system is confidently reliable to perform the TMF tests.

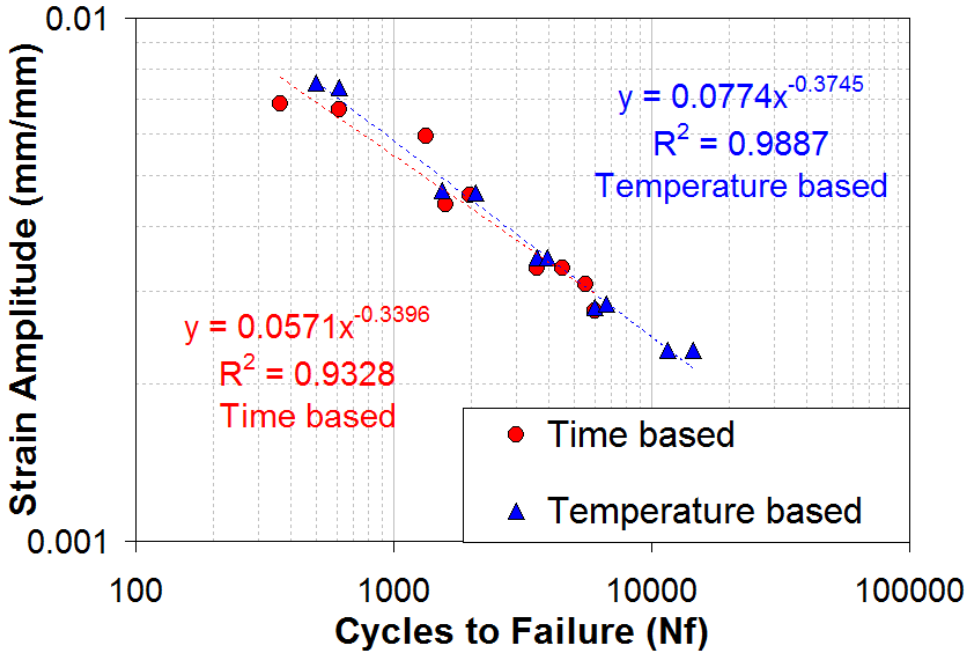

Figure 2.22 Comparisons of Time and Temperature Based TMF tests

2.3.4 Biaxial TMF test with Internal Pressure

To calculate the value of internal pressure used in this investigation, dimensions of a coke drum fabricated by Sumitomo Heavy Industries is implemented. The inner radius (r) of the drum is 3810 mm, and the wall thickness (t) is 39.5 mm. The maximum operating pressure (p) is 0.647 MPa. The axial and hoops stresses can be calculated as the following:

$$\sigma_{axial} = \frac{P \cdot r}{2t} \text{ or } \sigma_{hoop} = \frac{P \cdot r}{t} \tag{2.9}$$

The normal and hoop stresses in this drum are calculated to be 31.2 and 62.4 MPa respectively. To have similar stress level caused by internal pressure in the thin-walled tubular TMF specimen (as shown in Fig. 2.16), the following calculation is performed.

The inner radius (r) of the specimen is 9.017 mm, and the wall thickness (t) is 1.016 mm. The value of pressure inside the tubular specimen is:

$$P = \frac{\sigma_{hoop} \cdot t}{r} = \frac{62.4MPa \cdot 1.016mm}{9.017mm} = 7.03MPa = 1.02ksi \tag{2.10}$$

The tests are performed under temperature-dependent strain-controlled condition, and in-phase thermal-mechanical loading is applied at the same cycle rate of 0.02Hz. The temperature is cycled between 100°C and 480°C throughout the test. Thermal cycling is applied at the beginning of each test and the thermal strain is recorded. Subsequently, the pressure is applied before the mechanical load applied. Under the load-controlled mode, the strain is zeroed, and then the test is carefully switched to strain-controlled mode. From this point, the test starts and runs like the uniaxial TMF test. However, the pressure may fluctuate slightly in the first few cycles due to thermal cycling. The needle valves at the top and bottom of the cooling cells can be adjusted rigorously to minimize the fluctuation. It is recorded that the oscillation of the pressure between 100°C and 480°C inside the specimen is about ±2.5% of the preset value. When a through-wall crack appears in the specimen, the pressure starts to drop. When the pressure drops to 80% of the full pressure, the program will turn off the pressure valve, which the internal pressure will no longer supply to the tubular specimen. At each strain level, there are still at least two tests conducted to insure the repeatability of the test data.

The specimen is subjected to constant axial and hoop stress due to the constant pressure applied. Therefore, the tensile mean stress should be considered in the evaluation of the fatigue life. Morrow [20] introduced mean stress correction model in the stress-life equation 2.7, and the equation becomes:

$$\frac{\Delta\varepsilon_e}{2} = \frac{\sigma'_f - \sigma_m}{E}(2N_f)^b \tag{2.11}$$

Similarly, Manson and Halford [21] modified both the elastic and plastic terms of the strain-life equation to maintain the independence of the elastic-plastic strain ratio from mean stress. The total strain-life relation becomes:

$$\frac{\Delta\varepsilon}{2}=\frac{\sigma'_f-\sigma_m}{E}(2N_f)^b+\varepsilon'_f\left(\frac{\sigma'_f-\sigma_m}{\sigma'_f}\right)^{c/b}(2N_f)^c \tag{2.12}$$

The equivalent stress can be calculated as:

$$\sigma_{eq,m}=\frac{1}{\sqrt{2}}\left[\left(\sigma_{1,m}-\sigma_{2,m}\right)^2+\sigma_{2,m}^2+\sigma_{1,m}^2\right]^{1/2} \tag{2.13}$$

The fatigue lives of TMF and biaxial TMF are shown in Fig. 2.23. The fatigue life of TMF under biaxial loading is apparently shorter than under uniaxial loading. The life under biaxial loading is estimated by Eq. 2.12. The comparison of fatigue lives between estimated and test results is shown in Fig. 2.24. The method with considering mean stress gives fairly accurate prediction on the fatigue life of the specimen under internal pressure. Moreover, the mean stress in hoop direction gives ratcheting strain in that direction, which results accumulative bulging in the circumferential direction of the specimen as seen in Fig. 2.25.

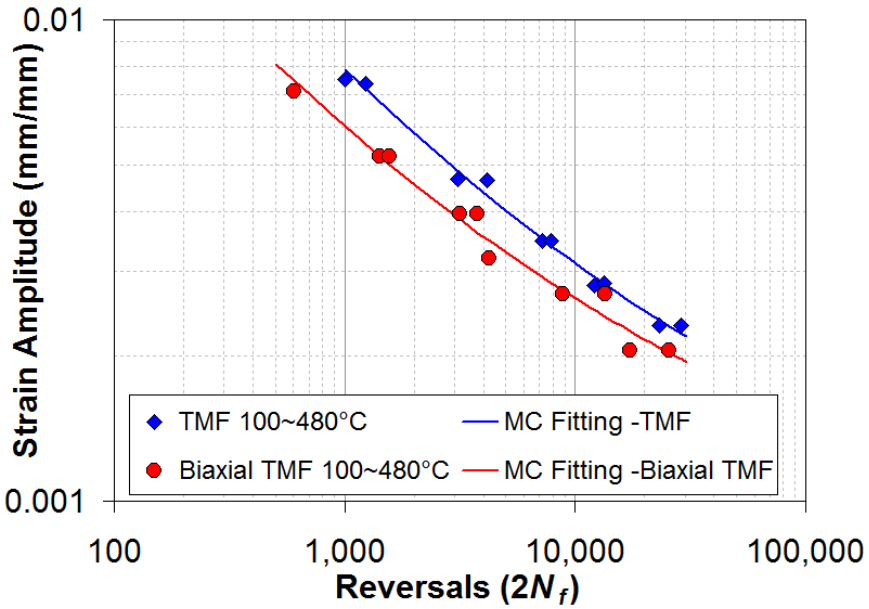

Figure 2.23 Fatigue lives of TMF and Biaxial TMF

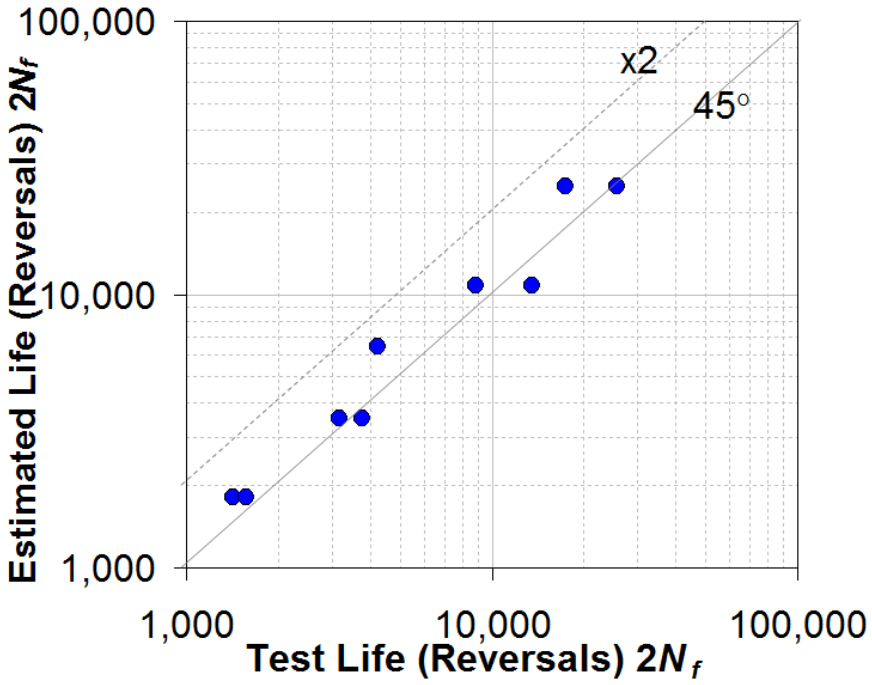

Figure 2.24 Comparison of estimated and test lives

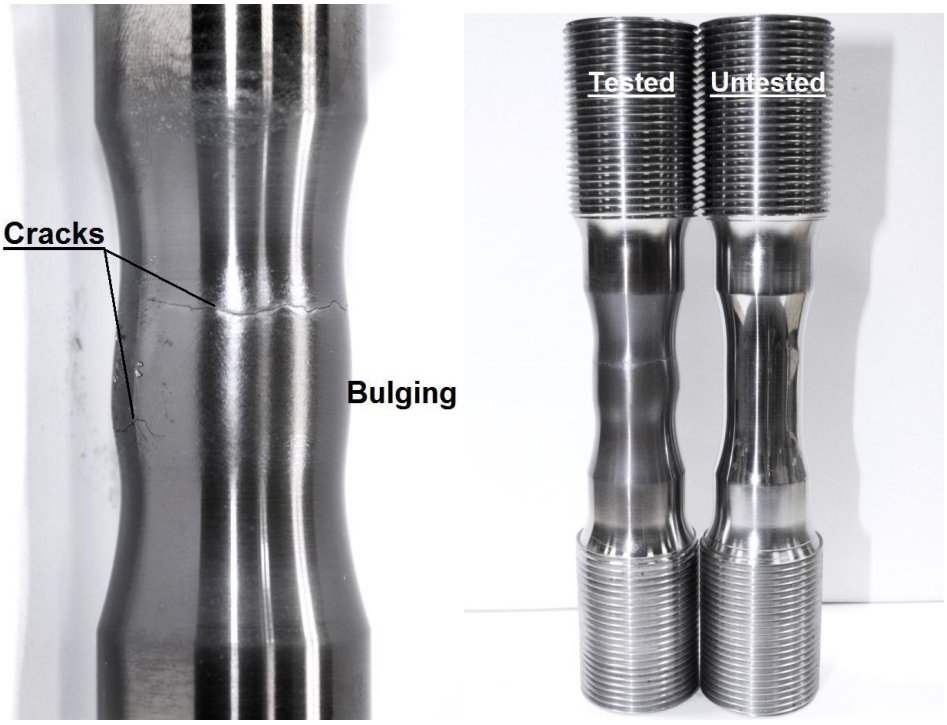

Figure 2.25 Pictures of tested and untested tubular specimen

2.4 Conclusions

To simulate complex thermal mechanical loading condition, an independent strain and temperature controlling with computer-controlled laboratory equipment is successfully designed and developed. The developed TMF testing system is capable of generating simultaneous thermal and mechanical loading as well as bi-axial loading condition on the thin-walled tubular specimen. It has been fully tested and verified to satisfy the requirement of simulating the thermal mechanical loading which is similar to the load experienced by coke drums. An investigation is carried out on a clad material of coke drums by the developed system. From the test results, the TMF life of TP 410S cycling between 100°C and 480°C is slightly shorter than ILCF at 480 °C. From the microstructural exam on the tested specimen, creep damage has more influence on the fatigue life of TP 410S under thermal mechanical loading. Furthermore, from the investigation of biaxial TMF test, the internal pressure causes mean strain in hoop direction, which will result in accumulative bulging for the thin-wall tubular specimen, which may reduce the fatigue life.

References

[1] Warren, J. R., Cowles, B. A., "A simplified thermal mechanical fatigue (TMF) test method", Journal of Engineering for Gas Turbines and Power, 108 (1986), 515-520

[2] Jin, L. , Pelloux, R. M., Xie, X., "Thermomechanica fatigue behaviour of a Nickel base superalloy", Chin. J. Met. Sci. Technol., 5 (1989) 1-7

[3] Bartsch, M., Baufeld, B.. et al., "Multiaxial thermo-mechanical fatigue on material systems for gas turbines", Mat.-wiss. U. Werkstofftech, 38 -9 (2007), 712-719

[4] ASTM E4-10, Standard practices for force verification of testing machines, ASTM international, West Conshohocken, PA, (2010) www.astm.org

[5] ASTM E467-08, Standard practice for verification of constant amplitude dynamic forces in an axial fatigue testing system, ASTM international, West Conshohocken, PA, (2008) www.astm.org

[6] Tao, G., Xia, Z., "A non-contact real-time strain measurement and control system for multiaxial cyclic fatigue tests of polymer materials by digital image correlation method", Polymer Testing, 24 (2005), 844-855

[7] Hyde, C. J., Sun, W., Leen, S. B., "Cyclic thermo-mechanical material modelling and testing of 316 stainless steel", International journal of pressure vessels and piping, 87 (2010) 365-372

[8] Affeldt, E. E., Hammer, J., Huber, U., Lundblad, H., "Analysis of thermal gradients during cyclic thermal loading under high heating rates", Thermomechanical fatigue behavior of materials, 4 (2003), 312-324

[9] Brendel, T., Affeldt, E., Hammer, J., Rummel, C., "Temperature gradients in TMF specimens. Measurement and influence on TMF life", International Journal of Fatigue, 30 (2008), 234-240

[10] Haehner, P., Affeldt, E., Beck, T., Klingelhoeffer, H., Loveday, M., Rinaldi, C., "Validated code-of-practice for strain controlled thermo-mechanical fatigue testing", ECReport EUR 22281 EN, ISBN92-79-02216-6, (2006)

[11] ASTM E2368-10, Standard Practice for Strain Controlled Thermomechanical Fatigue Testing, ASTM international, West Conshohocken, PA, (2010) www.astm.org

[12] Beck, T., Rau, K., "Temperature measurement and control methods in TMF testing - a comparison and evaluation", International Journal of Fatigue, 30 (2008) 226-233

[13] ASTM E1012-05, Standard practice for verification of test frame and specimen alignment under tensile and compressive axial force application, ASTM International, West Conshohocken, PA, US (2005) www.astm.org

[14] ASME E606-04, Standard Practice for Strain-Controlled Fatigue Testing, ASTM International, West Conshohocken, PA, US (2004) www.astm.org

[15] ASTM E2207-08, Standard practice for strain-controlled axial-torsional fatigue testing with thin-wall tubular specimens, ASTM International, West Conshohocken, PA, US (2008) www.astm.org

[16] Chen, J., 2010, "Experimental Study of Elastoplastic Mechanical Properties of Coke Drum Materials", Masters Dissertation, University of Alberta, Edmonton

[17] Basquin, O.H. "The exponential law of endurance tests", ASTM proceeding. 10(1910) 625-630

[18] Coffin, L. F. Jr., “A study of the effects of cyclic thermal stresses on a ductile metal”, Trans. ASME, 76 (1954) 931-950

[19] Manson, S.S., “Behaviour of materials under conditions of thermal stress”, Heat Transfer Symposium, University of Michigan, 1953, 9-75. See also NACA-TN-2933, (1953)

[20] Morrow, J.D. Fatigue design handbook, section3.2. SAE Advanced in Engineering, 4, 21–29. (1968)

[21] Manson, S.S., Halford, G.R., “Practical implementation of the double linear damage rule and damage curve approach for treating cumulative fatigue damage”, International Journal of Fracture, Vol. 17, No. 2, (1981), 169-172

CHAPTER 3 An Alternative Approach for Strain Measurement and Control in Fatigue Tests at Elevated Temperature[2]

For strain-controlled fatigue tests, especially at elevated temperature, implementation of knife-edges and punching dimples within gauge length of specimen are common practices to mount extensometers. Premature failure within the test section of the specimens may be introduced by implementing these techniques. In this chapter, an alternative approach is introduced to control and measure the strains in fatigue tests. Two dimples outside the gauge length section are punched and used to mount the extensometer. Then the correlation between the controlled (measured) strain and the strain within the gauge length section is established. For the isothermal fatigue tests (strain cycling at constant elevated temperature), the correlation can be established either through analytical analysis or finite element analysis (FEA). By comparing the hysteresis loops obtained through the correlation and the one directly measured within the gauge length, it is found that the correlation obtained from FEA has better agreement with the latter result. In addition, this technique can also be used for thermal-mechanical fatigue tests (TMF, both temperature and strain cycling). However, it is found that the correlation obtained from FEA is not accurate enough. Therefore, the correlation should be established through a cyclic test, in which two extensometers are mounted on a specimen, one to measure the strain within the gauge length and the other to measure the strain outside the gauge length.

[2] Chapter 3 of this thesis has been submitted to *Journal of Testing and Evaluation* in 2013

3.1 Introduction

Fatigue tests are increasingly being performed to simulate and investigate real-world failures of components in various structures. Performance of these tests is usually quite expensive and time-consuming especially if elevated temperature or thermal fatigue is involved. In most fatigue tests, accurate control and measurement of the strain in the specimen is by use of some forms of extensometers. In addition, the tests commonly require a selection of specimen shape. The fundamental requirement of a suitable specimen is that the material behaviour determined is independent of the geometry in the specimen gauge length area.

There are commonly two basic shapes suitable to uniaxial fatigue testing: the parallel cylindrical gauge length (PCGL) and the hourglass specimens. For PCGL specimens, one possible approach of attaching the extensometer is to have ridges near the end of the gauge length, for example, see refs. [1-2]. The benefit of this method is to have firm attachment of extensometer on the specimens. However cracks may initiate at or near the ridges and premature failure can occur. Furthermore, the difference in effective strain in gauge length and in ridges can be substantial if without proper calibrations. Another class of extensometer known as the side contact axial extensometer is popular technique to measure and control the strain by means of extension probes attached onto the specimen by using light springs. Raske and Burke [3] produced a design of extensometer which probes are made of ceramic rods with knife-edges tips. The extensometer probes are attached to the specimen by using a pulley wheel system. Walters and his colleague [4] designed an extensometer with independent stainless steel rods with knife-edges. Two pre-loaded springs push the extensometer probes to the specimen gauge section. Carden [5] in 1969 was one of the first to use an extensometer with ceramic probes with conical tips fitting into the dimples on the gauge section of a specimen. Later on, Lohr [6] designed a similar extensometer with radial spring loads to hold the extensometer probes against the gauge length. The ceramic rods can have conical tips or knife edges that press into dimples on the gauge length. Additionally, there are several different types of commercially available elevated temperature side-loaded

extensometers. They are commonly made of ceramic rods with knife-edges attached to the specimen gauge length by suitable compressive force. For elevated temperature strain-controlled fatigue tests, implementation of knife-edges and punching dimples within gauge length of specimen are common practices to mount the extensometer probes. The advantage of this method is that they provide direct measure and control of the strain along the gauge length. However, for fatigue tests, the knife edges or dimples may introduce local damage on specimen surface and premature failure on the test section of the specimen might be introduced. As shown in Fig. 3.1, crack can be initiated from the punched dimples or knife edges during fatigue testing. Implement of knife edge for fatigue test requires minimum force of attachment of probe arms to produce negligible surface damage. However, insufficient compressive force to the specimen gauge length, especially with long extensometer probes, may result slippage or other moves in relation to the gauge length. Therefore, the fatigue life of the specimen could also be greatly influenced by these factors.

The other commonly used specimen geometry in fatigue testing is hourglass specimen. Strain is controlled and measured at the minimum diameter by means of a diametral extensometer. Hirschberg [7] and Slot et al. [8] in 1969 used hourglass specimens for their fatigue tests at high temperature. Lord and Coffin [9] suggested that diametral strain ranges should be less than 0.02 mm/mm for testing to be accurate. There are several researchers [10-13] successfully used hourglass shape specimens to test fatigue behaviour of several metals at different temperatures in very high cycle fatigue region. Nogami et al. [14] studied the effect of specimen shape on the low cycle fatigue test results. They compared the fatigue lives of round bar and hourglass specimens and found that the effect of specimen shape on the low cycle fatigue life and fracture mode was almost negligible. The hourglass specimen has the advantage that the diametral extensometer can be more securely mounted with relatively lower contact forces, and thus less damage to the specimen's surface. However, there are some drawbacks associated with this type of extensometer. The diametral strain has to be converted to axial stain for control purposes, and substantial errors may be introduced from this conversion. In addition, diametral extensometer measures the strain in one plane and so

there is no averaging effect. Therefore, it may not be accurate for materials with anisotropic property. Furthermore, oxide layer can develop on the surface of the specimen in air especially at elevated temperature, and it may cause a slow ratcheting strain which influence the accuracy of the strain reading [18].

In many investigations associated with environmental chambers, the special specimen gripping arrangement, heating system and in-direct or not-direct contact extensometers are designed and incorporated with them. Wood et al. [15] tested fatigue behaviour of two steels in a helium mixture at elevated temperature. Strain was controlled by two extensometers contacting near the shoulder ends. The relation between the strain at shoulders and strain in gauge length was first established at different strain levels before the testing by two extensometers. However, no further detail was released. Furuya et al. [16] performed fatigue tests of 316 stainless steel at different elevated temperatures in a vacuum environment. An in-direct strain measurement was used. The total strain was obtained by subtracting the total elastic displacement of the specimen shoulders and load train from the actuator displacement. Kschinka and Stubbins [17] also tested fatigue lives of 2.25Cr-1Mo steel at 565°C in a vacuum with in-direct measurement. A correction factor is obtained by two extensometers, one is on the gauge section and the other one is on the shoulders. Three separate correlation tests have good agreement. However, this in-direct strain measurement has its drawbacks. A careful calibration is required to correlate the gauge length strain with the shoulder movement under cyclically stable conditions. This method is only approximate since the gauge length to shoulder movement relation changes as the material cyclically hardens or softens. If cyclic stabilization is not achieved during the strain controlled test, the correlation is debatable.

From the above reviews, it can be seen that there are always advantages and drawbacks associated with each approach. Each situation has its merits and deficiencies and the final decision regarding the test method is usually a compromise [18]. To avoid premature failure of specimens introduced by knife-edge or divots in gauge section, in this chapter, an alternative in-direct approach is introduced to control and measure the strain in fatigue tests at elevated temperature. The strain is measured between two

dimples, which are punched at two sections outside the gauge length and have slightly larger cross sectional area. In this case, the increased cross sectional area will help to prevent crack initiation on these punched dimples, and direct strain correlation between gauge section and dimple location can be established. Two methods, analytical analysis and finite element analysis are implemented to establish the strain correlation for 2¼Cr-1Mo steel. By comparing the coefficient obtained through the correlation and the one directly measured within the gauge length, it is found that the correlation obtained from FEA has better agreement with the latter result. In addition, this technique can also be used for thermal-mechanical fatigue tests (TMF, both temperature and strain cycling). However, it is found that the correlation obtained from FEA is not accurate enough. Therefore, the correlation should be established through a cyclic test, in which two extensometers are simultaneously mounted on a specimen, one measures the strain within the gauge length and the other measures the strain outside the gauge length.

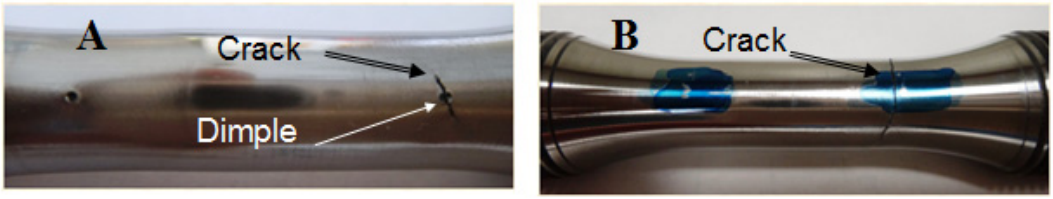

Figure 3.1 Photos of premature failure caused by (A) dimple and (B) knife-edge Ref. [19]

3.2 Material and Specimen Geometry

In this study, ASME SA387 Gr 22 CL 2 (SA387) is selected as an example to demonstrate this method. This material is commonly used as base-material in coke drum construction, and its nominal chemical composition contains 2¼% of Chromium and 1% of Molybdenum. The isothermal low cycle fatigue (ILCF) tests of the coke drum material are conducted at 100ºC and 480ºC, respectively. The specimen geometry for the isothermal fatigue tests is shown in Fig. 3.2. The gauge length of the specimen is 15.24 mm (0.6 in), and the diameter of the gage length is 10.16 mm (0.4 in). A tubular specimen with inner diameter of 6.35 mm (0.25 in) is designed for TMF testing in order

to minimize the thermal gradient along the radial direction and to reduce the required heating and cooling times. All specimens are machined along the rolling direction of the stock plates. The gauge section of the specimens is carefully polished by 3M sandpaper gradually to a grit size of 600 (average particle diameter 16 μm), and the inner surface of the TMF specimen is also polished to the same surface roughness.

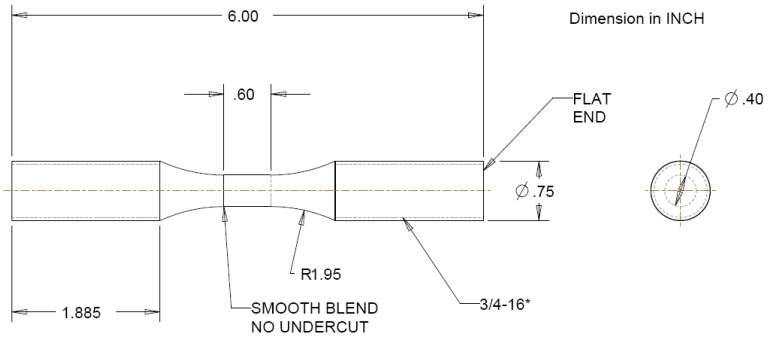

Figure 3.2 Drawing of isothermal fatigue tests specimen

In this investigation of fatigue life of coke drum material, a pair of dimples at one inch (25.4 mm) distance is punched outside the gauge length of the specimen as shown in Fig. 3.3. The punched dimples (with 1" or 25.4 mm distance) are located on the cross sections outside the effective gauge length (0.6” or 15.24 mm) of the test section. Due to the increased cross sectional area, the crack initiation on these dimples will be prevented. However, since the controlled strain is from 1” (25.4mm) distance, a strain correlation between the gauge length and dimple length should be carefully established and verified for the fatigue testing.

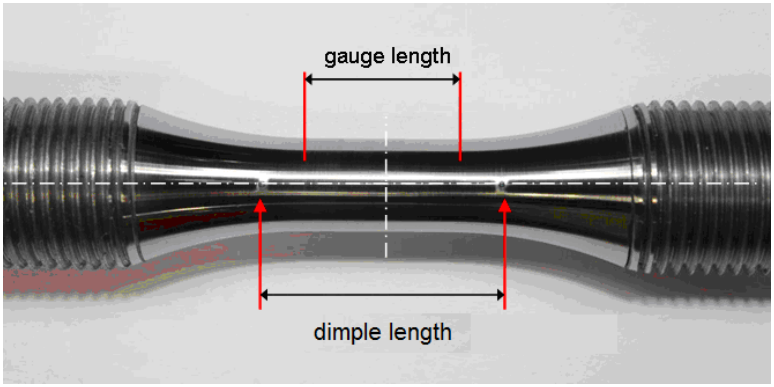

Figure 3.3 Picture of the specimen with two dimples at 1” (25.4mm) distance

3.3 Experimental Setup and Extensometer

A high temperature fatigue test system, as shown in Fig. 3.4, was developed in our lab to conduct ILCF test. The testing system primarily consists of a servo-controlled hydraulic MTS machine, an electric resistance heating furnace, a set of water-cooled grips with band heaters, an in-house developed extensometer and, a data acquisition and control system. A thermocouple is carefully spot-welded in the center of the specimen for each test, which is recommended by ASTM E2368 [20]. In addition, there is no crack initiation observed in the thermocouple weld spot throughout the tests. The specimen temperature can be digitally controlled from ambient temperature to 500 ± 0.1^{o}C in dynamic or steady state mode. The advantage of using an electric resistance heating furnace and water-cooled grips with band heaters is to minimize the thermal gradients along the axial direction of specimen's gauge length. By adjusting the water flow-rate and position of the band heaters, the thermal gradient along the two dimples location can be held within ± 5^{o}C at 500^{o}C or 1% of the testing temperature. However, due to the furnace setup, a side-contact axial extensometer with quartz probes has to be used to measure the strain at elevated temperature. All system components are calibrated and verified before testing according to ASTM E 606 [21].

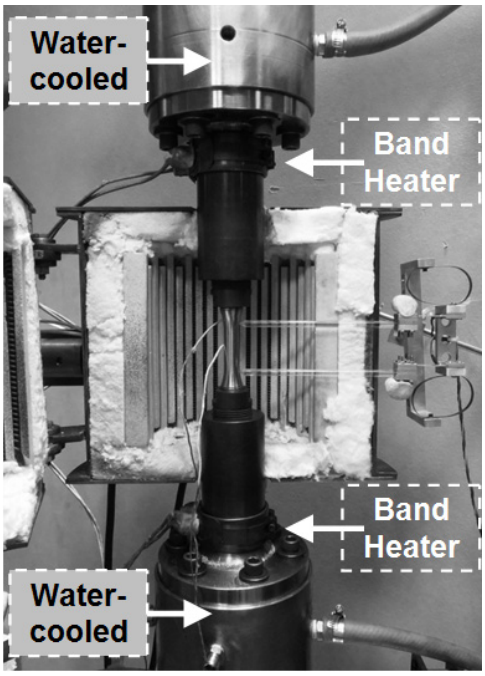

Figure 3.4 Picture of high temperature fatigue test system

The entire uniaxial extensometer system consists of a fixture frame, a uniaxial extensometer, two spring loops, and an air nozzle. The uniaxial extensometer is connected with an aluminum fixture frame by two loop springs, which can apply sufficient compressive force when mounting the extension quartz rods onto a test specimen. The uniaxial extensometer consists of two quartz rods with conical tips, two aluminum bending beams and a C-shaped frame. The aluminum bending beam is connected with C-shaped frame at one end and with quartz rod at the other end. Two strain gages are in pair mounted on the top and bottom of each beam. Two 80° angle dimples are carefully punched on the specimen, and the probe end is machined to be 50° angle with spherical points as shown in Fig. 3.5. In this way, the tip can pivot freely and securely inside the dimple when specimen is uniaxially pulled or pushed. The detailed design and development of the entire system are described in [22].

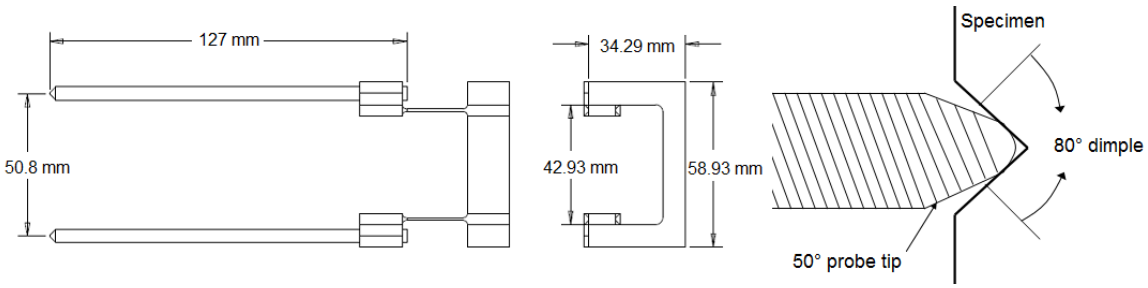

Figure 3.5 Drawing of high temperature side-contact axial extensometer

3.4 Establishment and Verification of Strain Correlation

Two methods, analytical analysis and finite element analysis are implemented to correlate the strains between gauge length and dimple length. The results are then compared with experiments to verify the established correlations.

3.4.1 Analytical Analysis

As shown in Fig. 3.6, a model of one quarter cross section of the specimen is established. The dimple is located 0.5” (12.7mm) from the symmetrical line of the

specimen. The radius of the test section is 0.2" (5.08mm). The correlation coefficient is defined as:

$$C_{inst.} = \frac{\varepsilon_{gauge}}{\varepsilon_{\text{dimple}}} \tag{3.1}$$

Where $\varepsilon_{\text{dimple}}$ is the strain measured at dimple length, and $\varepsilon_{\text{gauge}}$ is the strain measured at gauge length. These strains are engineering strains, which are defined as ratio between the elongation and the original length of a specimen. C_{inst} represents the ratio of strains measured between gauge length and dimple length. The strain at gauge length can be determined if the strain at dimple length and corresponding coefficient C_{inst} are known. Since the strain is controlled and measured at dimple length as described earlier to prevent premature failure, it needs to determine the corresponding correlation coefficients at different strains at dimple length. The procedure for establishing this strain correlation is outlined in the following:

The section AB, as seen in Fig. 3.6, has variable cross sectional areas, and it can be thought of as being composed of a number of individual sections (*n*). Each individual section has length ΔL. The radius of the cross section with respect to incremental length can be expressed as:

$$r_i = r_o + (r_f - r_f \cos(\sin^{-1}(\frac{\Delta L * i}{r_f})), i = 0,1,...,n \tag{3.2}$$

where r_o is the radius of the gauge length, and r_f is the radius of the fillet.
The averaged radius of each individual section, $r_{ave,}$ can be expressed by:

$$r_{ave,i+1} = \frac{(r_i + r_{i+1})}{2}, i = 0,1,...,n-1 \tag{3.3}$$

The corresponding cross sectional area of each individual section will be

$$A_i = \pi r_{ave,i}^2, \ \ i = 1,2,...,n \tag{3.4}$$

By applying an axial load P and assuming uniform distribution of stress and strain at each cross section, the stress in each individual section is

$$\sigma_i = \frac{P_i}{A_i} \tag{3.5}$$

Since the ILCF test is tested under fully-reversed cyclic loading, it is appropriate to represent the stress-strain relation by cyclic stress-strain curve (CSSC). Therefore, by implementing Ramberg-Osgood equation [23] for CSSC, the strain amplitude can also be expressed in this equation as a function of stress:

$$\frac{\Delta\varepsilon}{2} = f(\Delta\sigma) = \left(\frac{\Delta\sigma}{2E}\right) + \left(\frac{\Delta\sigma}{2K'}\right)^{\frac{1}{n'}} \tag{3.6}$$

Where E is Young's modulus, K' is the cyclic strength coefficient and n' is the cyclic strain hardening exponent, which depend on the material being considered. Similarly, the strain range of each individual section can be found:

$$\Delta\varepsilon_i = f(\Delta\sigma_i) = \Delta\varepsilon_e + \Delta\varepsilon_p = \left(\frac{\Delta\sigma_i}{E}\right) + 2\left(\frac{\Delta\sigma_i}{2K'}\right)^{\frac{1}{n'}} \tag{3.7}$$

The displacement of each individual section can be expressed as:

$$\delta_i = \varepsilon_i \Delta L_i \tag{3.8}$$

The total displacement of section AB can be found:

$$\delta_{AB} = \sum_{i=1}^{n} \delta_i \tag{3.9}$$

Since the section BC in Fig. 3.6 has uniform cross sectional area, the displacement δ_B under the applied load P can be found through the equation (3.6) as,

$$\varepsilon_{gauge} = \left(\frac{P}{\pi r_o^2 E}\right) + \left(\frac{P}{\pi r_o^2 K'}\right)^{\frac{1}{n'}} \tag{3.10}$$

$$\delta_{BC} = \varepsilon_{gauge} \cdot L_{BC} \tag{3.11}$$

The measured strain ε_{dimple} can be calculated by

$$\varepsilon_{\text{dimple}} = \left(\frac{\delta_{AB} + \delta_{BC}}{L_{AB} + L_{BC}}\right) \tag{3.12}$$

Finally, the corresponding coefficient of strain correlation can be obtained in Eq. (3.1).

This method provides a direct assessment of the correlation for strains between gauge length and dimple length for isothermal fatigue test. The accurate CSSC of the material at the corresponding constant temperature must be applied in this analysis. The

parameters required are Young's modulus E, cyclic strength coefficient *K'*, and cyclic strain hardening exponent *n'* from the cyclic test at the same constant temperature as the fatigue test. In this method, it is assumed that the stresses/strains are uniformly distributed along the cross sections. Therefore, errors may be introduced by these idealized factors.

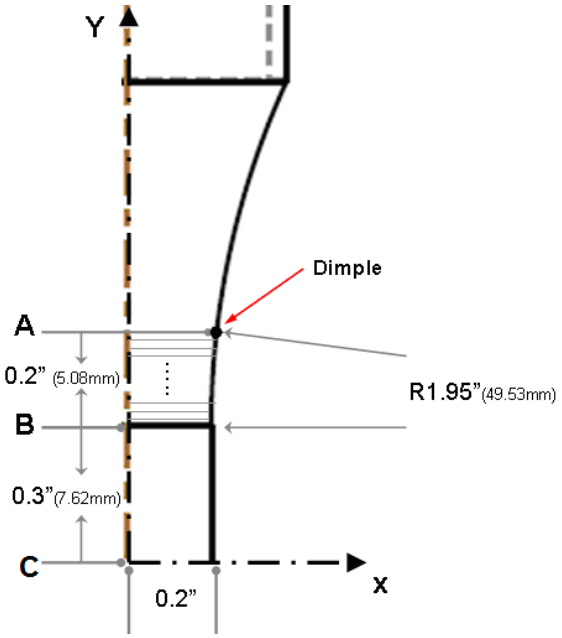

Figure 3.6 Schematics of one quarter cross section of the specimen

3.4.2 Finite Element Method

An axisymmetric finite element model is created to correlate the strains between the gauge length and dimple length. A quarter of the cross section of the specimen is modeled as shown in Fig. 3.7.

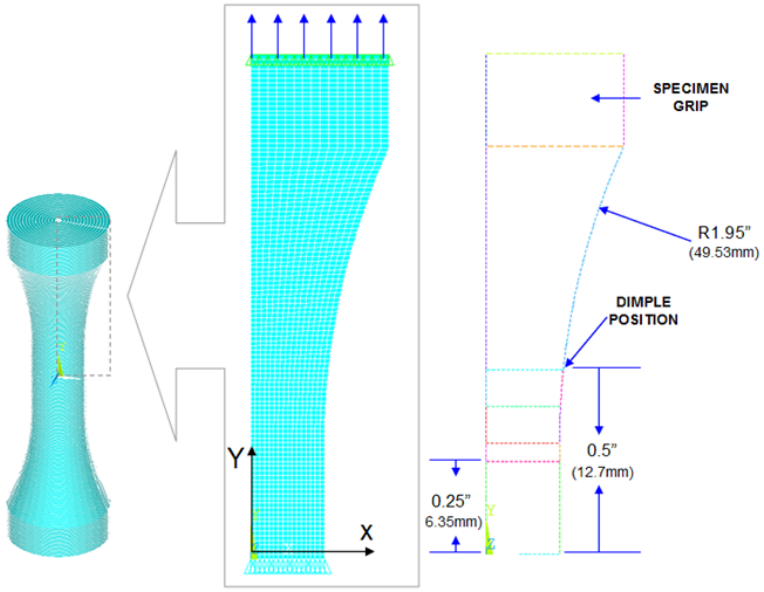

Figure 3.7 Geometry of FE model and dimensions

Commercial finite element analysis (FEA) code ANSYS is used for this analysis. First, CSSC must be obtained from the experiment at the same constant temperature as the fatigue test and to be input into the FEA model as a material property. The following boundary conditions are applied on this FEA model to simulate uniaxial loading on the specimen: The bottom edge (symmetry line of the specimen) is constrained in Y direction, and the top edge of the specimen grip is under plane-remain-plane condition. The displacement or load is also placed on the top edge to simulate the uni-axial loading in Y direction.

From the result, the incremental displacements of gauge length and dimple length are found. The engineering strains at these two locations can then be calculated by:

$$\varepsilon_{\text{dimple}} = \frac{\delta_{\text{dimple}}}{L_{\text{dimple}}} \quad and \quad \varepsilon_{gauge} = \frac{\delta_{gauge}}{L_{\text{gauge}}} \tag{3.13}$$

The corresponding correlation coefficient C_{inst} can be established according to Eq. (3.1).

The advantage of implementing FEA approach is that the stress distribution and Poisson's ratio are all being considered. It may yield more accurate result. However, the results obtained from both approaches will be compared with the experimental results at room temperature.

3.4.3 Experimental Verification

Due to the furnace setup, it is difficult to accommodate two extensometers inside the furnace to verify the strain correlation at elevated temperature. Therefore, the correlation is to be assessed for the case at room temperature. If the strain correlation can be verified at room temperature, the approach can then be applied at elevated temperature by using the CSSC at corresponding temperature. The experimental approach is to setup a test, which includes two installed extensometers with gauge distances of 0.5" (12.7 mm) and 1" (25.4 mm), respectively, as shown in the Fig. 3.8. The designed high temperature side-contact extensometer with quartz probes measures the strain at dimple length. The MTS side-contact extensometer with knife-edges measures the strain at gauge length of the specimen. The test is under strain-controlled fully reversed cyclic loading condition with same strain rate as the fatigue test. The two extensometers measure the strains in a synchronized manner. The recorded strains are then compared, and the strain correlation is established by Eq. (3.1).

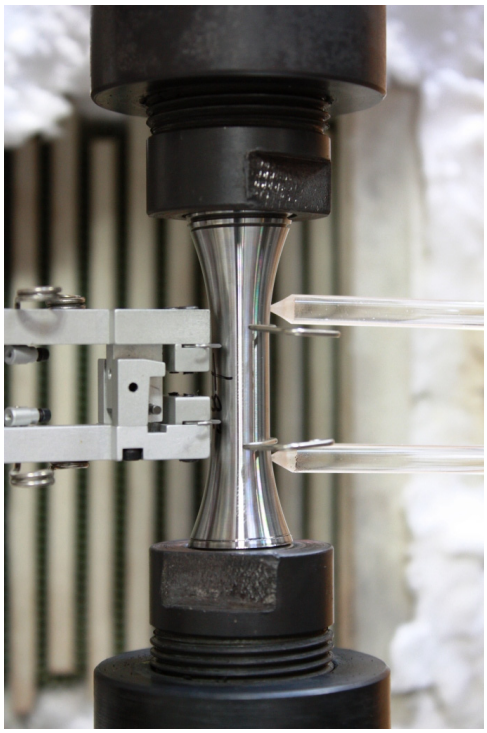

Figure 3.8 Setup of experimental validation

3.5 Results and Discussion

3.5.1 Characterization of CSSC of SA387 Gr 22 CL 2 at Constant Temperatures

To obtain CSSC of this material at different temperatures, three fully-reversed strain-controlled stepped cyclic tests are carried out at room temperature, 100 °C, and 480 °C, respectively. The strain is controlled by the side-contact axial extensometer with 0.5" (12.7 mm) leg distance. The specimen, as shown in Fig. 3.2, is used throughout this characterization, and the extensometer measures the strain inside the gauge length of the specimen. A strain rate of 0.005/sec is applied throughout the tests. At each strain level, the test will run until the hysteresis loop is stabilized (load is stabilized under strain control), and then the strain will increment to a higher level. From these stress-strain hysteresis loops, the cyclic stress-strain curves of this material at room temperature, 100 °C, and 480 °C can be obtained by connecting the saturated point of each loop, as an example shown in Fig. 3.9. The three CSSCs fitted by the Ramberg-Osgood equation [23] are shown and summarized in Fig. 3.10 and Table 3.1. The obtained CSSCs are then put into the analytical and FEA methods to obtain the strain correlation at different temperatures.

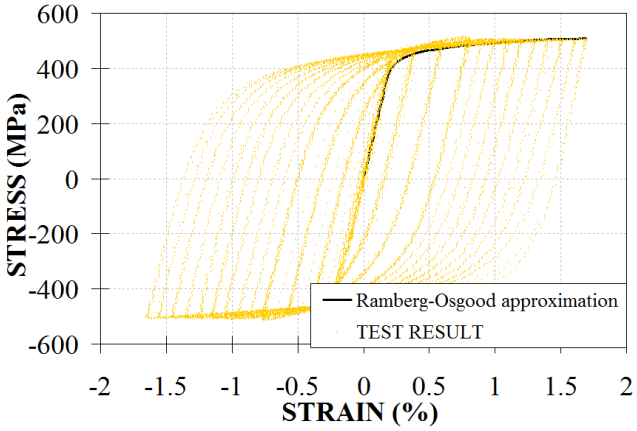

Figure 3.9 Example of hysteresis loop of SA 387 Gr 22 CL2 at room temperature

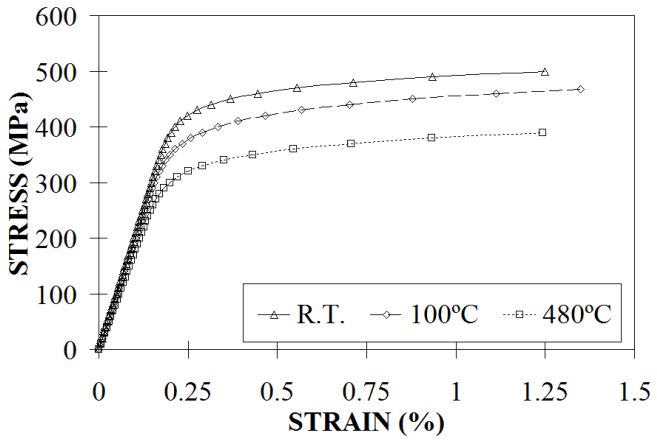

Figure 3.10 Cyclic stress/strain curves of SA387-22-2 at different temperatures

Table 3.1 Material constants of cyclic stress strain curves for SA387 Gr 22 CL2

	R.T.	100ºC	480ºC
E	204000	196000	176000
K'	644	615	545
n'	0.055	0.059	0.073

3.5.2 Analytical Analysis

As shown in Fig. 3.6, the section A is divided by *n* sub-sections. A sensitivity test is first carried out to find the number of divisions to give a converged result. In this case, 100 sub-sections are found to yield a converged result. CSSC properties of SA387, including *E, K', n'*, at room temperature (R.T.), 100°C, and 480°C are input into the program. A uniaxial tensile loading is applied on the specimen at each temperature. The three correlation curves at R.T., 100°C, and 480°C are shown in Fig. 3.11, it can be seen that as the temperature increases, the coefficient of strain correlation slightly decreases. It implies that at higher temperature, the difference between gauge length strain and dimple length strain is getting smaller. This is mainly due to the lowered stress strain curve at higher temperature (Fig. 3.10). It is also seen that when dimple length strain reaches 0.2%, the gage length strain is 3 to 4% higher than it. As higher strain (up to 0.9%) applied at dimple length, the gage length strain can be more than 10% higher.

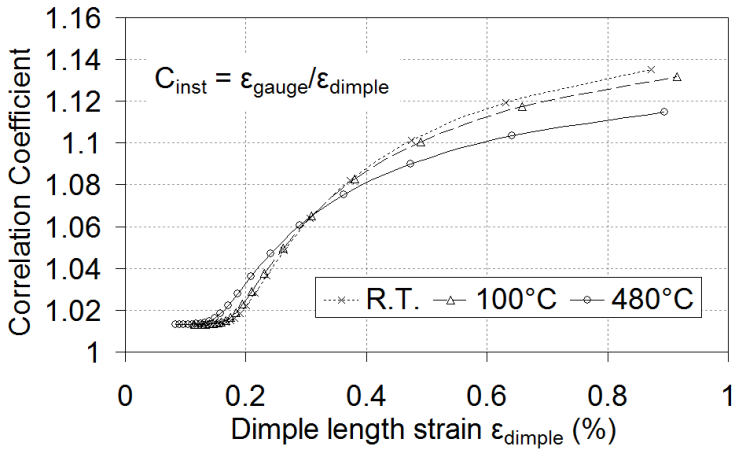

Figure 3.11 Analytical results of strain correlation

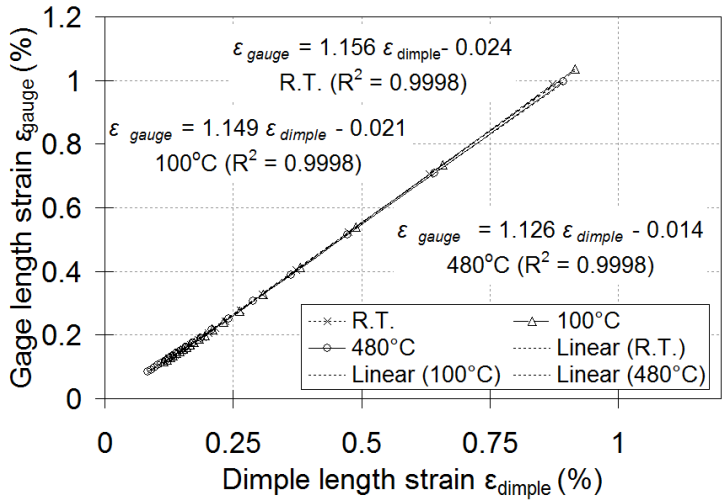

Figure 3.12 Analytical results of ε_{gauge} vs. ε_{dimple} at different temperatures

The results of gauge length strain versus dimple length strain at different temperatures are plotted in Fig. 3.12. The relation between the two strains can be estimated by a linear function:

$$\varepsilon_{gauge} = C \cdot \varepsilon_{\text{dimple}} + B \tag{3.14}$$

where C and B are constants from linear regression. As seen in Fig. 3.12, the constant C decreases as the temperature increases which has the identical trends as the correlation coefficient $C_{inst.}$. By implementing this function, any instant gauge length strain can be identified directly from the corresponding dimple length strain.

3.5.3 Finite Element Method

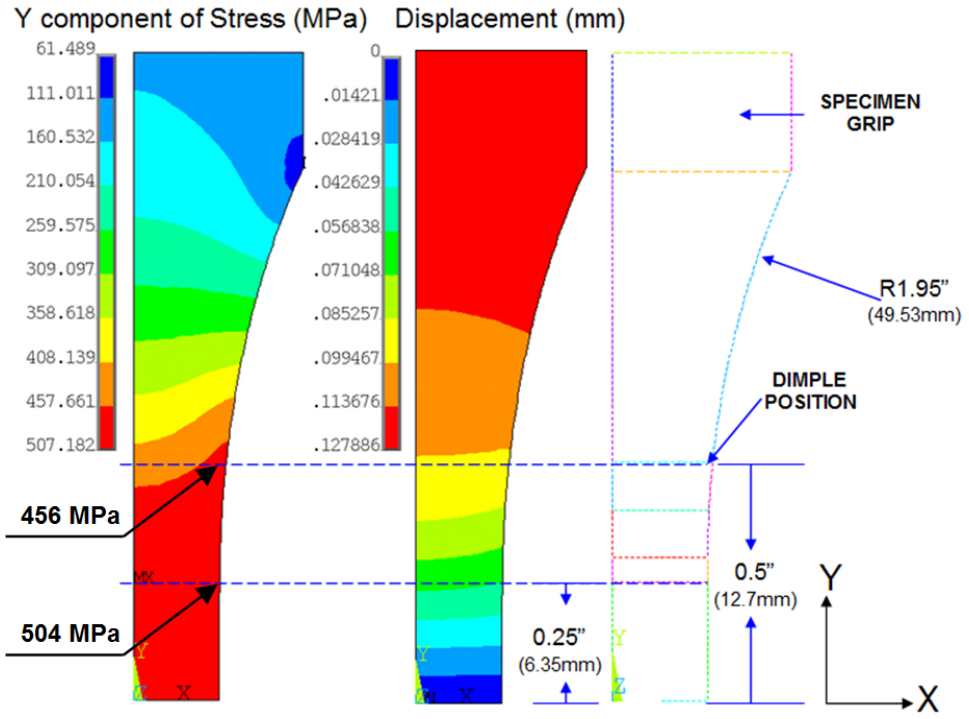

Figure 3.13 Contour results of FEA at room temperature

A finite element analysis (FEA) on correlating strains between gauge length and dimple length is carried out at room temperature, 100ºC, and 480 ºC, respectively. The material parameters, E, K', and n' at the above three temperatures obtained from the experiments, are input into the FEA code. To achieve approximate identical strain at dimple position as the analytical result, the maximum loads, 40 *kN*, 37.5 *kN*, and 31 *kN*, are applied on top edge of the grip by time increment at the three temperatures, respectively. The contour results of axial stress and axial displacement at room temperature, as an example, are shown in Fig. 3.13. Due to the increased cross sectional areas in dimple position, the stress is lower than that of gauge length. Therefore, the crack initiation will be prevented due to the lowered stress level at that location.

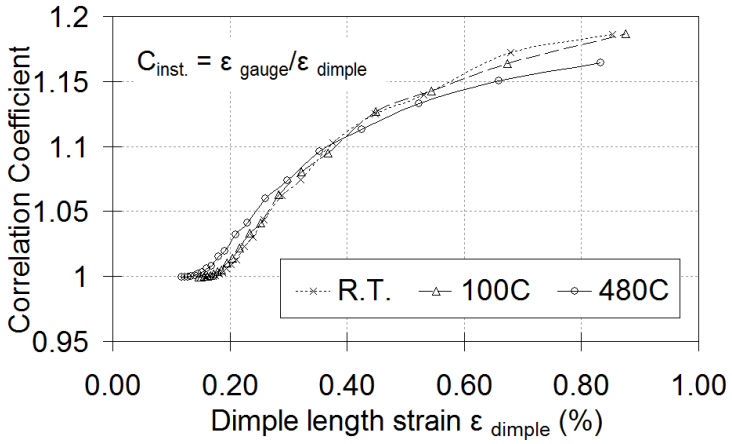

Figure 3.14 FEA results of strain correlations

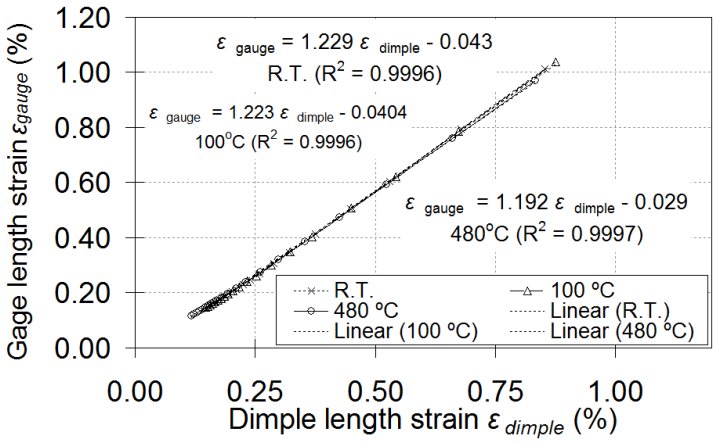

Figure 3.15 FEA results of ε_{gauge} vs. ε_{dimple}

The three curves of the correlation coefficient versus dimple length strains at room temperature, 100ºC, and 480 ºC, respectively, are shown in Fig. 3.14. As higher strain (up to 0.9%) applied at dimple length, the gage length strain can be more than 15% higher. In addition, at the largest strain 0.9%, the difference in coefficient from room temperature and 480°C is about 2%. Therefore, it can be seen that, even though the difference in CSSC at different temperatures is quite large, the difference in correlation coefficient at different temperatures is quite small. By comparing the coefficient obtained from analytical and FEA method, it is found that the coefficients obtained in the FEA are about 5% higher than that of analytical result at each corresponding temperature. This is

mainly due to that non-uniform stress and strain distribution outside the gauge length is being more accurately considered in the FE analysis.

The results of gauge length strain versus dimple length strain at different temperatures are plotted in Fig. 3.15. It can be seen that the relations between the two strains can also be well estimated by a linear function, Eq. (3.14).

For fatigue tests, the strain range and stress-strain hysteresis loops (The area of hysteresis loop represents dissipated plastic strain energy per cycle) are commonly used to relate the fatigue life of materials. Figures 3.16 A to C show the relation of gauge length strain and dimple length strain during cyclic loading at room temperature, 100°C, and 480°C, respectively, from the FEM analysis. It can be seen that for either tensile or compressive strains, the correlation between the gauge length and the dimple length are very well fitted by the linear regression according to Eq. (3.14). Therefore, by implementing this linear function, the strain ranges at gauge length can also be accurately obtained from the corresponding dimple length strain ranges.

The list of instant correlation coefficients for three temperatures obtained from Analytical and FEA are shown in Table 3.2 for a comparison.

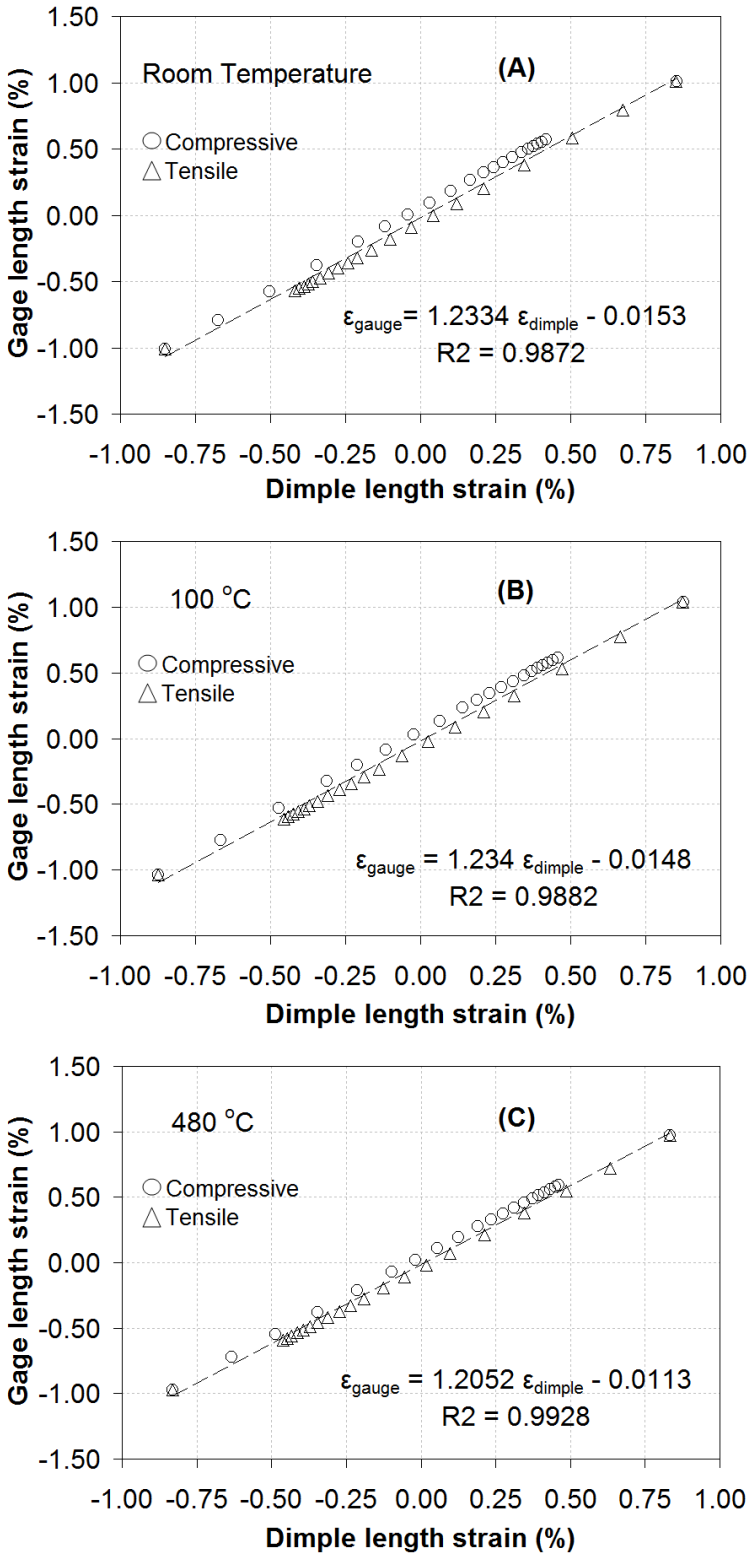

Figure 3.16 Results of ε_{gauge} vs. ε_{dimple} under cyclic loading

Table 3.2 Summary of strain correlation coefficients from FEA and analytical

	$C_{inst.}$ at R.T.		$C_{inst.}$ at 100°C		$C_{inst.}$ at 480°C	
ε_{dimple}	FEA	Analytical	FEA	Analytical	FEA	Analytical
0.15	1.000	1.013	1.000	1.013	1.000	1.016
0.2	1.009	1.022	1.014	1.029	1.026	1.036
0.3	1.062	1.061	1.064	1.065	1.074	1.061
0.5	1.138	1.104	1.136	1.101	1.132	1.092
0.6	1.163	1.119	1.160	1.114	1.150	1.096
0.7	1.172	1.128	1.170	1.124	1.160	1.110
0.9	1.190	1.136	1.191	1.130	1.166	1.113

3.5.4 Experimental Verification

As shown in Fig. 3.8, both gauge length and dimple length strains are recorded concurrently by the two extensometers. Two fully-reversed cyclic loading tests at room temperature are conducted to verify the predicted correlations by the analytical and the FEA methods. For the first specimen, step-increment cyclic loading test is tested up to a strain level of 0.62%; for the second specimen, the step-increment cyclic test is at larger strain level between 0.62% and 0.84% which is the maximum strain amplitude considered in our fatigue testing.

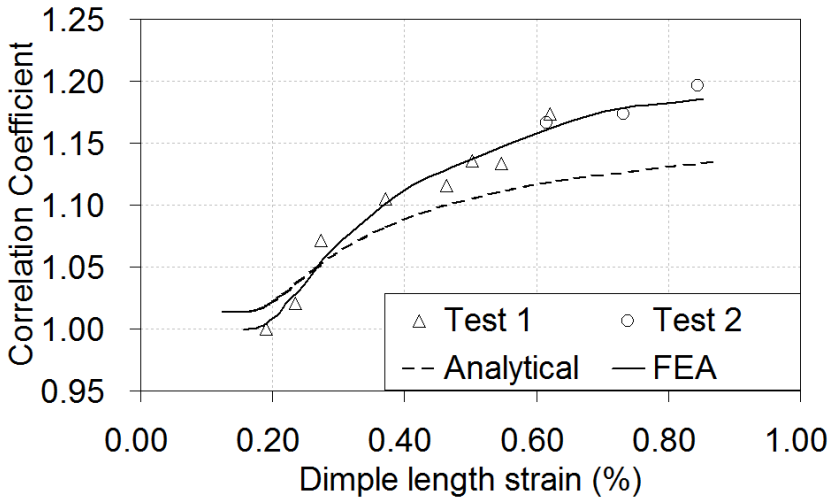

Figure 3.17 Comparison of room temperature correlation coefficients C_{inst}

The instant correlation coefficients between the experiment and the two analysis methods are first shown in Fig. 3.17. At each strain level, the instant coefficient is calculated from the gauge length and dimple length strains based on Eq. (3.1), and the determined coefficient is plotted corresponding to its dimple length stain. It can be seen that the FEA results have a good agreement with experimental results. However, the difference of the correlation coefficients predicted by the analytical and FE methods is less than 4% when the strain is up to 0.8%. Therefore, the error generated by the analytical analysis is considerablely small.

The stress-strain hysteresis loops obtained from experiment, correlated by analytical method, and by FEA according to the linear function Eq. (3.14) are shown in Fig. 3.18 as an example. The test is controlled by the dimple length strain corresponding to the smaller loop in dashed line in Fig. 3.18. The larger loop in solid line is the hysteresis loop recorded based on the strains from the gauge length extensometer. The triangle symbol in Fig. 3.18 represents the hysteresis loop correlated by the FEA method and the circle symbolizes the loop correlated by the analytical method. It can be seen that the former closely tracks the measured hysteresis loop by the gauge length extensometer. However, the hysteresis loop predicted by the analytical method has larger deviation from the experimental result. Therefore, the hysteresis loop at gauge length can be more accurately correlated by the dimple length strain integrated with coefficient obtained from FEA in the form of Eq. (3.14). However, it should be cautious when use this method at large strain amplitude during fully-reversed loading. The instability or buckling of the specimens may present during large compressive strain, and deviation may be significantly magnified by these factors.

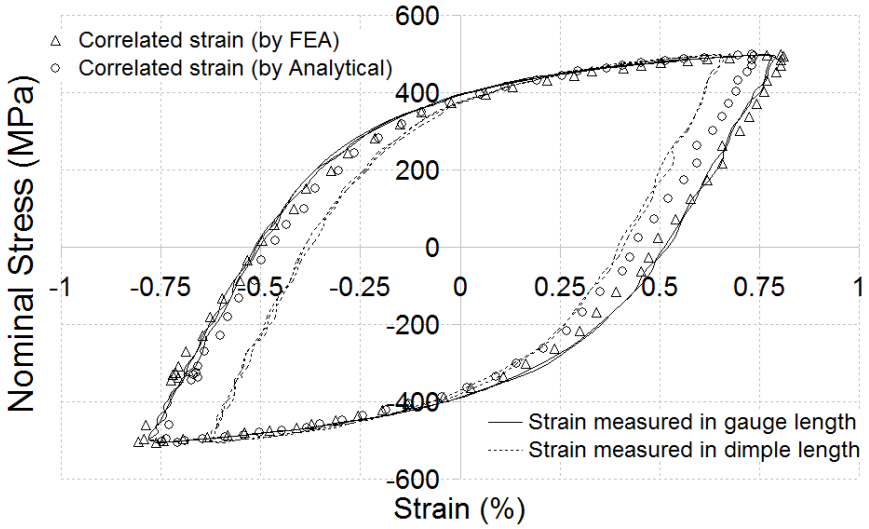

Figure 3.18 Comparison of hysteresis loops

3.5.5 Comparison of Fatigue Data

To verify the accuracy of the correlated result, a group of fatigue tests for SA 387 is conducted at 480°C. The ILCF tests are performed under strain-controlled condition at a strain rate of 0.005/sec throughout all tests. The strain is controlled and measured at dimple length for each test, and the strain of gauge length is correlated thereafter. The tests are conducted under fully-reversed cyclic loading. At each strain level, there are at least two tests conducted to insure the repeatability and accuracy of the data. Each fatigue test stops when the maximum load decreases to 6 *kN* for the ILCF solid specimens. The reasons for this failure criteria are: (1) to protect the equipment from the sudden rupture of the specimen; (2) the set failure point is very close to the final separation, and it covers over 95% of the entire life; (3) the intact specimen provides ease in disassembling of the tested specimen.

Another ILCF data for SA 387 (2¼ Cr-1Mo) at 500°C is taken from NRIM fatigue data sheet [24]. The data is obtained from the tests performed under strain-controlled fully-reversed cyclic loading at a strain rate of 0.005/sec. The criterion for the failure is when the specimen separates completely into two parts. The specimen surface is finished by longitudinal polishing with 600 grade silicon carbide paper.

For the sake of comparison, the total strain amplitude versus fatigue life is separated into plastic amplitude and elastic amplitude versus fatigue life as shown in Fig. 3.19 A and B for two sets of data respectively. The fatigue life curve can be accurately represented by Coffin-Manson [25, 26] relation:

$$\frac{\Delta\varepsilon}{2} = \frac{\Delta\varepsilon_e}{2} + \frac{\Delta\varepsilon_p}{2} = \frac{\sigma'_f}{E}(2N_f)^b + \varepsilon'_f(2N_f)^c \tag{3.15}$$

Where $2N_f$ is reversals to failure (2*cycles to failure), σ'_f is fatigue strength coefficient, and b is fatigue strength exponent. ε'_f is the fatigue ductility coefficient, and c is the fatigue ductility exponent. As shown in Fig. 3.19C, the fatigue life with correlated strain is very well agreed with the data from NRIM. The little deviation may be caused by small difference in testing temperature (20°C difference) and failure criteria. However, this

well agreed result verifies that our proposed strain control technique and correlation method can produce accurate and reliable fatigue life data.

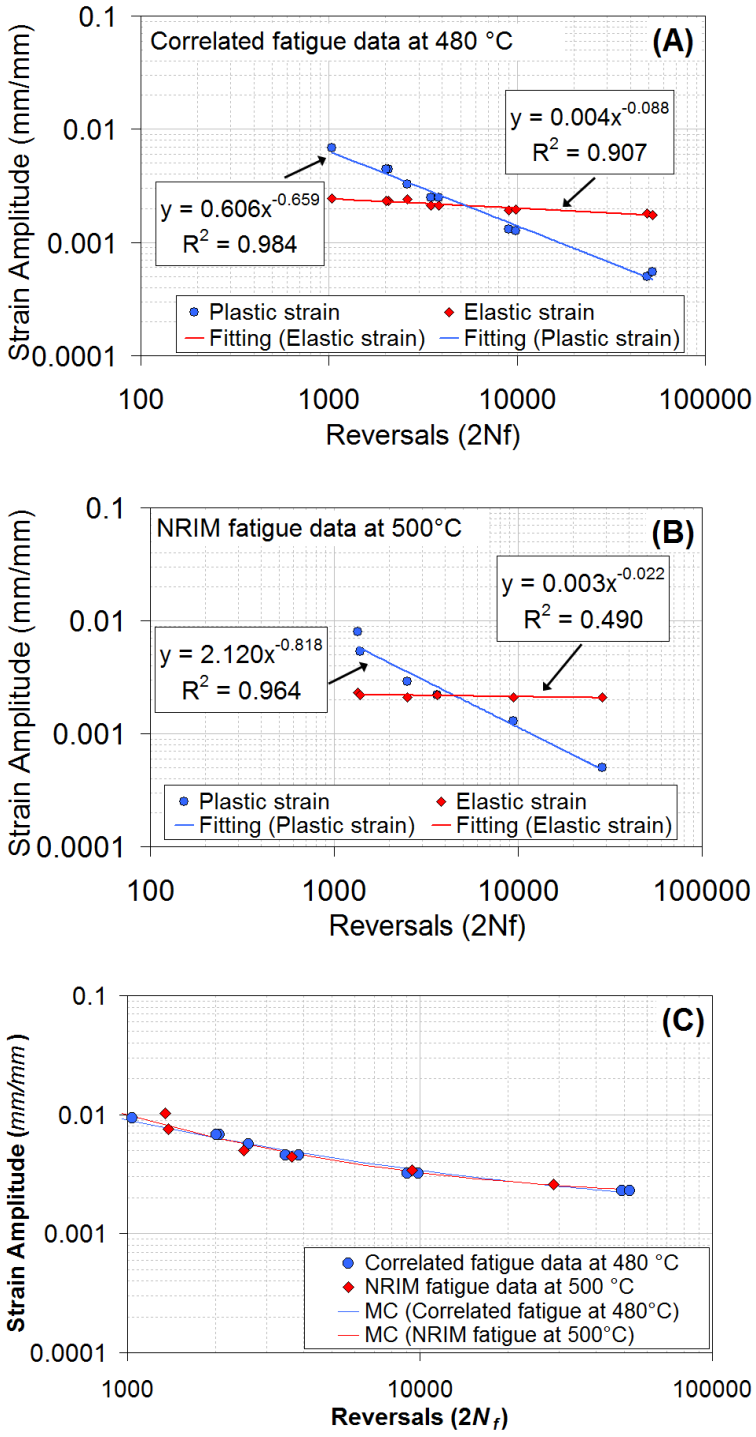

Figure 3.19 Comparison of correlated fatigue data and NRIM fatigue data

3.6 Strain Correlation for Thermal-Mechanical Fatigue (TMF)

This alternative strain measurement technique can also be implemented in Thermal-Mechanical Fatigue (TMF) test. Same material ASME SA387 Gr 22 CL 2 (SA387) is used as an example to demonstrate this method. However, in this investigation, an induction unit is used as a heating device in TMF instead of closed furnace. It is significantly time efficient to apply thermal cycling on specimens, and also it provides open space to locate two extensometers to measure the strains at high temperature directly. By optimizing the coil configuration of the induction system, the dynamic thermal gradient along the two dimple locations can be minimized to about 1% of the max temperature. The developed TMF test system is designed and calibrated according to ASTM E2368-10 [20] and EUR 22281 EN [27]. The detailed development of the test system can be referred to chapter 2 and [28]. To investigate the strain correlation, a TMF tubular specimen is placed in the center of the work coil of the induction system, and two high temperature extensometers are located on the specimen, as shown in Fig. 3.20. One extensometer, with smaller gauge length, is located in the gauge length of the specimen to measure the strain inside the gauge length. The other extensometer, with larger gauge length, is positioned slightly outside the gauge section to control the strain dynamically. Therefore, the correlation between both strains (ε_{gauge} and ε_{dimple}) can be directly established experimentally. Furthermore, a study of FEA on correlation coefficients is compared with experimental result to verify its feasibility.

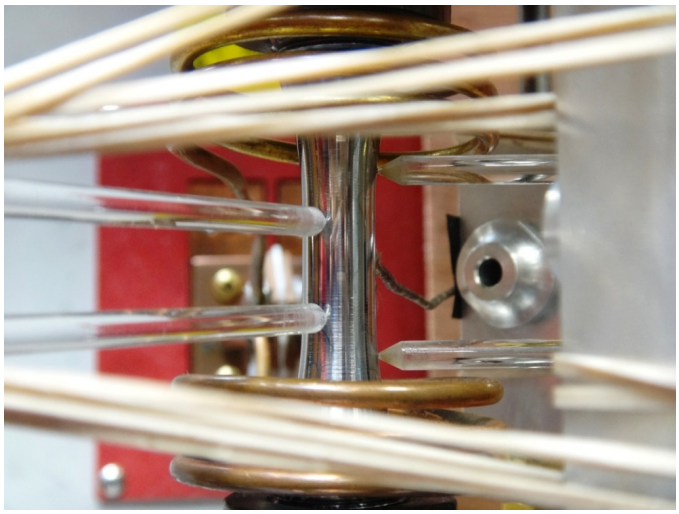

Figure 3.20 Picture of TMF specimen and extensometers

The thermal cycling is carried out at the beginning of each test until the thermal cycle is stabilized, and then the thermal strains at T_{max} and T_{min} are recorded. Thermal strain according to each temperature can be obtained during the thermal cycling and it can be expressed by a third order polynomial function:

$$\varepsilon_{thermal} = f(T) = C_1 \cdot T^3 + C_2 \cdot T^2 + C_3 \cdot T + C_4 \tag{3.16}$$

The instantaneous coefficient of thermal expansion (CTE) can be calculated in the following for SA387 during the thermal cycling between 100°C and 480°C:

$$CTE = \frac{d\varepsilon_{thermal}}{dT} = 3C_1 \cdot T^2 + 2C_2 \cdot T + C_3 \tag{3.17}$$

where $C_1 = 1.4460E\text{-}12;\ C_2 = 2.0808E\text{-}09;\ C_3 = 1.2238E\text{-}05;\ C_4 = -2.3229E\text{-}04$

The instantaneous CTE at different temperatures for SA 387 is shown in Fig. 3.21 and Table 3.3 and it will be used in FE analysis.

The total strain ε_{total} at two extreme temperatures are summation of the mechanical and thermal strains:

$$\varepsilon_{total}^{100^oC} = \varepsilon_{mech}^{100^oC} + \varepsilon_{thermal}^{100^oC} \tag{3.18}$$

$$\varepsilon_{total}^{480^oC} = \varepsilon_{mech}^{480^oC} + \varepsilon_{thermal}^{480^oC} \tag{3.19}$$

Then, the total strains at two extreme temperatures are controlled at dimple length. The dynamic mechanical strain can be obtained by subtracting the thermal strain from the measured total strain.

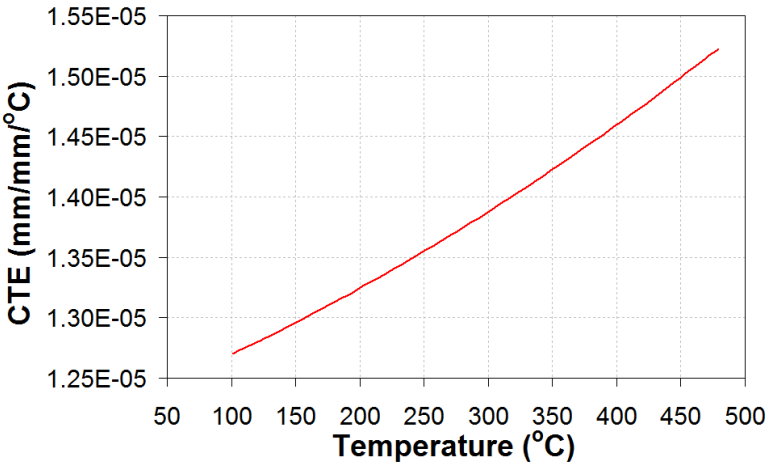

Figure 3.21 Chart of thermal expansion during thermal cycling

Table 3.3 Instantaneous Coefficient of Thermal Expansion of SA387 Gr 22 Cl 2

Temperature (°C)	20°C	100 °C	250 °C	480 °C
CTE (mm/mm/ °C)	12.32E-6	12.70E-6	13.54E-6	15.23E-6

For the sake of comparison, a FEA model is created according to the test specimen, and the cyclic stress-strain curves (Fig. 3.10), material properties (Table 3.1), and CTE (Table 3.3) at different temperatures are input into the FEA model. Additionally, a multi-linear kinematic hardening model is used in this model. Same boundary condition is applied on the FEA model as that for the isothermal model in Fig. 3.7.

Four correlation coefficients are shown in Fig. 3.22 as an example. They are used for correlating the strain range between gauge length and dimple length. The coefficient of test result is up to 10% larger than that of FEA at strain range of 1.45%. By comparing stress strain history from test result and FEA, it is found that there is deviation in stress-strain path between test and FEA modeling under thermal mechanical loading, as seen in Fig. 3.23. Four different CSSCs at room temperature, 100°C, 250°C, and 480°C are input into the FEA program as well as instantaneous CTE obtained from experiment. Kinematic hardening model is used to constitute the stress strain relation. It is found that linear interpolation is used in FEA model to accommodate the stress strain relation with changing in temperature. However, the material behaviour under thermal mechanical

loading could be more complicated than that. Therefore, relatively large error could be introduced by the FE modeling.

The linear function Eq. (3.14), is also used to establish the relation between $\Delta\varepsilon_{gauge}$ and $\Delta\varepsilon_{dimple.}$. The linear function, as shown in Fig. 3.24, can accurately represent the relation between gauge length and dimple length strain ranges. Figure 3.25 shows the comparison between the hysteresis loops from the strains directly measured from the extensometers and from the correlated strains. The test is controlled by the dimple length strain corresponding to the smaller loop in dashed line in Fig. 3.25. The larger loop in solid line in that figure is the hysteresis loop recorded based on the strains from the gauge length extensometer. The triangle symbol in the figure represents the hysteresis loop correlated by FEA method and the circle symbolizes the loop correlated by the experiment. The result shows that hysteresis loop correlated from Eq. (3.14) obtained experimentally is more accurate than that obtained by FEA. The hysteresis loop of gauge length can be accurately correlated from that of dimple length by experimental method. There are noticeable deviations in the reversals of the hysteresis loop correlated by the FEA method. Therefore, this strain control and measurement technique can also be applied in TMF testing to prevent premature failure of the specimen. However, a strain correlation based on experiment has to be established to obtain the gauge length strain and hysteresis loop. The correlation based on FEA may introduce significant errors depending on the complexity of the specimen geometry and material models.

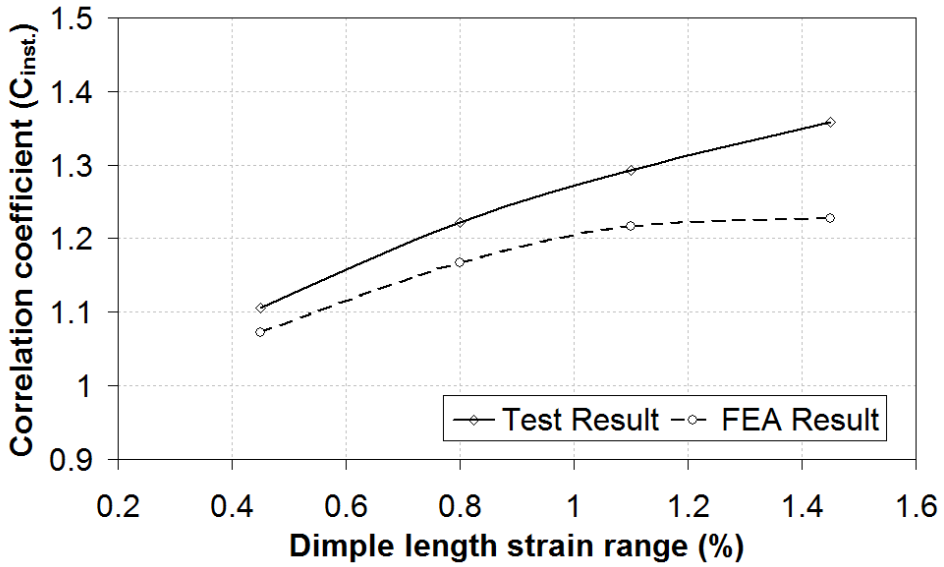

Figure 3.22 Comparison of Coefficient for TMF

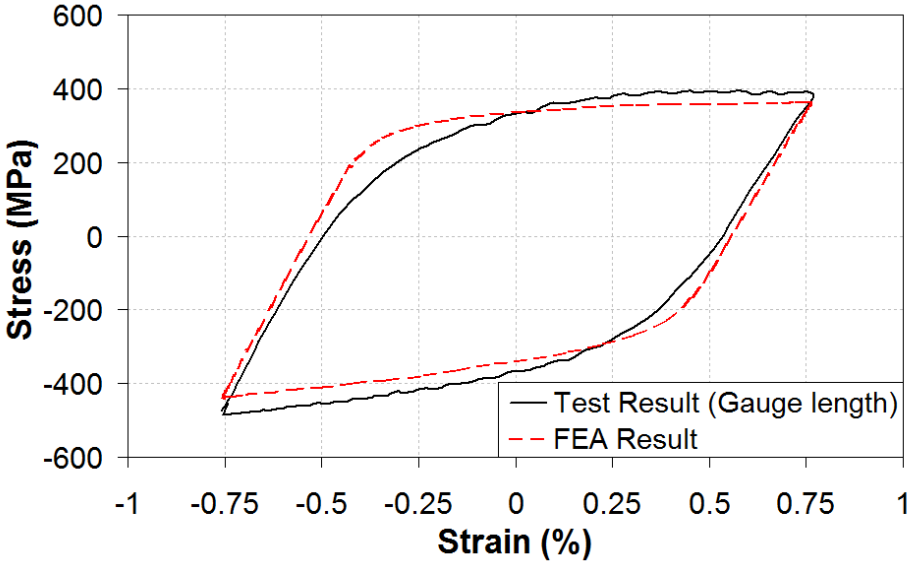

Figure 3.23 Comparison of hysteresis loops between test and FEA

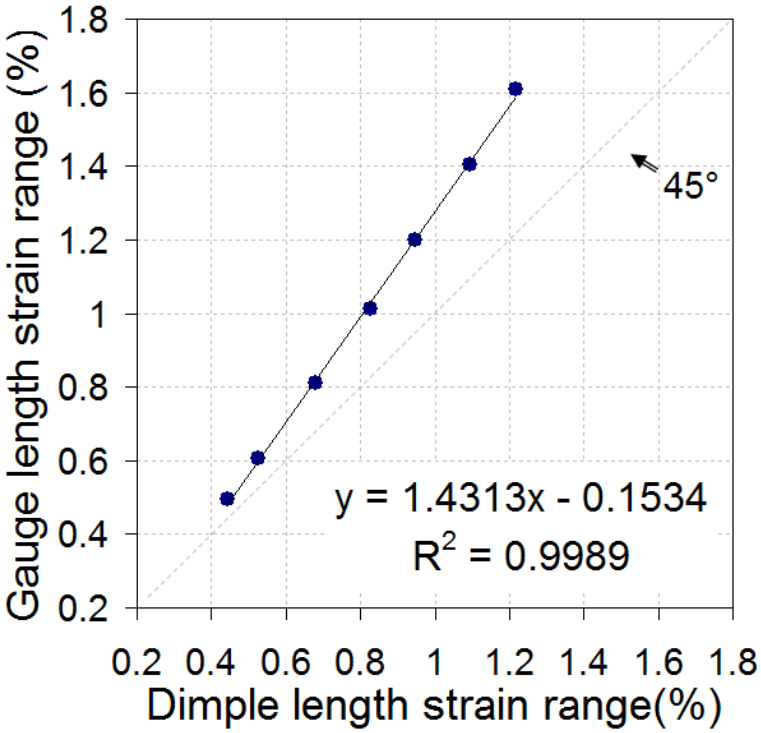

Figure 3.24 Experimental results on gauge and dimple strain ranges

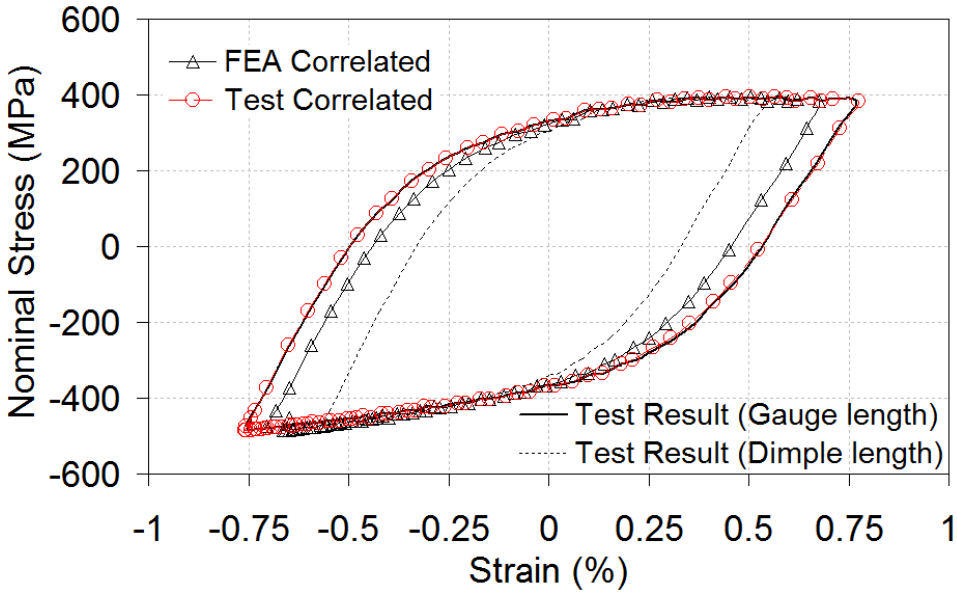

Figure 3.25 Comparison of measured hysteresis loop and correlated ones

3.7 Conclusions

Fatigue tests are increasingly being performed to simulate and investigate real-world failures of structural components. Premature failure of the specimens can be introduced by knife-edge or divots in gauge section during the control and measurement of the strain, which can significantly affect the accuracy of the result. In this chapter, an alternative in-direct approach is introduced to control and measure the strains for fatigue tests, especially at elevated temperatures. Two approaches, analytical and finite element analysis (FEA) are implemented to establish the strain correlations at room temperature, 100ºC and 480ºC, respectively for material SA387 Gr 22 CL 2. The results are then compared with the experiments to verify and validate the established correlations at room temperature. From the results, it can be seen that the FEA results have a good agreement with experimental results. However, the difference of the correlation coefficients predicted by the analytical and FE methods is less than 4% when the strain is up to 0.8%. By comparing the hysteresis loops predicted from the FEA and analytical method with the one obtained from the tests, it is shown that the prediction from the correlation obtained from FEA has better agreement with the experimental result.

This technique can also be used in TMF test. However, the correlation coefficient at each strain level should be directly established from the experiment. The correlation relation between the strain at dimple length and strain at gauge length based on FEM analysis has relative large deviations from the experimentally established correlation relation. This may be attributed to that the materials can have more complicated stress-strain behaviours under thermal-mechanical cyclic loadings, which may not be accurately simulated by the material model used in the current FEM analysis.

References

[1] Wells, C. H., "Elevated temperature testing methods", ASTM 465, (1969), P. 87

[2] Ellison, E. G. and Patterson, A. J. F., "Creep-fatigue interaction in a 1Cr Mo V steel", Proc. I. Mech. E, 190 (12/76), (1976), 321-350

[3] Raske, D. T. and Burke, W. F., "An extensometer for low cycle fatigue tests on anisotropic materials at elevated temperature", J. Phys. E. Sci. Instru., (1979), 12, 175

[4] Walters, D. J. and Hales, R. "An extensometer for creep fatigue testing at elevated temperatures and low strain ranges", J. Strain Anal., (1981), 16, 145

[5] Carden, A. E., "Thermal fatigue evaluation", ASTM STP 465, (1969), P. 163

[6] Lohr, R. D., "The role of extensometry in modern materials testing", Transducer/Tempcon 82 Conference, Wembley, UK, (1982)

[7] Hirschberg, M. H., "A low cycle fatigue testing facility", ASTM STP 465, (1969), P67

[8] Slot, T., Stentz, R. H. and Berling, J. T., "Controlled strain testing procedures", ASTM STP 465,(1969), P.100

[9] Lord, D. C. and Coffin, L. F., "High temperature materials behaviour", ASTM STP 465, (1969), P. 129

[10]Shiozawa, K., Murai, M., Shimatani, Y., and Yoshimoto, T., "Transition of fatigue failure mode of Ni-Cr-Mo low-alloy steel in very high cycle regime", International Journal of Fatigue, 32(3), (2010), 541-550

[11]Mochizuki, Y., Nakajima, M., and Shimizu, T., "High Cycle Fatigue Properties and Failure Mode in Ni-Cr-Mo steel Tempered at Low Temperature", Advance in Fracture and Damage Mechanics VII, Key Engineering Materials, 385-387, (2008), 185-188

[12] Ono, Y., Yuri, T., Sumiyoshi, H., Matsuoka, S., and Ogata, T., "High-cycle fatigue properties and sub-surface crack initiation in Ti-5%Al-2.5%Sn ELI alloy", Journal of the Japan Institute of Metals, 69-8, (2003), 391-397

[13]Shiozawa, K., and Lu, L., "Very high-cycle fatigue behaviour of shot-peened high-carbon-chromium bearing steel", Fatigue and Fracture of Engineering Materials and Structures, 25:8-9, (2002), 813-822

[14]Nogami, S., Sato, Y., Tanaka, A., Hasegawa, A., Nishimura, A., and Tanigawa, H., "Effect of Specimen Shape on the Low Cycle Fatigue Life of Reduced Activation Ferritic/Martensitic Steel", Journal of Nuclear Science and Technology, 47-1, (2010), 47-52

[15] Wood, D.S., Slattery, G.G., Wynn, J., Connaughton, M.D., and Lambert, M.E., "Preliminary results of the effect of environment on low cycle fatigue of type 316 and 9Cr1Mo steels", in: The influence of environment on fatigue, Inst. Mech. Engrs., London, (1977), 11-20,

[16] Furuya, K., Nagata, N. and Watanabe, R., " Low cycle fatigue properties of type 316 stainless steel in vacuum", J. Nucl. Mater., 89, (1980), 372-382

[17] Kschinka, B. and Stubbins, J.F., "Creep-fatigue-environment interaction in a bainitic 2.25 wt.%Cr-1 wt.%Mo steel forging", Mater. Sci. Eng., A110, (1989), 89-102

[18] Sumner, G., "Techniques for high temperature fatigue testing", London : Elsevier Applied Science, c1985. print

[19] Chen, J., Yamatomo, T., Xia, Z., Esaki, K., "Experimental Evaluation of Fatigue Life of Coke Drum Materials with Weld Sections", Proceeding of ASME Pressure Vessel and Piping Conference (2013): PVP2013-97095

[20] ASTM E2368-10, 2010, "Standard Practice for Strain Controlled Thermomechanical Fatigue Testing", ASTM international, West Conshohocken, PA, 2010, DOI: 10.1520/E2368-10

[21] ASTM E606-04, 2004, "Standard Practice for Strain-controlled Fatigue Testing", ASTM international, West Conshohocken, PA, 2004, DOI: 10.1520/E606-04

[22] Chen, J., 2010, "Experimental Study of Elastoplastic Mechanical Properties of Coke Drum Materials", Masters Dissertation, University of Alberta, Edmonton

[23] Ramberg, W., & Osgood, W. R., "Description of stress-strain curves by three parameters" Technical Note No. 902, National Advisory Committee for Aeronautics, Washington DC, 1943

[24] Anonym. "Data Sheets on Elevated-Temperature, Low-Cycle Fatigue Properties of SCMV 4 (2.25Cr-1Mo) Steel Plate for Pressure Vessel" *NRIM Fatigue Data Sheet (1991): 1. TEMA.* Web. 20 Nov. 2013

[25] Coffin, L. F. Jr., "A study of the effects of cyclic thermal stresses on a ductile metal", Trans. ASME, 76 (1954) 931-950

[26] Manson, S.S., "Behaviour of materials under conditions of thermal stress", Heat Transfer Symposium, University of Michigan, 1953, 9-75. See also NACA-TN-2933, 1953)

[27] Hahner, P., Affeldt, E., Beck, T., Klingelhoffer, H., Loveday, M., Rinaldi, C. "Validated Code of Practice for Strain-controlled Thermo-Mechanical Fatigue Testing" EC- EUR 22281 EN – Directorate General, Joint Research Centre – Institute for Energy, (2006)

[28] Chen, J., Xia, Z., "Thermal Mechanical Fatigue of Coke Drum Materials", Proceeding of 13th International Conference on Fracture, June 16-21, 2013, Beijing, China

CHAPTER 4 A Comparative Study on Fatigue Lives of 2¼Cr-1Mo and C-½Mo Base Materials Used for the Construction of Delayed Coke Drums[3]

Since the nineteen eighties, new drum material selection has been towards increasing chrome -molybdenum alloy content. Steels with higher Cr and Mo contents are presumed to have better thermal cycling resistance because of their higher yield strength and better creep resistance. However, there is not enough evidence to demonstrate the improved reliability of these materials in this specific service. In this paper, a comparative study of fatigue lives of C-½Mo and 2¼Cr-1Mo steels is performed at elevated temperature. The results show that the isothermal low cycle fatigue (ILCF) life of C-½Mo steel is longer than that of 2¼Cr-1Mo steel at test temperatures of 100°C and 480°C. By comparing thermal mechanical fatigue (TMF) lives of these two materials, it is shown that the TMF life of C-½Mo steel is about 3 times longer than that of 2¼Cr-1Mo steel. Therefore, the former might be a better base material than the latter from the standpoint of the ILCF and TMF lives. This observation is also consistent with the survey data of the American Petroleum Institute (API). Finally, a simple life prediction method, the Universal Slopes Equation, USE is tested in this study. It is found that the USE can give reasonable prediction for C-½ Mo steel at 100°C, only. However, it cannot predict fatigue life accurately at elevated temperatures.

[3] Chapter 4 of this thesis has been submitted to *Journal of Pressure Vessels and Piping* in 2013

4.1 Introduction

Coke drums are normally constructed of carbon or low alloy carbon steels and internally clad with stainless steel to protect the coke drums from corrosion [1]. There are limited studies on the fatigue life estimation for coke drums materials [2-6]. These are based on single material at isothermal condition, which do not consider cyclic temperature conditions. There are few study related to the comparative evaluation of alternative coke drum materials from fatigue life point of view.

In recent years, new drum material selection has been towards increasing chrome-molybdenum alloy content. API survey [7] data shows that 13 out of 22 coke drums installed between 1950 and 1969 were made of C-Mo steels, but only 2 of 22 drums that were installed between 1980 and 1997. However, in those two periods, 2 out of 22 coke drums were made of Cr-Mo steels between 1950 and 1969 while 19 of 22 were installed between 1980 and 1997. Steels with higher Cr and Mo contents are presumed to have better thermal cycling resistance because of their higher yield strength and better creep resistance. However, there is little evidence to demonstrate the improved fatigue endurance of these materials. The coke drums constructed from these materials still experience the same type of damage and failure in sometimes notably shorter exposure times.

In this chapter, two coke drum base materials (C-½Mo and 2¼Cr-1Mo) are investigated and compared under isothermal and thermal-mechanical cyclic loadings. In addition, a comparative study between isothermal and thermal mechanical fatigue lives of these materials is conducted. The Universal Slopes Equation (USE), first proposed by Manson [8, 9], is attempted to predict the isothermal and thermal-mechanical fatigue lives of both materials at elevated temperatures.

4.2 Specimen Geometry and Materials

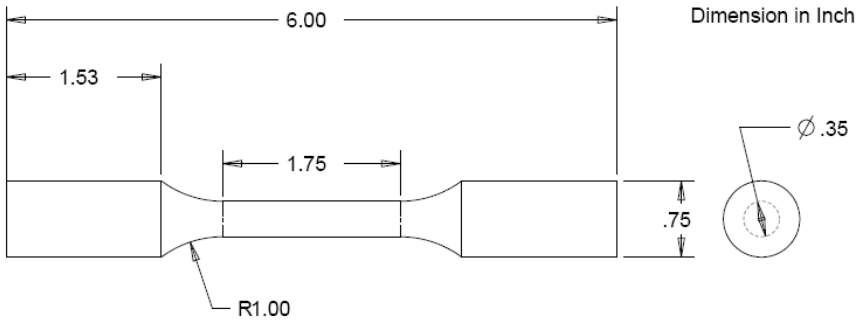

Figure 4.1 Drawing of uniaxial tensile test specimen

There are three different types of specimens used in this study: uniaxial tensile test specimen (Fig. 4.1), isothermal low cycle fatigue (ILCF) specimen (Fig. 3.2) and thermal-mechanical fatigue (TMF) test specimen (Fig. 2.15). All specimens are machined along the rolling direction of the stock plates. The gauge section of the specimens is carefully polished by 3M sandpaper gradually to a grit size of 600 (average particle diameter 16 μm), and the inner surface of the TMF specimen is also polished to the same surface roughness.

Two base materials, ASME SA 387 Gr 22 CL 2 (SA 387) and ASME SA 204 Gr C (SA 204C) are investigated in this study. The nominal chemical composition of SA 387 Gr 22 CL 2 and SA 204 Gr C are 2¼ Cr- 1Mo and C-½Mo respectively. Both plates were normalized and tempered after fabrication. The detailed chemical compositions of the plates are listed in Table 4.1.

Table 4.1 Chemical Composition* for SA 387 Gr 22 CL2 and SA 204 Gr C

	C	Cr	Mn	Mo	P	S	Si	Heat Treat
SA 387 Gr 22 CL 2	0.12	2.33	0.52	0.95	0.007	0.007	0.2	Normalize Temper
SA 204 Gr C	0.23	0.142	0.899	0.492	0.008	0.0004	0.387	Normalize Temper

*Source: Manufacturing test certificate report, American Alloy Steel

4.3 Experimental Equipment and Test Procedures

The same high temperature fatigue test system discussed in chapter 3 is used to conduct ILCF testing in this investigation. The more detailed design and development of this system are described in [10].

To achieve a relatively faster thermal cycling rate in TMF testing, a TMF test system is successfully developed and installed in the lab. The detailed description of development of the system can be found in chapter 2 and [11]. All the components are calibrated before this investigation according to ASTM standard E2368 Standard Practice for Strain Controlled Thermo-Mechanical Fatigue Testing [12].

ILCF tests are first conducted at 100°C and 480°C for the SA 387 and SA 204C materials. The selected test temperature of 480°C represents the upper bound of usual operational temperatures for coke drums. The uni-axial ILCF tests are carried out as benchmark tests for comparison. The ILCF tests are performed under strain-controlled condition at a strain rate of 0.005/sec throughout all tests. The tests are conducted for fully-reversed cyclic loading at both 100°C and 480°C. Afterwards, TMF tests are carried out on both materials. The tests are performed under temperature-dependent strain-controlled condition, and in-phase thermal-mechanical loading is applied at a cycle rate of 0.02Hz. The temperature is cycled between 100°C and 480°C throughout the test. At each strain level, there are at least two tests conducted to insure the accuracy of the data. Each fatigue test stops when the maximum load decreases to 6 *kN* for the ILCF solid specimens and 3.7 *kN* for the TMF tubular specimens as failure criterion in this investigation.

4.4 Mechanical Properties of Tested Materials

Uniaxial tensile and stepped fully-reversed cyclic tests (in order to obtain cyclic stress-strain curve) are first conducted at 100°C and 480°C for the SA 387 and SA 204C specimens. The mechanical properties from both temperatures, obtained from the tests, are summarized in Table 4.2. For uniaxial monotonic tensile tests, the variation of elongation and reduction of area for SA 387 is less sensitive to temperature than for SA 204C. Young's modulus, yield strength (at 0.2% offset strain), and ultimate tensile strength of SA 387 at 100°C and 480°C are higher than that of SA 204C at corresponding temperatures (See Table 4.2). This is mainly due to the higher content of Cr-Mo in SA 387. This observation is consistent with the API survey [7] trend for new drum material selection. The specific measured mechanical properties of SA 387 are superior to that of SA 204C at corresponding temperature for the monotonic tensile tests. However, by comparing the monotonic stress-strain curves (MSSC) with cyclic stress-strain curves (CSSC) at 100°C and 480°C for both materials in Fig. 4.2, it is found that SA 387 experiences cyclic softening (MSSC is above CSSC) while cyclic hardening (CSSC is above MSSC) is observed at elevated temperature for SA 204C. Cyclic hardening indicates increased resistance to deformation. Therefore, the material's cyclic hardening is more beneficial for resisting deformation under cyclic loading. From Table 4.2 and Fig. 4.2, the cycle stress curves indicate that Young's moduli for the two materials are almost the same at 100°C and 480°C. At 100°C, the yield strength of SA 204C is still lower than that of SA 387 (372 MPa versus 415 MPa), however, at 480°C, the yield strength of SA 204C becomes higher than that of SA 387 (388 MPa versus 349 MPa) Therefore, it may be concluded that the mechanical properties of SA 387 may not be superior to that of SA 204C under cyclic fatigue loading conditions, especially at higher temperatures.

Table 4.2 Tensile and Cyclic Properties of SA 387 Gr 22 Cl 2 and SA 204 Gr C

	SA 387 Gr 22 CL 2		SA204 Gr C	
	100°C	480°C	100°C	480°C
Properties obtained from tensile tests				
Young's Modulus (GPa) – E	202.7	157.6	195.4	154.8
Yield Strength (MPa) – $\sigma_{0.2\%}$	484.7	405.8	371.1	256.8
Ultimate Tensile Strength (MPa) - σ_{UTS}	605.9	505.6	532	474.3
Elongation (%)	34.4	32	38.8	36.9
Reduction of Area (%) – RA	76.9	76.7	68	81.6
True Fracture Strength (MPa) - σ_f	1363.4	767	1114.3	1152.5
Properties obtained from cyclic tests				
Young's Modulus (GPa) – E	198	158.2	195.2	154.3
Yield Strength (MPa) – $\sigma_{0.2\%}$	415	349	372	388

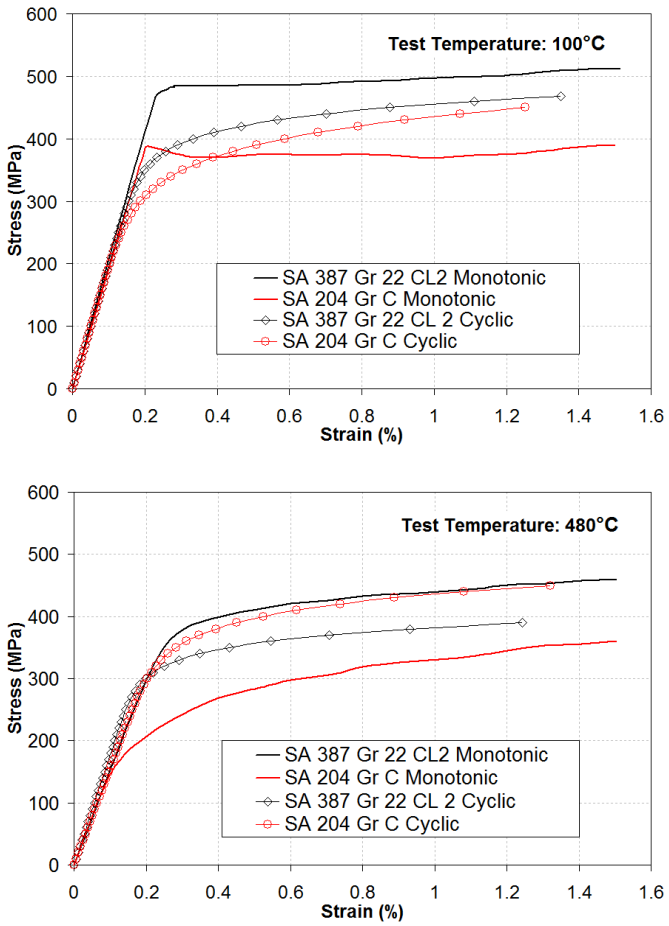

Figure 4.2 Comparison of MSSC and CSSC for SA 387 and SA 204C

4.5 Fatigue Test Results and Discussion

4.5.1 Isothermal low Cycle Fatigue Tests

Table 4.3 Summary of ILCF test results for SA387-22-2 and SA204C

ASME SA 387 Gr. 22 CL 2				ASME SA 204 Gr. C			
100°C		480°C		100°C		480°C	
$\Delta\varepsilon_{mech}/2$ (*mm/mm*)	$2N_f$ (*reversals*)	$\Delta\varepsilon_{mech}/2$ (*mm/mm*)	$2N_f$ (*reversals*)	$\Delta\varepsilon_{mech}/2$ (*mm/mm*)	$2N_f$ (*reversals*)	$\Delta\varepsilon_{mech}/2$ (*mm/mm*)	$2N_f$ (*reversals*)
0.00260	46980	0.00221	49060	0.00286	42440	0.00301	23680
0.00260	50280	0.00221	52280	0.00277	55648	0.00301	19580
0.00440	11920	0.00322	9032	0.00431	14952	0.00444	4324
0.00440	12812	0.00322	9860	0.00431	15360	0.00439	5130
0.00568	5720	0.00458	3466	0.00535	10828	0.00665	2354
0.00568	6760	0.00458	3848	0.00671	4448	0.00665	2256
0.00696	3400	0.00679	2064	0.00660	6480	0.00901	1178
0.00696	3422	0.00679	2012	0.00775	3742	0.00901	1674
0.00944	1620	0.00930	700	0.00890	2254	0.01044	1176
0.00944	1740	0.00930	1040	0.00890	2714	0.01044	1132

Table 4.3 lists the isothermal fatigue test results for SA 387 and SA 204C steels at 100°C and 480°C respectively. Figure 4.3 shows the relation between mechanical strain amplitude versus number of reversals ($2N_f$) for SA 387 and SA 204C at 100°C and 480°C. To accurately express the strain-life relation, same Coffin-Manson-Basquin's relation [13-15], discussed in chapter 2, is used, and the total strain verse fatigue life can be rewritten as elastic and plastic portions:

$$\frac{\Delta\varepsilon}{2}=\frac{\Delta\varepsilon_e}{2}+\frac{\Delta\varepsilon_p}{2}=\frac{\sigma'_f}{E}(2N_f)^b+\varepsilon'_f(2N_f)^c \tag{4.1}$$

The detailed decomposition of total strain into plastic and elastic portions versus reversals for SA 387 and SA 204C at 100°C and 480°C are shown in Fig. 4.4. It can be seen that the data is well fitted by linear regression as the form of Eq. 4.1 for plastic and

elastic portions correspond. The parameters obtained from this procedure are summarized in Table 4.4. The data for mechanical strain amplitude versus reversals, in Fig. 4.3, are fitted by the Coffin-Manson-Basquin relation (Eq. 4.1). It can be seen that as the test temperature increases the fatigue lives of both materials decrease noticeably. The ILCF life of SA 204C is longer than that of SA 387 at the same test temperature. By comparing the elongation of both materials from tensile tests, it is found that the elongations of SA 204C at both temperatures are greater than that of SA 387 which implies that SA 204C is more ductile than SA 387. Since ductility mainly dominates the fatigue life within LCF region [16], therefore, it may be evident that SA 204C has longer life than SA 387 from this point of view.

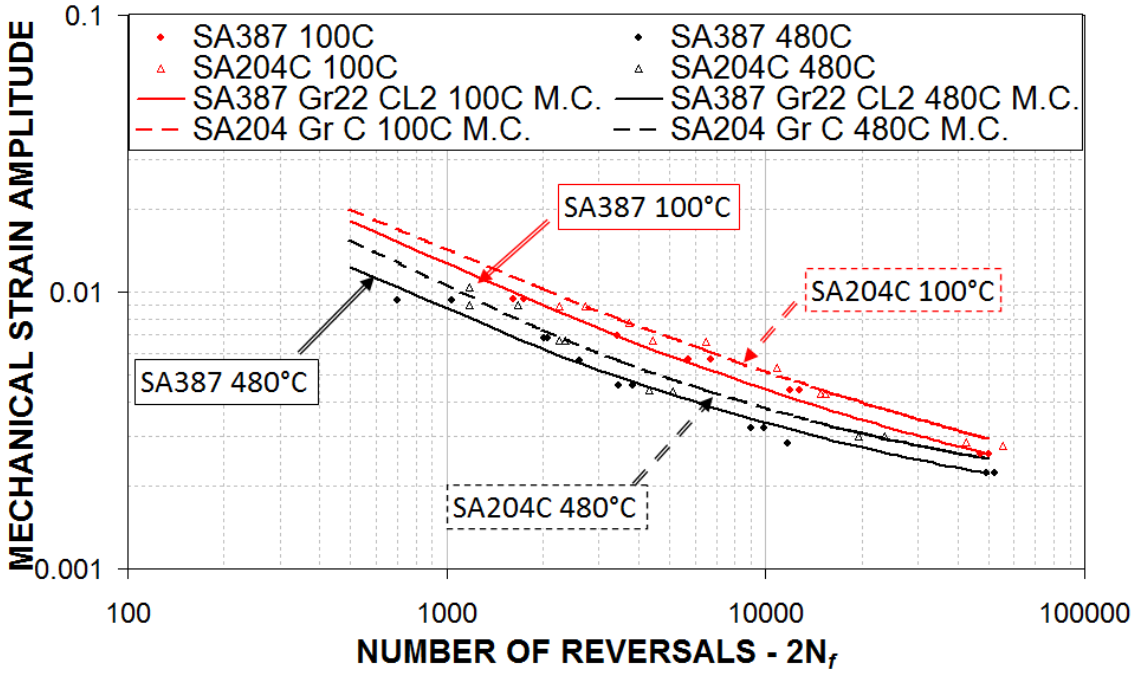

Figure 4.3 Summary of isothermal LCF results of SA 387 and SA 204C

Table 4.4 Summary of Fatigue Coefficients of SA387-22-2 and SA204-C

	SA 387 Gr 22 CL 2		SA 204 Gr C	
	100°C	480°C	100°C	480°C
Young's Modulus (GPa) – E	202.7	157.6	195.4	154.8
Fatigue strength coefficient (MPa) - σ'_f	1418.9	788	1563.2	774
Fatigue strength exponent – b	-0.128	-0.098	-0.139	-0.084
Fatigue ductility coefficient - ε'_f	0.727	0.563	0.596	0.991
fatigue ductility exponent – c	-0.625	-0.655	-0.576	-0.705

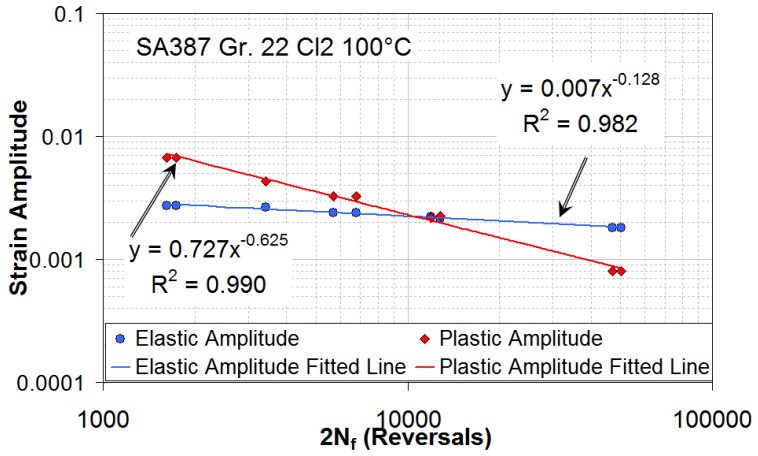

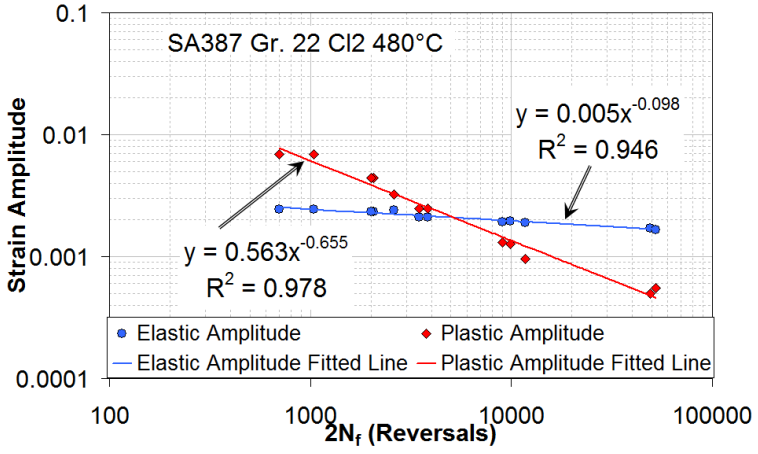

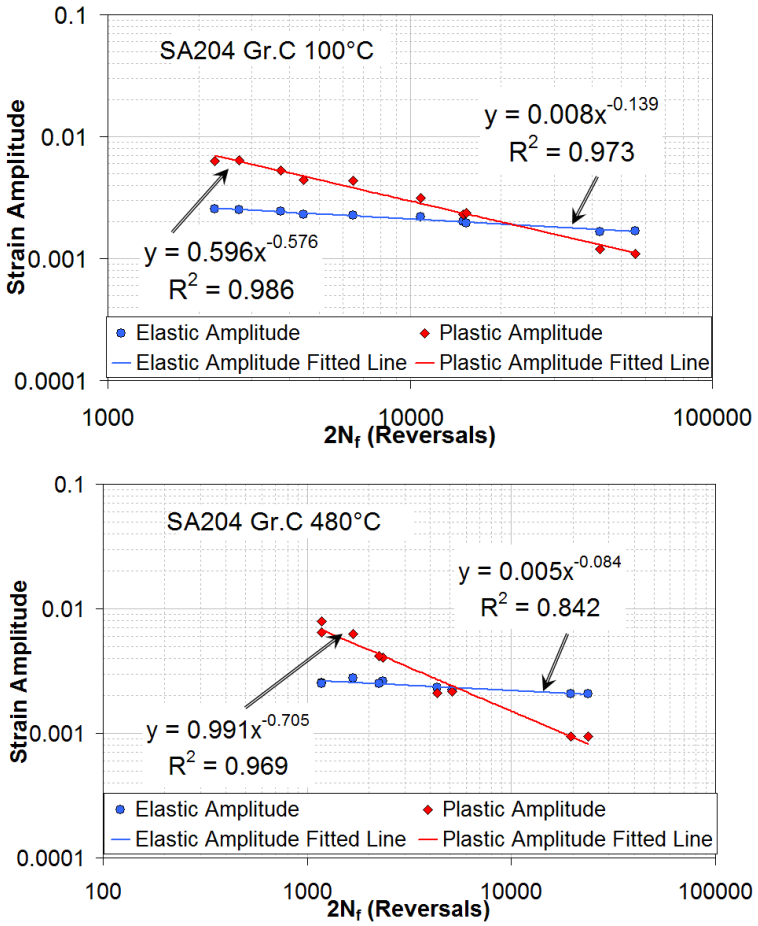

Figure 4.4 Summary of elastic amplitudes and plastic amplitudes vs. $2N_f$

4.5.1.1 Universal Slopes Method (USM) for ILCF

In 1965, Manson [8] proposed the universal slopes method to predict the isothermal fatigue lives of metal materials based on ultimate tensile strength, Young's modulus and reduction of area from tensile tests. It assumes that the slopes of the elastic and plastic lines are the same for all materials. The slopes of the elastic and plastic lines are assumed to be equal to -0.12 and -0.6. Manson shows that the intercept of the elastic line is equal to $[ln(1/(1\text{-}RA))]^{0.6}$ at a life of $N_f = 1$. The intercept of the plastic line is equal to $3.5(\sigma_u/E)$ at a life of $N_f = 1$. Therefore, the Universal Slopes Equation (USE) developed by Manson [8] is given by

$$\Delta\varepsilon = 3.5\frac{\sigma_u}{E}\left(N_f\right)^{-0.12} + \left[\ln\left(\frac{1}{1-RA}\right)\right]^{0.6}\left(N_f\right)^{-0.6} \tag{4.2}$$

Rewritten in the form of strain amplitude versus reversals, the equation becomes

$$\frac{\Delta\varepsilon}{2} = 1.9018\frac{\sigma_u}{E}\left(2N_f\right)^{-0.12} + 0.7579\left[\ln\left(\frac{1}{1-RA}\right)\right]^{0.6}\left(2N_f\right)^{-0.6} \tag{4.3}$$

The comparison of tested fatigue lives for SA 387 and SA 204C at 100°C and 480°C with the predictions by the USE is shown in Fig. 4.5A. In this figure, the closer to the 45° reference line the test points are, the more accurate are the predictions by the universal slope method, Eq. (4.3). One can see that the test points for SA 204C at 100°C are close to the 45° reference line, which implies that the fatigue lives are well predicted by the USE. The test points for SA 387 at 100°C are all above the 45° reference line but with only a small deviation. (USE predicted points on ordinate and test results on abscissa). However, the test points for both materials at 480°C are well above the 45° reference line indicating that the USE predictions are non-conservative. Therefore, based on the current test data, the USE provides a reasonable prediction for SA 204C at 100°C. It cannot be directly applied to the test cases at elevated temperature of 480°C.

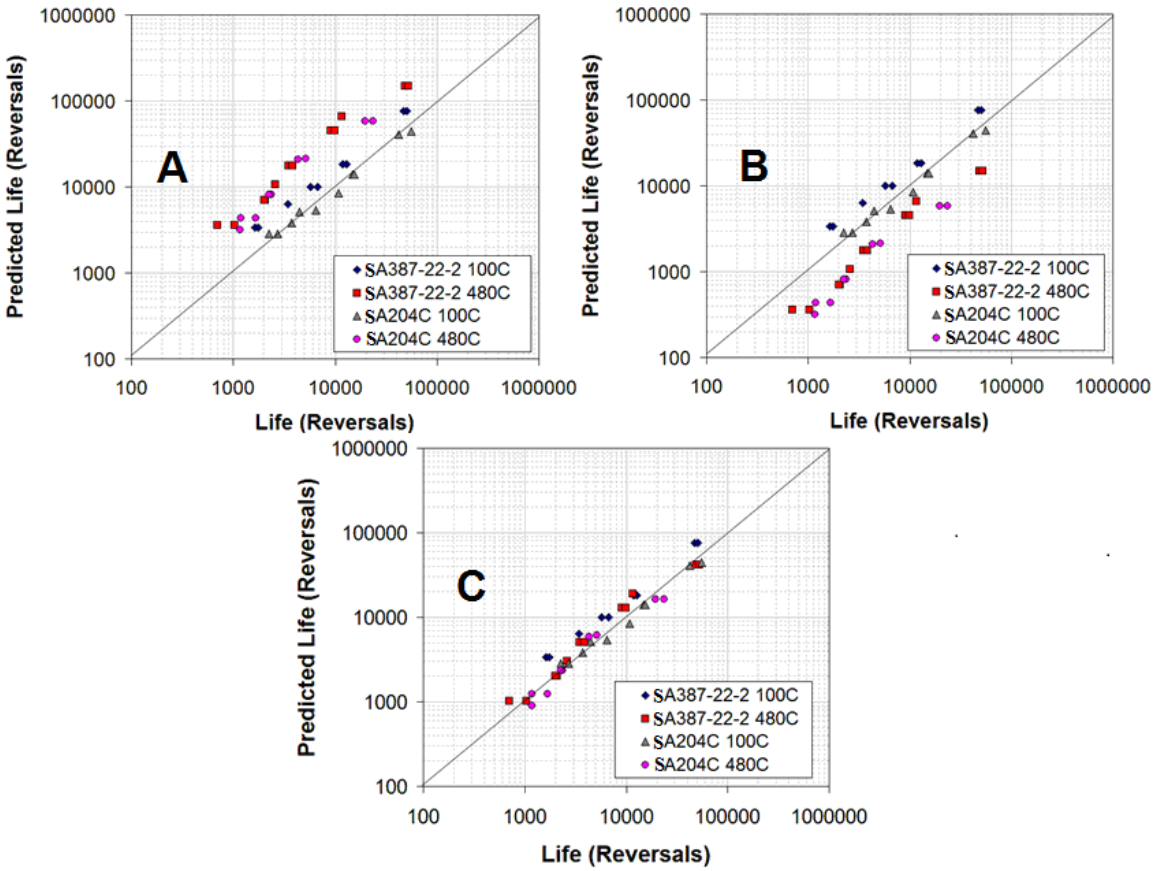

Figure 4.5 Comparison of predicted life by USE and test life

(A) by USE; (B) by 10% rule; (C) by reduction factor of 3.5 (USE predicted points on ordinate and test results on abscissa)

In 1968, Manson [9] proposed a simple "10% Rule" for estimating high temperature low cycle fatigue lives. The USE is first used to determine fatigue life, and this life is simply divided by a factor of 10 as the fatigue life at elevated temperatures. The USE is a simple method to estimate fatigue lives of materials based on their tensile test properties. As shown in references [8] and [9], it can provide good predictions of fatigue lives for some materials including stainless steels, nickel alloys, etc. By implementing this rule as seen in Fig. 4.5B, it is found that the prediction becomes quite conservative for the isothermal tests at 480°C for the two materials. By modifying the reduction factor and using a value of 3.5 instead of 10, all the data points from the four groups of fatigue tests lie very close to the 45° reference line as shown in Fig. 4.5C. Therefore, it should be cautious when use the simple Universal Slopes Equation (USE) method to estimate fatigue lives of materials, especially at elevated temperatures.

4.5.2 Thermal-Mechanical Fatigue Tests

Table 4.5 Summary of TMF test results for SA387-22-2 and SA204-C

ASME SA 387 Gr 22 Cl 2		ASME SA 204 Gr C	
TMF (100°C ~ 480°C)		TMF (100°C ~ 480°C)	
$\Delta\varepsilon_{mech}/2$ (*mm/mm*)	$2N_f$ (*reversals*)	$\Delta\varepsilon_{mech}/2$ (*mm/mm*)	$2N_f$ (*reversals*)
0.0079	1242	0.0072	2676
0.0079	1436	0.0072	2604
0.0049	3768	0.0060	3060
0.0049	3630	0.0060	3340
0.0035	7362	0.0047	8134
0.0035	8978	0.0047	7236
0.0025	26562	0.0033	38904
0.0025	16488	0.0033	22232

The TMF tests are conducted on SA 387 and SA 204C under in-phase temperature-controlled thermal mechanical loading conditions. Table 4.5 lists the results for SA 387 and SA 204C steels. The mechanical strain is obtained by subtracting the thermal strain from the total strain. The total mechanical strain amplitude versus reversals is then separated into elastic and plastic portions versus reversals, as seen in Fig. 4.6. The data is well fitted by linear regression according to the power function of Eq. 4.1. The lines of total mechanical amplitude versus reversals fitted by Eq. 4.3 are then plotted in Fig. 4.7 for both materials. By comparing TMF lives of the two materials, it is shown that the TMF life of SA 204C is about 3 times longer than SA 387. TMF testing simulates the thermal and mechanical loading conditions experienced by coke drums. Therefore, it is further demonstrated that SA 204C (C-½Mo) is a better base material than SA 387 (2¼Cr-1Mo) from a fatigue life standpoint.

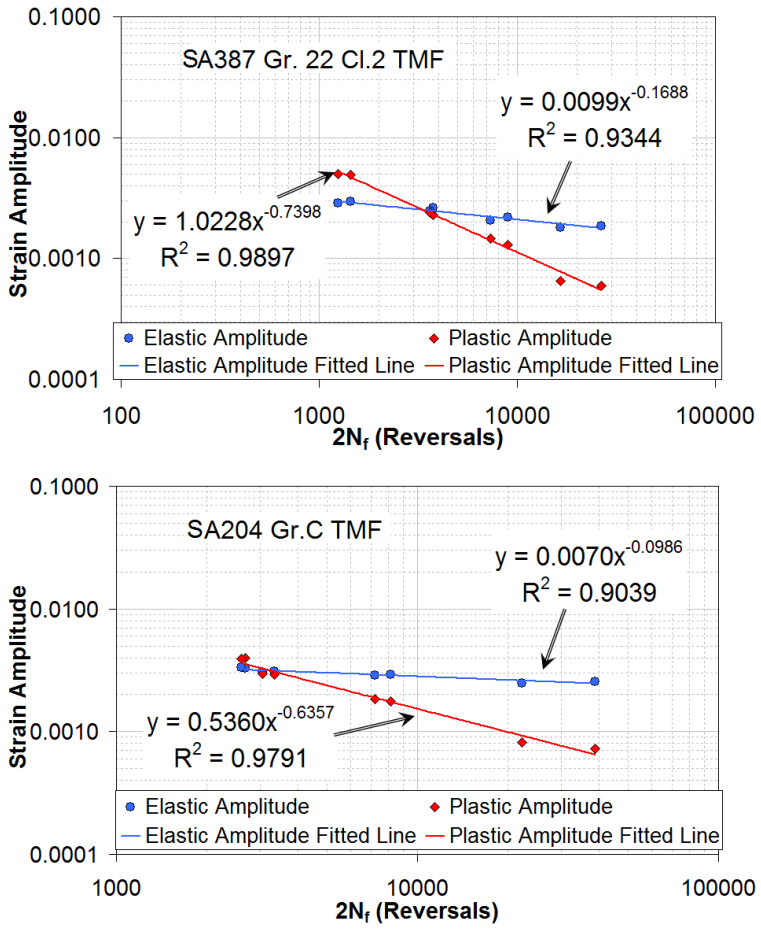

Figure 4.6 Summary of elastic and plastic lines for TMF results

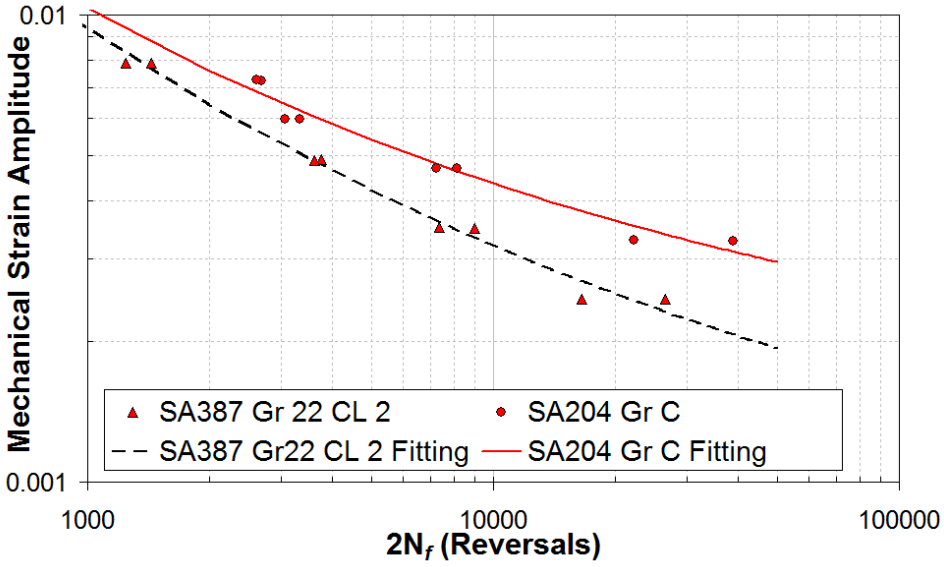

Figure 4.7 Comparison of TMF lives for SA 387 and SA 204C

4.5.2.1 Universal Slopes Method (USM) for TMF

A prediction of TMF lives of SA 387 and SA 204C is also attempted by the USE. The properties of ultimate tensile strength, Young's modulus and reduction of area from tensile tests at 480°C are used in the prediction of TMF lives. Similar with prediction of isothermal LCF at 480°C, Eq. 4.3 are first used for predicting TMF lives of SA 204C and SA 387 respectively. As seen in Fig. 4.8A, the predicted lives are significantly longer than the test results for both materials (non-conservative). By attempting the "10% rule" to predict TMF life, it is also found that the prediction is too conservative as shown in Fig. 4.8B. Furthermore, the same reduction factor of 3.5 instead of 10 is tried. As shown in Fig. 4.8C, the data points become closer to the 45° reference line while for SA 387 the data points are higher than the reference line and for SA 204C they are lower than the reference line.

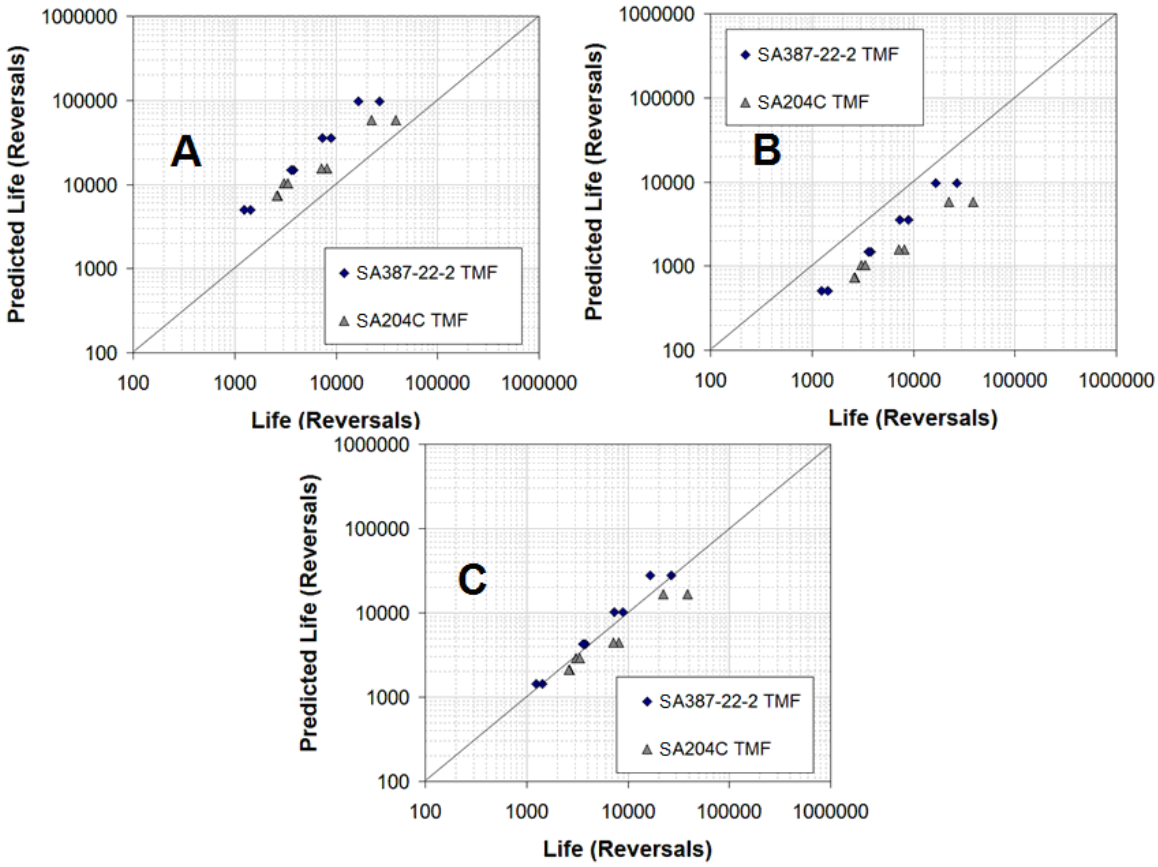

Figure 4.8 Comparison of predicted life by USE and test life

(A) by USE; (B) by 10% rule; (C) by reduction factor of 3.5 (USE predicted points on ordinate and test results on abscissa)

4.5.3 Comparison of ILCF and TMF lives

As shown in Fig. 4.9, comparisons of ILCF and TMF lives on SA 387 and SA 204C are performed. The TMF life of SA 387 becomes slightly shorter than ILCF at 480°C up to mechanical strain amplitude of 0.004. The fatigue lives for ILCF at 480°C and TMF coincide between mechanical strain amplitude of 0.004 and 0.006. Thereafter, the TMF curve is a little higher than that of ILCF. Overall, for SA 387, the TMF fatigue curve is very close to the ILCF fatigue curve at the same maximum temperature of 480°C. In contrast, the TMF life of SA 204C is longer than that of ILCF at 480°C up to mechanical strain amplitude of 0.008. This means that, if prediction of the TMF life of SA 204C is based on the ILCF fatigue curve at 480°C, it will yield a conservative prediction. Overall, the longer TMF life of SA 204C than that of ILCF life at the same maximum temperature implies that the expected service life of SA 204C drums is longer than predicted by ILCF results and is beneficial to operators of this equipment.

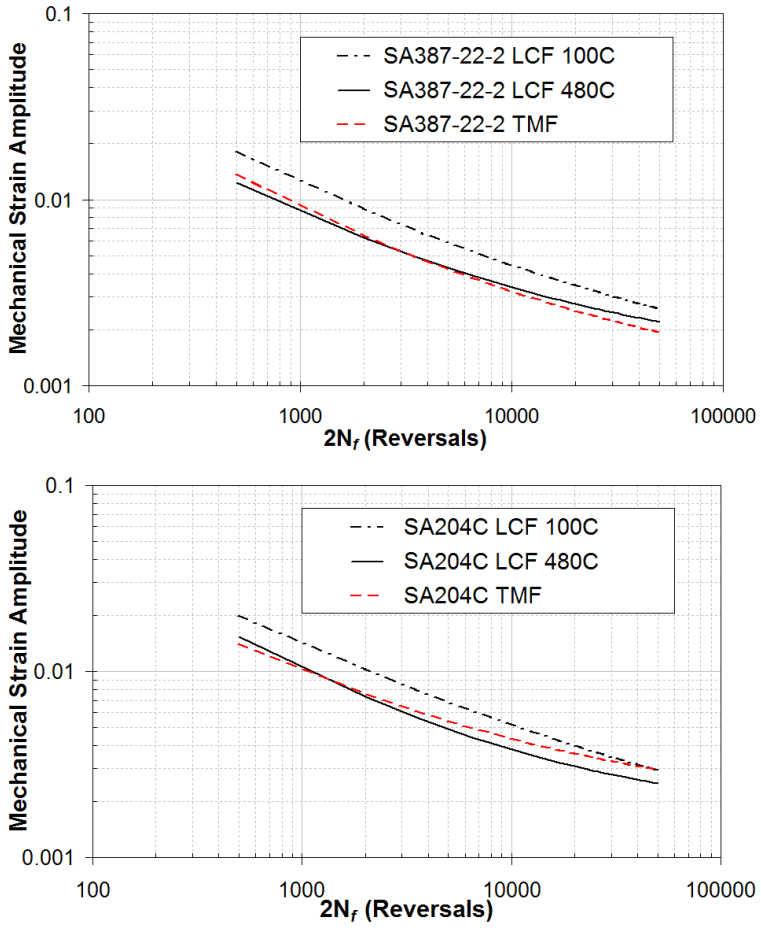

Figure 4.9 Comparisons of LCF and TMF lives on SA 387 and SA 204C

4.5.4 Comparison to API Survey Data

Table 4.6 presents API survey data on crack and bulge damage of coke drums made of C-½Mo (SA 204C) and Cr-Mo (SA 387) steels. It is divided into two sections: one is the number of cycles to first through wall crack, and the other one is cycles to first bulge. Coke drums fabricated from C-½Mo indicate a lower minimum cycle to first through wall crack and first bulge than ones fabricated from Cr-Mo. The tensile strength and yield strength of SA 387 is higher than that of SA 204C; therefore, it appears reasonable to conclude that coke drums fabricated from SA 204C could have less resistance to damage than coke drums fabricated from Cr-Mo; but this would be valid only for the initial operational cycles. Recall the data presented in Table 4.2 and Fig. 4.2,

showing that SA 204C has cyclic hardening behaviour, especially at elevated temperature, and SA 387 has cyclic softening behaviour, in contrast. Cyclic hardening indicates increased resistance to deformation and cyclic softening indicates decrease resistance. Therefore, the SA 204C material is stronger than SA 387 after a cyclic stable stage is achieved. Table 4.6 also shows that coke drums fabricated from SA 204C have maximum of 9,386 cycles without crack indication, but coke drums fabricated from SA 387 have a maximum of 5,994 cycles without crack indication. It is also shown that coke drums made of C-0.5Mo can have maximum 9386 cycles without bulging, but coke drums made of Cr-Mo can only have maximum 4745 cycles without bulging. The field data appears to support that the lab finding that SA 204C (C-Mo) steels could be a better base material than SA 387 (Cr-Mo) from the standpoints of ILCF and TMF lives.

Table 4.6 API survey of coke drum damage

	Cycles to first through wall crack		Cycles to first bulge	
Material	Minimum	Maximum without crack	Minimum	Maximum without bulge
C-½Mo	1,286	9,386	346	9,386
Cr-Mo	2,025	5,994	1,286	4,745

* Reference [7]

4.6 Conclusions

In recent years, new coke drum material selection has been towards increasing the chrome-moly alloy content. API survey [7] data shows that the number of coke drums made of C-Mo decreased from 13 to 2 and Cr-Mo increased from 2 to 19 units (total 22 units surveyed) between the years of 1950 to 1997. In this paper, a comparative study on isothermal low cycle fatigue and thermal-mechanical fatigue of ASME SA 387 Gr 22 CL2 (2¼Cr-1Mo) and ASME SA 204 Gr. C (C-½Mo) is presented. The following conclusion can be drawn from this study:

1. The monotonic tensile strength, Young's modulus, yield strength (at 0.2% strain offset), and ultimate tensile strength of SA 387 at 100°C and 480°C are found to be superior to SA 204C at corresponding temperature.

2. Under cyclic testing, Young's moduli of the two materials are almost the same at 100°C and 480°C. The cyclic yield strength of SA 204C at 100°C remains lower than that of SA 387; but at 480°C, the cyclic yield strength of SA 204C becomes greater than that of SA 387. This is mainly due to the cyclic hardening of SA 204C and cyclic softening of SA 387, and more so at elevated temperature.

3. The ILCF life of SA 204C is longer than that of SA 387 at the same test temperature. As the temperature increases, the fatigue life of both materials decreases.

4. The TMF life of SA 204C is found to be about 3 times longer than that of SA 387. As the mechanical strain amplitude becomes smaller, the difference in TMF lives of the two materials becomes larger.

5. The TMF life of SA 387 can be reasonably predicted based on the ILCF life at the same maximum temperature of 480°C.

6. The longer TMF life of SA 204C than that of ILCF life at the same maximum temperature implies that the expected service life of SA 204C drums is longer than predicted by ILCF results and is beneficial to operators of this equipment.

7. Based on the current experimental study and, in combination with the API survey data, it is shown that SA 204C (C-½Mo) is a better base material than SA 387 (2¼Cr-Mo) from the standpoints of ILCF and TMF lives.

8. A simple fatigue life prediction method, the Universal Slopes Equation, is applied to the ILCF and TMF test data in this study. It is found that the USE method can give reasonable estimation of fatigue lives for SA 204C at constant temperature of 100°C. However, it should be cautious when it is used for other cases and especially at elevated temperatures.

References

[1] Penso, J. A., Lattarulo, Y. M., Seijas, A. J., Torres, J., Howden, D., and Tsai, C. L., "Understanding Failure Mechanisms to Improve Reliability of Coke Drum," PVP (Am. Soc. Mech. Eng.), 395, pp. 243–253. (1999)

[2] Ramos, A., Rios, C. and Vargas, J., "Mechanical Integrity Evaluation of Delayed Coke Drums", PVP-Vol.359, Fitness for Adverse Environments in Petroleum and Power Equipment, ASME (1997)

[3] Ramos, A., Rios, C., Johnsen, E., Gonzalez, M., and Vargas, J., "Delayed Coke Drum Assessment Using Field Measurements and FEA," Analysis and Design of Composite, Process, and Power Piping and Vessels, ASME, New York, 368, (1998), 231–237.

[4] Ramos, A. J., Rios, C. and Vargas, J.A.R., "Fatigue Life Prediction of Delayed Coke Drums", Vision Techenologica, Vol.6, 93-100,(1999)

[5] Boswell R.S., Ferraro T., "Remaining Life Evaluation of Coke Drums", Plant Engineering, Design and Responsibility Symposium, Energy Engineering Conference, (1997)

[6] Sohel M Panwala M, K. N. Srinviasan, S. L. Mehta, "Creep-fatigue interaction in coke drums: An approach based on API 579-1/ASME FFS-1 2007", Proceeding of the ASME, Pressure Vessels and Piping Division conference (2009): PVP2009-77483

[7] API Proceedings "1996 APE Coke Drum Survey-Final Report", 1996 American Petroleum Institute, Washington, DC

[8] Manson, S.S., "Fatigue: A complex subject – Some Simple Approximations," Proceedings, Society of Experimental Stress Analysis, Vol. 12, No. 2, (1965)

[9] Manson, S.S., "A simple procedure for estimating high-temperature low cycle fatigue", Experimental Mechanics, (1968), 349-355

[10] Chen, J., "Experimental Study of Elastoplastic Mechanical Properties of Coke Drum Materials", Masters Dissertation, University of Alberta, Edmonton, (2010)

[11] Chen, J., Xia. Z., "Thermal Mechanical Fatigue of Coke Drum Materials", Proceeding of 13th International Conference on Fracture, June 16-21, 2013, Beijing, China

[12] ASTM E2368, 2010 "Standard Practice for Strain Controlled Thermomechanical Fatigue Testing", ASTM International, West Conshohocken, PA, 2003 , DOI: 10.1520/E2368-10, www.astm.org.

[13] Basquin, O. H. "The exponential law of endurance tests", ASTM proceeding. 10 (1910) 625-630

[14] Coffin, L. F. Jr., "A study of the effects of cyclic thermal stresses on a ductile metal", Transaction of ASME, 76 (1954) 931-950

[15] Manson, S.S., "Behaviour of materials under conditions of thermal stress", Heat Transfer Symposium, University of Michigan, (1953), 9-75. See also NACA-TN-2933, (1953)

[16] Bannantine, J.A., "Fundamental of metal fatigue analysis", Englewood Cliffs, N.J. : Prentice Hall, (1990). Print.

CHAPTER 5 A Fatigue Life Prediction Method for Coke Drum Base, Weld, and HAZ Materials from Tensile Properties[4]

The importance of material fatigue information in design has been well recognized. There are a few existing fatigue life prediction methods based on materials tensile properties. Some of these fatigue life prediction methods can be successfully applied for non-heat affected materials. However, industrial components, such as pressure vessel, pipelines etc. are commonly constructed by welding parts together. The fatigue lives of welded section and its surrounding material could be greatly affected by the welding process. Therefore, it is beneficial to develop a fatigue life prediction model for the weld and surrounding heat affected zone (HAZ) materials based on their tensile testing data. In this chapter, fatigue lives of base material and its weld and HAZ materials for constructing coke drums are studied. Mechanical properties are first obtained from the tensile tests. Then, fully-reversed strain-controlled fatigue tests are performed. It is found that the fatigue life of pure base material is roughly twice of the weld and four time of the HAZ at the same strain amplitude. Four-point correlation (FPC) method by Manson can reasonably predict the life of base material. However, it over-predicts the lives of weld and HAZ. By introducing two reduction factors $R_{plastic}$ and $R_{elastic}$ for the weld and HAZ material respectively into the FPC method, the over-prediction can be rectified. Therefore, the proposed modified FPC method could be applied in predicting fatigue lives of weld and HAZ materials.

[4] Chapter 5 of this thesis has been published in *Materials & Design* vol. 63, 575-583, 2014

5.1 Introduction

Fatigue tests are increasingly being performed to simulate and investigate real-world failures of components in various structures. However, performance of these tests is usually quite costly and time-consuming especially if environmental effect is involved. Consequently, for the initial design phase, it is greatly valuable to estimate the fatigue life from knowledge of the material properties more easily obtained such as through uniaxial tensile test. There are a few existing fatigue life prediction methods based on tensile data. In 1965, Manson [1] independently proposed two methods to predict the isothermal fatigue lives of metal materials based on ultimate tensile strength, true fracture strength, Young's modulus and reduction of area from tensile tests. In 1977, Socie et al [2] introduced another fatigue life prediction method based on monotonic properties. In that method, a few adjustments on parameters based on strain-life equation are made. In 1988, Muralidharan and Manson [3] modified Manson's universal slopes method to improve its prediction over the entire life range. There are several other research works to predict fatigue life by modifying the existing strain-fatigue life equation based material properties from tensile test [4-7]. Ong [8] has evaluated three commonly used methods, the four-point correlation method, the universal slopes method and Socie's method based on 49 steels, and found that the four-point correlation (FPC) method gives the best solution of the three methods for estimating fatigue life in terms of material properties from uniaxial tensile test. However, these fatigue life prediction methods are effective only for non-heat affected materials. The fatigue lives of heat affected materials could apparently be different from that of the non-heat affected one due to the metallurgical alterations. Industrial components, such as pressure vessel, pipelines, etc. are commonly constructed by welding different sections together. The welded section and its surrounding heat affected zone (HAZ) material could be greatly affected by the welding process. There are relatively limited fatigue life data available in literature for weld and HAZ materials. Therefore, it is beneficial to develop a fatigue life prediction method for the weld and HAZ materials based on their more easily obtained data, such as tensile properties.

Coke drums are normally constructed of carbon or low alloy carbon steels and internally clad with stainless steel to protect the coke drums from corrosion. The whole drum is built by sub arc welding the courses together. Many researches found that low cycle fatigue (LCF) is considered the failure mode for coke drums. [9-11] However, there are limited studies on the fatigue life estimation for coke drums which are only based on the base material [12-14]. Some [15, 16] have used the ASME fatigue design curve of base material to evaluate the fatigue life of coke drums. However, the ASME design curve would not be expected to give an accurate prediction of service life for a coke drum. The bulges are normally found near the circumferential weld seams, yield strength of which normally is higher. The base material finally tends to become thin and fails via cracking as the result of the restraint caused by the weld seams [11, 15, 17, 18]. As a result, there are a lot of cases observed that cracks are near or within the weld seams. Therefore, more reliable evaluation of fatigue lives of coke drums should also consider the fatigue lives of the weld and HAZ.

In this chapter, a group of base material and its weld and HAZ materials for constructing coke drums are selected. Their uniaxial tensile stress-strain curves and cyclic stress-strain curves are first obtained and compared. Micro-structural examination is then performed on base, weld, and HAZ materials. Low cycle fatigue (LCF) tests at elevated temperature of 250°C are carried out on these materials. Based on the above data, a modified FPC method for predicting fatigue lives of weld and HAZ materials from their tensile properties is proposed. The prediction of the modified method shows in better agreement with the experimental result.

5.2 Specimen Geometry and Materials

There are three different types of specimens used in this study: uniaxial tensile test specimen (Fig. 4.1), isothermal LCF specimen (Fig. 3.2) and HAZ - LCF test specimen (Fig. 5.1). The tensile test specimen is designed according to ASTM E8 [19]. Pure Base and pure weld specimens are machined to this geometry from the base and weld plates, respectively. The HAZ specimens are manufactured to this profile (Fig. 5.1)

from the welding joint shown in Fig. 5.2, and the gauge section mainly covers the weld and HAZ materials only. The nominal volume ratio between HAZ and weld is about 1.5 within the gauge length. Additionally, the cyclic stress-strain curves of base and weld materials are obtained through stepped cyclic tests performed on specimens with LCF specimen. The HAZ specimens are designed with sufficient amount of HAZ materials while minimized the gage length. The gage length is 25.4 mm (1 in), and the diameter within the gage length is 11.94 mm (0.47 in). The welding is performed by the same procedure as that in the coke drum construction. Post Weld Heat Treatment is performed after welding according to ASME Sec. VIII Div. 1 [20]. All specimens are machined along the rolling direction of the stock plates. The gauge section of the specimens is carefully polished by 3M sandpaper gradually to a grit size of 600.

SA 387 Gr. 11 Class 2, which is commonly used material for fabricating coke drum base shell, is selected for this investigation. The weld filler also uses the same material. The nominal chemical composition of SA 387 Gr. 11 CL.2 is 1¼ Cr-½ Mo.

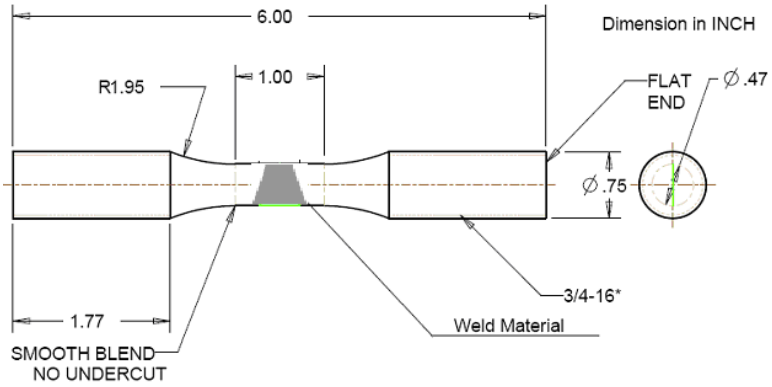

Figure 5.1 Drawing of HAZ - LCF specimen

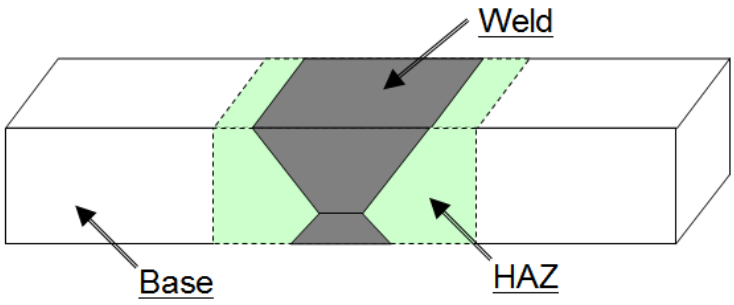

Figure 5.2 Drawing of welding joint of drum shell

5.3 Experimental Setup and Procedures

The same high temperature fatigue test system discussed in chapter 3 was used to conduct LCF testing in this investigation. The more detailed design and development of this system are described in [21].

From an in-field measurement by using high temperature strain gauges and thermocouples, it is observed that extreme strains on coke drum shell surface occurs during the quenching stage when the temperature drops to the range between 300°C and 200°C [22]. Therefore, the testing temperature is chosen at 250°C. A specimen with 3 thermocouples is initially used to verify the thermal gradient along the axial direction. After the temperature reached to 250°C and stabilized, the test starts after the strain is re-zeroed. Strain rate is set at 0.005/sec for all tests. At each strain amplitude, at least two tests are conducted to insure the repeatability and accuracy of the data. Each fatigue test stops when maximum load reaches 17% of the load at $N_f/2$ (stabilized maximum load). The reasons for this failure criteria are: 1. It protects the equipment from the sudden rupture of the specimen; 2. The set failure point is very close to the final separation, and it covers over 95% of the life. The tensile tests are performed, at similar strain rate, according to ASTM standards [19, 23].

5.4 Mechanical Properties and Microstructures

Uniaxial tensile and stepped fully-reversed cyclic tests are first conducted for base, weld, and HAZ specimens. A repeated test is performed on each material to confirm the accuracy of the result. The mechanical properties from two tests of each material are summarized in Table 5.1. The Young's modulus of base materials is moderately higher than both of weld and HAZ materials. The yield strength ratio of weld to base is averagely equal to 1.08. However, there is no evident dissimilarity in ultimate tensile strength among these materials. The elongation measured after the test shows the decline trend from base, weld to HAZ materials. However, the reduction of area shows similarity in base, weld and HAZ. By comparing the monotonic stress-strain curves with cyclic

stress-strain curves for three materials in Fig. 5.3 (B), it is found that all three materials experience cyclic softening, and no apparently difference in cyclic stress-strain curves.

Table 5.1 Tensile and Cyclic Properties of SA387-11-2 Base, Weld and HAZ

	Base		Weld		HAZ	
	Test 1	Test 2	Test 1	Test 2	Test 1	Test 2
Properties from tensile tests						
Young's Modulus (GPa) – E	196.59	198.7	186.1	192.1	183.8	186.1
Yield Strength (MPa) – $\sigma_{0.2\%}$	426.9	424.1	458.4	461.9	445.1	458.4
Proportional limit (MPa) – $\sigma_{prop.}$	414.3	411.5	454.9	456.3	401	390.5
Ultimate Tensile Strength (MPa)	555.7	550.8	545.8	552.9	550.1	543.1
Elongation (%)	23.93	23.57	18.50	19.29	16.79	17.71
Reduction of Area (%) – RA	75.47	75.57	74.43	74.14	75.88	74.43
True Fracture Strength (MPa) – σ_f	1270.4	1243.2	1135.9	1147.6	1153.4	1111.3

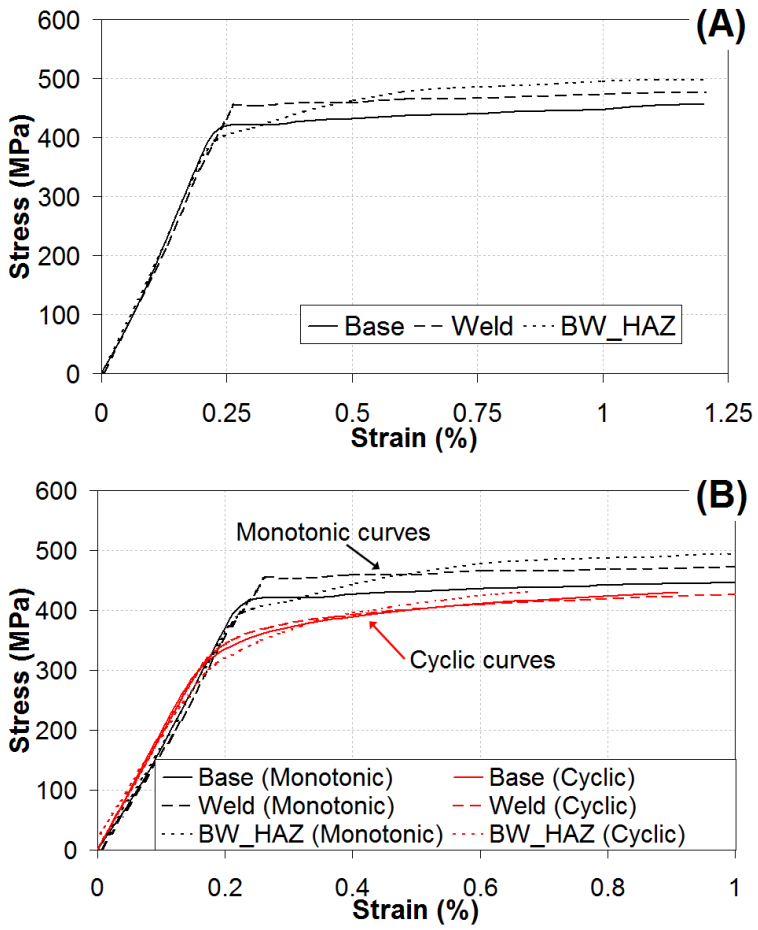

Figure 5.3 Monotonic and cyclic stress strain curves at 250°C

(A) Monotonic stress strain curves (B) Comparisons of monotonic and cyclic curves

Plastic deformation is mainly due to the motion of dislocations. The yield strength of a metal can usually be increased by introducing obstacles to dislocations. Such obstacles can be tangles of dislocations, grain boundaries, and distorted crystal structures due to small particles dispersed in the crystal structures. From comparison of microstructures of base and weld materials, shown in Fig. 5.4, it is found that the grain size of base metal is much larger and more regular than weld. Therefore, it is first evident that the yield strength of weld material is higher than that of base metal and the ductility of weld material is lower than that of base material. In addition, a more irregular pattern of microstructure of HAZ can be seen in Fig. 5.5.

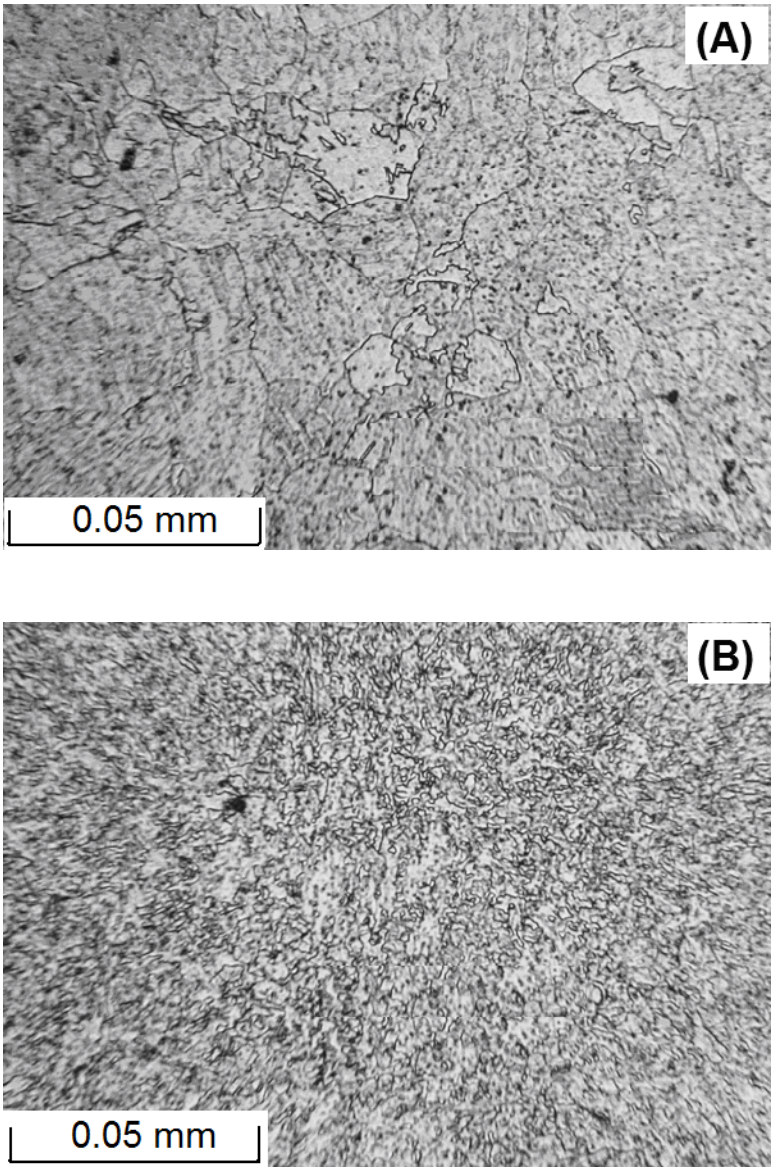

Figure 5.4 Pictures of microstructures of base and weld materials
(A) pure base and (B) pure weld materials

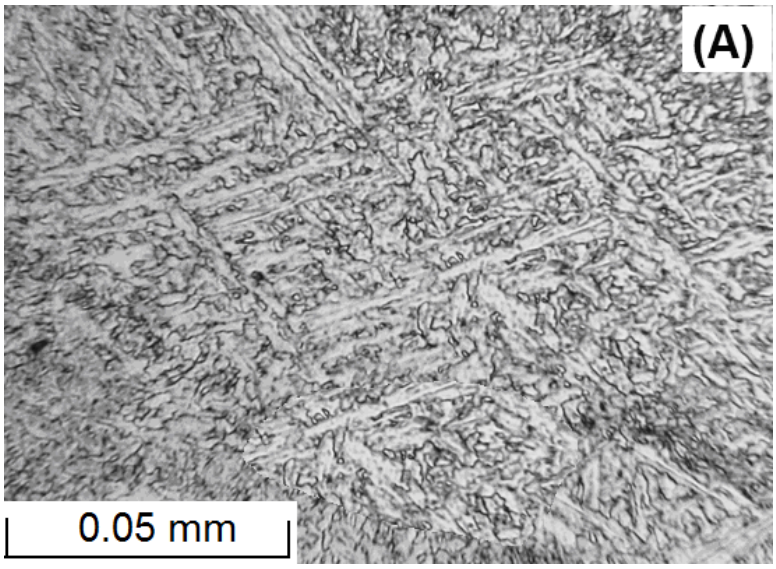
(A)
0.05 mm

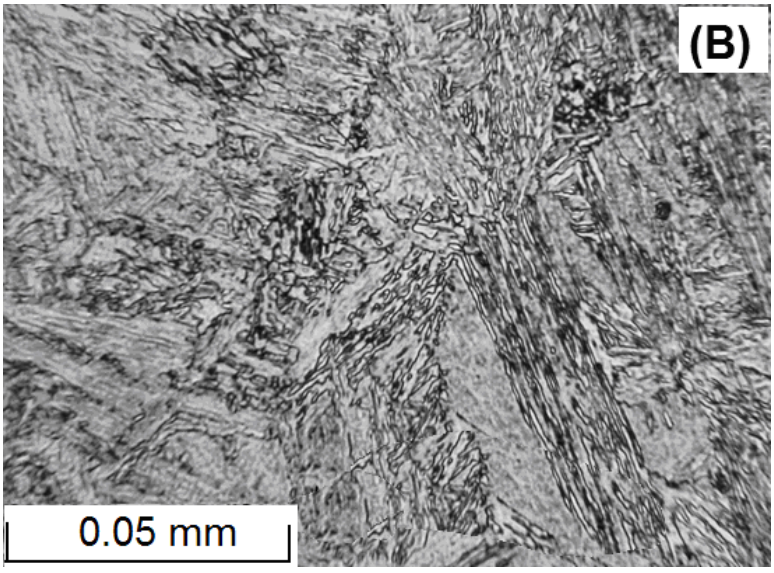
(B)
0.05 mm

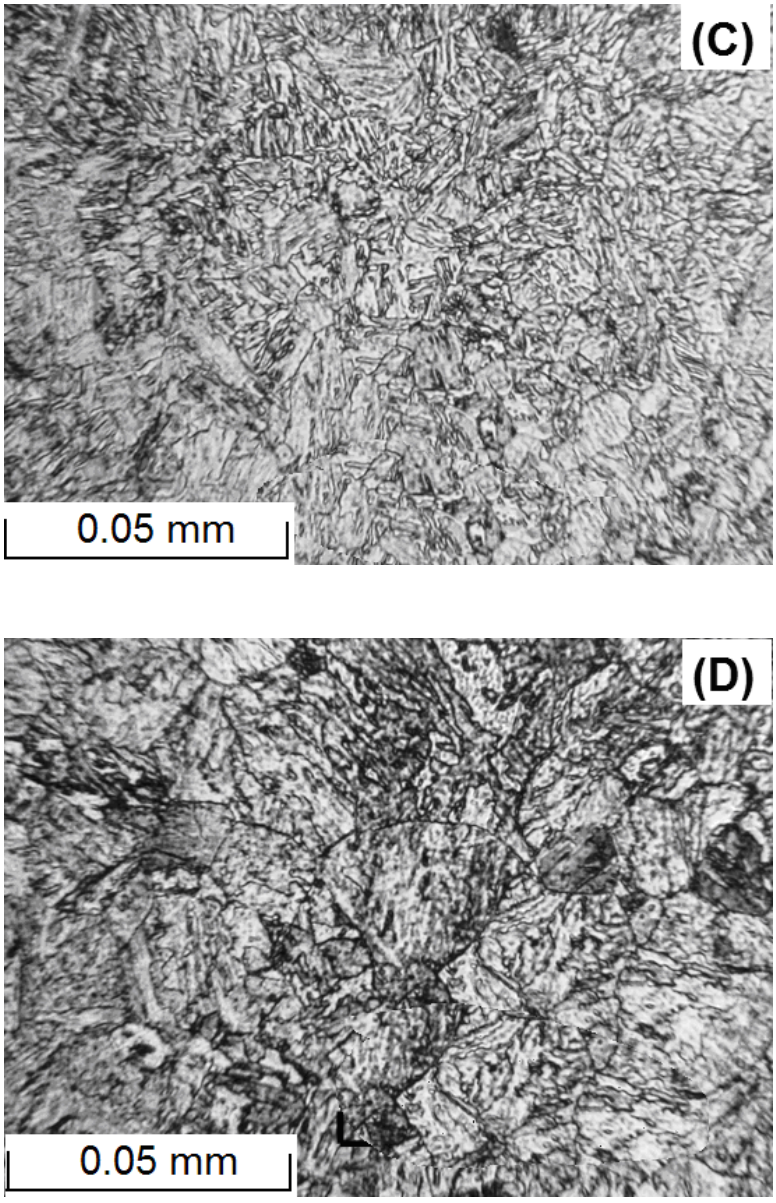

Figure 5.5 Pictures of microstructures of HAZ from close weld to close base (A to D)

5.5 Fatigue Test Results and Discussion

To accurately correlate fatigue life with elastic and plastic strain, same Coffin-Manson-Basquin's relation [24-26], more details discussed in chapter 2, is used. The total strain verse fatigue life can be rewritten as:

$$\frac{\Delta\varepsilon}{2} = \frac{\sigma'_f}{E}(2N_f)^b + \varepsilon'_f(2N_f)^c \tag{5.1}$$

where $\Delta\varepsilon_e/2$ and $\Delta\varepsilon_p/2$ are the elastic and plastic strain amplitude respectively, σ'_f is fatigue strength coefficient, and b is fatigue strength exponent. ε'_f is the fatigue ductility coefficient, and c is the fatigue ductility exponent. $2N_f$ is reversals to failure (2*cycles to failure).

The detailed decomposition of total strain into elastic and plastic portions versus reversals for base, weld, and HAZ are shown in Fig. 5.6 (A-C). It can be seen that the data is well fitted by linear regression as the form of Eq. 5.1 for elastic and plastic portions correspondingly. The parameters obtained from this procedure are summarized in Table 5.2. Figure 5.6 (D) shows the relation between total mechanical strain amplitude versus number of reversals ($2N_f$) for base, weld, and HAZ materials. The fatigue life of base is apparently longer than both weld and HAZ. Quantitatively, it is shown that the life of the base is roughly twice of the weld and four time of the HAZ at the same strain amplitude. In addition, the life of HAZ is almost identical to weld at 0.8% strain amplitude, and it declines dramatically at small strain amplitude, see Fig. 5.6 (D). Table 5.3 lists the fatigue test results of SA387 Gr. 11 Cl 2 base, weld, and HAZ materials.

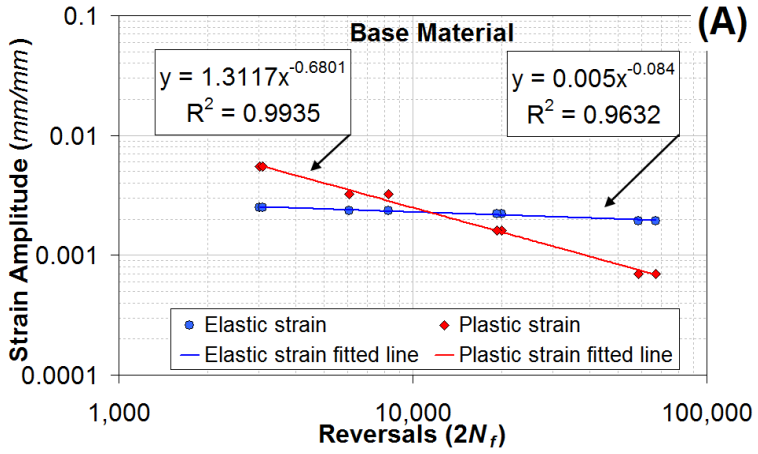
(A)
Base Material
y = 1.3117x^-0.6801
R^2 = 0.9935
y = 0.005x^-0.084
R^2 = 0.9632
Elastic strain
Plastic strain
Elastic strain fitted line
Plastic strain fitted line
Strain Amplitude (mm/mm)
0.1
0.01
0.001
0.0001
1,000
10,000
100,000
Reversals (2N_f)

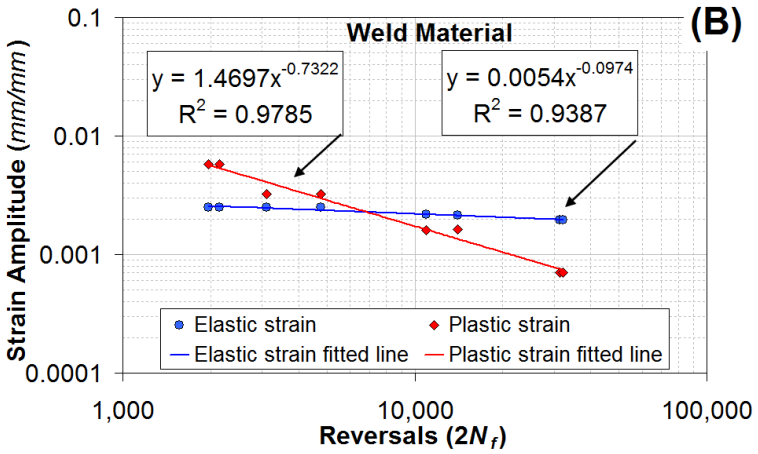
(B)
Weld Material
y = 1.4697x^-0.7322
R^2 = 0.9785
y = 0.0054x^-0.0974
R^2 = 0.9387
Elastic strain
Plastic strain
Elastic strain fitted line
Plastic strain fitted line
Strain Amplitude (mm/mm)
0.1
0.01
0.001
0.0001
1,000
10,000
100,000
Reversals (2N_f)

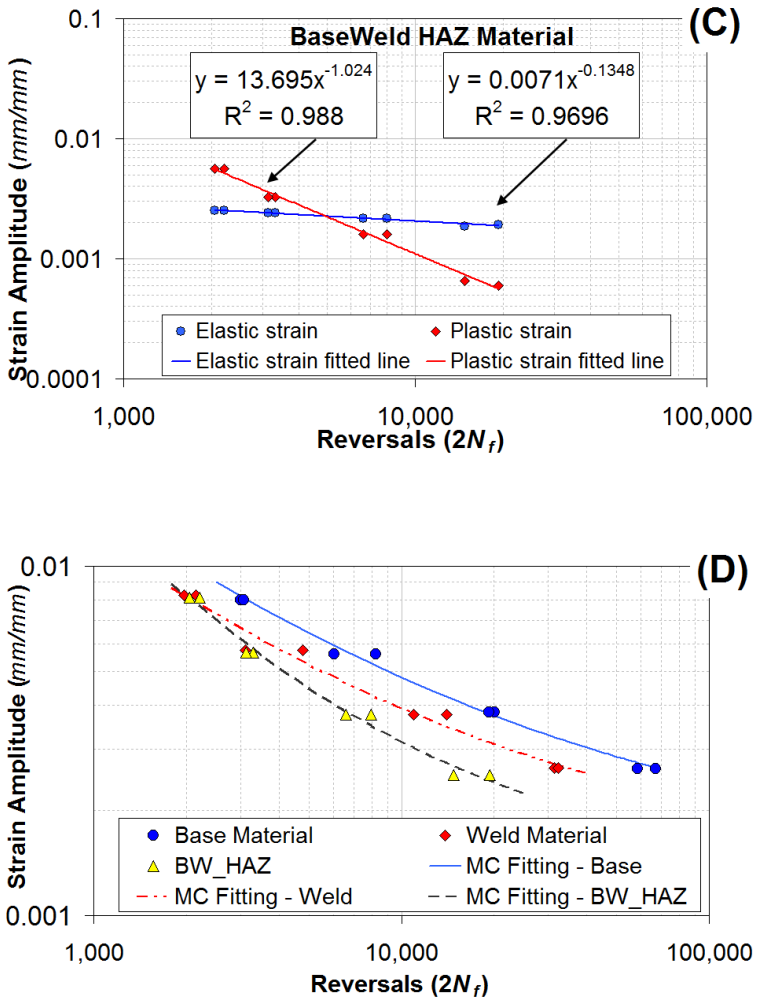

Figure 5.6 Summary of elastic amplitudes and plastic amplitudes vs. $2N_f$

Table 5.2 Summary of Fatigue Coefficients of SA387-11-2 Base, Weld and HAZ

	Base	Weld	BW_HAZ
Young's Modulus (GPa) - E	197.6	189.1	184.9
Fatigue strength coefficient (MPa) - σ'_f	988	1021.1	1312.8
Fatigue strength exponent - b	-0.084	-0.0974	-0.1348
Fatigue ductility coefficient - ε'_f	1.3117	1.4697	13.6948
fatigue ductility exponent - c	-0.6801	-0.7322	-1.024

Table 5.3 Summary of LCF test results of SA387-11-2 Base, Weld and HAZ

Base Material			Weld Material			BW_HAZ		
$\Delta\varepsilon/2$ (mm/mm)	$\Delta\sigma/2$ at $N_f/2$ (MPa)	Reversals ($2N_f$)	$\Delta\varepsilon/2$ (mm/mm)	$\Delta\sigma/2$ at $N_f/2$ (MPa)	Reversals ($2N_f$)	$\Delta\varepsilon/2$ (mm/mm)	$\Delta\sigma/2$ at $N_f/2$ (MPa)	Reversals ($2N_f$)
0.0080	403.7	3,004	0.0082	416.7	2,148	0.0081	415.8	2,052
0.0080	403.7	3,084	0.0082	417.2	1,964	0.0081	414.9	2,214
0.0056	389.5	6,060	0.0058	395.1	4,782	0.0056	400.6	3,306
0.0056	382.3	8,262	0.0058	397.2	3,106	0.0056	402.3	3,138
0.0038	362.5	20,080	0.0038	373.1	10,940	0.0038	384.3	7,980
0.0038	362	19,320	0.0038	370.1	14,000	0.0038	384.6	6,620
0.0026	346.4	67,140	0.0026	352.1	31,460	0.0025	361.5	19,360
0.0026	345.3	58,480	0.0026	353.4	32,240	0.0025	368.1	14,780

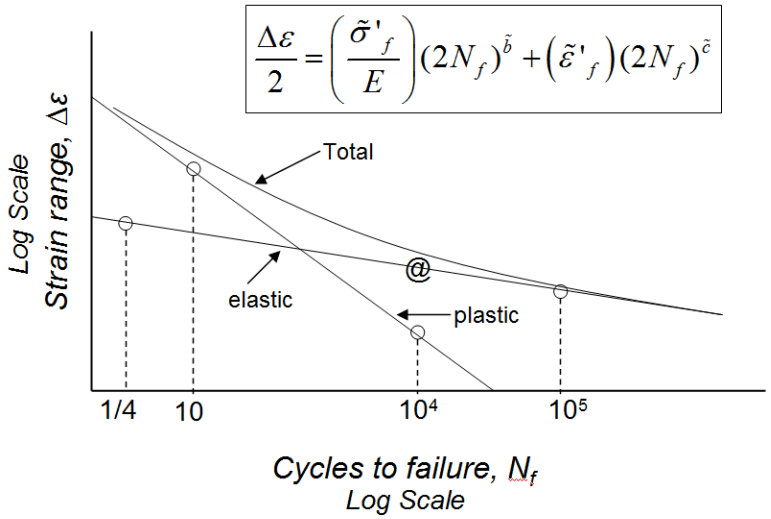

Figure 5.7 Demonstration of four-point correlation method

In 1965, Manson [1] independently proposed a fatigue life prediction method, called Four-Point Correlation (FPC) method. The fatigue life can be predicted based on ultimate tensile strength, true fracture strength, Young's modulus and reduction of area from tensile tests. As shown in Fig. 5.7, this approach uses two points on elastic and two points on the plastic lines, respectively, to construct the Coffin-Manson-Basquin's relation. Eq. (5.1). On the elastic line, a point is located at ¼ cycle with a strain range estimated as $2.5\sigma_f/E$, where σ_f is the true fracture strength of the material obtained by dividing the load at the time of complete fracture in the tensile test by the cross sectional area measured after the separation of the specimen. Another point is at 10^5 cycles whose strain range is estimated as $0.9\sigma_u/E$, where σ_u is the ultimate tensile strength measured during a tensile test. In both cases, E is the Young's modulus. On the plastic line, a point located at 10 cycles is determined, and the corresponding strain range is $1/4D^{3/4}$, where $D = \ln [1/ (1 - RA)]$ is the logarithmic ductility of the material and RA is reduction in cross sectional area. Another point on the plastic line is located at 10^4 cycles. The point shown by the @ symbol at 10^4 cycles is first located on the elastic line and the strain range is observed, and then the strain range on plastic line is obtained by $(0.0132 - \Delta\varepsilon_e^{@})/1.91$.

From the above defined four points, the Manson-Coffin equation in Fig. 5.7 can be obtained through algebraic manipulations as

$$\frac{\Delta\varepsilon}{2}=\frac{\tilde{\sigma}_f^{'}}{E}(2N_f)^{\tilde{b}}+\tilde{\varepsilon}_f^{'}(2N_f)^{\tilde{c}} \tag{5.2}$$

where

$$\tilde{\sigma}_f^{'}=\frac{1}{2}E\times 10^{\tilde{b}\log 2+\log\left(2.5\sigma_f/E\right)} \tag{5.3}$$

$$\tilde{b}=\frac{\log\left[2.5\sigma_f/0.9\sigma_u\right]}{\log\left[1/(4\times 10^5)\right]} \tag{5.4}$$

$$\tilde{\varepsilon}_f^{'}=\frac{1}{2}\times 10^{\tilde{c}\log\frac{1}{20}+\log\left[\frac{1}{4}\left[\ln\{1/(1-RA)\}\right]^{3/4}\right]} \tag{5.5}$$

$$\tilde{c}=\frac{1}{3}\log\left[(0.0132-\Delta\varepsilon_e^{@})/1.91\right]-\frac{1}{3}\log\left\{\frac{1}{4}\left[\ln\left\{1/\left(1-RA\right)\right\}\right]^{3/4}\right\} \tag{5.6}$$

$$\Delta\varepsilon_e^{@}=10^{\tilde{b}\log(4\times 10^4)+\log\left[2.5\sigma_f/E\right]} \tag{5.7}$$

where $\Delta\varepsilon_e^{@}$ is the strain located on the elastic line at 10^4 cycles.

The comparison of tested fatigue lives with the predictions by the FPC method is shown in Fig. 5.8. In this figure, the closer to the 45° reference line the points are, the more accurate are the predictions. Each mechanical property used in this prediction is obtained from the averaged value of two tensile tests for each material. The result shows that the FPC can reasonably predict the fatigue lives of the base material. However, there is a significant deviation between test and predicted fatigue lives for weld and HAZ. Based on the FPC method, the differences in tensile properties of weld and HAZ from the base material do not cause apparent differences in predicted fatigue lives between the three different materials. The predicted fatigue lives of the weld and HAZ by the FPC method are almost two times and four times of the tested fatigue lives of weld and HAZ, respectively, as shown in Fig. 5.8. Therefore, the FPC method cannot be directly applied to the weld and HAZ materials.

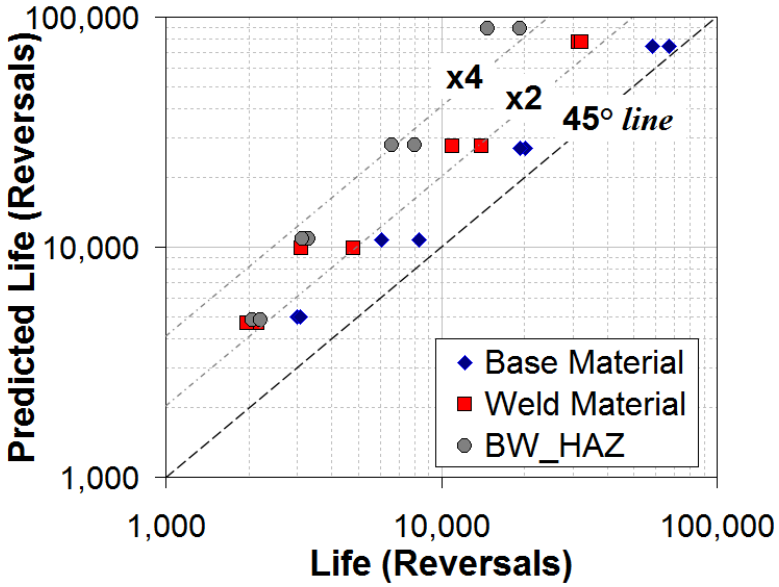

Figure 5.8 Comparison of predicted life by FPC and test life

5.5.1 Proposed Fatigue Life Method

Two reduction factors $R_{plastic}$ and $R_{elastic}$ are introduced to take account of the weld and HAZ materials in the fatigue life prediction. From the study, it is found that at 10^4 cycles, $R_{plastic}$ = 1.5 for weld material and 2.9 for HAZ, and at 10^5 cycles, $R_{elastic}$ = 1.1 for weld material and 1.3 for HAZ. It also assumed that there is no obvious divergence in fatigue lives between them at very short LCF region as seen in Fig. 5.6 (D). Therefore, the parameters $\tilde{b}$ and $\tilde{c}$ become:

$$\tilde{b} = \frac{\log\left[2.5\sigma_f \cdot R_{elastic} / 0.9\sigma_u\right]}{\log\left[1/(4\times 10^5)\right]} \tag{5.8}$$

$$\text{Where } R_{elastic} = \begin{cases} 1 & , \ Base \\ 1.1 & , \ Weld \\ 1.3 & , \ HAZ \end{cases}$$

$$\tilde{c} = \frac{1}{3}\log\left[(0.0132 - \Delta\varepsilon_e^{@})/(1.91\cdot R_{plastic})\right] - \frac{1}{3}\log\left\{\frac{1}{4}\left[\ln\left\{1/(1-RA)\right\}\right]^{3/4}\right\} \tag{5.9}$$

$$\text{Where } R_{elastic} = \begin{cases} 1 & , \quad Base \\ 1.5 & , \quad Weld \\ 2.9 & , \quad HAZ \end{cases}$$

Furthermore, there is not always available for the data of true fracture strength in the literatures. Therefore, it is more convenient to substitute this parameter by more easily accessible properties such as ultimate tensile strength. Reference [1] suggested that the true fracture strength could be approximated by multiplying the ultimate tensile strength by the factor (1+*D*), thus,

$$\sigma_f = \sigma_u (1 + D) = \sigma_u \left\{ 1 + \ln\left[1/\left(1 - RA\right)\right]\right\} \tag{5.10}$$

However, by comparing true facture strength with ultimate tensile strength of all materials in this study, it is found that it is more accurate to correlate the two by the factor [1+ (1+ε_f)].

$$\sigma_f = \sigma_u \left[1 + \left(1 + \varepsilon_f\right)\right] \tag{5.11}$$

where ε_f is the strain measured at the time of complete fracture in the tensile test. A standard tensile test specimen (as shown in Fig. 4.1) with 1" gauge length was used to measure ε_f. If different specimen geometries and gauge lengths were used, it may result in different values of ε_f .

By comparing with the true fracture strengths correlated from reduction of area (RA) and elongation at failure in Fig. 5.9 for base, weld, and HAZ, the values obtained from elongation draw more closely on the measured values.

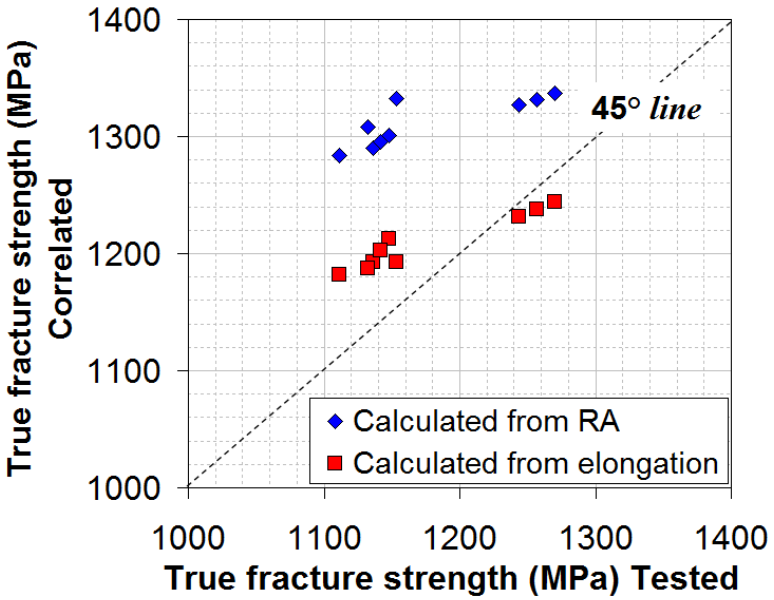

Figure 5.9 Comparison of true facture strengths

In this case, the true fracture strength in Eq. (5.8-5.9) can be substituted by ultimate tensile strength. Therefore, only Young's modulus, ultimate tensile strength and elongation at specimen failure from tensile test will be sufficient to predict the fatigue life for base, weld, and HAZ. The equations then become:

$$\tilde{\sigma}_f' = \frac{1}{2}E \times 10^{\log\left(0.9\sigma_u/(R_{elastic}\cdot E)\right)-\tilde{b}\log(2\times10^5)} \tag{5.12}$$

$$\tilde{b} = \frac{\log\left[2.5\left[1+\left(1+\varepsilon_f\right)\right]\cdot R_{elastic}/0.9\right]}{\log\left[1/(4\times10^5)\right]} \tag{5.13}$$

$$\tilde{c} = \frac{1}{3}\log\left[(0.0132-\Delta\varepsilon_e^{@})/(1.91\cdot R_{plastic})\right] - \frac{1}{3}\log\left[\frac{1}{4}\left(1+\varepsilon_f\right)^{3/4}\right] \tag{5.14}$$

$$\tilde{\varepsilon}_f' = \frac{1}{2}\times10^{\log\left[(0.0132-\Delta\varepsilon_e^{@})/(1.91\cdot R_{plastic})\right]-\tilde{c}\log(2\times10^4)} \tag{5.15}$$

$$\Delta\varepsilon_e^{@} = 10^{\log(0.9\sigma_u/(E\cdot R_{elastic}))-\tilde{b}} \tag{5.16}$$

Figure 5.10 shows comparison of the modified FPC method with experimental result. From the comparison with the original FPC method on base, weld and HAZ

materials in Fig. 5.8, the modified method has more accurate prediction than the original one for the weld and HAZ materials.

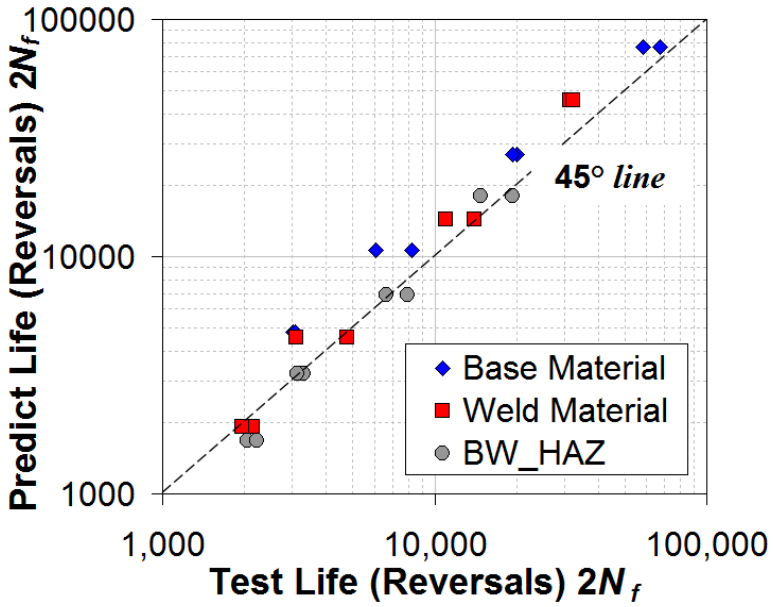

Figure 5.10 Comparison of modified FPC method with test results

To further verify predictive capability of the modified method, fatigue tests on Cr-Mo and its weld and HAZ are found and taken from the literature [27, 28]. The test is conducted by strain-controlled condition at room temperature. All tests are tested under zero mean strain at the strain rate of 10^{-3}. Figure 5.11 A shows comparison of Manson's FPC method and test result, and Fig. 5.11 B shows the prediction of modified four point method using Young's modulus, ultimate tensile strength and elongation at failure. From the Fig. 5.11 A, it shows that all lives of weld and HAZ are over-predicted more than 5 times. However, the predicted lives of weld and HAZ by modified method have better agreement with test result. Therefore, the modified FPC method could have favourable performance in prediction lives of weld and HAZ materials.

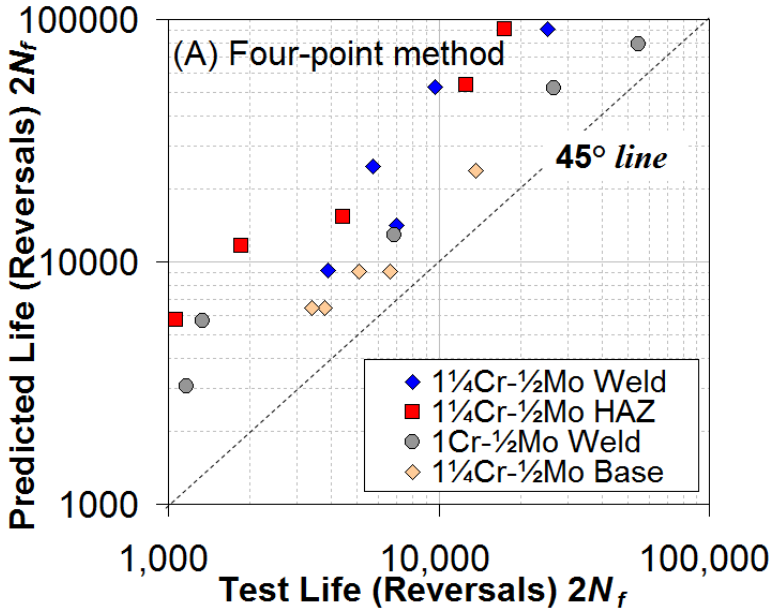

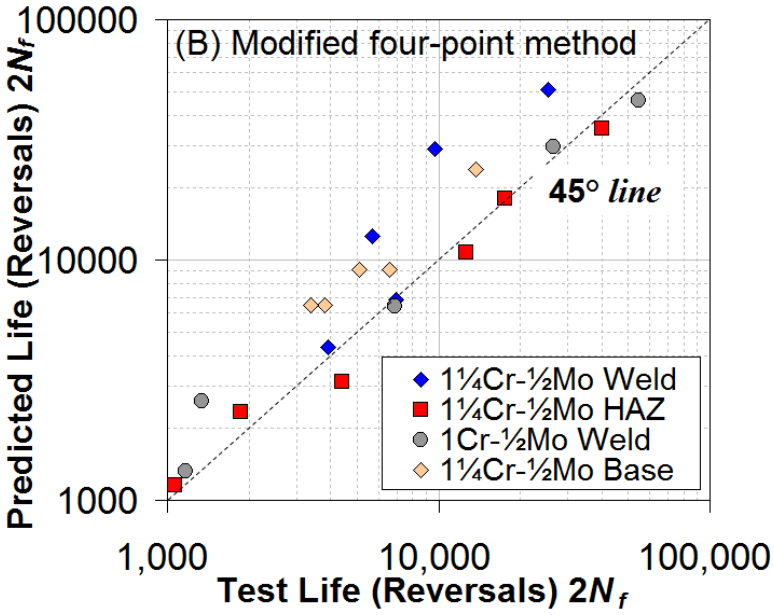

Figure 5.11 Comparison of FPC and Modified methods

Figure 5.12 shows the nominal stress changes in number of cycles of the three materials during the fatigue tests with strain amplitudes of 0.38% and 0.26% and the abscissa of the figures shows in log scale. From the plots, it is seen that after cyclically stabilized at early stage of their life, all materials (base, weld, and HAZ) show a gradually decline of stress range before a sudden drop. Table 5.4 summarizes load decline rate for all three materials at the strain amplitude of 0.38% and 0.26%. It first points out the ratio of number of cycles measured at 10% load declined from stabilized level to number of cycles at failure. This may indicate the period for crack initiation with respect to its final life, $N_{10\%}/N_f$. From the table, it is confirmed that HAZ has the shortest period for crack initiation among the others. In addition, the decline rate of the load from the time when load drops to 10% of the stabilized level to failure might be also an indicator for the crack growth rate during this period. From the result, the load of HAZ declines 3 times faster than base, and 1.5 to 2 times quicker than weld. Therefore, it is proven that the HAZ not only has the shorter period for crack initiation, but also has the faster crack growth rate than base and weld.

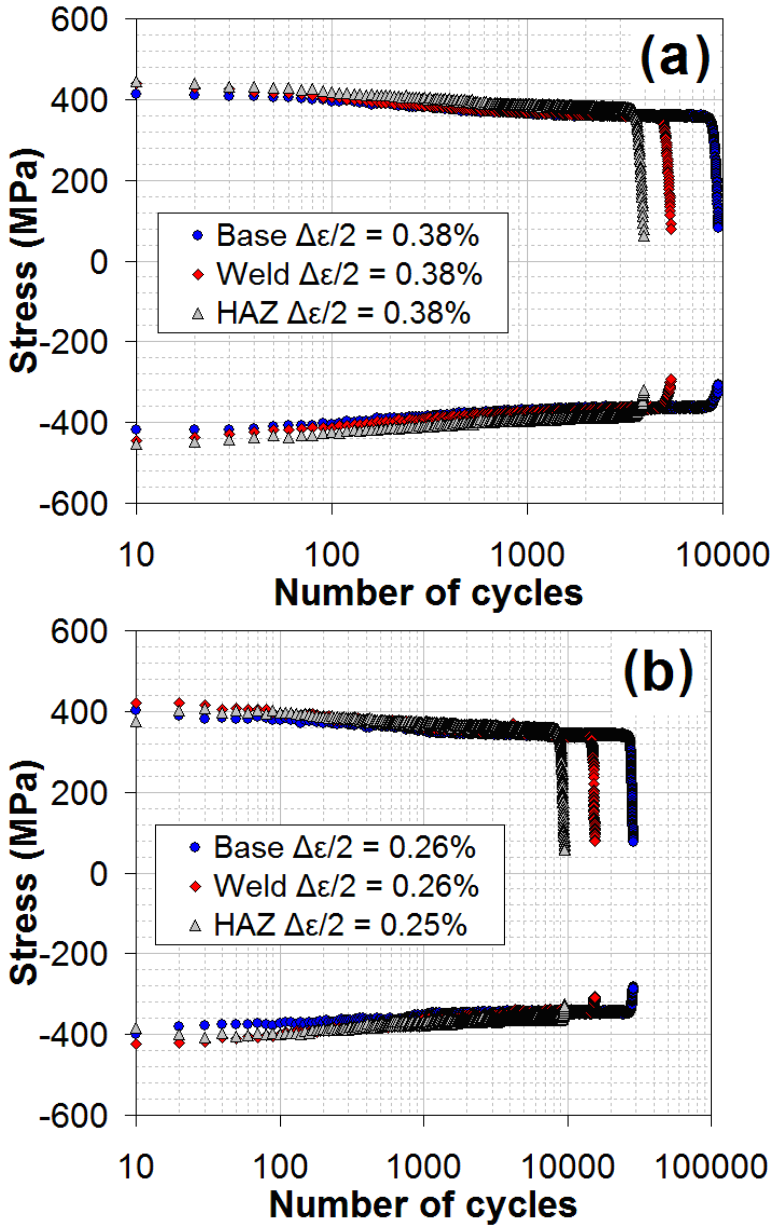

Figure 5.12 Plots of stress level vs. number of cycles

Table 5.4 statistical of load decline path

	Δε/2 = 0.38%		Δε/2 = 0.26%	
	$N_{10\%}/N_f$ (%)	$L/N_{10\%\sim f}$ (kN/cycle)	$N_{10\%}/N_f$ (%)	$L/N_{10\%\sim f}$ (kN/cycle)
Base	93.6%	0.033	95.8%	0.016
Weld	93.0%	0.051	95.8%	0.034
HAZ	92.3%	0.106	93.7%	0.052

Figure 5.13 shows the pictures of the tested specimens for HAZ, base, and Weld. There are total 8 specimens tested for each material. All HAZ specimens ruptured closely along the interface between base and weld. Therefore, it indicated that the heat affected zone is the weak spot of the weld joint.

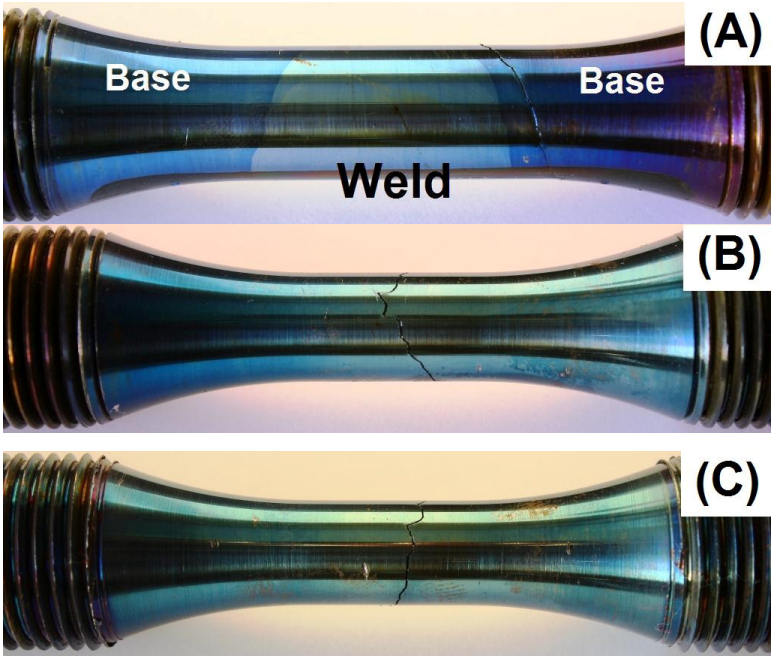

Figure 5.13 Photos of test fatigue specimens (A) HAZ (B) base (C) weld

5.6 Conclusions

Fatigue tests are increasingly being performed to simulate and investigate real-world failures of components in various structures. There are a few existing fatigue life prediction methods based on material's uniaxial tensile test data. There are lots of industrial components, such as pressure vessel, piping, etc., are commonly constructed by welding different sections together. However, there are even fewer effective fatigue life prediction methods applicable to the heat affected materials. In this study, coke drum material SA 387 Gr. 11 CL. 2 are used to help in developing fatigue life prediction models for base, weld, and HAZ materials based on their uniaxial tensile test data.

The fatigue life of base is roughly twice of the weld and four time of the HAZ at the same strain amplitude. The comparison of tested fatigue lives with the predictions by the FPC method shows that the FPC method can reasonably predict the fatigue lives of base material. However, there is a significant deviation between test and predicted lives for weld and HAZ materials. Two reduction factors $R_{plastic}$ and $R_{elastic}$ are then introduced into the FPC method to account for the heat-affected effect in the weld and HAZ materials. In addition, true facture strength could be better correlated with ultimate tensile strength by the factor of $[1+ (1+\varepsilon_f)]$. The predicted fatigue lives of weld and HAZ by the modified FPC method have good agreement with test results. Finally, from the investigation of load decline rate for all three materials, it is proven that the HAZ not only has the shorter period for crack initiation, but also has the faster crack growth rate than base and weld materials.

References

[1] Manson, S.S., "Fatigue: A complex subject – Some Simple Approximations," Proceedings, Society of Experimental Stress Analysis, Vol. 12, No. 2, (1965)

[2] Socie, D.F., Mitchell, M.R. and Caulfleld, E.M. 'Fundamentals of modern fatigue analysis' Fracture Control Program Report No. 26 (University of Illinois, USA, 1977)

[3] Muralidharan, U., Manson, S. S., "A modified universal slopes equation for estimate of fatigue characteristics of metals", Journal of Engineering Materials and Technology, Vol. 110, (1988) 55-58

[4] Ong, J. H., "An improved technique for the prediction of axial fatigue life from tensile data", International Journal of Fatigue, Vol. 15-3 , (1993) 213-219,

[5] Baumel, A., Seeger, T., "Material data for cyclic loading", Amsterdam: Elsevier Science Publishers (supplement I); (1990)

[6] Park, J. H., Song, J. H., "New estimation method of fatigue properties of aluminum alloys", Journal of Engineering Materials and Technology, Transactions of the ASME Vol. 125, (2003) 208-214

[7] Roessle, M. L., Fatemi, A., "Strain-controlled fatigue properties of steels and some simple approximation", International Journal of Fatigue, Vol. 22, (2000) 495-511,

[8] Ong, J. H., "An evaluation of existing methods for the prediction of axial fatigue life from tensile data", International Journal of Fatigue, Vol. 15, (1993) 13-19,

[9] Penso, J. A., Lattarulo, Y. M., Seijas, A. J., Torres, J., Howden, D., and Tsai, C. L., "Understanding Failure Mechanisms to Improve Reliability of Coke Drum," PVP (Am. Soc. Mech. Eng.), 395, (1999), pp. 243–253.

[10] Pieper, C.J., Shockley, L.R. and Stewart, C.W. "Coke Drum Design-Longer Life through Innovation", AIChE 2000 Spring National Meeting, Atlanta, GA, March 5-9, (2000).

[11] Richard Boswell, "Coke Drum Bulges", Stress Engineering Services, May, (2001).

[12] Ramos, A., Rios, C., Vargas, J., Tahara, T., and Hasegawa, T., "Mechanical Integrity Evaluation of Delayed Coke Drums," Fitness for Adverse Environments in Petroleum and Power Equipment, ASME, New York, Vol. 359,(1997), pp.291–298.

[13] Ramos, A., Rios, C., Johnsen, E., Gonzalez, M., and Vargas, J., "Delayed Coke Drum Assessment Using Field Measurements and FEA," Analysis and Design of Composite, Process, and Power Piping and Vessels, ASME, New York, Vol. 368, (1998), pp. 231–237.

[14] Ramos, A. J., Rios, C. and Vargas, J.A.R., "Fatigue Life Prediction of Delayed Coke Drums", Vision Techenologica, Vol.6, (1999), pp. 93-100.

[15] Boswell R.S., Ferraro T., "Remaining Life Evaluation of Coke Drums", Plant Engineering, Design and Responsibility Symposium, Energy Engineering Conference, (1997).

[16] Sohel M Panwala M, K. N. Srinviasan, S. L. Mehta, "Creep-fatigue interaction in coke drums: An approach based on API 579-1/ASME FFS-1 2007", Proceeding of the ASME 2009 Pressure Vessels and Piping Division conference 2009, Prague, Czech Republic

[17] API Proceedings "1996 APE Coke Drum Survey-Final Report", 1996 American Petroleum Institute, Washington, DC

[18] Stewart, C. W., Stryk, A. M., and Presley, L., "Coke drum design", Chicago Bridge & Iron, PTQ Q3, (2006).

[19] ASTM, E8 "Standard Test Methods of Tension Testing of Metallic Materials," ASTM Standards, American Society for Testing and Materials, (2008).

[20] ASME Boiler and Pressure Vessel Code, Section VIII, Division 2, Design and Fabrication of Pressure Vessels, (2010).

[21] Chen, J., "Experimental Study of Elastoplastic Mechanical Properties of Coke Drum Materials", Masters Dissertation, University of Alberta, Edmonton, (2010).

[22] Yamamoto, t., Huhetaoli, K. A., Niimoto, S., Ohata, M., Tagawa, T., Minami, F. "Investigation of Bulging Behavior of Coke Drum -A practical analysis of bulging under complex quench conditions-", Proc. Pressure Vessels & Piping Division Conf., ASME (2011): PVP2011- 57428.

[23] ASTM, E21 "Test Methods for Elevated Temperature Tension Tests" ASTM Standards, American Society for Testing and Materials, 2008

[24] Basquin, O.H. "The exponential law of endurance tests", ASTM proceeding. 10,(1910), pp.625-630.

[25] Coffin, L. F. Jr., "A study of the effects of cyclic thermal stresses on a ductile metal", Trans. ASME, 76, (1954), pp. 931-950.

[26] Manson, S.S., "Behaviour of materials under conditions of thermal stress", Heat Transfer Symposium, University of Michigan, 1953, 9-75. See also NACA-TN-2933, (1953).

[27] Sasaki, Y., Niimoto, S., “Study on skirt-to-shell attachment of coke drum by evaluation of fatigue strength of weld metal”, Proc. Pressure Vessels & Piping Division Conf., ASME(2011): PVP2011- 57314.

[28] Anonym. “Data Sheets on Low-Cycle Fatigue Properties at Elevated-Temperature for Weld and Base Metals of SCMV2-2NT (1Cr-0.5Mo) Low Alloy Steel Plate for Boiler and Other Pressure Vessels” *NRIM Fatigue Data Sheet (1993):1. TEMA*. Web. 22 Jan. (2014).

CHAPTER 6 Temperature-Dependent Fatigue Life Prediction Method for Coke Drum Materials

Fatigue life data has more and more important role in design and failure analysis. There are a few existing methods for life prediction based on material tensile properties. However, few estimation methods are proposed with considering the factor of temperature. Yet, a large number of industrial equipments are operating at elevated temperatures. It is more accurate and reasonable to evaluate their lives at elevated temperatures. Due to the consideration of cost and time, it is not easy to conduct the fatigue test at elevated temperatures. The fatigue life data of some materials is quite limited, especially at elevated temperature. Therefore, it is beneficial for the industries and academic research to have a method that can accurately estimate the material lives at both lower and elevated temperatures, only based on tensile properties. In this study, several commonly used coke drum materials are selected in this evaluation. Modified universal slopes and median methods give the best prediction for these materials at lower (20°C~100°C) and elevated temperatures (400°C~500°C), respectively. None of the methods can give accurate estimation at both temperature ranges. A new temperature-dependent method, which only uses tensile strength, Young's modulus and elongation at fracture, is then proposed. By comparing with other existing methods at both temperature ranges, the new proposed method gives better prediction to the test result.

6.1 Introduction

Fatigue life data and information play a significant role in engineering design and failure analysis. Safer and more confident product and equipment can be designed with the consideration of fatigue factors. However, accessibility of the accurate fatigue data is not always guaranteed for certain materials. Meanwhile, performance of these tests is usually quite costly and time-consuming especially if environmental effect is involved. Consequently, for the initial design phase, it is greatly helpful to estimate the fatigue life from knowledge of the more easily obtained material properties such as from uniaxial tensile test.

One of the first methods for prediction of fatigue life based on the tensile test was proposed by Manson [1], which is called four point correlation method. The fatigue life can be predicted based on ultimate tensile strength, true fracture strength, Young's modulus and reduction of area from tensile tests. At the same time, Manson [1] proposed another method, based on tensile data, called universal slope method. This method has less complicated expressions for each fatigue parameters, and it assumes that the slopes of the plastic and elastic – lives lines are constants for all materials. Due to its simplicity of the equation, this method has been widely used. Muralidharan and Manson [2] proposed a modified universal slopes method based on the original one to improve its accuracy. The modified method is still based on the same tensile data except that the coefficients and exponents of the expression had been modified. Later on, Socie et al [3] proposed a method based on correlating the slope of the elastic line with the ultimate tensile strength. Baumel and Seeger [4] proposed an expression, called uniform material law, used for unalloyed and low alloy steels. It is assumed that the slopes of plastic and elastic lines for the whole group of materials are very close to the values in the modified universal slopes method. This method uses only tensile strength and Young's modulus of the material for estimation of strain-fatigue life relations. Based on Manson's four point correlation method, Ong [5] proposed a modified method based on 49 steels. All fatigue parameters are correlated with tensile data differently than the original method. However, the coefficient of the elastic line is assumed to be equal to the true fracture strength of the

material. The coefficient of plastic line is approximated to be equal to the logarithmic ductility of the material. These assumptions make the expression less perplexed than the original one. Meggiolaro and Castro [6] proposed a median method and used 724 steels to statically analyze the fatigue parameters based on different fatigue prediction methods. Based on the 724 steels, the median values of each of these four fatigue parameters, which are assumed to be constant values except the fatigue strength coefficient, are estimated.

Ong [7] has evaluated three commonly used methods, the four-point correlation method, the universal slopes method and Socie's method based on 49 steels, and found that the four-point correlation and universal slopes methods give the best solution of the three methods for estimating fatigue life in terms of material properties from uniaxial tensile test. Based on the evaluation of fraction of data within a life factor of 5, the four point correlation method has the highest fraction falling within that range from the experimental values. Later on, Park and Song [8] evaluated six prediction methods mentioned above except the median method. There are 116 steels, 16 aluminum alloys and six titanium alloys used in this evaluated based on the tensile properties. The modified universal slopes method provides best results. Based on the reviewed methods, it is found that most of the methods were proposed only for room temperature fatigue life estimation or at lower temperature ranges. Some of the methods [6] were proposed by using the material data at temperatures varying from 21 to 800°C, without considering the temperature influence on the fatigue life. Therefore, there is lack of life estimation methods taking into consideration of temperature.

In this study, several different coke drum materials are selected in this evaluation. Coke drums are vertical pressure vessels used in the delayed coking process in petroleum refineries and oil sands plants. They are normally constructed of carbon or low alloy carbon steels and internally clad with stainless steel to protect the coke drums from corrosion. Many researches found that low cycle fatigue (LCF) is considered the failure mode for coke drums. [9-11] However, there are limited studies on the fatigue life estimation for coke drums which are only based on the base material at a single

temperature [12-14]. Some [15, 16] have only used the ASME fatigue design curve of base material to evaluate the fatigue life of coke drums, which could have huge divergence in real service life. Therefore, the fatigue life data of coke drum materials is quite limited, especially at elevated temperature. It is beneficial for the industries and academic research to have a method to accurately estimate coke drum materials at both lower and elevated temperatures only based on tensile properties.

In this chapter, three coke drum materials are tested at 100°C and 480°C respectively, and four more coke drum materials, which has both tensile and fatigue life data available, are selected from the literature at room temperature, 400°C and 500°C. Seven estimation methods are first evaluated based on the selected coke drum materials data at these temperature ranges. A new temperature-dependent method is proposed. It only uses Young's modulus, ultimate tensile strength, elongation at fracture and temperature as input data to estimate strain-life relations.

6.2 Specimen and Materials

Two different types of specimens used in this study: Uniaxial tensile test specimen (Fig. 4.1) and isothermal low cycle fatigue (LCF) specimen (Fig. 3.2). The more detailed geometry of LCF specimen is discussed in Chapter 3. The tensile test specimen is designed according to ASTM E8 [17], and the more detailed dimension is described in chapter 4.

In this study, three different materials are tested at 100°C and 480°C. Two base materials, SA387 Gr 22 CL2 and SA204 Gr C, and one clad material, SA204 TP410S, are selected and tested. The nominal chemical composition of SA 387 Gr 22 CL 2 and SA 204 Gr C are 2¼ Cr- 1Mo and C-½Mo respectively. The 410S stainless steel has nominal chemical composition of 13Cr. Both plates were normalized and tempered after fabrication. The data from these steels in addition to three other base steels of coke drums at room temperature and 500°C published by National Research Institute for Metals (NRIM) [18-20] and Sumitomo Heavy Industries [21] were then used to examine

correlations among the various monotonic and fatigue properties. These include relationships between ultimate tensile strength, logarithmic ductility and fracture strength with fatigue strength coefficient, fatigue strength exponents, fatigue ductility coefficient, and fatigue ductility exponent. These additional base materials include SA387 Gr 11 CL 2 with nominal composition of 1¼Cr-½Mo, SA387 Gr 12 CL 2 with nominal composition of 1Cr-½Mo, and SA387 Gr 22 CL 2 with nominal composition of 2¼Cr-1Mo. These chosen materials cover most of the base and clad materials for present coke drum constructions. Therefore, there are total seven groups of materials data at lower temperature (room temperature and 100°C) and 6 groups of data at elevated temperatures (400~500°C) in this evaluation.

6.3 Experimental Equipment and Procedures

The high temperature fatigue test system discussed in chapter 3 was used to conduct LCF testing in this investigation. A thermal couple is carefully placed in the center of the specimen for each test, which is recommended by ASTM E2368 [22]. All system components are calibrated and verified before testing according to ASTM E606 [23]. The more detailed design and development of this system are described in [24].

The uniaxial tensile tests are performed, at a strain rate of 0.005/sec, according to ASTM standards [17, 25]. The tests are conducted at 100°C and 480°C respectively for SA 387 Gr 22 CL 2 (SA 387), SA 204 Gr C (SA 204C) and SA 240 TP 410S (410S). The selected test temperature of 480°C represents the upper bound of usual operational temperature for coke drums. The specimens are pulled till complete separation, and then the mechanical properties are obtained from the test data. The LCF tests are performed under strain-controlled condition at the same strain rate of 0.005/sec throughout all tests. The tests are conducted for fully-reversed cyclic loading ($R = \varepsilon_{\min}^{mech} / \varepsilon_{\max}^{mech} = -1$) at both temperatures. There are two tests conducted at each strain amplitude to insure the repeatability and accuracy of the data. Each fatigue test stops when maximum load reaches 17% of the load at $N_f/2$ (stabilized maximum load).

6.4 Mechanical Properties

There are two tests performed for each material at 100°C or 480°C. The averaged mechanical properties obtained from both tests, such as Young's modulus, yield strength, ultimate tensile strength, elongation at fracture, reduction of area, and true fracture strength of the coke drum materials, are summarized in Table 6.1. For uniaxial monotonic tensile tests, the variation of elongation and reduction of area for SA 387 is less sensitive to temperature than for SA 204C and 410S. Young's modulus, yield strength (at 0.2% offset strain), and ultimate tensile strength of SA 387 at 100°C and 480°C are higher than that of SA 204C at corresponding temperatures. This is mainly due to the higher content of Cr-Mo in SA 387. The yield strength and ultimate tensile strength of 410S have the lowest values among the ones of SA 387 and SA 204C.

Table 6.1 Mechanical properties of SA387-22-2, SA204-C, TP410S

ASME	SA 387 Gr 22 CL2	SA 204 Gr C	SA 240 TP 410S	SA 387 Gr 22 CL2	SA 204 Gr C	SA 240 TP 410S
Nominal Chemical Composition	2¼ Cr-1Mo	C-½Mo	13Cr	2¼ Cr-1Mo	C-½Mo	13Cr
Test Temperature	100°C	100°C	100°C	480°C	480°C	480°C
Young's Modulus (GPa) – E	202.7	195.4	184.5	175	154.8	165.7
Yield Strength (MPa) – $\sigma_{0.2\%}$	484.7	371.1	253	405.8	256.8	161.5
Ultimate Tensile Strength (MPa)σ_U	605.9	532	400	505.6	474.3	276.5
Elongation (%) - ε_f	34.4	38.8	39.3	32	36.9	31.9
Reduction of Area (%) – RA	76.9	68	81.5	76.7	81.6	80.2
True Fracture Strength (MPa) - σ_f	1363.4	1114.3	1110	767	1152.5	657

6.5 Fatigue Life Results

Basquin [26] first proposed that the fatigue life could be correlated with stress or elastic strain. Later on, Coffin [27] and Manson [28] found that it is more accurate to correlated fatigue life with plastic strain by a similar power law function, especially at LCF region as shown in Fig. 6.1. Therefore, in combining Coffin-Manson-Basquin's relation, the total strain verse fatigue life can be rewritten as

$$\frac{\Delta\varepsilon}{2}=\frac{\Delta\varepsilon_e}{2}+\frac{\Delta\varepsilon_p}{2}=\frac{\sigma'_f}{E}(2N_f)^b+\varepsilon'_f(2N_f)^c \tag{6.1}$$

where $\Delta\varepsilon_e/2$ and $\Delta\varepsilon_p/2$ are the elastic and plastic strain amplitude respectively, σ'_f is fatigue strength coefficient, and b is fatigue strength exponent. ε'_f is the fatigue ductility coefficient, and c is the fatigue ductility exponent. $2N_f$ is reversals to failure (2*cycles to failure). Table 6.2 summarizes the fatigue parameters of all coke drum materials used in the evaluation of the prediction methods. It includes wide range of base materials and one clad material at both lower temperature (room temperature and 100°C) and elevated temperatures (400°C ~500°C) in this evaluation.

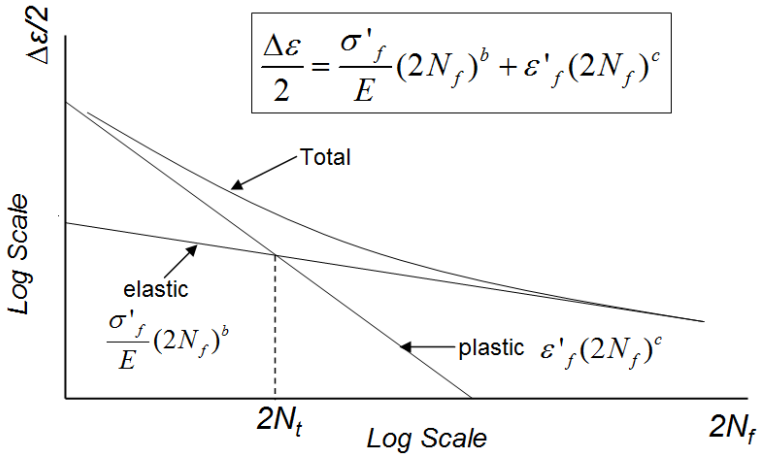

Figure 6.1 Demonstration of elastic and plastic strain vs. fatigue lives

Table 6.2 Summary of fatigue parameters for SA387, SA204-C, TP410S

	σ'_f/E	b	ε'_f	c
2¼ Cr- 1Mo (100°C)*	0.0074	-0.1301	0.7048	-0.6217
C-½Mo (100°C)*	0.0076	-0.1387	0.5959	-0.5755
13Cr (100°C)*	0.0063	-0.1313	0.4110	-0.5331
2¼ Cr- 1Mo (RT)**	0.0036	-0.0455	1.0401	-0.7139
1Cr-½Mo (RT)**	0.0058	-0.1268	0.4183	-0.5313
1¼Cr-½Mo (RT)**	0.0042	-0.0845	0.3963	-0.5518
1¼Cr-½Mo (RT)***	0.0040	-0.0661	0.6692	-0.6195
2¼ Cr- 1Mo (480°C)*	0.0046	-0.0943	0.5271	-0.6440
C-½Mo (480°C)*	0.0045	-0.0788	1.1084	-0.7169
13Cr (480°C)*	0.0019	-0.0251	0.5652	-0.6043
2¼ Cr- 1Mo (500°C)**	0.0026	-0.0219	2.1200	-0.8187
1Cr-½Mo (400°C)**	0.0035	-0.0575	1.8520	-0.7541
1¼Cr-½Mo (500°C)**	0.0038	-0.0838	0.7566	-0.7071

* Tested materials ** NRIM *** Sumitomo

6.6 Review of Fatigue Life Prediction Methods

There are seven commonly used fatigue life prediction methods based on tensile data evaluated in this study. They are briefly described in the following:

6.6.1 Four-Point Correlation Method (FPCM)

Manson [1] independently proposed a fatigue life prediction method, called four-point correlation method. The fatigue life can be predicted based on ultimate tensile strength, true fracture strength, Young's modulus and reduction of area from tensile tests. This approach uses two points on elastic and plastic lines respectively to correlate them. Coefficients used in Eq. (6.1) for this method can be characterized by the following relations:

$$\sigma_f^{'} = \frac{1}{2} E \times 10^{b\log 2 + \log\left(2.5\sigma_f / E\right)} \tag{6.2}$$

$$b = \frac{\log\left[2.5\sigma_f / 0.9\sigma_u\right]}{\log\left[1/(4\times10^5)\right]} \tag{6.3}$$

$$\varepsilon_f^{'} = \frac{1}{2}\times10^{c\log\frac{1}{20}+\log\left[\frac{1}{4}\left[\ln\{1/(1-RA)\}\right]^{3/4}\right]} \tag{6.4}$$

$$c = \frac{1}{3}\log\left[(0.0132-\Delta\varepsilon_e^{@})/1.91\right]-\frac{1}{3}\log\left\{\frac{1}{4}\left[\ln\left\{1/\left(1-RA\right)\right\}\right]^{3/4}\right\} \tag{6.5}$$

$$\Delta\varepsilon_e^{@} = 10^{b\log(4\times10^4)+\log\left[2.5\sigma_f/E\right]} \tag{6.6}$$

where $\Delta\varepsilon_e^{@}$ is the strain located on the elastic line at 10^4 cycles.

6.6.2 Universal Slope Method (USM)

Manson [1] proposed the universal slopes method to predict the isothermal fatigue lives of metal materials based on ultimate tensile strength, Young's modulus and reduction of area from tensile tests. It assumes that the slopes of the elastic and plastic lines are the same for all materials. The slopes of the elastic and plastic lines are assumed to be equal to -0.12 and -0.6 in Eq. (6.1). The Universal Slopes Equation (USE) developed by Manson [1] is given by

$$\Delta\varepsilon = 3.5\frac{\sigma_u}{E}\left(N_f\right)^{-0.12}+\left[\ln\left(\frac{1}{1-RA}\right)\right]^{0.6}\left(N_f\right)^{-0.6} \tag{6.7}$$

Rewritten in the form of strain amplitude versus reversals, the equation becomes

$$\frac{\Delta\varepsilon}{2} = 1.9018\frac{\sigma_u}{E}\left(2N_f\right)^{-0.12}+0.7579\left[\ln\left(\frac{1}{1-RA}\right)\right]^{0.6}\left(2N_f\right)^{-0.6} \tag{6.8}$$

6.6.3 Modified Universal Slope Method (MUSM)

Muralidharan and Manson [2] proposed a Modified Universal Slopes Method based on the original USM to improve its accuracy. The modified method is still based on ultimate tensile strength, Young's modulus and reduction of area. The slopes of the

elastic and plastic lines become to be equal to -0.09 and -0.56 instead. This modified equation is determined to be:

$$\Delta\varepsilon = 1.17\left[\frac{\sigma_u}{E}\right]^{0.832}\left(N_f\right)^{-0.09} + 0.0266\left[\ln\left(\frac{1}{1-RA}\right)\right]^{0.155}\left[\frac{\sigma_u}{E}\right]^{-0.53}\left(N_f\right)^{-0.56} \qquad (6.9)$$

Rewritten in the form of strain amplitude versus reversals, the equation becomes

$$\frac{\Delta\varepsilon}{2} = 0.6227\left[\frac{\sigma_u}{E}\right]^{0.832}\left(2N_f\right)^{-0.09} + 0.0196\left[\ln\left(\frac{1}{1-RA}\right)\right]^{0.155}\left[\frac{\sigma_u}{E}\right]^{-0.53}\left(2N_f\right)^{-0.56} \qquad (6.10)$$

6.6.4 Method Proposed by Socie et al (MPS)

Socie et al [3] proposed a method based on correlating fatigue strength coefficient with ultimate tensile strength. In this method, the true fracture stress σ_f is equal to fatigue strength coefficient σ'_f in Eq. (6.1). However, it is proposed that $\sigma'_f = \sigma_u + 345$ MPa for steel with hardness below 500 BHN. In addition, the elastic slope *b* is obtained by jointing a point at 10^6 reversals and the other point at one reversal which can be approximated to true fracture strength or $\sigma_u + 345$. The plastic portion is similar like USM's except the coefficients. The Resulting equation of this method becomes:

$$\frac{\Delta\varepsilon}{2} = \frac{\sigma_f}{E}\left(2N_f\right)^{-\frac{1}{6}\log(2\sigma_f/\sigma_u)} + \left[\ln\left(\frac{1}{1-RA}\right)\right]\left(2N_f\right)^{-0.6} \qquad (6.11)$$

Rewritten in the form of ultimate tensile strength, the equation becomes

$$\frac{\Delta\varepsilon}{2} = \frac{\sigma_u + 345}{E}\left(2N_f\right)^{-\frac{1}{6}\log[2+(690/\sigma_u)]} + \left[\ln\left(\frac{1}{1-RA}\right)\right]\left(2N_f\right)^{-0.6} \qquad (6.12)$$

6.6.5 Uniform Material Law Method (UMLM)

Baumel and Seeger [4] proposed an expression used for unalloyed and low alloy steels. It is assumed that the value of *b* and *c* in Eq. (6.1) are constant for the whole group of materials and they are very close to the values in the modified universal slopes method. A conditional coefficient is added in front of the plastic term. The expression is written in:

$$\frac{\Delta\varepsilon}{2}=1.5\frac{\sigma_u}{E}\left(2N_f\right)^{-0.087}+0.59\psi\left(2N_f\right)^{-0.58} \tag{6.13}$$

Where

$$\frac{\sigma_u}{E}\le 0.003,\quad \psi=1$$

$$\frac{\sigma_u}{E}> 0.003,\quad \psi=1.375-125\frac{\sigma_u}{E}$$

6.6.6 Modified Four-Point Correlation Method (MFPCM)

Ong [5] proposed a modified four-point correlation method based on Manson's method. The fatigue strength coefficient is assumed to be equal to the true fracture strength of the material. The fatigue ductility coefficient is approximated to be equal to the logarithmic ductility of the material. The fatigue strength exponent and fatigue ductility exponent are determined by implementing of the ultimate tensile strength, young's modulus, and plastic and elastic strains determined at 10^6 and 10^4 reversals. Therefore, the coefficients are modified into the following forms:

$$\sigma_f^{'}=\sigma_f=\sigma_u(1+\ln[1/(1-RA)]) \tag{6.14}$$

$$b=\frac{1}{6}\left\{\log\left[0.16\left(\frac{\sigma_u}{E}\right)^{0.81}\right]-\log\left(\frac{\sigma_f}{E}\right)\right\} \tag{6.15}$$

$$\varepsilon_f^{'}=\ln[1/(1-RA)] \tag{6.16}$$

$$c=\frac{1}{4}\log\left(\frac{0.00737-\Delta e_e^*/2}{2.074}\right)-\frac{1}{4}\log\left\{\ln[1/(1-RA)]\right\} \tag{6.17}$$

$$\frac{\Delta\varepsilon_e^*}{2}=\frac{\sigma_f}{E}\left[10^{\frac{2}{3}\left\{\log\left[0.16\left(\sigma_u/E\right)^{0.81}\right]-\log\left(\sigma_f/E\right)\right\}}\right] \tag{6.18}$$

where $\Delta\varepsilon_e^*$ is the strain located on the elastic line at 10^4 cycles.

6.6.7 Median Method (MM)

Meggiolaro and Castro [6] proposed a median method and used 724 steels to statically analyze the fatigue parameters based on different fatigue prediction methods. They found that the fatigue ductility coefficient is poorly correlated with the monotonic tensile properties. Based on the 724 steels, the median values of each of these four fatigue parameters, which are assumed to be constant values except the fatigue strength coefficient σ_f', are estimated. The complete form of this method for steels is:

$$\frac{\Delta\varepsilon}{2} = 1.5\frac{\sigma_u}{E}\left(2N_f\right)^{-0.09} + 0.45\left(2N_f\right)^{-0.59} \tag{6.19}$$

6.7 Evaluation of the Reviewed Methods

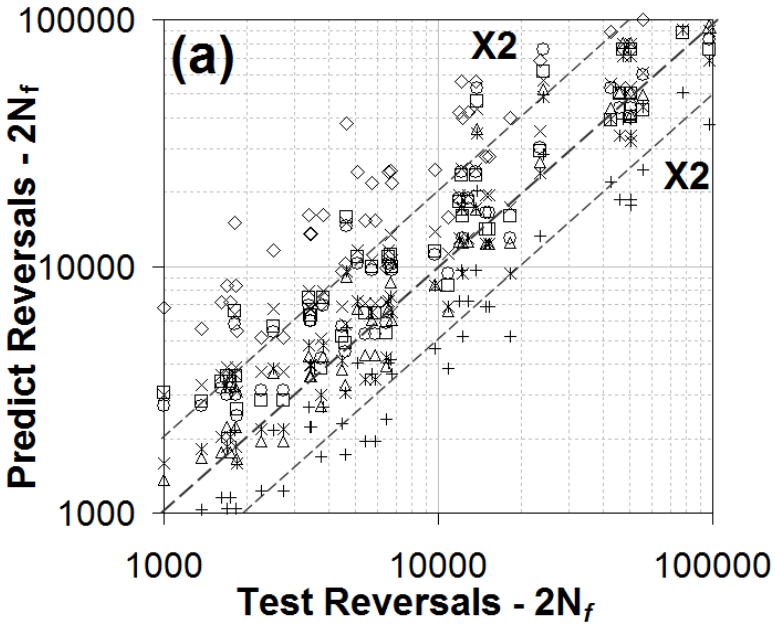

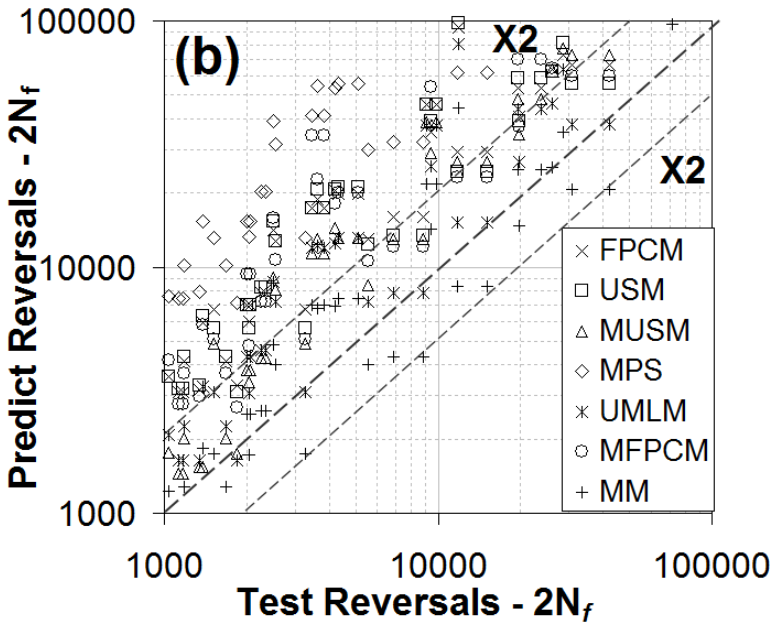

Figure 6.2 Comparison between predicted and test lives

(a) at lower temperatures (R.T. and 100°C) (b) at elevated temperatures (400°C and 500°C)

Figure 6.2 (a) and (b) shows the comparison between predicted reversals by different methods and test reversals for all selected coke drum materials at lower and elevated temperatures respectively. At lower temperatures, as shown in Fig. 6.2 (a), most of the methods yield reasonably accurate prediction within the x2 band. However, the method of MPS performs the worst among the seven chosen methods. It averagely over-predicts the life by five times. This is mainly caused by assuming the fatigue ductility coefficient ε_f' is equal to logarithmic ductility D which is calculated from Reduction of Area (RA). However, the investigated materials have fairly larger RA than the MM method studied, which could introduce significant deviation. There are some other methods, such as USM and FPCM, showing some weakness on predicting certain materials. However, they overall give fairly satisfactory prediction on coke drum materials. The MM method apparently under-predicts the life by a factor of three. This method assumes that all materials could have predicted lives based only on ultimate tensile strength and Young's modulus and all materials have constant fatigue strength exponent, fatigue ductility strength and exponents. However, from Table 6.2, it shows

that these parameters from different materials can have significant variation, which might cause under-prediction for some materials. At elevated temperature, as shown in Fig. 6.2 (b), all methods significantly over-predict the lives up to ten times except the MM method which also shows the under-prediction at elevated temperatures. This is because that the MM method only relies on the ratio between ultimate tensile strength and Young's modulus which decreases moderately at elevated temperatures. The UMLM method shows some accurate predictions on some of the data points. However, it still over-predicts the lives of the materials by two times in general. Therefore, some of the methods could give pretty good prediction for coke drum materials at lower temperatures based on the tensile data. However, none of them could provide satisfactory prediction at both lower and elevated temperatures.

To quantitatively elevate the accuracy of the selected prediction method, there are three approaches are used here to perform the evaluation. The first approach is correlation coefficient which is numerical measure of the strength of the linear relationship between two variables. The correlation coefficient is usually denoted by the letter *r*, and it can be expressed by:

$$r = \frac{1}{n-1}\sum_{i=1}^{n}\left(\frac{N_{f,i}^{test} - \bar{N}_f^{test}}{S_{N_f^{test}}}\right)\left(\frac{N_{f,i}^{pred} - \bar{N}_f^{pred}}{S_{N_f^{pred}}}\right) \tag{6.20}$$

Where $\bar{N}_f$ and S_{N_f} are the mean and standard deviations of the test and predict final lives. The correlation coefficient is always between -1 and 1. Positive values of the coefficient imply that the least squares line has a position slope. Values close to 0 indicate a poor linear relation between the two sets of points. The correlation coefficients close to 1 indicate that a strong linear relation between the two sets data. The coefficient is equal to 1 only when the points in the plot lie exactly on a straight line of positive slope. Therefore, the correlation coefficient measures how close the test and predict lives are linearly correlated in this case.

The second evaluation criterion is goodness of fit between predicted and experimental values E_a, and it was first used by Park and Song [8] to evaluate the

accuracy of the fatigue life prediction methods. The relation between predicted and test lives is expressed by a least-squares line as:

$$\log(N_f^{pred}) = \alpha + \beta \log(N_f^{test}) \tag{6.21}$$

It can be seen that the closer the values of α and β are to 0 and 1respectively, the better the prediction is. For the condition of α greater than zero, the value of β less than unity yields better prediction than greater than one. For the condition of α less than zero, the value of β greater than unity yields better prediction than smaller than one. Therefore, the summation of α and β can also be as an additional evaluation criterion. Thus, the goodness of fit between the predicted and test values, E_a can be expressed as:

$$E_a = \frac{\left(1-|\alpha|\right)+\left(1-|1-\beta|\right)+\left(1-|1-(\alpha+\beta)|\right)}{3} \tag{6.22}$$

The third evaluation criterion is fraction of data within a specified range s, in this study, a factor of 2 is employed for life prediction, and then E_f can be written as:

$$E_f = \frac{\text{Number of data}\left\langle 0.5 \le \dfrac{N_f^{pred}}{N_f^{test}} \le 2 \right\rangle}{\text{Number of total data}} \tag{6.23}$$

Table 6.3 summarizes the calculated factors of the evaluation for predictions at both lower and elevated temperatures. The Modified Universal Slopes Method (MUSM) gives the best prediction among the others for prediction at lower temperatures based on the three elevation criteria and their average value. However, at elevated temperatures, the averaged criterion indicates that the Median Method's prediction provides the best result. However, the criteria of correlation coefficient and goodness of fit shows the MUSM performs better than MM in terms of linearity and closeness of fitting. By comparing the fraction of data within a range of 2, the MUSM has only half of the predicted lives laid in this range, and the rest is over-predicted more than two times. By considering the same range factor, the MM has about 90% of the data falling into this range, but, nearly half of these data are under-predicted. Therefore, it is difficult to decide which method would give better prediction for these materials at elevated temperatures.

A temperature-dependent method is favourable to help in prediction accurately at both lower and elevated temperatures.

Table 6.3 Summary of the evaluation coefficients for all prediction methods

	FPCM	USM	MUSM	MPS	UMLM	MFPCM	MM
	Lower temperature (RT~100°C)						
r	0.956	0.930	**0.969**	0.922	0.940	0.894	0.935
E_a	0.398	0.413	**0.993**	0.386	0.804	0.599	0.949
E_f	0.706	0.784	**0.961**	0.157	0.922	0.804	0.627
$\bar{E}$	0.687	0.709	**0.974**	0.488	0.889	0.766	0.837
	Elevated temperature (400~500°C)						
r	0.730	0.721	**0.734**	0.701	0.677	0.269	0.667
E_a	0.269	0.254	**0.907**	0.196	0.695	0.761	0.845
E_f	0.109	0.196	0.457	0.000	0.435	0.239	**0.891**
$\bar{E}$	0.369	0.390	0.699	0.299	0.602	0.423	**0.801**

6.8 Development of Temperature Dependent Four Point Correlation Method (TDFPCM)

For the sake of simplicity and accessibility of the tensile data, it is found that Young's modulus, ultimate tensile strength and elongation at fracture are the most commonly available data for metal materials. Therefore, these three tensile properties are attempted as input parameters for life prediction of temperature dependent case.

This method is developed based on the similar methodology as Manson's Four Point Correlation Method [1]. It uses two points on elastic and plastic lines respectively to correlate them. The relation at each point is obtained based on the correlation of the strain amplitude and tensile properties of the selected materials at corresponding fatigue life. For example, on the elastic line, a point is located at ¼ cycle with a strain amplitude

estimated as $1.157[\sigma_u(2+\varepsilon_f)/E][-0.1226(T/100)+1.1226]$. Another point is at $5\text{x}10^4$ cycles which the strain amplitude estimated as $0.62\sigma_u/E$, where σ_u is the ultimate tensile strength measured during a tensile test, and E is the Young's modulus in both cases. On the plastic line, a point is located at 10 cycles determined, and the corresponding strain amplitude is $(\sigma_u/E)(100\varepsilon_f)$, where ε_f is the strain measured after the specimen completely fractured. A standard tensile test specimen (as shown in Fig. 4.1) with 1" gauge length was used to measure ε_f. If different specimen geometries and gauge lengths were used, it may result in different values of ε_f. Another point on the plastic line is obtained at 10^4 cycles, and the corresponding strain amplitude is $\varepsilon_f\,(1000/E)[-0.143(T/100)+1.143]$, where T is the temperature, and $T = 100$ when T is measured $\leq 100°C$, which assumes no difference in fatigue lives between room temperature and 100°C for same material. Therefore, the four fatigue parameters can be rewritten as:

$$\sigma'_f = 1.157\sigma_u(2+\varepsilon_f)\left[-0.1226\left(\frac{T}{100}\right)+1.1226\right]\cdot 2^b \tag{6.24}$$

$$b = \frac{\log\left\{1.866\left(2+\varepsilon_f\right)\left[-0.1226\left(\frac{T}{100}\right)+1.1226\right]\right\}}{\log\left[1/\left(2\times 10^5\right)\right]} \tag{6.25}$$

$$\varepsilon'_f = \frac{\sigma_u}{E}\left(\varepsilon_f\cdot 100\right)\left(\frac{1}{20}\right)^c \tag{6.26}$$

$$c = \frac{1}{3}\log\left\{\left(\frac{10}{\sigma_u}\right)\left[-0.143\left(\frac{T}{100}\right)+1.143\right]\right\} \tag{6.27}$$

Where $T = 100$ when T is measured $\leq 100°C$

Figure 6.3 shows the comparison between the predicted lives with tested lives at lower and elevated temperatures. Figure 6.3 (a) shows between TDFPCM and MUSM at lower temperatures (RT~100°C) and (b) between TDFPCM and MM at elevated temperatures (400~500°C). Based on the evaluation on the selected seven prediction methods, MUSM and MM are the most accurate prediction methods among the others for lower and elevated temperatures respectively. By performing the same quantitative

evaluation on these methods with TDFPCM at lower and elevated temperatures, it shows that the TDFPCM has outstanding performance at both temperature ranges as shown in table 6.4. Furthermore, to assess the developed method on predicting at mid-temperature ranges, three fatigue data of base material (1¼Cr-½Mo, 1Cr-½Mo, and 2¼Cr-1Mo) at 300°C are also chosen from [18-20], and another base material of 1¼Cr-½Mo at 250°C was selected from [29]. Three methods, MUSM, MM and TDFPCM, are attempted to predict the fatigue lives of these base materials at 250°C and 300°C based on the corresponding tensile data. As shown in Fig. 6.4, MUSM gives about two times over-prediction of fatigue lives on most of the materials. Meanwhile, MM under-predicts half of the data by approximate two times. In general, the developed TDFPCM gives the overall best prediction among the three methods. This conclusion is also proven through the quantitative evaluation as summarized in Table 6.5.

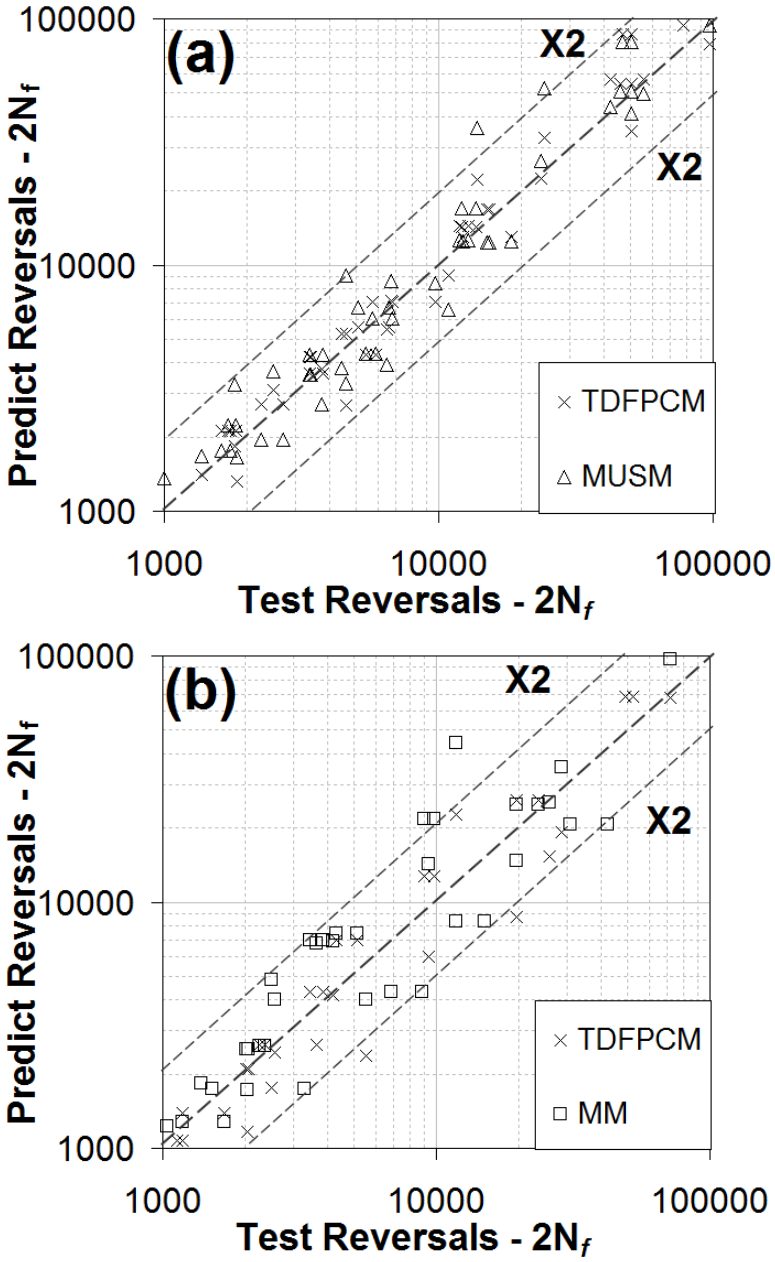

Figure 6.3 Comparison of test and predicted lives

(a) between TDFPCM and MUSM at low temperatures (RT~100°C) (b) between TDFPCM and MM at elevated temperatures (400~500°C)

Table 6.4 Summary of the evaluation coefficients for TDFPCM, MSUM and MM

	TDFPCM	MUSM	TDFPCM	MM
	RT~100°C		400~500°C	
r	0.949	0.969	0.732	0.667
Ea	0.993	0.993	0.979	0.845
Ef	1.000	0.961	0.957	0.891
$\bar{E}$	**0.981**	0.974	**0.889**	0.801

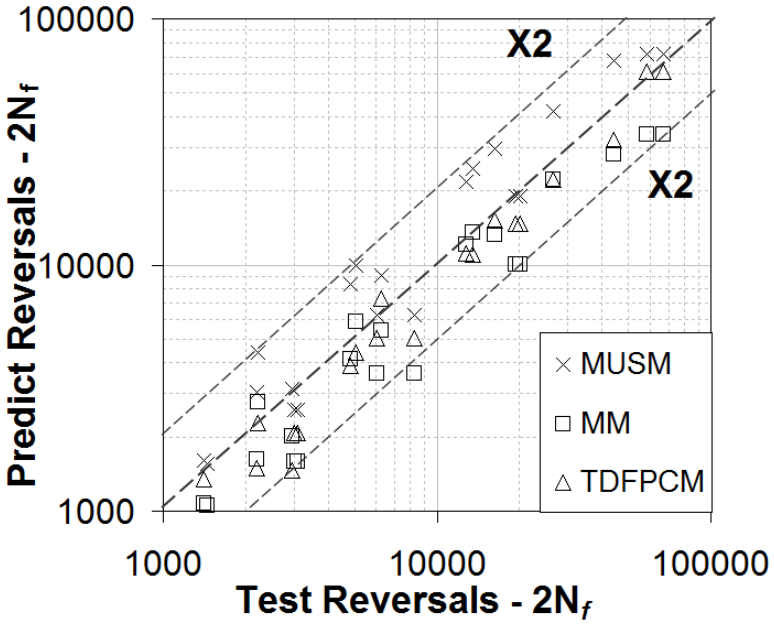

Figure 6.4 Comparison of test and predicted result at 250~300°C

Table 6.5 Evaluation coefficients for MUSM, MM and TDFPCM at 250°C

	MUSM	MM	TDFPCM
	250~300°C		
r	0.995	0.994	0.998
E_a	0.920	0.900	0.800
E_f	0.609	0.870	1.000
$\bar{E}$	0.841	0.921	**0.933**

6.9 Conclusions

In this chapter, three coke drum materials are first tested at 100°C and 480°C, and four more coke drum materials, which has both tensile and fatigue life data available, are selected from the literature at room temperature, 400°C and 500°C. Seven existing fatigue life prediction methods are evaluated based on the selected coke drum materials data at lower and elevated temperature ranges. It is found that modified universal slopes give the best prediction for these materials at lower temperature (20°C~100°C) and median method is superior to others at elevated temperatures (400°C~500°C). However, none of the methods can give accurate estimation at both temperature ranges. A new temperature-dependent method, which only uses tensile strength, Young's modulus and elongation at fracture, is proposed. By comparing with the other existing methods at both temperature ranges and even at mid-temperature range, the new proposed method has closer predicted lives to the test ones.

References

[1] Manson, S.S., "Fatigue: A complex subject – Some Simple Approximations," Proceedings, Society of Experimental Stress Analysis, Vol. 12, No. 2, (1965).

[2] Muralidharan U, Manson SS. Modified universal slopes equation for estimation of fatigue characteristics. Journal of Engineering Materials and Technology, Trans. of ASME (1988): pp.55 – 8.

[3] Socie, D. F., Mitchell, M. R. and Caulfield, E. M., "Fundamentals of Modern Fatigue Analysis", *Fracture Control Program report No. 26*, University of Illinois, USA, (1977).

[4] Baumel, A, Seeger T. Materials data for cyclic loading. Amsterdam: Elsevier Science Publishers, (1990).

[5] Ong, J.H. "An improved technique for the prediction of axial fatigue life from tensile date", International Journal of Fatigue , (1993), pp.213 – 9.

[6] Meggiolaro MA, Castro JTP. Statistical evaluation of strain-life fatigue crack initiation predictions. Int J Fatigue, 26(5), (2004), pp. 463 – 76.

[7] Ong, J. H., "An evaluation of existing methods for the prediction of axial fatigue life from tensile data", International Journal of Fatigue, Vol. 15, (1993), pp. 13-19.

[8] Park, J.H., Song, J.H. "Detailed evaluation of methods for estimation of fatigue properties" International Journal of Fatigue , Vol. 17, (1995), pp.365 – 73.

[9] Penso, J. A., Lattarulo, Y. M., Seijas, A. J., Torres, J., Howden, D., and Tsai, C. L., "Understanding Failure Mechanisms to Improve Reliability of Coke Drum," ASME (1993): PVP-Vol. 395, pp. 243–253.

[10] Pieper, C.J., Shockley, L.R. and Stewart, C.W. , "Coke Drum Design-Longer Life through Innovation", AIChE 2000 Spring National Meeting, Atlanta, GA, March 5-9, (2000).

[11] Boswell, R. S., "Coke Drum Bulges", Stress Engineering Services, May, (2001).

[12] Ramos, A., Rios, C., Vargas, J., Tahara, T., and Hasegawa, T., "Mechanical Integrity Evaluation of Delayed Coke Drums," Fitness for Adverse Environments in Petroleum and Power Equipment, ASME (1997): Vol. 359, pp.291–298.

[13] Ramos, A., Rios, C., Johnsen, E., Gonzalez, M., and Vargas, J., "Delayed Coke Drum Assessment Using Field Measurements and FEA," Analysis and Design of Composite, Process, and Power Piping and Vessels, ASME (1998): Vol. 368, pp. 231–237.

[14] Ramos, A. J., Rios, C. and Vargas, J.A.R., "Fatigue Life Prediction of Delayed Coke Drums", Vision Techenologica, Vol.6, (1999), pp. 93-100.

[15] Boswell R.S., Ferraro T., "Remaining Life Evaluation of Coke Drums", Plant Engineering, Design and Responsibility Symposium, Energy Engineering Conference, (1997).

[16] Sohel, M., Panwala, M., Srinviasan, K. N. and Mehta, S. L., "Creep-fatigue interaction in coke drums: An approach based on API 579-1/ASME FFS-1 2007", Proceeding of the ASME Pressure Vessels and Piping Division conference (2009).

[17] ASTM, E8-04, 2004, "Standard Test Methods of Tension Testing of Metallic Materials," ASTM international, West Conshohocken, PA, (2004), DOI:10.1520/E0008-04, www.astm.org

[18] Anonym. “Data Sheets on Low-Cycle Fatigue Properties at Elevated-Temperature for Weld and Base Metals of SCMV2-2NT (1Cr-0.5Mo) Low Alloy Steel Plate for Boiler and Other Pressure Vessels” NRIM Fatigue Data Sheet (1993):1. TEMA. Web. 22 Jan. (2014).

[19] Anonym. “Data Sheets on Elevated-Temperature Low-Cycle Fatigue Properties of SCMV3 (1.25Cr-0.5Mo) Steel Plate for Pressure Vessels” NRIM Fatigue Data Sheet (1981):1. TEMA. Web. 22 Jan. (2014).

[20] Anonym. “Data Sheets on Elevated-Temperature Low-Cycle Fatigue Properties of SCMV4 (2.25Cr-1Mo) Steel Plate for Pressure Vessels” NRIM Fatigue Data Sheet (1987):1. TEMA. Web. 22 Jan. (2014).

[21] Sasaki, Y., Niimoto, S., “Study on skirt-to-shell attachment of coke drum by evaluation of fatigue strength of weld metal”, Proc. Pressure Vessels & Piping Division Conf., ASME (2011): PVP2011- 57314.

[22] ASTM E2368-10, 2010, “Standard Practice for Strain Controlled Thermomechanical Fatigue Testing”, ASTM international, West Conshohocken, PA, 2010, DOI: 10.1520/E2368-10, www.astm.org

[23] ASTM E606-04, 2004, “Standard Practice for Strain-controlled Fatigue Testing”, ASTM international, West Conshohocken, PA, 2004, DOI: 10.1520/E606-04, www.astm.org

[24] Chen, J., “Experimental Study of Elastoplastic Mechanical Properties of Coke Drum Materials”, Masters Dissertation, University of Alberta, Edmonton, (2010).

[25] ASTM, E21-09, 2009, “Test Methods for Elevated Temperature Tension Tests" ASTM international, West Conshohocken, PA, 2009, DOI:10.1520/E0021-09, www.astm.org

[26] Basquin, O.H. "The exponential law of endurance tests", ASTM proceeding. Vol. 10, (1910), pp. 625-630.

[27] Coffin, L. F. Jr., "A study of the effects of cyclic thermal stresses on a ductile metal", Trans. ASME, Vol.76, (1954): pp. 931-950.

[28] Manson, S.S., "Behaviour of materials under conditions of thermal stress", Heat Transfer Symposium, University of Michigan, (1953), pp.9-75. See also NACA-TN-2933, 1953)

[29] Chen, J., Yamatomo, T., Xia, Z. and Esaki, K., "Experimental Evaluation of Fatigue Life of Coke Drum Materials with Weld Sections", Proceeding of ASME pressure vessel and piping Conference, (2013).

CHAPTER 7 Experimental Evaluation of Fatigue Life of Coke Drum Materials with Weld Sections[5]

It is observed that most cracks were near or within the weld seams of coke drums. In order to better understand fatigue damage mechanisms of the coke drum materials with their weld sections, an experimental investigation of fatigue lives of these materials are carried out. It is a common consideration that the yield strength of the weld should be within a close percentage to that of base material in order to keep strength uniformity throughout the drum shell sections. However, this effect of the yield strength matching on the shell durability has not yet clarified quantitatively. From this point of view, two different types of specimens have been designed and manufactured: base material only, base with base weld. In addition, three groups of base with weld materials with different ratios of weld to base yield strengths are prepared. Low cycle fatigue tests at elevated temperature of 250°C are carried out on the above specimens. Through study on the recorded stress-strain hysteresis loops and observation on the fracture surfaces, damage mechanisms of different types of specimens are analyzed. Their strain range - fatigue life curves are also compared. Furthermore, finite element analyses based on the actual specimens' geometries and properties are conducted to help in understanding the experimental observations. This experimental evaluation of fatigue life of coke drum materials with welds may provide a good reference for better design of coke drums in the future.

[5] Chapter 7 of this thesis has been published in the proceeding of ASME 2013 Pressure Vessels and Piping Conference, Volume 3: Design and Analysis, Paris, France, July 14-18, 2013 ISBN: 978-0-7918-5567-6

7.1 Introduction

Coke drums are normally constructed of carbon or low carbon alloy steels and internally clad with SA 240 Type 410S or Type 405 stainless steel to protect the coke drums from corrosion [1]. It is found that shell bulging is one of the causes contributing to cracking and failure in the vessel shell of coke drums [2]. The bulges are normally found near the circumferential weld seams which normally have higher yield strength, and the base material finally tend to become thin and fails via cracking as the result of the restraint caused by the weld seams [3-5]. As a result, there are a lot of cases observed that cracks were near or within the weld seams. In recent years, new drum material selection has been towards increasing Chrome-Moly alloy content [5]. Steels with higher Cr and Mo contents are considered to have better thermal cycling resistance because of their higher yield strength and better creep resistance. However, there is still not enough evidence to demonstrate the improved reliability due to use of these materials. The coke drums constructed from these materials still experience same type of damage or failure.

In order to better understand fatigue damage mechanisms of the coke drum materials with their weld sections, an experimental investigation of fatigue lives of these materials are carried out. It is a common consideration that the yield strength of the weld should be within a close percentage to that of base material in order to keep strength uniformity throughout the drum shell sections. However, this effect of the yield strength matching on the shell durability is not yet clarified quantitatively.

In this chapter, two different types of specimens have been designed and manufactured: base material only, base with base weld. Three groups of base-weld with different ratios of weld to base yield strengths are prepared. Low cycle fatigue tests at elevated temperature of 250°C are carried out on these specimens. Furthermore, finite element analyses based on the actual specimens' geometries and properties are conducted to help in understanding the experimental observations.

7.2 Specimen Preparation and Materials

There are three different types of specimens used in this study: tensile test specimen (Fig. 4.1), pure-base fatigue (Fig. 3.2) and base-weld fatigue specimens (Fig. 5.1). The more detailed geometries of these specimens are discussed in the previous chapters. The pure-base specimens were directly machined from the base plate. The base-weld specimens were cut from the plate with centered weld section. To prevent buckling of the specimen under fully-reversed cyclic loading, the specimens were designed with sufficient amount of weld and base materials while minimize the gage length.

SA-387 Gr. 11 Class 2, base and weld materials are selected for this experimental investigation. The nominal chemical composition of SA 387 Gr. 11 CL.2 is 1¼ Cr-½ Mo. The uni-axial tensile tests are conducted at room temperature on base and case 1, 2 and 3 weld materials. The yield strengths of the materials are obtained from the monotonic stress-strain curves. The yield strength ratios (S_w/S_b) between weld and base are found to be: for case 1 weld, $S_{w1}/S_b = 1.166$ (monotonic at R.T.); for case 2 weld, $S_{w2}/S_b = 1.055$ (monotonic at R.T.); for case 3 weld, $S_{w3}/S_b = 1.128$ (monotonic at R.T.). Since the fatigue tests are carried out at 250°C under fully-reversed strain-controlled cyclic loading, it is more reasonable to based on the cyclic stress-strain curves to determine the yield strength ratio (S_w/S_b) because it represents the actual stable stress-strain relations in cyclic fatigue tests. The cyclic tests of base and weld materials are performed at 250°C. Two repeating tests are carried out for the case 1, 2 and 3 weld materials, respectively. The cyclic stress strain curves, Fig. 7.1, are obtained by passing the saturated point of each hysteresis loop. It is found that the ratios of S_w/S_b obtained from the cyclic stress-strain curves at temperature of 250°C are lower than the corresponding values obtained from the monotonic stress-strain curves at room temperature (R.T.) as shown in Fig. 7.1 and Table 7.1.

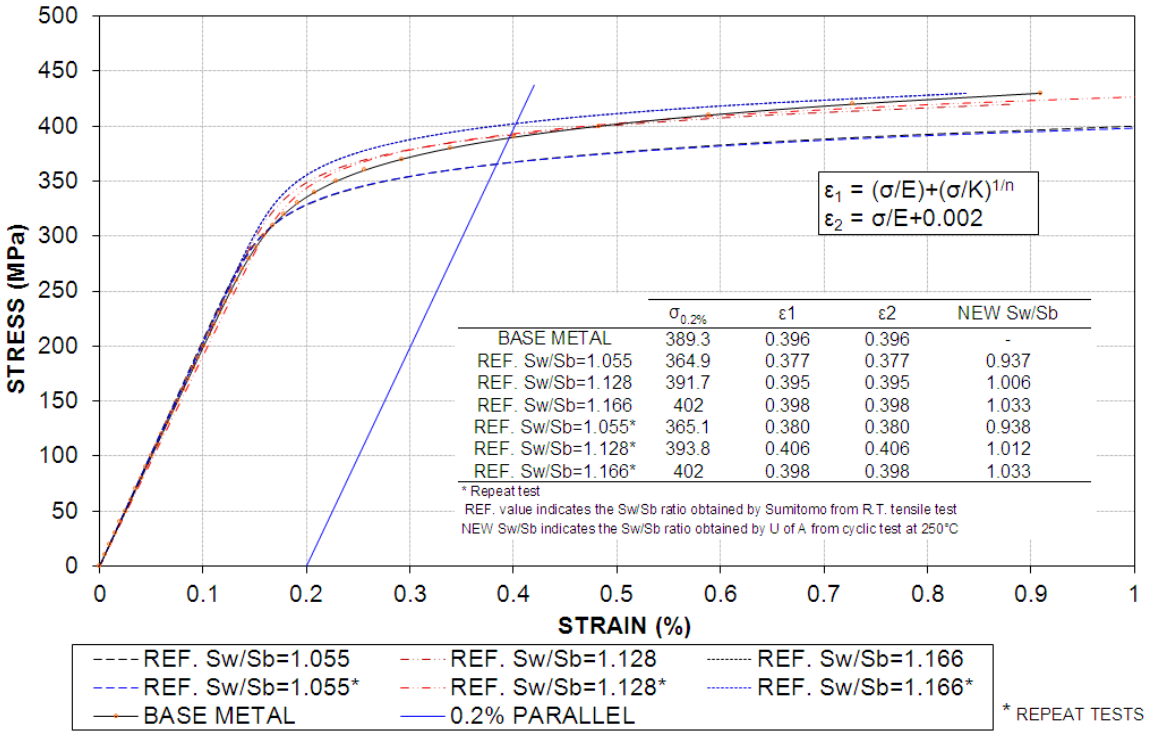

	$\sigma_{0.2\%}$	ε1	ε2	NEW Sw/Sb
BASE METAL	389.3	0.396	0.396	-
REF. Sw/Sb=1.055	364.9	0.377	0.377	0.937
REF. Sw/Sb=1.128	391.7	0.395	0.395	1.006
REF. Sw/Sb=1.166	402	0.398	0.398	1.033
REF. Sw/Sb=1.055*	365.1	0.380	0.380	0.938
REF. Sw/Sb=1.128*	393.8	0.406	0.406	1.012
REF. Sw/Sb=1.166*	402	0.398	0.398	1.033

* Repeat test
REF. value indicates the Sw/Sb ratio obtained by Sumitomo from R.T. tensile test
NEW Sw/Sb indicates the Sw/Sb ratio obtained by U of A from cyclic test at 250°C

Figure 7.1 SA 387 Gr. 11 CL.2 for 250°C cyclic stress strain curves

Table 7.1 Comparison of S_w/S_b ratios for case 1, case 2 and case 3

	S_w/S_b (R.T. monotonic)	S_w/S_b (250°C cyclic)
CASE 1 WELD	1.166	1.033
CASE 2 WELD	1.055	0.937
CASE 3 WELD	1.128	1.006
CASE 1 WELD $_{repeat}$	1.166	1.033
CASE 2 WELD $_{repeat}$	1.055	0.938
CASE 3 WELD $_{repeat}$	1.128	1.012

7.3 Experimental Setup and Procedures

The same high temperature fatigue test system discussed in chapter 3 is used to conduct LCF testing in this investigation. The more detailed design and development of this system are described in [6].

Fully-reversed strain-controlled fatigue tests are performed at constant temperature of 250°C. From an in-field measurement by using high temperature strain gauges and thermocouples, it is observed that extreme strains on shell surface occurs during the quenching stage when the temperature drops to the range between 300°C and 200°C [7]. Therefore, the testing temperature is chosen at 250°C. A specimen with 3 thermocouples (TCs) is initially used to verify the thermal gradient along the axial direction. Two TCs are spot-welded on the cross sections parallel to the dimples, and the other one are located in center of the specimen as a control TC. After the temperature reached to 250°C and stabilized, the test starts after the strain is re-zeroed. Straining rate is set at 0.005/sec for all tests. Four strain amplitudes are controlled and measured for each case. There are at least two tests conducted at each strain amplitude to insure the repeatability and accuracy of the data. Each fatigue test stops when maximum load reaches to 7 kN or 17% of the load at Nf/2 (stabilized maximum load).

7.4 Test Results and Discussion

Table 7.2 has listed all the fatigue test results for pure base specimens and three groups of base-weld specimens. Figure 7.2 shows the relations of strain range vs. fatigue life Nf for the above four groups of specimens. The test data points for each group of specimens can be fitted accurately by Manson-Coffin's [8-10] equation:

$$\Delta\varepsilon_t = \Delta\varepsilon_p + \Delta\varepsilon_e = C_p\left(N_f\right)^{-k_p} + C_e\left(N_f\right)^{-k_e} \tag{7.1}$$

where Δε is strain range, C_p, k_p, C_e *and* k_e are constants from fitting.

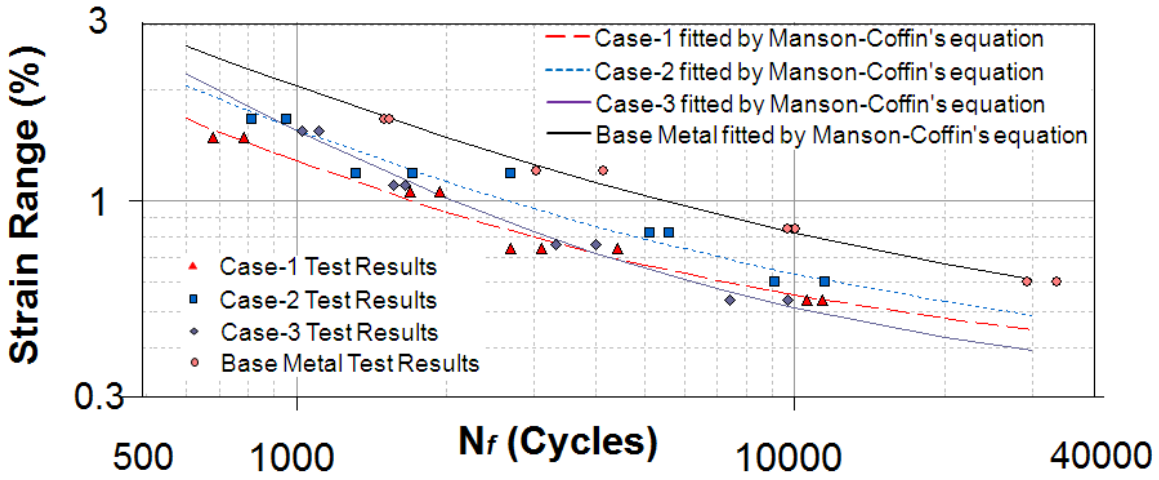

Figure 7.2 Fatigue test results of pure base, Case 1, 2 and 3 base-weld

It can be seen from Fig. 7.2 that the fatigue life of case 2 which has lower yield strength ratio (S_w/S_b) is longer than that of case 1. The fatigue life of case 3 is fitted in between case 1 and 2 up to strain range of 0.7%, and then starting to be lower than the curve of case 1. Due to the material uniformity of the pure-base specimens, the fatigue data is more repeatable and better fitted than base-weld specimens. In addition, the fatigue life of pure-base material is considerably longer than three cases of base-weld specimens.

There are three rupture modes observed from the total 26 tests of base-weld specimen, as seen in Fig. 7.3. There are 18 out of 26 specimen ruptured closely along the interface between base and weld (mode A). There are four from case 2 specimens cracked in the weld section of the specimen (mode B) and four from case 1 specimens ruptured in the base metal a little away from the base-weld interface (mode C). All case 3 specimens are cracked along the interface between base and weld (Fig. 7.3). It can also be seen that, there is no rupture mode B showing in case 1 specimens, and there is no rupture mode C showing in case 2 specimens. There is only rupture mode A showing in case 3 specimens. The pictures of ruptured specimens for mode A, B, and C are shown in Fig. 7.4 as an example. The mid-section with lighter color is weld material, and the rest is base material.

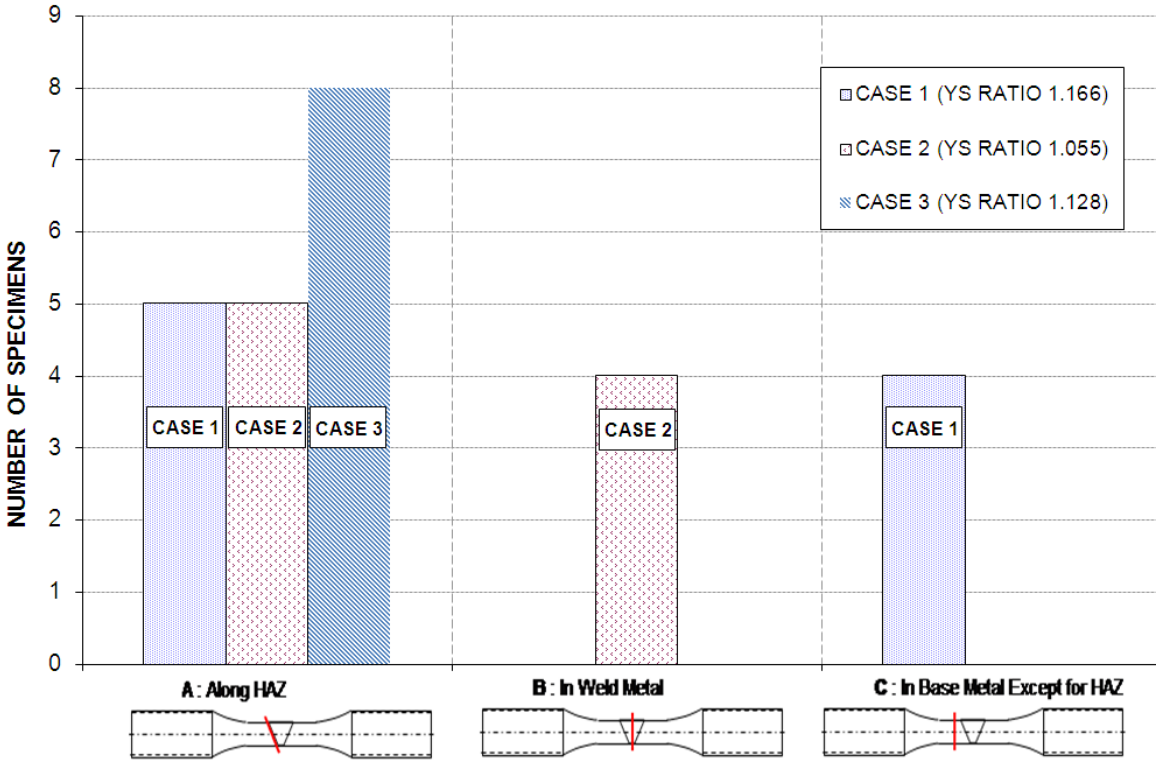

Figure 7.3 Rupture modes for case 1, case 2, and case 3base-weld specimen

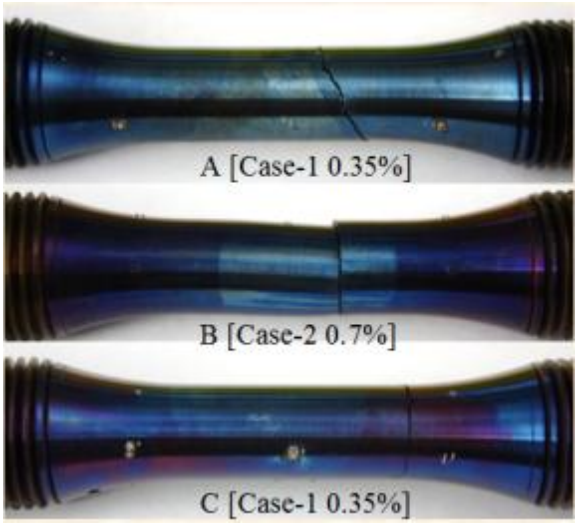

Figure 7.4 Pictures of ruptured specimens

Table 7.2 Summary of fatigue test results for base-weld specimens

	Specimen #	$\Delta\varepsilon_{gauge}$	N_f
CASE 1 (YS RATIO =1.166)	1_2_1	1.48%	785
	1_2_2	1.48%	680
	1_1_1	1.06%	1942
	1_2_3	1.06%	1690
	1_3_1	0.74%	2690
	1_3_2	0.74%	4410
	1_3_3	0.74%	3100
	1_4_1	0.53%	11390
	1_4_2	0.53%	10610
CASE 2 (YS RATIO =1.055)	2_2_1	1.66%	812
	2_2_2	1.66%	954
	S_2_1	1.18%	1314
	2_1_1	1.18%	2700
	2_4_1	1.18%	1710
	2_3_1	0.83%	5120
	2_3_2	0.83%	5600
	S_2_3	0.59%	11490
	2_4_2	0.59%	9120
CASE 3 (YS RATIO =1.128)	3_1_1	1.54%	1026
	3_1_2	1.54%	1107
	3_2_1	1.10%	1653
	3_2_2	1.10%	1569
	3_3_1	0.77%	3990
	3_3_2	0.77%	3310
	3_4_1	0.55%	9680
	3_4_2	0.55%	7390
PURE BASE	B-1	1.67%	1502
	B-2	1.67%	1542
	B-3	1.19%	3030
	B-4	1.19%	4131
	B-5	0.83%	10040
	B-6	0.83%	9660
	B-7	0.60%	33570
	B-8	0.60%	29240

7.5 FEA and Comparison with Experiments

7.5.1 FEA Model Setup

A 3-D finite element model of specimen is created, as shown in Fig. 7.5. The symmetric plane of the specimen is constraint in vertical direction, and the center point of that plane is fixed in both x and z directions. Fully-reversed uni-axial cyclic displacement is applied at the top edge of the grip. The cyclic stress strain curves, Fig. 7.1, obtained from cyclic tests are inputted into the program as elastic-plastic properties.

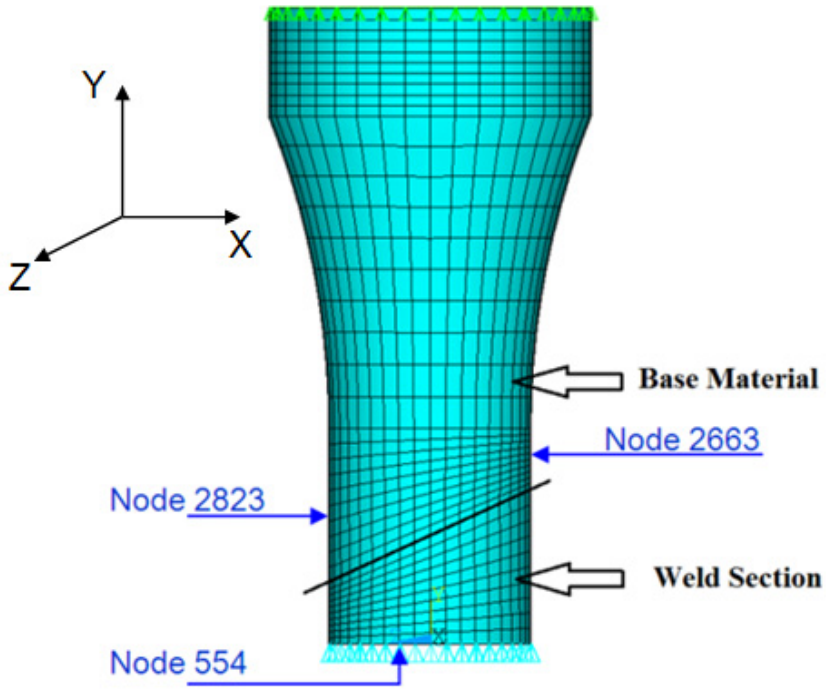

Figure 7.5 Finite element model of base-weld specimen

7.5.2 FEA Results

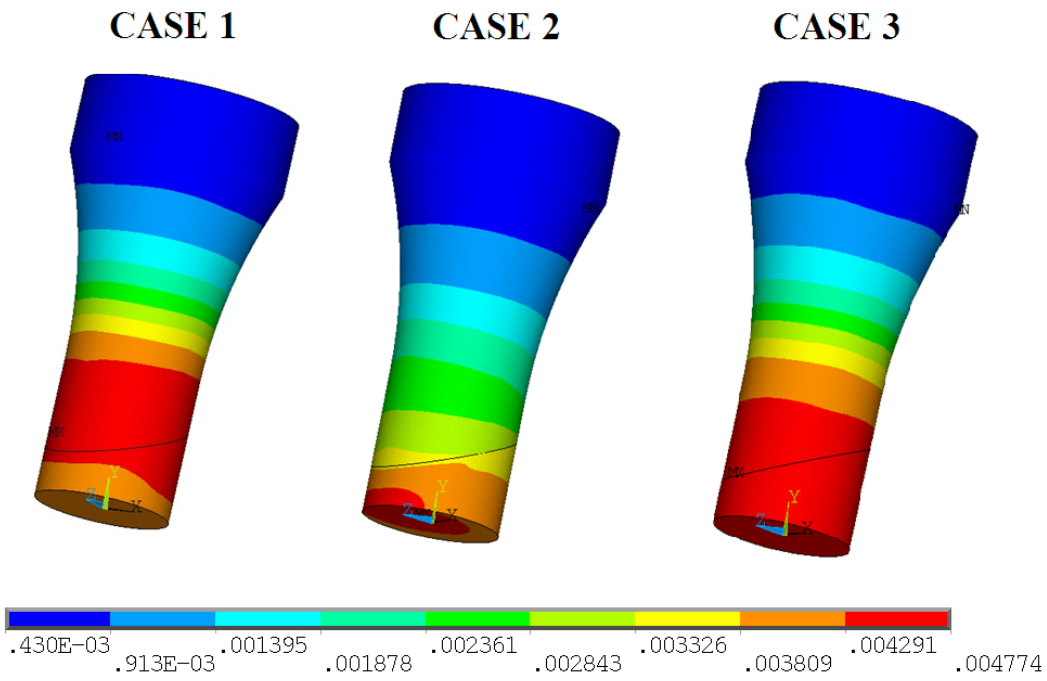

Figure 7.6 FEA results of axial elastic-plastic strain

The results of axial total elastic-plastic strain, as seen in Fig. 7.6, show that for the case 1 (S_w/S_b=1.033 at 250°C, cyclic) the maximum value occurs in the base section of the specimen (node 2823, Fig. 7.5); for case 2 (S_w/S_b =0.937 at 250°C, cyclic) the maximum value occurs in the weld section of the specimen (node 554, Fig. 7.5). for case 3 (S_w/S_b =1.006 at 250°C, cyclic) the maximum value occurs in the interface between base and weld of the specimen. This is mainly due to the different yield strengths of the weld materials. By comparing this result with experimental observations, it agrees that for case-2, weld section is more susceptible to failure; for case-1, base section is more vulnerable to failure; and for case-3, the interface is the weakest point. However, due to heat affection during the welding process, the interface between base and weld seems weaker under cyclic loading. Therefore, the FEA results are in good consistent with the failure modes observed experimentally for the case 1, case 2, and case 3 specimens.

However, the ratios of S_w/S_b obtained from cyclic stress strain curves for case 1, case 2 and case 3 do not have significant difference from uniformed strength condition

S_w/S_b =1.0. To more clearly show the effect of S_w/S_b on the fatigue life, a special case is assumed. As seen in Fig. 7.7, a stress-strain curve of weld material which results in S_w/S_b = 1.2 (at 250°C, cyclic) is assumed. This set of stress-strain curves are input into the FE model, Fig. 7.5 and the calculation is repeated. Figure 7.8 shows that the axial elastic plastic strain is much higher in the case of S_w/S_b = 1.2 (at 250°C, cyclic) than that of S_w/S_b = 1.033 (at 250°C, cyclic). In addition, by comparing the largest stress-strain hysteresis loops between S_w/S_b =1.2 (at 250°C, cyclic) and 1.033(at 250°C, cyclic) as shown in Fig. 7.9, the former ratio results in larger hysteresis loop. The closed area of the hysteresis loop is the dissipated strain energy per cycle which may be directly related to the low-cycle fatigue life for same material under same constant temperature. Therefore, it concludes that significantly higher ratio of S_w/S_b may significantly reduce the fatigue life for coke drums. The closer yield strength ratio between weld and base materials is beneficial from the fatigue life point of view for coke drums.

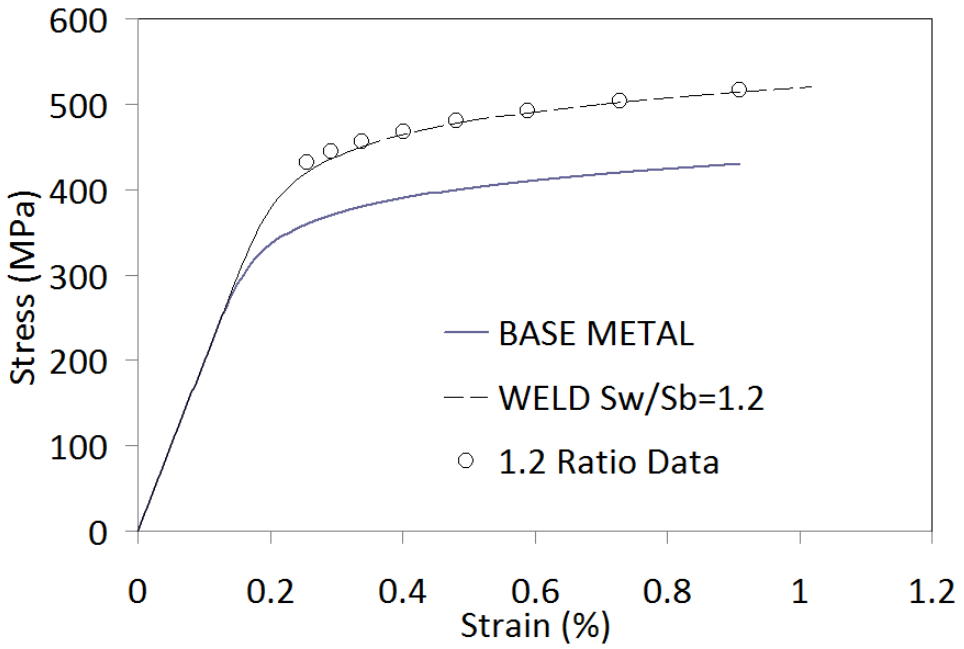

Figure 7.7 Assumed stress strain input curves for weld

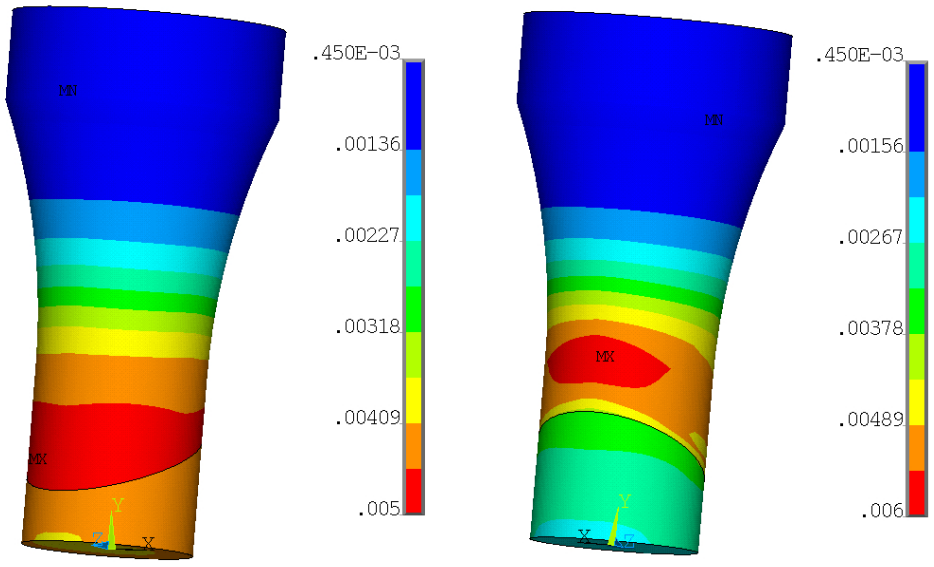

Figure 7.8 FEA results of axial elastic plastic strain

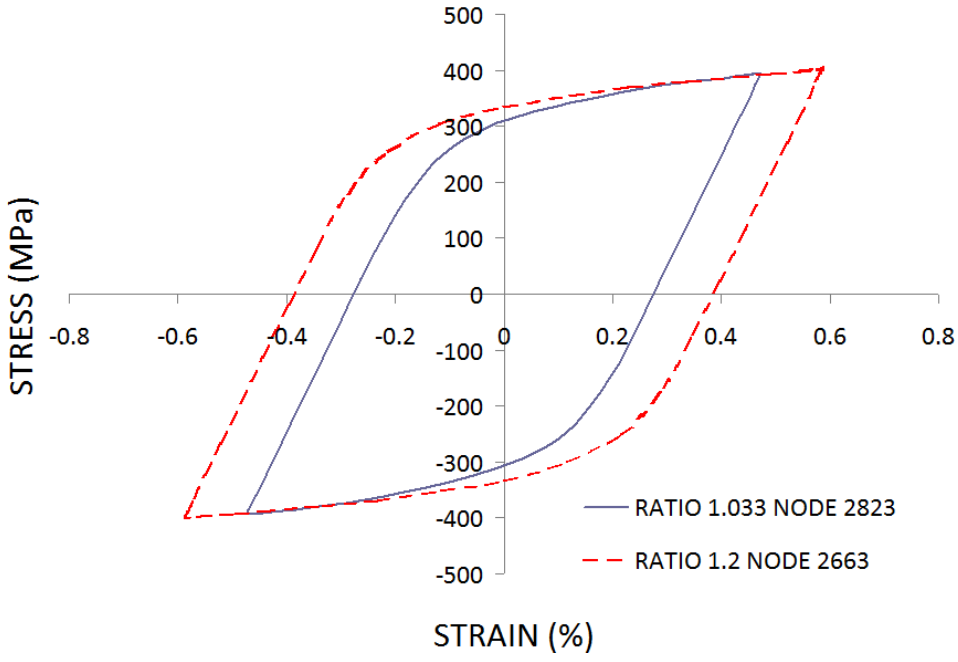

Figure 7.9 Hysteresis loops at nodes

7.6 Conclusions

In order to better understand fatigue damage mechanisms of coke drum materials with their weld sections, an experimental investigation of fatigue lives of these materials are carried out. Two different types of specimens have been designed and manufactured: base material only, base with base weld. In addition, three groups of base with weld materials with different ratios of weld to base yield strengths are prepared. The yield strength ratios are characterized from the monotonic tensile test at room temperature and cyclic test at temperature of 250°C. Low cycle fatigue tests at elevated temperature of 250°C are carried out on the above specimens. The following conclusions can be drawn from the current study:

1. The higher strength ratio of S_w/S_b results in shorter fatigue life as in comparison of the strain amplitude-fatigue life curves for the case 1 and case 2 specimens;

2. The pure base material has longer fatigue life than that of the base-weld specimens. This is due to the material uniformity of the pure-base specimens and without the heat affected zone (HAZ) introduced by the welding process;

3. Most of the base-weld specimen ruptured near the interface between the weld and base materials. There is no rupture mode occurred in the weld section for specimens with higher $S_w/S_b > 1$ (Case 1). There is no rupture mode occurred in the base zone for specimens with lower $S_w/S_b < 1$ (Case 2). The rupture modes observed for each case are consistent with the numerical analysis results on the FE models with actual specimen's geometry and mechanical properties.

4. The closer matching yield strength ratio between the weld and base materials should be beneficial for extension of the service life of coke drums.

References

[1] Penso, J. A., Lattarulo, Y. M., Seijas, A. J., Torres, J., Howden, D., and Tsai, C. L., "Understanding Failure Mechanisms to Improve Reliability of Coke Drum," ASME (1999): PVP-Vol. 395, pp. 243–253.

[2] Pieper, C.J., Shockley, L.R. and Stewart, C.W., "Coke Drum Design-Longer Life through Innovation", AIChE 2000 Spring National Meeting, Atlanta, GA, March 5-9, (2000).

[3] Richard Boswell, "Coke Drum Bulges", Stress Engineering Services, May, (2001).

[4] Boswell R.S., Ferraro T., "Remaining Life Evaluation of Coke Drums", Plant Engineering, Design and Responsibility Symposium, Energy Engineering Conference, (1997).

[5] API Proceedings "1996 APE Coke Drum Survey-Final Report", American Petroleum Institute, Washington, DC, (1996).

[6] Chen, J., "Experimental Study of Elastoplastic Mechanical Properties of Coke Drum Materials", Masters Dissertation, University of Alberta, Edmonton, (2010).

[7] Yamamoto, T., Arii, K., Huhetaoli, Niimoto, S., Ohata, M., Tagawa, T., Minami, F., "Investigation of Bulging Behavior of Coke Drum -A practical analysis of bulging under complex quench conditions-", Proc. Pressure Vessels & Piping Division Conf., ASME (2011): PVP2011- 57428.

[8] Basquin, O.H. "The exponential law of endurance tests", ASTM proceeding. Vol. 10, (1910): pp. 625-630.

[9] Coffin, L. F. Jr., “A study of the effects of cyclic thermal stresses on a ductile metal”, Trans. ASME(1954): Vol.76, pp. 931-950.

[10] Manson, S.S., “Behaviour of materials under conditions of thermal stress”, Heat Transfer Symposium, University of Michigan, (1953), pp. 9-75. See also NACA-TN-2933, 1953)

CHAPTER 8 Investigation on the Effect of Weld Yield Strength on the Fatigue Life of Clad Shell Structure of Coke Drums[6]

In order to better understand the influence of this effect on the fatigue life of coke drum, an experimental investigation of fatigue lives of a type of specimens similar to the wall structure of coke drums, is carried out. The structural specimens consist of four different materials: base, base-weld, clad, and clad-weld. Additionally, three groups of the structural specimens with different yield strength ratios of base weld to base are prepared. Low cycle fatigue tests at elevated temperature of 250°C are carried out on the structural specimens. Through study on the fatigue lives and failure modes, damage mechanisms of different types of specimens are analyzed. Their strain range - fatigue life curves are also compared. Furthermore, finite element analysis based on the specimen's geometry and properties are performed to help in understanding and verifying the experimental observations. This experimental study on fatigue lives of the structural specimens may provide a good reference for better design and maintenance of coke drums in the future.

[6] Chapter 8 of this thesis has been submitted to *Journal of Pressure Vessels and Piping* in 2013

8.1 Introduction

Coke drums are normally constructed of carbon or low carbon alloy steels and internal clad with stainless steel to protect the coke drums from corrosion [1]. Some researchers state that the root cause of the shell bulging is the intense thermal cycling during the operation of filling-quenching cycle [2]. The bulges are normally found near the circumferential weld seams, yield strength of which normally is higher. The base material finally tends to become thin and fails via cracking as the result of the restraint caused by the weld seams [3-5].

There are very few investigations on the influence of yield strength ratio between the weld and the base on the fatigue lives of coke drums. It is a common consideration that the yield strength of the weld should be close to that of base material in order to keep strength uniformity throughout the drum shell sections. This effect of the yield strength matching on the shell durability is investigated by using specimens consisting of base and base-weld in the previous chapter and [6]. In that study, fatigue lives of three groups of specimens with different yield strength ratios of base-weld to base are evaluated at an elevated temperature of 250°C. It is found that higher strength ratio of S_w/S_b results in shorter fatigue life. However, this study does not consider the clad section (clad and clad-weld) of the actual clad wall structure of coke drums.

In this chapter, a structural specimen has been designed and manufactured based on the cross section structure of coke drum wall. It consists of four different materials: base, base-weld, clad, and clad-weld. Additionally, three groups of the structural specimens with different yield strength ratios of base-weld to base are prepared. Low cycle fatigue tests at elevated temperature of 250°C are carried out on these specimens. Furthermore, finite element analysis based on the actual specimen's geometry and material properties are conducted to help in understanding the experimental observations.

8.2 Structural Specimen Design and Materials

The structural specimen is designed as shown in Fig. 8.1. The specimens were directly cut and machined from a coke drum wall plate with materials of base, base-weld, clad and clad-weld. Because of thin thickness of the clad, a special machining procedure is implemented to minimize removal of the clad materials. The test section is required to contain all four sections of coke drum wall and their interfaces. The gauge length of the specimen is also minimized to reduce the instability due to cyclic loading. The machined thicknesses of clad and base are 3.048 mm (0.12") and 13.716 mm (0.54"), respectively. The total length of the specimen is 152.5mm (6"), and the gage length is 25.58mm (1.125"). The width and thickness of the gauge length is 16.764mm (0.66") and 8.89mm (0.35"), respectively. The specimen is heat tinted after heated to the temperature of 250°C as seen in Fig. 8.2. The sections can be distinguished by different formed colors due to different oxidation resistance of materials.

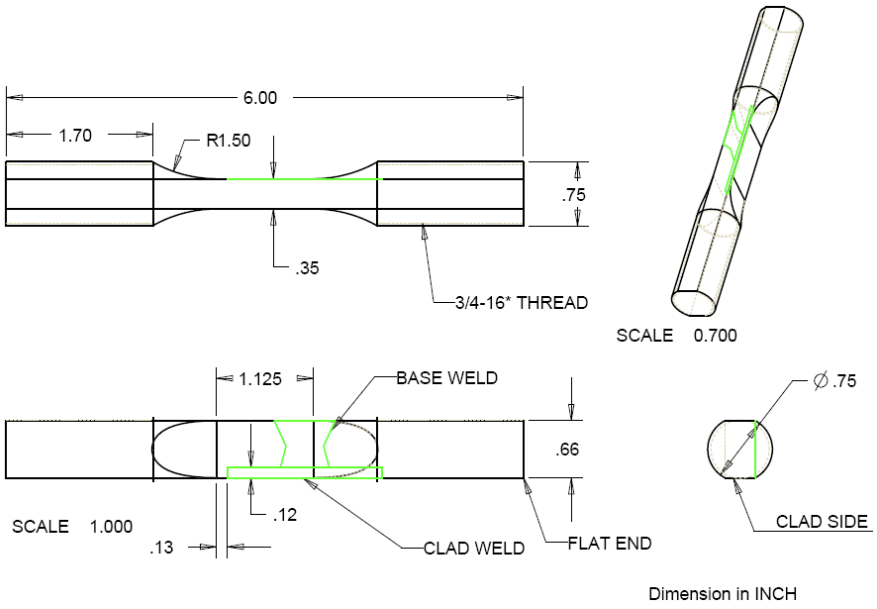

Figure 8.1 Detailed drawing of structural specimen

Figure 8.2 Photo of structural specimen after heated to 250°C

SA 387 Gr. 11 Class 2 base and weld materials are selected for this experimental investigation. The nominal chemical composition of SA387 Gr. 11 Cl. 2 is 1.25 Cr - 0.25 Mo. The clad material is SA 240 TP 410S stainless steel, and its nominal chemical composition is 13Cr. The clad weld material is ERNiCr-3 (INCO 82) with nominal chemical composition of 72 Ni, 20 Cr, 3 Mn, and 2.5 Nb.

It is common to characterize material's strength based on yield strength at room temperature (RT) in the industry. Therefore, the yield strengths of the cases 1 to 3 base-welds and base metal were first obtained from monotonic stress-strain curves at RT. The yield strength ratios (S_w/S_b) between base-weld and base are then established for each case: for case 1, 2, and 3, S_w/S_b = 1.166, 1.005 and 1.128 respectively. Since the fatigue tests were performed at 250°C under fully-reversed strain-controlled cyclic loading, it is more reasonable to determine the yield strength ratio (S_w/S_b) based on the cyclic stress-strain curves at 250°C. It represents the actual stable stress-strain relations in cyclic fatigue tests. The cyclic stress strain curves of one base and three weld materials are shown in Fig. 8.3. A repeated cyclic test is performed for each case of base-weld materials to ensure the accuracy of the results, and the maximum ratio difference between two identical tests is found to be within a negligible value of 0.6%.

The RT monotonic and 250°C cyclic stress strain curves of the clad and clad-weld are shown in Fig. 8.4, respectively. From the RT monotonic stress-strain curves, the ratio of yield strength between clad and clad-weld is found to be 1.3, which is much higher than the ratios between the base-weld and base. According to the 250°C cyclic-stress strain curves, the ratio of the yield strengths between the clad and clad-weld is found to

be 1.52 . In addition, to ensure the accuracy of this result, a repeated test of clad-weld is performed, and it is found that the scatter is within 4%.

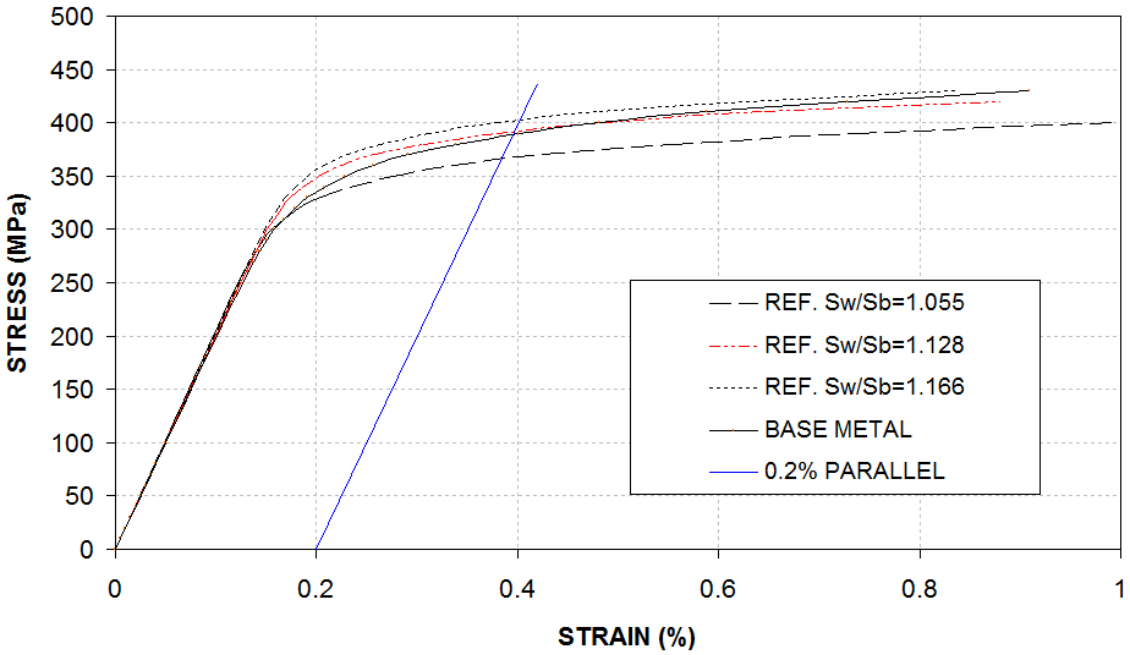

Figure 8.3 SA 387 Gr. 11 CL.2 (base and weld) 250°C cyclic stress train curves

Table 8.1 S_w/S_b ratios from different temperatures and tests

	S_w/S_b (R.T. monotonic)	S_w/S_b (250°C cyclic)
CASE 1 WELD	1.166	1.033
CASE 2 WELD	1.055	0.937
CASE 3 WELD	1.128	1.006

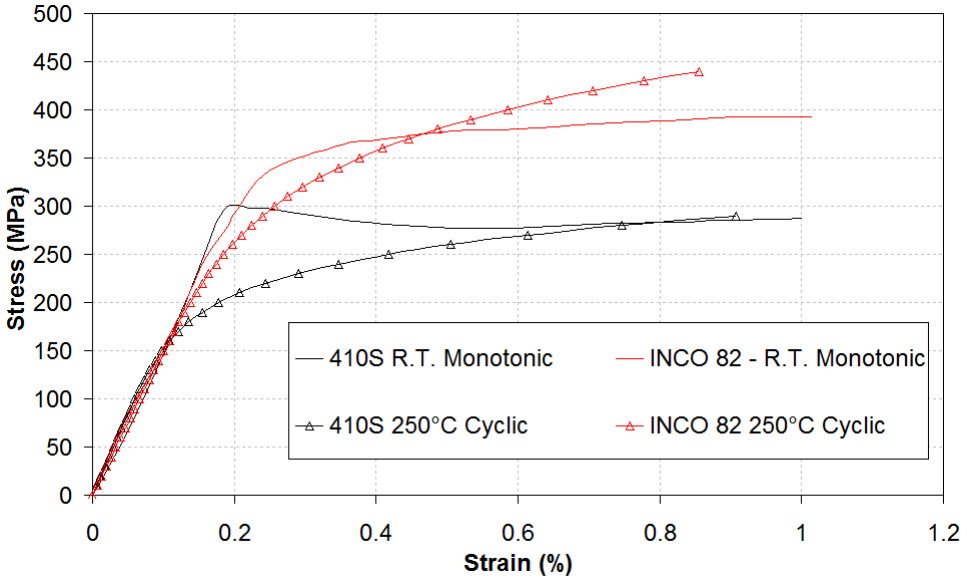

Figure 8.4 Stress strain curves comparison between 410S and INCO82

8.3 Experimental Setup and Procedures

The same high temperature fatigue test system discussed in chapter 3 was used to conduct isothermal fatigue testing in this investigation. The more detailed design and development of this system can be found [7].

Fully-reversed strain-controlled loading condition was applied on the specimens at constant temperature of 250°C. From an in-field measurement by using high temperature strain gauges and thermocouples, it is observed that extreme strains on shell surface occurs during the quenching stage when the temperature drops to the range between 300°C and 200°C [8]. Therefore, the testing temperature is set at 250°C to investigate the fatigue life. As shown in Fig. 8.5, three thermocouples, one in the center of the gauge section and other two on the two edges of the test section, were initially spot-welded on the specimen to verify the thermal gradient along the axial direction at 250°C. It is found that the thermal gradient along the axial direction is within 1% of T_{max} (250°C) which is fulfilled the recommendation by ASTM E606 [9]. After the temperature reached to 250°C and stabilized, the test starts after the strain is re-zeroed. Straining rate

is set constant at 0.5%/sec for the entire tests. Four strain ranges, 0.5%, 0.7%, 1% and 1.2% are controlled and measured at the gauge length. There are at least two tests conducted at each strain range to confirm the repeatability and accuracy of the data. Each fatigue test stopped when maximum load reached to 10% of the load at $N_f/2$ (stabilized maximum load).

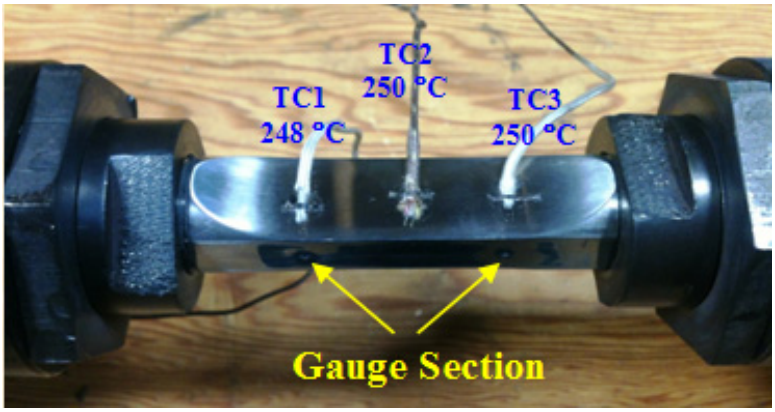

Figure 8.5 Thermocouple welded on the Specimen

8.4 Test Results and Discussion

The fatigue lives of case 1~3 structural specimens are plotted in log-log scale, as shown in Fig. 8.6. In addition, the fatigue life of pure base material at 250°C (adopted from reference 6) is shown in this plot for a comparison. The test data for each case of specimens can be well fitted by Manson-Coffin's [Eq. 7.1] relation:

$$\Delta\varepsilon_t = \Delta\varepsilon_p + \Delta\varepsilon_e = C_p\left(N_f\right)^{-k_p} + C_e\left(N_f\right)^{-k_e} \tag{8.1}$$

where Δε is strain range, C_p, k_p, C_e *and* k_e are constants by least square method.

Figure 8.6 shows case 1 specimens, which has largest value of S_w/S_b = 1.166 (monotonic at R.T.), have the shortest fatigue lives. However the fatigue lives of case 2 and 3 specimens do not have obvious deviations. At lower strain ranges, the fitting curve of case 2 is higher than that of case 3 (longer fatigue lives) while at larger strain range, the former case is lower than that of the latter case (shorter fatigue lives). This trend is also consistent with the experimental observations reported in reference [6] where three

cases of base and base-weld (without clad and clad weld) specimens with the same three different values of S_w/S_b are tested. Figure 8.6 also shows that the specimens of pure base material have the longest fatigue lives than the fatigue lives of all specimens including any weld section. This can be attributed to the detrimental effects of the weld, which may introduce non-matched yield strength ratio of S_w/S_b and HAZ in the base material.

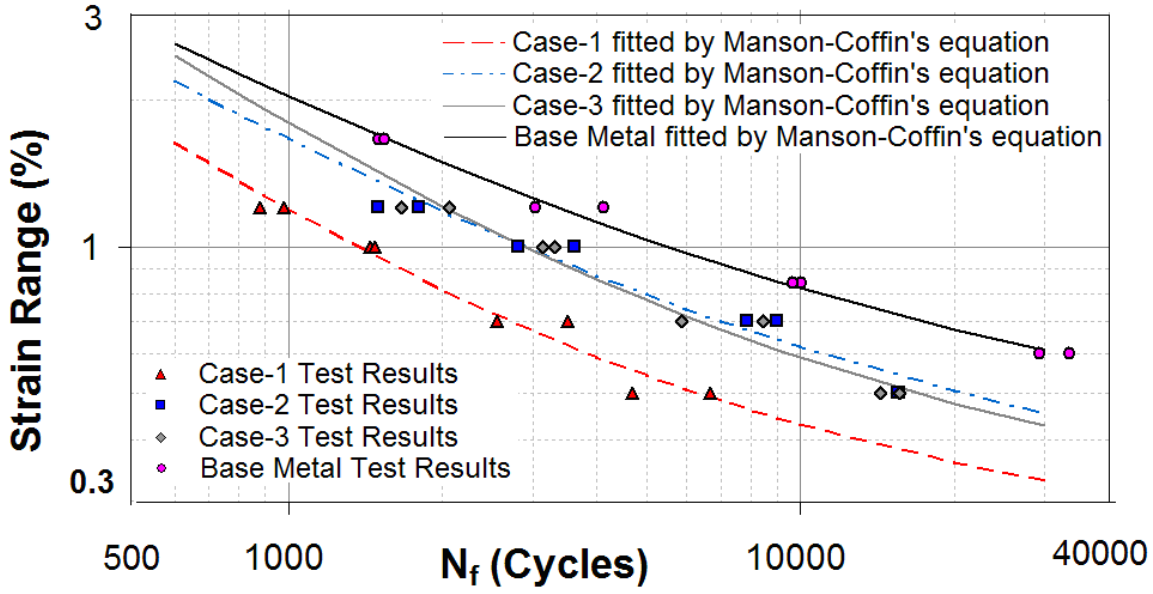

Figure 8.6 Fatigue test results of pure base, Case 1~3 structural specimens

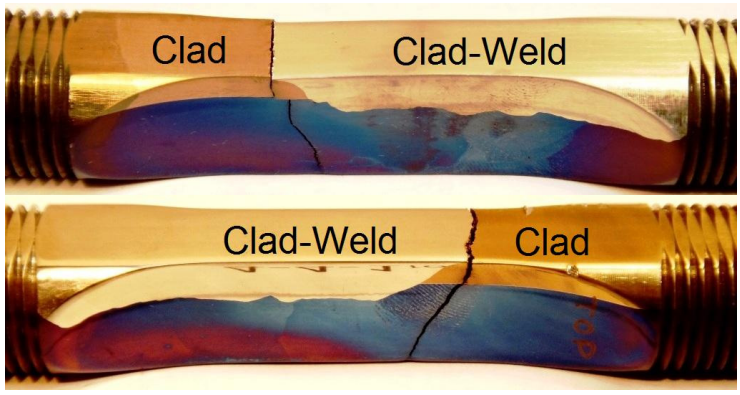

Figure 8.7 Example of rupture mode 1

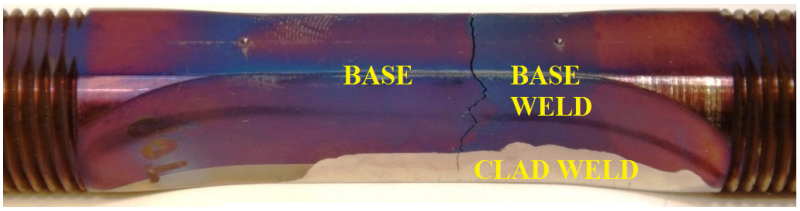

Figure 8.8 Example of rupture mode 2

Table 8.2 has listed fatigue failure lives and rupture modes for each case of 1 to 3 structural specimens. It is observed that for most of the specimens (23 of 25) cracks initiated from the interface between clad and clad-weld and then propagated into the base and base-weld area (some may also propagated first along the base-clad interface and then into the base and base-weld area), as shown in Fig. 8.7. It is noted that the yield strength ratio between the clad-weld (INCO82) and clad (410S) has much higher value (1.3, from RT monotonic curve and 1.52 from cyclic curve at 250°C) than that between base-weld and base. Under strain-controlled cycling, the soft clad material 410S could experience largest plastic deformation range. Therefore, for the current structural specimens, the weakest zone should be at clad 410S material very near to the interface between the clad and clad-weld. There is one specimen from case 2 which has crack initiated from the interface between base and base-weld and continuously grow into the clad weld, as shown in Fig. 8.8. One specimen from case 3 has crack initiated from the base (away from interface). The reasons for these two exceptional observations are not clear. It might be related to certain pre-existed defects in certain particular base or base-weld zones.

Table 8.2 Summary of fatigue test results for structural specimens

	Specimen	$\Delta\varepsilon$	N_f	RUPTURE
CASE 1 (YS RATIO 1.166)	4-1-1	1.2%	878	1
	4-2-1	1.0%	1477	1
	4-3-1	0.7%	2560	1
	4-4-1	0.5%	4710	1
	4-1-2	1.2%	981	1
	S4-1	1.0%	1442	1
	4-3-2	0.7%	3520	1
	4-4-2	0.5%	6670	1
CASE 2 (YS RATIO 1.055)	5-1-1	1.2%	1801	2
	5-2-1	1.0%	2817	1
	5-3-1	0.7%	9000	1
	5-4-1	0.5%	15640	1
	5-2-3	1.2%	1632	1
	5-4-3	1.0%	3495	1
	5-3-3	0.7%	7860	1
	5-4-2	0.5%	15530	1
CASE 3 (YS RATIO 1.128)	6-1-2	1.2%	2064	1
	6-2-1	1.0%	3308	1
	6-3-1	0.7%	8460	3
	6-4-1	0.5%	14320	1
	6-1-3	1.2%	1660	1
	6-2-2	1.0%	3144	1
	6-3-2	0.7%	5870	1
	6-4-2	0.5%	15590	1
	6-1-1	1.4%	1569	1

1. Crack initiated from interface of clad and clad-weld
2. Crack initiated from interface of base and base-weld
3. Crack initiated from base section

8.5 Finite Element Analysis and Discussion

8.5.1 FEA Model Setup

As shown in Fig. 8.9, 2D model of the test section of the specimen is created, and the meshing pattern of the 2D model is shown in the right side figure. The cyclic stress-strain curves at 250°C, plotted in Fig. 8.3 and 8.4, of base, case 1 to 3 welds, clad, and clad-weld are input into the ANSYS FEA code. In addition, the instantaneous linear coefficients of thermal expansion (CTE) at 250°C, Table 8.3, are considered and entered into the code to simulate the effect of thermal stress along the materials. It should be noted that the possible changes in properties in HAZ zones are not considered in the FE modeling.

The following boundary conditions are applied on the FEA model: the bottom edge is constraint in vertical direction, and the center node of the bottom edge is also fixed in horizontal direction. The nodes on the top surface are constrained to have same vertical displacements (plane-remains-plane). The temperature 250°C is first applied on the test section, and the displacement is then applied, which is equivalent to 0.35% of axial strain, on the top edge to simulate the axial fully-reversed cyclic loading.

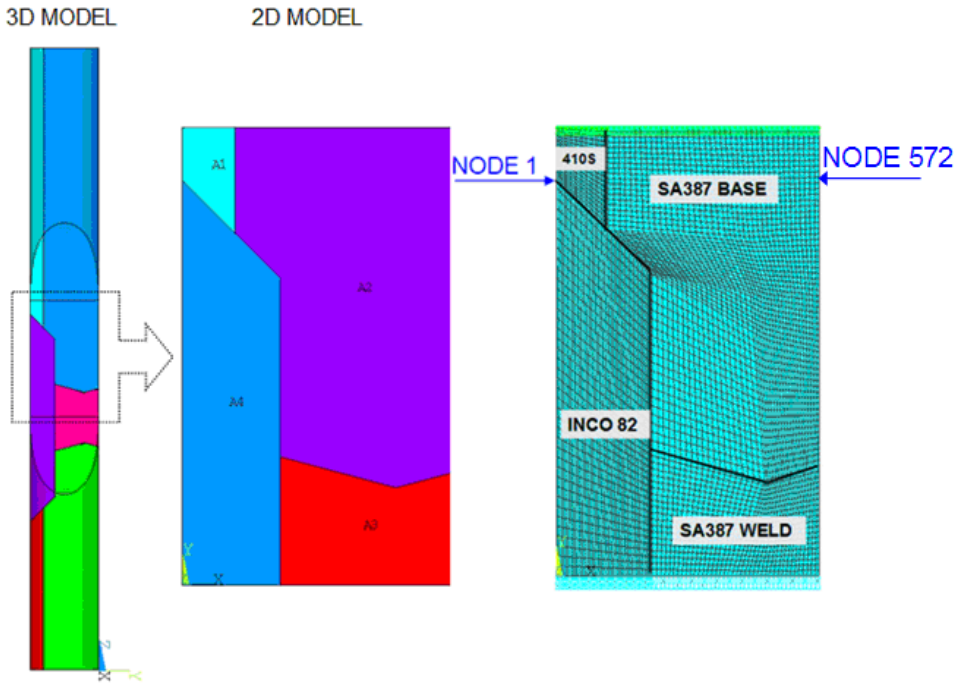

Figure 8.9 FEA modelling of structural specimen

Table 8.3 Instantaneous linear CTE at 250°C for base, clad and welds

	410S*	SA387 Gr.11CL2*	INCO82**
CTE (10^{-6} ε/°C)	12.1	14.3	11.3

* [10] ** [11]

8.5.2 FEA Results and Discussion

After the temperature of 250°C is applied on the model, the results of thermal and mechanical strains and stresses due to difference of CTEs are shown in Fig. 8.10. It can be seen that this temperature increase causes tensile mechanical strains and stresses in the clad and clad-weld and compressive mechanical strains and stresses in the base and base-weld. The highest mechanical strain is located in the clad and clad-weld near the interface between them (Node 1), and the highest tensile stress (axial direction) can also be indentified in that region from the results. This is due to the INCO82 and 410S have lower CTEs than that of base and base-weld, see Table 8.3. Therefore, it draws attention that considerable tensile stress and strain had been existed in the clad and clad-weld due

to their mismatched CTEs with base and base-weld materials. After the body temperature of 250°C is applied on the model, upon the thermal expansion, further displacement of the top edge corresponding cyclic strain range of 0.7% is applied. In this way, the loading condition is completely simulated according to the experiment.

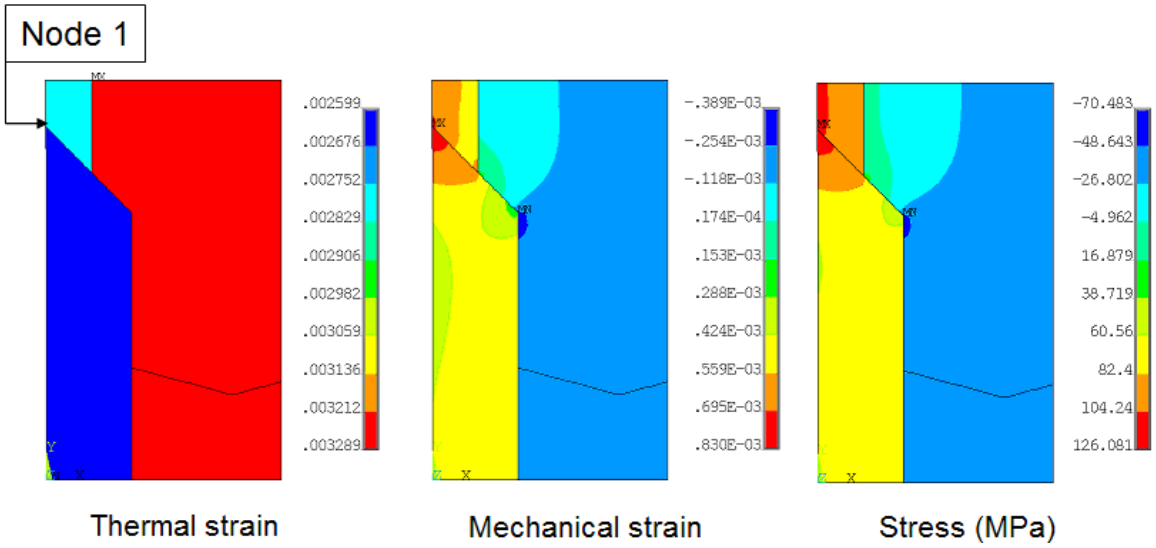

Figure 8.10 Thermal-mechanical strains and stress after heated to 250°C

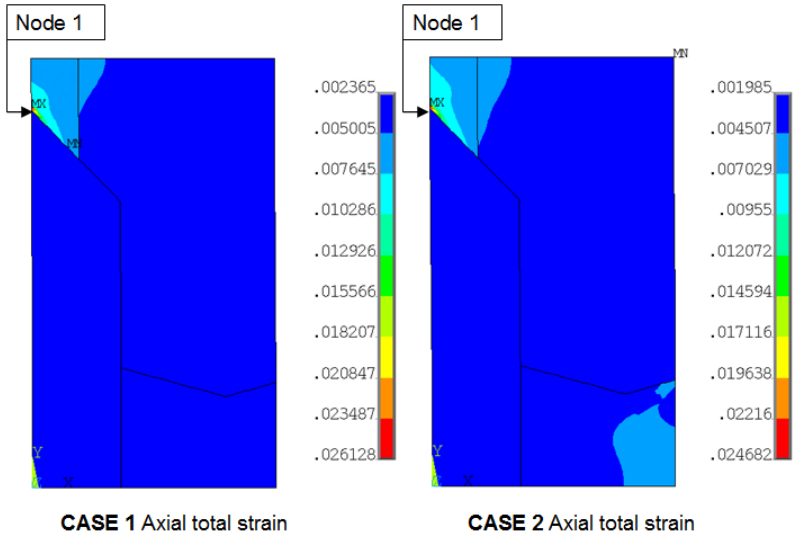

Figure 8.11 Contour results of axial strains of case 1 and 2

Figure 8.11 shows the contour results of axial strain for case 1 and 2. It can be seen that the maximum strain occurs at the same location, i.e. at the free edge and

interface between clad and clad-weld, Node 1 (in clad material). The maximum strain in the clad material near node 1 is due to the largest yield strength ratio, S_{cw}/S_c, between the clad-weld and clad. The hysteresis loops (axial direction) of case 1 and 2 at node 1 are shown in Fig. 8.12. The hysteresis loop of case 2 has less positive mean strain and slightly smaller strain range than that of case 1. It is known that the larger area of stress-strain hysteresis loop and more positive mean strain can result in earlier crack initiation. Therefore, for most specimens of this investigations (23 of 25) the cracks are initiated from the same location, node 1 (Fig. 8.11), due to higher maximum strain values and larger dissipated strain energy per cycle (the area of stress-strain hysteresis loop), but this process could take even shorter time for the case 1 and results in relatively shorter fatigue lives of specimens due to the higher positive mean strain of case 1.

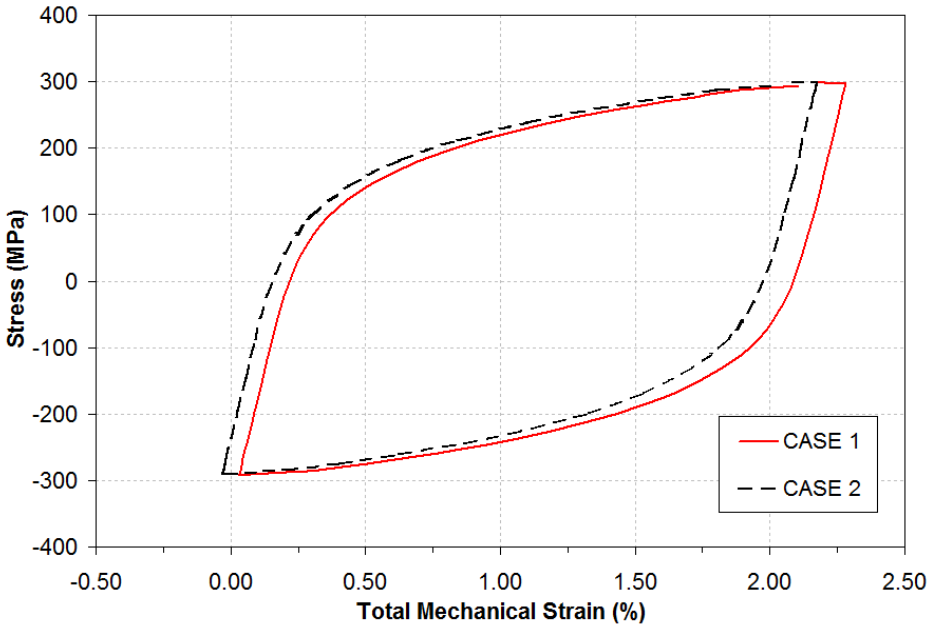

Figure 8.12 Hysteresis loops of case 1~3 on node 1 (Fig. 8.9)

Figure 8.13 shows the hysteresis loops of another point, node 572 (refer Fig. 8.9), in base material. This node is chosen on the edge of base material and on the same horizon to node 1. It can be seen that the enclosed area of the hysteresis loop for case 1 is significant larger than that of case 2. Therefore, it implies that for case 1 specimens, the cracks not only can initiate earlier at the interface between clad and clad-weld, but also

can propagate faster in the base material than that of case 2 specimens, resulting in shorter fatigue lives. As shown in Fig. 8.14, case 1 not only has shorter crack initiation period than that of case 2, but also it has shorter crack propagation period than case 2.

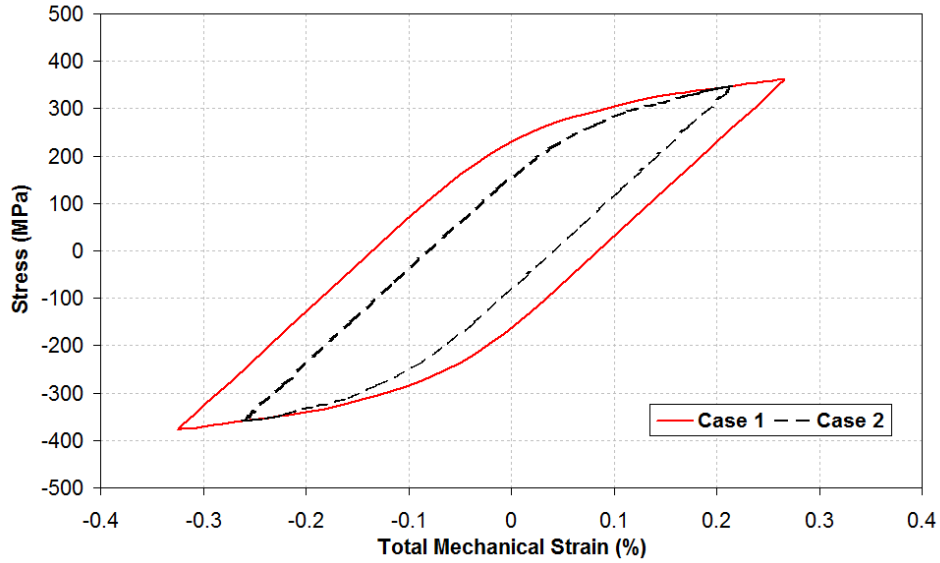

Figure 8.13 Hysteresis loops of case 1 and 2 on node 572 (Fig. 8.9)

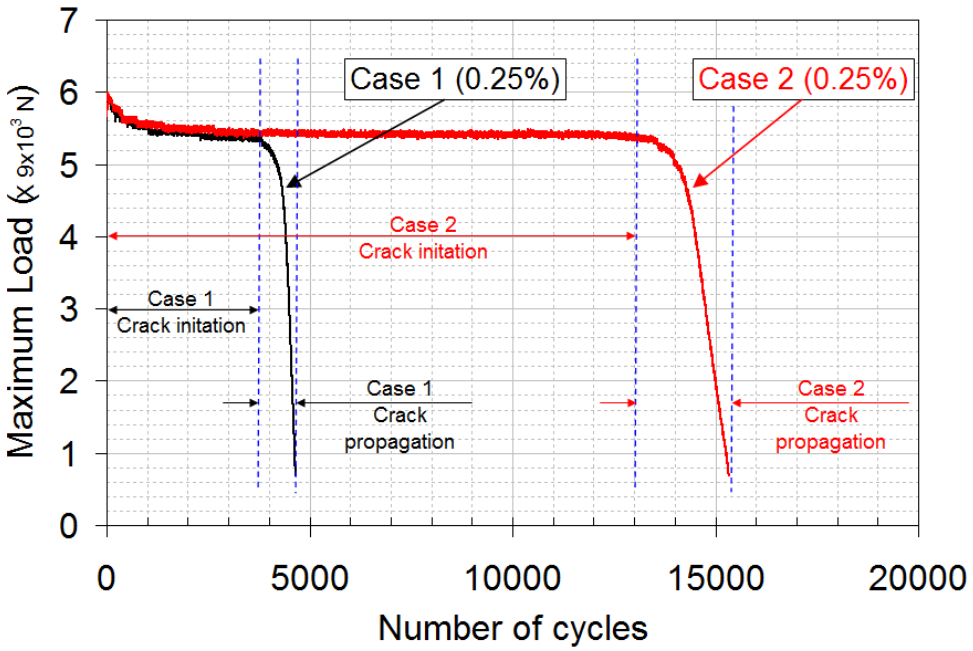

Figure 8.14 Plots of Maximum load vs. number of cycles for case 1 and 2

All the above comparisons are made for case 1 and case 2, which have different yield strength ratio between base and base-weld materials. However, from cyclic stress strain curves at 250°C (Fig. 8.4), the ratio of yield strength between clad and clad-weld materials is found to be the largest (1.3, from RT monotonic curve and 1.52 from cyclic curve at 250°C), which may cause the cracking in the interface between clad and clad weld. In order to investigate this effect, another two FEA results are compared. The first is assumed that the clad and clad-weld have uniform properties of INCO 82, and the second is assumed that they have the same properties of 410S. For the two assumptions, the properties of base and base-weld of case 2 are used. Figure 8.15b and 8.15c show the axial strain distributions for these two assumed cases of matched properties of clad and clad-weld. For a comparison the strain distribution of case 2 in Fig. 8.11b is replaced in Fig. 8.15a. It can be seen that the maximum strain loactions are moved to the interfaces between the Inco82 and base-weld (Fig. 8.15b) and between 410S and base (Fig. 8.15c). Furthermore, the maximum strain values of these two ideal cases (0.004644 and 0.006560) are much smaller than that for the actual non-mathed clad and clad-weld (0.02468).

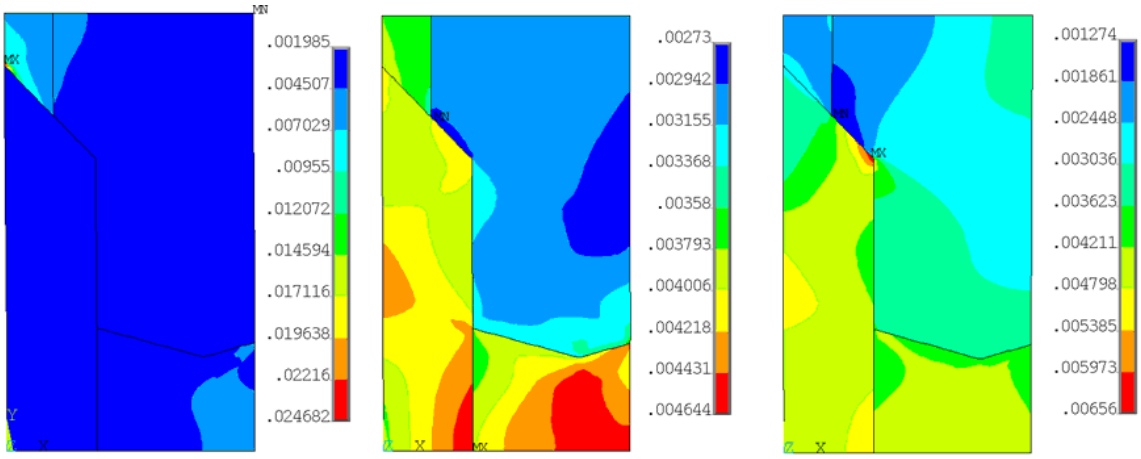

Figure 8.15 Contour results of total axial strains for case 2 and assumed perfectly matched clad and clad-weld

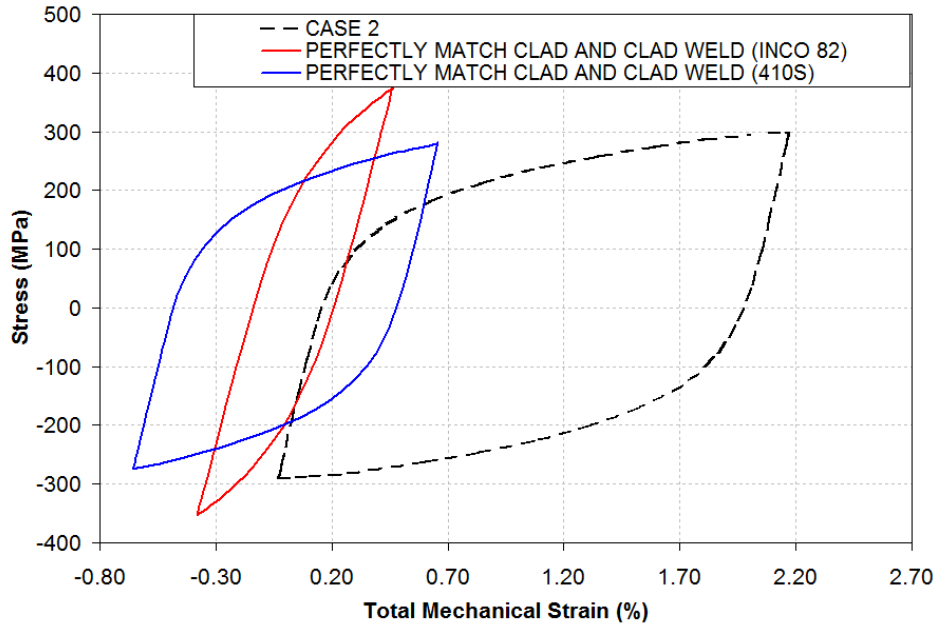

Figure 8.16 Hysteresis loops of case 2 and perfectly matched clad and its-weld at node 1

Figure 8.16 shows the stress-strain hysteresis loops at node 1 for the two assumed ideal cases and the actual case 2. It is obvious that the actual case 2 has much larger hysteresis loop and much larger positive mean strain. Therefore, the FEA results has further proved that for the current specimens simulating wall structure of coke drum the weakest point is at node 1, the interface between the clad and clad-weld, due to the largest yield strength difference between the two materials and due to larger difference of CTEs between the clad and base materials. If clad and clad-weld materials had more matched yield strengths, crack might not start from the location of the interface between the clad and clad-weld, and the clad wall structure of coke drums could have significant longer fatigue lives.

8.6 Conclusions

In order to better understand fatigue damage mechanisms of coke drums, an experimental investigation on fatigue lives of structural specimens similar to clad wall structure of coke drums, has been carried out. The structural specimens consist of four different materials: base (SA387), base-weld (SA387), clad (TP410S), and clad-weld (Inco82). Additionally, three groups of the structural specimens with different ratios of yield strength of base-weld to base are prepared. Low cycle fatigue tests at elevated temperature of 250°C are carried out on the structural specimens. The following conclusions can be drawn from the current study:

1. For the studied material combination of the structural specimens of coke drums the weakest area is in the clad (TP410S) near the interface between the clad and clad-weld (Inco82). Crack most possibly initiates from the free edge of the interface. This is due to the yield strength ratio between the clad-weld and clad, S_{cw}/S_c, has the highest value and the clad-weld and clad have lower CTEs than that of the base and base-weld;

2. The yield strength ratio between the base-weld and base, S_w/S_b, also has influence on the fatigue lives of the structural specimens as shown from the strain amplitude-fatigue life curves for the case 1 and case 2 specimens. The harder base-weld material results in shorter fatigue lives of the structural specimens;

3. The pure base material has longer fatigue life than any type of the specimens containing weld-sections. This is due to the material uniformity of the pure-base specimens and without heat affected zone (HAZ) introduced by the welding process;

4. The FEA results based on a model, similar to the structural specimen, are in consistence with the experimental observations. The numerical results explain the crack initiation and propagation mechanisms of the clad specimens.

5. There seems great potential to improve thermal-mechanical fatigue resistance of coke drums by optimal combination of the clad, clad-weld, base and base-weld materials. Two rules of thumb in materials selection are:

a. The CTEs of clad and clad-weld materials must be closer to the CTEs of base and base-weld materials;

b. The yield strength ratios between clad-weld and clad and between base-weld and base must be as closer as possible.

References

[1] Penso, J. A., Lattarulo, Y. M., Seijas, A. J., Torres, J., Howden, D., and Tsai, C. L., "Understanding Failure Mechanisms to Improve Reliability of Coke Drum," ASME (1999): PVP-Vol. 395, pp. 243–253.

[2] Pieper, C.J., Shockley, L.R. and Stewart, C.W., "Coke Drum Design-Longer Life through Innovation", AIChE 2000 Spring National Meeting, Atlanta, GA, March 5-9, (2000).

[3] Richard Boswell, "Coke Drum Bulges", Stress Engineering Services, May, (2001).

[4] Boswell R.S., Ferraro T., "Remaining Life Evaluation of Coke Drums", Plant Engineering, Design and Responsibility Symposium, Energy Engineering Conference, (1997).

[5] API Proceedings "1996 APE Coke Drum Survey-Final Report", American Petroleum Institute, Washington, DC, (1996).

[6] Chen, J., Yamatomo, T., Xia, Z., Esaki, K., "Experimental Evaluation of Fatigue Life of Coke Drum Materials with Weld Sections", Proceeding of ASME pressure vessel and piping Conference, July 14-18, (2013).

[7] Chen, J., "Experimental Study of Elastoplastic Mechanical Properties of Coke Drum Materials", Masters Dissertation, University of Alberta, Edmonton, (2010).

[8] Yamamoto, T., Arii, K. , Huhetaoli, S. Niimoto, S., Ohata, M., Tagawa, T., Minami, F., "Investigation of Bulging Behavior of Coke Drum -A practical analysis of bulging under complex quench conditions-", Proc. Pressure Vessels & Piping Division Conf., ASME (2011): PVP2011- 57428.

[9] ASME E606-04, “Standard Practice for Strain-Controlled Fatigue Testing”, ASTM International, West Conshohocken, PA, US (2004).

[10] ASME Boiler & Pressure Vessel Code Section II-Materials-Part D-Properties, (2011), New York, NY, USA

[11] Panneerselvam, G. et al. "A study on the thermal expansion characteristics of Inconel-82 filler wire by high temperature X-ray diffraction", Materials Letters, Vol.58 1-2, (2003), pp. 216-221.

CHAPTER 9 Fatigue Life Estimation of Coke Drums under Global and Local Loadings[7]

To accurately predict the safety lives of coke drums, a statistical fatigue life evaluation method is proposed in our group. To implement this method, simplified thermal-elasto-plastic analytical models are used to calculate maximum equivalent strain amplitudes for global cycling and local hot and cold spot events. Statistical analysis of temperature data on a coke drum shell is also performed to get the probabilities of each event. The final statistical fatigue life evaluation model is based on Palmgren-Miner's damage accumulation rule with consideration of maximum equivalent strain amplitudes from global and local loadings and thermal-mechanical fatigue life curves of coke drum materials. The present analysis shows that the safety life of the coke drum is about 5,000 operational cycles, which are in good agreement with the surveyed lives provided by American Petroleum Institute (API) coke drum survey.

[7] Part of this chapter has been submitted to *Engineering Failure Analysis* in July 2014

9.1 Introduction

Coke drums are traditionally not designed for cyclic loads. It is has not been the usual practice to give serious consideration to the possibility of fatigue failure. However, due to the severe cyclic thermal and mechanical loads, their operational life is normally much shorter than other pressure equipment in refineries. Coke drums are susceptible to cracking and sometimes associated with bulging deformation after several thousands of operational cycles [1, 2]. These damages may lead to unexpected failure of coke drums, which may interrupt the production and thus result in huge economic losses to the oil companies. Therefore, it is beneficial to conduct the reliable lifetime assessment of coke drums.

Coke drums are typically constructed from alloy 410S stainless steel [12Cr] cladding and 1Cr-1/2Mo to 2½-1Mo low alloy carbon steel base plate. It has been well recognized that low cycle thermal-mechanical fatigue (TMF) is the most common failure mechanism of a coke drum and is responsible for the initiation of cracks in coke drums [3]. References [4-9] studied the fatigue life estimation for the coke drums by conducting low cycle fatigue tests. However, these low cycle fatigue tests only conducted on base material under isothermal condition. Therefore, the reliable lives of coke drums should be estimated based on thermal-mechanical fatigue assessment of the vessels. In addition, hot and cold spots appear in the coke drum shell in the quenching stage due to the existence of uneven and random channelling flows of water through the residual coke mass during this period. The developed hot and cold spots may primarily contribute to the bulging of the shell and have been considered as another failure mechanism of a coke drum [10, 11]. As a result, the hot and cold spot effect should also be carefully taken into consideration in the assessment of the reliable lives of coke drums. It should be noted that such an effect is complicated since the location, the temperatures of the affected areas and their surrounding areas are most likely in a random nature. Therefore, a statistical fatigue life analysis method for coke drums instead of a deterministic one should be more appropriate.

The TMF life curves of the coke drum materials obtained previously in Chapter 2 and 4 are used to provide a more accurate fatigue life evaluation method, which represents a similar loading scenario experienced by coke drums during the operation. As mentioned before, the hot and cold spot effect in the quenching stage significantly influences the stress and strain levels in the coke drum shell, therefore, should be included in the fatigue life evaluation of coke drums. Zhang et al. [12] in our research group developed a simplified local stress analysis model for the estimation of hot and cold spot effect on the drum shell. In this model, the hot or cold spot is realized by imposing a temperature difference, either higher or lower, than the temperature of its surrounding material. Based on this developed model, the stress and strain induced by the hot and cold spot effect at both clad and base plates could be obtained accurately. It is also noticed that the occurrence of the hot and cold spots in a operational cycle is absolutely arbitrary due to the random channelling formations on the inner wall of coke drums. To quantitatively evaluate this phenomenon, Yan et al. [13] in our group examined the probability distributions of hot and cold spot from the measured temperature data.

In this chapter, a statistical fatigue life analysis method will be briefly introduced for coke drums. The development of this method depends on the thermal-mechanical fatigue test results, the developed simplified thermo-elasto-plastic models and the statistical analysis of temperature data on a coke drum shell. Finally, the statistical fatigue life evaluation model of coke drums is developed by combining Palmgren-Miner's cumulative damage rule and probabilities of various loading conditions. This methodology presented is considered to be more accurate for the fatigue life prediction of coke drums. The evaluation methodology developed in this study can be employed to predict the safety lives of coke drums and is expected to be helpful for the design and maintenance of the equipment.

9.2 Materials Properties and TMF Life Curves

A set of base and clad materials, ASME SA 387 Gr 22 CL 2 (SA 387) and ASME SA 240 TP410S (410S), are used in this investigation. The nominal chemical composition of SA 387 Gr 22 CL 2 and SA 204 Gr C are 2¼ Cr-1Mo and 12Cr, respectively. The TMF lives of coke drum base material SA 387 and clad material 410S are as shown in Fig. 9.1. $2N_f$ in this log-log plot is defined as the reversal to the final failure of the test specimen. From this figure, it can be seen that the fatigue life of the base material is slightly higher than that of the clad material at relatively large mechanical strain amplitude, while both materials show similar fatigue life behaviours when the mechanical strain amplitude is relatively low, i.e., below 0.3% of strain amplitude.

The fatigue life curves of both materials can be well represented by the Coffin-Manson-Basquin's relation [14-16] incorporating the mean stress [17] and mean strain effects as:

$$\frac{\Delta\varepsilon_{eqv}}{2}=\left(\frac{\sigma_f^{'}-\sigma_{meqv}}{E}\right)\left(2N_f\right)^b+\left(\varepsilon_f^{'}-\varepsilon_{meqv}\right)\left(2N_f\right)^c \tag{9.1}$$

in which $\Delta\varepsilon_{eqv}/2$ is the maximum equivalent strain amplitude; ε_{meqv} and σ_{meqv} are the equivalent mean strain and mean stress corresponding to the maximum equivalent strain amplitude; σ'_f and b are the fatigue strength coefficient and fatigue strength exponent; E is the Young's modulus at 100 °C; ε'_f and c are the fatigue ductility coefficient and fatigue ductility exponent. It should be mentioned that the mean stress and strain could appear in the stress and strain analysis of coke drums based on the developed models. Thus, it is necessary to incorporate these two terms in the final evaluation of fatigue life, as seen from Eq. (9.1). Table 9.1 shows the experimentally determined material constants of the both clad and base materials. As a result, the fatigue life of coke drum materials, under any determined maximum equivalent strain amplitude $\Delta\varepsilon_{eqv}$ with corresponding equivalent mean strain ε_{meqv} and mean stress σ_{meqv} could be predicted by using Eq. (9.1) and material constants listed in Table 9.1.

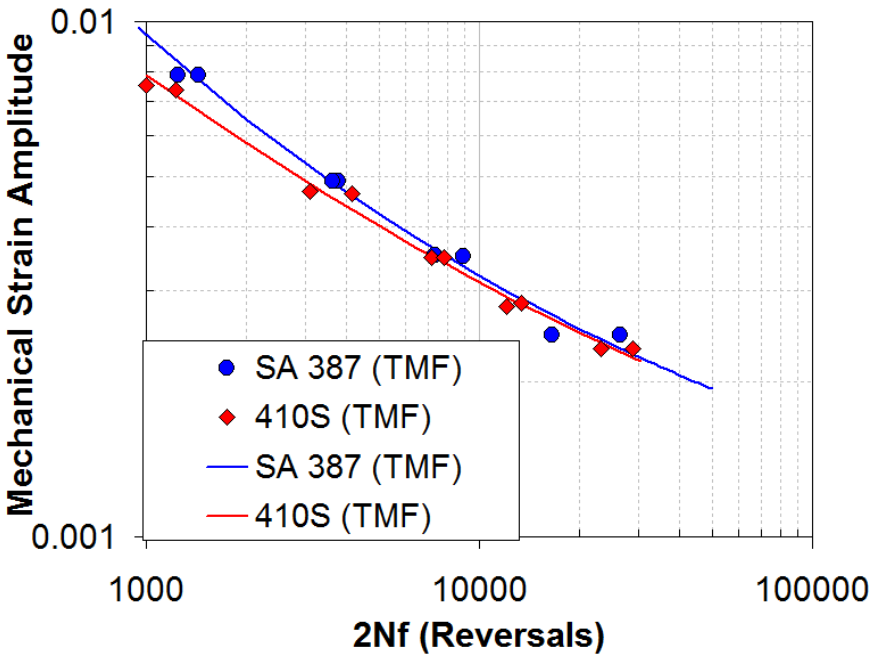

Figure 9.1 Thermal-mechanical fatigue lives of coke drum base and clad materials

Table 9.1 Fatigue properties of coke drum materials based on TMF tests

Material	σ'_f (MPa)	b	ε'_f	c	E (GPa)	Plate
SA387	2006.73	-0.1688	1.0228	-0.7398	202.7	Base
410S	795.5	-0.1112	0.3095	-0.5734	185	Clad

To calculate the maximum equivalent strain amplitudes, equivalent stress and strain means through simplified thermo-elasto-plastic models developed by Zhang [12] in our group, the temperature-dependent bi-linear material properties including Young' modulus E, yield strength σ_y and tangent modulus E_t should be determined first. Although they could be directly obtained from ASME Boiler and Pressure Vessel Code [18], the data provided there are the specified minimum values, which are too conservative to the practical uses of the materials. To obtain more practical material properties, the cyclic stress-strain curves (CSSC) of SA387 and TP 410S are first experimentally obtained at room temperature, 100 °C, 250 °C, and 480 °C, respectively as shown in Fig. 9.2. Fig. 9.3 shows an example of the stress-strain curve and the graphic definitions of the material

properties. The case is for clad material of the coke drum and the test temperature is set at 480°C. As seen from Fig. 9.3, a bilinear relationship of the stress-strain curve is assumed to determine the material properties. The Young's modulus E is obtained by a linear regression least-squares estimate of the slope in the proportional elastic region, which is line a; then construct a line b perpendicular to the abscissa that passes through $\varepsilon = 0.5\%$. This value is chosen since the absolute value of obtained strain is always lower than 0.5%. The tangent modulus E_t is obtained as the slope of the tangent (which is line c) to the stress-strain curve at the intersection of line b and the curve. Finally, the yield strength σ_y is defined as the stress of the intersection of line a and line c. Following the same procedure, the material properties of coke drum base and clad materials at different temperatures can be obtained. After that, a material property-temperature relationship can be determined and input in the analytical models. The coefficients of thermal expansion (CTE) of both materials, as shown in Fig. 9.4 are also experimentally measured and compared with ASME data [18], they both have fairly good agreement. The values of CTE also serve as input data in this model. The system setup for CTE measurement is introduced in Appendix C.

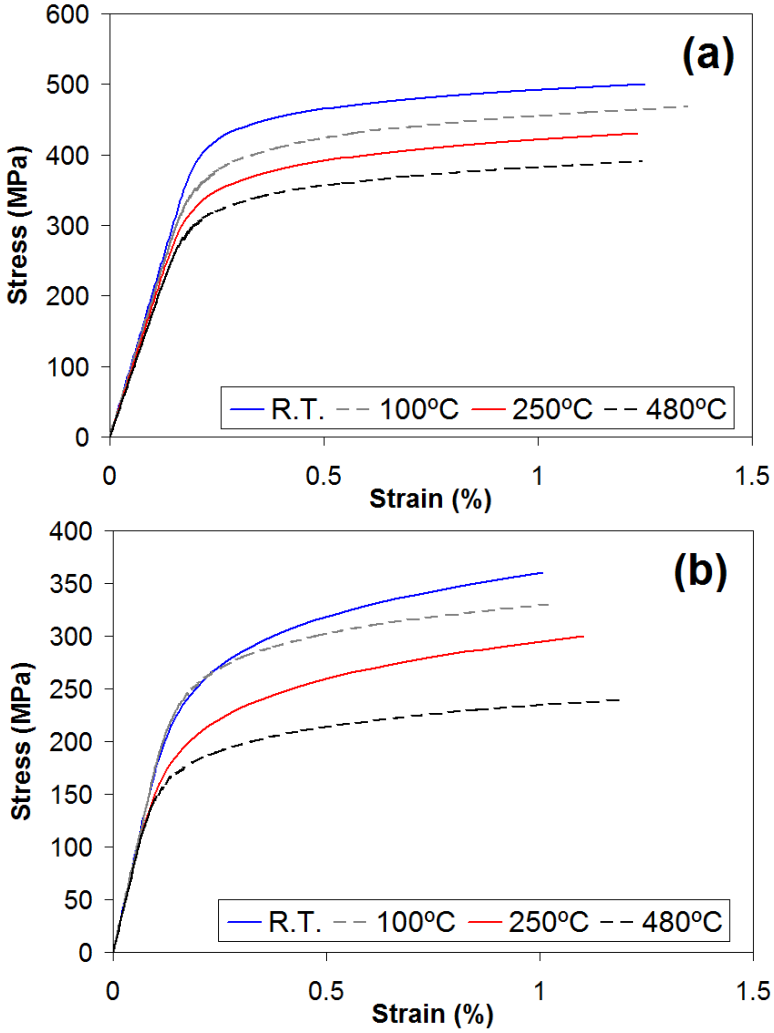

Figure 9.2 Cyclic stress strain curves (a) SA 387 (b) TP 410S

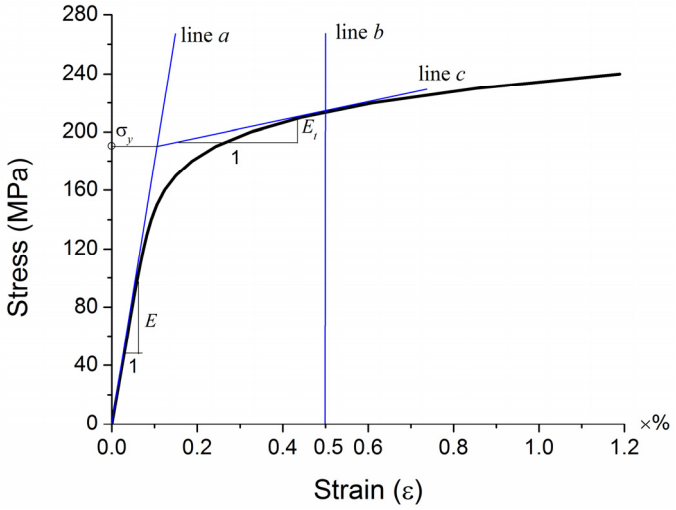

Figure 9.3 CSSC for clad material and the graphic definitions of material properties.

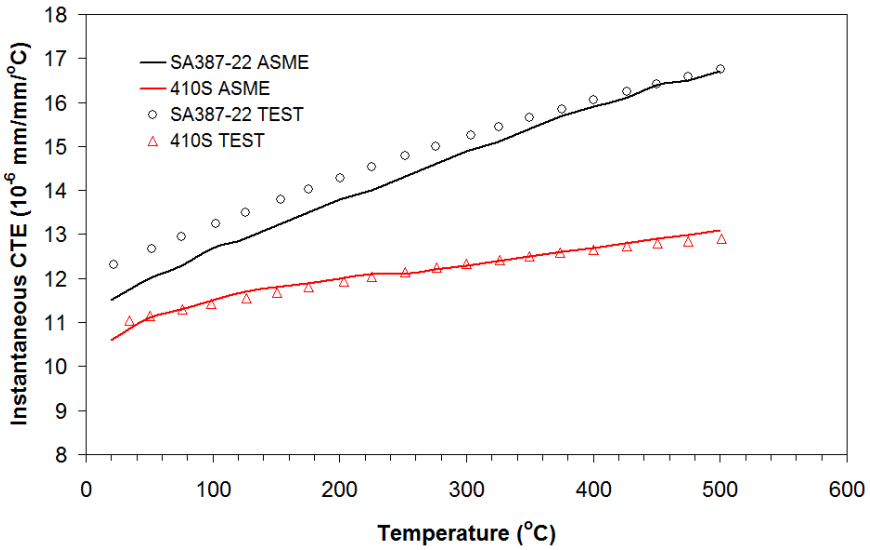

Figure 9.4 Coefficient of thermal expansion of SA 387 and TP 410S

9.3 Simplified Thermo-Elasto-Plastic Models

This work was undertaken by Dr. Zhang, Yanxiang. in our research group

Two simplified analytical models have been successfully developed to estimate stress and strain in coke drums. Global simplified analytical model is based on one clad element to estimate stress and strain induced mainly due to the difference of thermal expansion coefficients in clad and base materials. Internal pressure is taken into account in this model. Local simplified model is developed according to a clad circular plate with a central spot to simulate effects caused by hot and cold spot. A hot or cold spot is established by imposing a higher or lower temperature in the spot than the temperature of its surrounding area. More details about these two models can be referred to [12]. Validation of both models is verified by the good agreement of results from finite element analysis (FEA) and simplified models.

For global loading case, temperature applied increases from 37.8 °C to 450 °C and then decreases to 37.8°C whereas pressure is in-phase with temperature with the maximum pressure being 0.647 MPa. For local hot or cold spot loading case, a temperature difference between the central spot and its surrounding area is applied to the

simplified local model. The hot spot loading is defined as the temperature in the central spot is higher than its surrounding materials, and vice versa for the cold spot. The result shows that stress and strain in both clad and base change significantly and reach much higher level than those in global case, because both clad and base yield at this temperature difference. Therefore, the local hot and cold spot effect is significant and indispensible in the fatigue life prediction of coke drums.

After stress and strain components obtained for clad and base materials, the component strain range is determined. Equivalent strain amplitude is calculated based on von Mises yield criterion as:

$$\frac{\Delta\varepsilon_{eqv}}{2}=\frac{2}{\sqrt{3}}\sqrt{\left(\frac{\Delta\varepsilon_{hoop}}{2}\right)^2+\left(\frac{\Delta\varepsilon_{axial}}{2}\right)^2+\frac{\Delta\varepsilon_{hoop}}{2}\frac{\Delta\varepsilon_{axial}}{2}}; \tag{9.2}$$

Similarly, the equivalent mean stress σ_{meqv} and mean strain ε_{meqv} are calculated as:

$$\begin{aligned}\varepsilon_{m,eqv}&=\frac{2}{\sqrt{3}}\sqrt{\varepsilon_{m,hoop}^2+\varepsilon_{\mathrm{m},axial}^2+\varepsilon_{m,hoop}\varepsilon_{m,axial}};\\ \sigma_{m,eqv}&=\sqrt{\sigma_{m,hoop}^2+\sigma_{m,axial}^2-\sigma_{m,hoop}\sigma_{m,axial}}\end{aligned} \tag{9.3}$$

Then the maximum equivalent strain amplitude from equation (9.2) is chosen to be used in fatigue life equation (9.1). Meanwhile at the corresponding equivalent mean stress and strain are also adopted in fatigue life equation. Only positive mean strain or/and stress effect is considered in this case since it is favourable to the crack opening and thus is likely to shorten the fatigue life of the material. Therefore from Eq. (9.1) and using the material properties listed in Table 9.1, the fatigue life of coke drum materials under global loading condition or any local loading condition can be obtained.

9.4 Statistical fatigue life prediction method

This work was undertaken by Dr. Yan, Zhi. in our research group

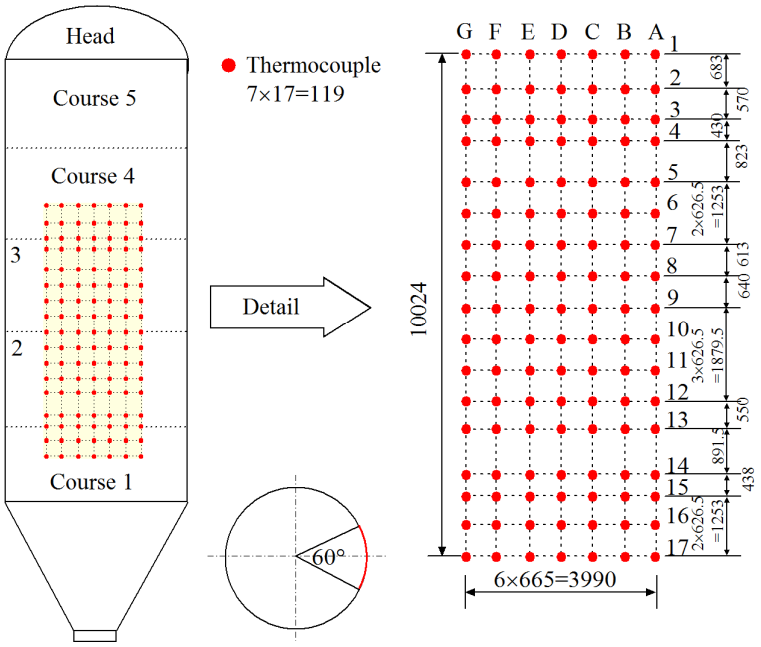

Figure 9.5 Thermocouple grid on a coke drum

Ref. [13]

The objective of the statistical analysis is to characterize the apparently random hot and cold spot event using statistical modeling theory and then to apply an appropriate methodology to relate fatigue lives of coke drums to the experimental fatigue life data which are obtained in a deterministic model. The temperature measurements at different locations of a certain area of the drum shell were recorded, as shown in Fig. 9.5. A total of 119 (7 columns by 17 rows) thermocouples were installed. The thermocouple grid spans 4 shell courses (Course 1 to Course 4) and covers 1/6 of the coke drum circumference. By investigating the temperatures at the different measurement locations, it is found that the temperature difference between the investigated central locations and their surrounding locations could be significant in the quenching stage of the operational cycle. The statistical analysis is conducted based on over 200 operational cycles of the measured coke drum. It is found that the largest temperature differences produced by both the hot and cold spots follow a Weibull-type generalized extreme value (GEV)

distribution [13]. The probability density function of the GEV distribution could be expressed as:

$$f(\Delta T)=\frac{1}{\sigma}\left[1+k\left(\frac{\Delta T-\mu}{\sigma}\right)\right]^{-1-\frac{1}{k}}\exp\left\{-\left[1+k\left(\frac{\Delta T-\mu}{\sigma}\right)\right]^{-\frac{1}{k}}\right\} \tag{9.4}$$

where k, σ and μ are shape parameter, scale parameter and location parameter of the temperature difference data, respectively. From the analysis, it is shown that the peak values of the probability densities occur at about 200°C temperature difference. Since the local strains can be calculated at any given temperature difference based on the simplified local analysis model, the statistical distribution of local strains can also be correlated in the same way. Figure 9.6 shows the histogram of maximum equivalent strain amplitude induced by the cold spot in base layer of the coke drum shell as an example.

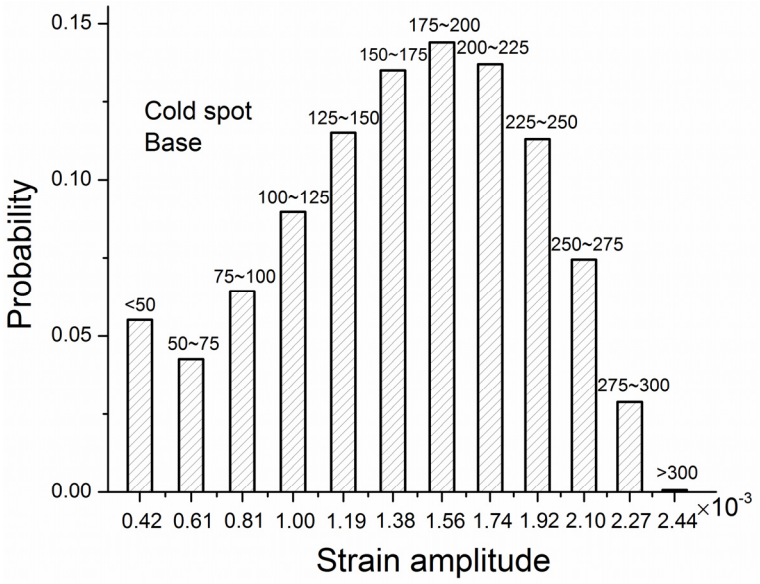

Figure 9.6 Histogram of strain amplitude induced by cold spot in base layer [13]

9.5 Estimation Based on Palmgreen-Miner's Rule

From the above analysis, it can be seen that coke drums are subjected to both global and local loadings. To predict the lifetime of the coke drums, cumulative damage rule should be applied. In this work, a statistical fatigue life estimation method is introduced based on Palmgreen-Miner's cumulative damage model, which can be expressed as [19]:

$$D = \sum_{i=1}^{n} \frac{n_i}{N_i} \tag{9.5}$$

in which n_i is the number of cycles at a given stress or strain amplitude; N_i is the number of cycles to failure at the same stress or strain amplitude; D is the damage index and the damage at failure is taken as $D = 1$. To incorporate the statistical analysis into the Palmgren-Miner's model, the following is assumed:

1. Hot or cold spot is considered when the temperature difference is greater than 50°C
2. Both global and local loadings are considered when the temperature difference is greater than 50°C
3. The occurrence of hot or cold spot is equal
4. 12 loading ranges corresponding to hot or cold spot in ΔT are considered

Therefore, for a coke drum having an service life of n_f, Eq. (9.5) can be rewritten as

$$\frac{n_f}{N_f^g} + \sum_{i=2}^{12} \frac{p_i^h n_f}{N_{fi}^h} + \sum_{i=2}^{12} \frac{p_i^c n_f}{N_{fi}^c} = 1 \tag{9.6}$$

in which N_f^g is the fatigue life of clad or base for the coke drum under global loading; N_{fi}^h and N_{fi}^c are the fatigue life of clad or base for the coke drum under *i*-th local loading ranges induced by different hot and cold spots, respective; p_i^h and p_i^c are the corresponding probabilities. From Eq. (9.6), the fatigue lives of the coke drum can be estimated based on strain amplitude according to both clad and base materials. The predicted fatigue lives of base and clad layers based only on strain amplitude from global

loading are $4.9x10^{10}$ and $1.7x10^{5}$, respectively. The predicted fatigue lives of base and clad layers based on strain amplitudes from both global and local loading are $2.04x10^{4}$ and $2.12x10^{4}$, respectively. Therefore, the local hot and cold spot attacks are more detrimental than global loading. Thus, the local hot and cold spot effect is crucial to be considered in the fatigue life prediction for coke drums. Moreover, the fatigue life of HAZ is roughly a quarter of pure base material at the same strain amplitude, as discussed in chapter 5. As a result, the fatigue lives become $5.1x10^{3}$ and $5.3x10^{3}$ cycles for HAZ of base and clad materials, respectively, under the severe hot and cold spot attack. These results are consistent with the findings in [1, 20], which indicated that coke drums are susceptible to damages after several thousands of operational cycles. The life of coke drums could be much shorter if more severe and frequent hot or cold attack occurs at some points.

9.6 Conclusions

In this study, a statistical fatigue life prediction method of coke drums is suggested with the consideration of the randomness of local hot and cold spot effect. The method is based on the thermal-mechanical fatigue test results, the simplified thermo-elasto-plastic global and local analysis models and the statistical analysis of temperature data on a coke drum. The experimentally obtained strain-life curves could determine the fatigue life of coke drum materials at a given maximum equivalent strain amplitude level, which can be calculated from simplified analysis models. The probabilities of multiple strain amplitudes observed in the coke drum service life are determined from the statistical distribution of the temperature difference. By incorporating the statistical results into Palmgren-Miner's rule, the damages of the coke drums under both global thermal-mechanical loading and additional local hot and cold spot attacks are accumulated. With consideration of life deduction for HAZ, the fatigue lives estimated are $5.1x10^{3}$ and $5.3x10^{3}$ cycles for base and clad materials, respectively. The life of coke drums could be much shorter if more severe and frequent hot or cold attack occurs at some points.

References

[1] Stewart, C., “Vertical Plate Technology Extends the Life of Coke Drums,” Welding Journal, Vol. 83, (2004), pp.34-36.

[2] ASME, “Boiler and Pressure Vessel Code VIII Rules for Construction of Pressure Vessels Division 1, ” ASME, New York, (2007).

[3] Penso, J. A., Lattarulo, Y. M., Seijas, A. J., Torres, J., Howden, D., and Tsai, C. L., “Understanding Failure Mechanisms to Improve Reliability of Coke Drum,” PVP (Am. Soc. Mech. Eng.), Vol. 395, (1999), pp. 243–253.

[4] Oka, M, et al. "Study On The Effects Of Switching Temperature On The Thermal Fatigue Life Of The Shell-To-Skirt Junction Of Coke Drum." Journal of Pressure Vessel Technology-Transactions of ASME 133.6, (2011).

[5] Sasaki, Y., and S. Niimoto. " Study on Skirt-to-Shell Attachment of Coke Drum by Evaluation of Fatigue Strength of Weld Metal." Proceedings of ASME Pressure Vessels and Piping Conference (2012): PVP2011-57314.

[6] Li, Z., Zhou X., Xu W., and Fenkun L., "Safe Life Estimation of Coke Drum in Service Environment." Journal of Pressure Vessel Technology134.3, (2012).

[7] Ramos, A., Rios, C. and Vargas, J., “Mechanical Integrity Evaluation of Delayed Coke Drums”, PVP-Vol.359, Fitness for Adverse Environments in Petroleum and Power Equipment, ASME, (1997).

[8] Ramos, A., Rios, C., etc., “Delayed Coke Drum Assessment Using Field Measurements and FEM”, PVP-Vol.368, Analysis and Design of Composite, Process, and Power Piping and Vessels, ASME , (1999).

[9] Ramos, A. J., Rios, C. and Vargas, J.A.R., "Fatigue Life Prediction of Delayed Coke Drums", Vision Techenologica, Vol.6, (1999), pp. 93-100.

[10] Ju, F., Aumuller, J., Xia, Z., and DuPlessis, P., "Global and Local Elastic-Plastic Stress Analysis of Coke Drum under Thermal-Mechanical Loadings," ASME J. Pressure Vessel Technol., Vol. 133, (2010), pp. 061202.

[11] Oka, M., Himsar A., Masashi D., and Hiroyuki F.. "Initiation of Bulges in a Coke Drum Subjected to Cyclic Heating and Cooling, also Cyclic Mechanical Loads" Journal of Thermal Stresses 33.10, (2010).

[12] Zhang, Y. X., and Xia, Z. H., "Simplified Thermo-Elasto-Plastic Analysis Models for Determination of Global and Local Stresses in Coke Drums," ASME 2013 Pressure Vessels and Piping Conference, 3, (2013), pp. V003T03A070.

[13] Yan, Z., Aumuller, J.J., Esaki, K., and Xia, Z. H., "Statistical Analysis of Shell Metal Temperature Data for a Coke Drum," Internal report, (2014).

[14] Basquin, O.H. "The exponential law of endurance tests", ASTM proceeding. 10 (1910) , pp.625-630.

[15] Coffin, L. F. Jr., "A study of the effects of cyclic thermal stresses on a ductile metal", Trans. ASME, Vol.76, (1954), pp. 931-950.

[16] Manson, S.S., "Behaviour of materials under conditions of thermal stress", Heat Transfer Symposium, University of Michigan, (1953), pp.9-75. See also NACA-TN-2933, (1953).

[17] Morrow, J.D. Fatigue design handbook, section3.2. SAE Advanced in Engineering, Vol.4, (1968), pp. 21–29.

[18] ASME, Boiler and Pressure Vessel Code II Part D Properties, ASME, New York, (2007).

[19] Miner, M.A., "Cumulative Damagein Fatigue," J. Appl. Mech., (1945), pp. A–159–164.

[20] API Proceedings "1996 APE Coke Drum Survey-Final Report", American Petroleum Institute, Washington, DC, (1996) .

CHAPTER 10 Summary of Research Contributions and Guidelines for Improving Reliability of Coke Drums

Coke drums are vertical pressure vessels used in the delayed coking process in petroleum refineries. The significant temperature variation during the delayed coking process, such as heating and quenching, causes the useful life of coke drums to be shortened comparing with other pressure vessels under non-cyclic thermal condition. Several thousands of dollars are spent to repair the units and the loss from the disruption of the production could be even much higher. There are relatively few investigations involving experiments to simulate and predict the damage and fatigue life of coke drums. However, these low cycle fatigue tests only conducted on base material under isothermal condition. In order to better understand the damage mechanism and extend the service life of coke drum from both design and operational improvement. A investigation of fatigue life of coke drum is carried out. From this research, the following contributions are achieved:

1. A biaxial thermal mechanical fatigue testing system is successfully developed and applied in this research

The developed thermal mechanical fatigue (TMF) testing system is capable of generating simultaneous thermal and mechanical loading. It has been fully tested and verified to satisfy the requirement of simulating the thermal mechanical loading which is similar to the loading experienced by coke drums. An investigation is carried out on a clad material of coke drums by the developed system. The TMF life of TP 410S cycling between 100°C and 480°C is slightly shorter than isothermal low cycle fatigue (ILCF) at 480 °C. Furthermore, from the investigation of biaxial TMF test, the strain-life relation from uniaxial TMF can give very good prediction on bi-axial case with consideration of mean stress.

2. An alternative in-direct approach is invented to control and measure the strains for fatigue tests

Two approaches, analytical and finite element analysis (FEA) are implemented to establish the strain correlations at elevated temperatures. The FEA results have a good agreement with experimental results. This technique can also be used in TMF test by directly established correlation from the experiment.

3. A fatigue life prediction method for weld and HAZ materials is proposed

Two reduction factors $R_{plastic}$ and $R_{elastic}$ are introduced into the four-point-correlation (FPC) method to account for the heat-affected effect in weld and HAZ materials. The predicted fatigue lives of weld and HAZ by the modified FPC method have better agreement with test results. In addition, true facture strength could be better correlated with ultimate tensile strength and elongation at fracture.

4. A temperature dependent fatigue life prediction method for coke drum materials is proposed

Seven existing fatigue life prediction methods are reviewed and evaluated based on the selected coke drum materials data at lower and elevated temperature ranges. It is found that none of the methods can give promising estimation at both temperature ranges. A new temperature-dependent method, which only uses tensile strength, Young's modulus and elongation at fracture, is developed. The new proposed method has better predicted lives to the tested ones.

5. A statistical fatigue life prediction method of coke drums is suggested

The method is based on the thermal-mechanical fatigue test results, the simplified thermo-elasto-plastic global and local analysis models and the statistical analysis of

temperature data on a coke drum. By incorporating the statistical results into Palmgren-Miner's rule, the damages of the coke drums under both global thermal-mechanical loading and additional local hot and cold spot attacks are accumulated. With consideration of life deduction for HAZ, the estimated fatigue life of a typical coke drum is about 5,000 cycles which has very good agreement with 1996 API survey.

There are some guidelines that may help to extend service lives of coke drums

1. Selection of base material

A comparative study on fatigue behaviours of 2¼Cr-1Mo and C-½Mo indicates that the lives of C-½Mo are longer than that of 2¼Cr-1Mo under both isothermal and thermal mechanical cyclic loadings. With further support of API survey, it is concluded that C-½Mo is a better base material than 2¼Cr-Mo for fabrication of coke drums from the standpoints of fatigue behaviours.

2. Selection of base, clad and weld materials

   i. The CTEs of the clad and clad-weld materials must be closer to the CTEs of base and base-weld materials
   ii. The yield strength ratios between clad-weld and clad and between base-weld and base must be as closer as possible.

This study leads to better understanding of damage mechanisms occurring in coke drums and provides useful guidelines and material data in optimal selection of materials, design and manufacturing of more robust new coke drums, as well as for extending service lives of the existing coke drums from the operational and maintenance point of view. The benefit of this study to industrial users is to design and construct new equipment that is more robust and to improve service life of existing equipment.

BIBLIOGRAPHY

Affeldt, E. E., Hammer, J., Huber, U., Lundblad, H., "Analysis of thermal gradients during cyclic thermal loading under high heating rates", Thermomechanical fatigue behavior of materials, 4 (2003), 312-324

Anonym. "Data Sheets on Elevated-Temperature Low-Cycle Fatigue Properties of SCMV3 (1.25Cr-0.5Mo) Steel Plate for Pressure Vessels" NRIM Fatigue Data Sheet (1981):1. TEMA. Web. 22 Jan. 2014

Anonym. "Data Sheets on Elevated-Temperature Low-Cycle Fatigue Properties of SCMV4 (2.25Cr-1Mo) Steel Plate for Pressure Vessels" NRIM Fatigue Data Sheet (1987):1. TEMA. Web. 22 Jan. 2014

Anonym. "Data Sheets on Elevated-Temperature, Low-Cycle Fatigue Properties of SCMV 4 (2.25Cr-1Mo) Steel Plate for Pressure Vessel" NRIM Fatigue Data Sheet (1991): 1. TEMA. Web. 20 Nov. 2013

Anonym. "Data Sheets on Low-Cycle Fatigue Properties at Elevated-Temperature for Weld and Base Metals of SCMV2-2NT (1Cr-0.5Mo) Low Alloy Steel Plate for Boiler and Other Pressure Vessels" NRIM Fatigue Data Sheet (1993):1. TEMA. Web. 22 Jan. 2014

API 579-1/ASME FFS, American Petroleum Institute, Washington, DC, (2007)

API Proceedings "1996 APE Coke Drum Survey-Final Report", American Petroleum Institute, Washington, DC, (1996)

ASME Boiler and Pressure Vessel Code (BPVC) Section II, New York, N.Y., American Society of Mechanical Engineers, (2007)

ASME Boiler and Pressure Vessel Code (BPVC) Section VIII Division 1, New York, N.Y., American Society of Mechanical Engineers, (2007)

ASME Boiler and Pressure Vessel Code (BPVC) Section VIII Division 2, New York, N.Y., American Society of Mechanical Engineers, (2007)

ASME Boiler and Pressure Vessel Code (BPVC) Section VIII Division 2, New York, N.Y., American Society of Mechanical Engineers, (2010)

ASME E606-04, Standard Practice for Strain-Controlled Fatigue Testing, ASTM International, West Conshohocken, PA, US (2004) www.astm.org

ASTM E1012-05, Standard practice for verification of test frame and specimen alignment under tensile and compressive axial force application, ASTM International, West Conshohocken, PA, US (2005) www.astm.org

ASTM E2207-08, Standard practice for strain-controlled axial-torsional fatigue testing with thin-wall tubular specimens, ASTM International, West Conshohocken, PA, US (2008) www.astm.org

ASTM E2368-10, Standard Practice for Strain Controlled Thermomechanical Fatigue Testing, ASTM international, West Conshohocken, PA, (2010) www.astm.org

ASTM E4-10, Standard practices for force verification of testing machines, ASTM international, West Conshohocken, PA, (2010) www.astm.org

ASTM E467-08, Standard practice for verification of constant amplitude dynamic forces in an axial fatigue testing system, ASTM international, West Conshohocken, PA, (2008) www.astm.org

ASTM E21, Test Methods for Elevated Temperature Tension Tests" ASTM Standards, American Society for Testing and Materials, ASTM international, West Conshohocken, PA, (2008) www.astm.org

ASTM E8-04, Standard Test Methods of Tension Testing of Metallic Materials, ASTM international, West Conshohocken, PA, (2004), www.astm.org

Bannantine, J.A., "Fundamental of metal fatigue analysis", Englewood Cliffs, N.J. : Prentice Hall, 1990. Print.

Bartsch, M., Baufeld, B.. et al., “Multiaxial thermo-mechanical fatigue on material systems for gas turbines”, Mat.-wiss. U. Werkstofftech, 38 -9 (2007), 712-719

Basquin, O.H. “The exponential law of endurance tests”, ASTM proceeding. 10(1910) 625-630

Baumel, A., Seeger, T., “Material data for cyclic loading”, Amsterdam: Elsevier Science Publishers - supplement I, (1990)

Beck, T., Rau, K., “Temperature measurement and control methods in TMF testing - a comparison and evaluation”, International Journal of Fatigue, 30 (2008) 226-233

Boswell R.S., Ferraro T., “Remaining Life Evaluation of Coke Drums”, Plant Engineering, Design and Responsibility Symposium, Energy Engineering Conference, (1997)

Boswell, R.S., “Coke Drum Bulges”, Stress Engineering Services, May, (2001)

Boswell, R.S., and Wright, B., "State-of-The-Art Improvements in Coke Drum Design and Life Extension Practices." Proceedings of ASME Pressure Vessels and Piping Conference (2008): CREEP2007-26254.

Brendel, T., Affeldt, E., Hammer, J., Rummel, C., "Temperature gradients in TMF specimens Measurement and influence on TMF life", International Journal of Fatigue, 30 (2008), 234-240

Carden, A. E., "Thermal fatigue evaluation", ASTM STP 465, 1969, P. 163

Chen, J., "Experimental Study of Elastoplastic Mechanical Properties of Coke Drum Materials", Masters Dissertation, University of Alberta, Edmonton, (2010)

Chen, J., Xia, Z., "Thermal Mechanical Fatigue of Coke Drum Materials", Proceeding of 13th International Conference on Fracture, June 16-21, 2013, Beijing, China

Chen, J., Yamatomo, T., Xia, Z., and Esaki, K., "Experimental Evaluation of Fatigue Life of Coke Drum Materials with Weld Sections", Proceeding of ASME pressure vessel and piping Conference, July 14-18, Paris, France, (2013)

Clark, R.D., Rytt, D. K., et al., "Coke Drum Life Improvement – A Combined Approach", AIChE 2002 Spring National Meeting, New Orleans, Louisiana, March 10-14, (2002)

Coffin, L. F. Jr., "A study of the effects of cyclic thermal stresses on a ductile metal", Trans. ASME, 76 (1954) 931-950

Ellison, E. G. and Patterson, A. J. F., "Creep-fatigue interaction in a 1Cr Mo V steel", Proc. I. Mech. E, 190 (12/76), 1976, 321-350

Furuya, K., Nagata, N. and Watanabe, R., " Low cycle fatigue properties of type 316 stainless steel in vacuum", J. Nucl. Mater., 89, 1980, P. 372-382

Hahner, P., Affeldt, E., Beck, T., Klingelhoffer, H., Loveday, M., Rinaldi, C. "Validated Code of Practice for Strain-controlled Thermo-Mechanical Fatigue Testing" EC-EUR 22281 EN – Directorate General, Joint Research Centre – Institute for Energy, Petten, NL., ISBN92-79-02216-6, (2006)

Hirschberg, M. H., "A low cycle fatigue testing facility", ASTM STP 465, 1969, P67

Hyde, C. J., Sun, W., Leen, S. B., "Cyclic thermo-mechanical material modelling and testing of 316 stainless steel", International journal of pressure vessels and piping, 87 (2010) 365-372

Jin, L. , Pelloux, R. M., Xie, X., "Thermomechanica fatigue behaviour of a Nickel base superalloy", Chin. J. Met. Sci. Technol., 5 (1989) 1-7

Ju, F., Aummuler, J., Xia, Z. and Plessis, P. D., "Global and Local Elastic-Plastic Stress Analysis of Coke Drum Under Thermal-Mechanical Loadings", Journal of Pressure vessel technology, 133 (2011)

Kschinka, B. and Stubbins, J.F., "Creep-fatigue-environment interaction in a bainitic 2.25 wt.%Cr-1 wt.%Mo steel forging", Mater. Sci. Eng., A110, 1989, P. 89-102

Li, Z., Zhou X., Xu W., and Fenkun L., "Safe Life Estimation of Coke Drum in Service Environment." Journal of Pressure Vessel Technology134.3 (2012)

Lohr, R. D., "The role of extensometry in modern materials testing", Transducer/Tempcon 82 Conference, Wembley, UK, 1982

Lord, D. C. and Coffin, L. F., "High temperature materials behaviour", ASTM STP 465, 1969, P. 129

Manson, S.S., "A simple procedure for estimating high-temperature low cycle fatigue", Experimental Mechanics, 1968, 349-355

Manson, S.S., "Behaviour of materials under conditions of thermal stress", Heat Transfer Symposium, University of Michigan, 1953, 9-75, See also NACA-TN-2933, (1953)

Manson, S.S., "Fatigue: A complex subject – Some Simple Approximations," Proceedings, Society of Experimental Stress Analysis, Vol. 12, No. 2, 1965

Manson, S.S., Halford, G.R., "Practical implementation of the double linear damage rule and damage curve approach for treating cumulative fatigue damage", Int. J. Fract., Vol. 17, No. 2, (1981), 169-172

Meggiolaro MA, Castro JTP. Statistical evaluation of strain-life fatigue crack initiation predictions. Int J Fatigue 2004;26(5):463 – 76.

Miner, M.A., "Cumulative Damagein Fatigue," J. Appl. Mech., pp. A–159–164. (1945)

Mochizuki, Y., Nakajima, M., and Shimizu, T., "High Cycle Fatigue Properties and Failure Mode in Ni-Cr-Mo steel Tempered at Low Temperature", Advance in Fracture and Damage Mechanics VII, Key Engineering Materials, 385-387, 2008, P. 185-188

Morrow, J.D., Fatigue design handbook, section3.2, SAE Advanced in Engineering, 4, 21–29, (1968)

Muralidharan, U., Manson, S. S., "A modified universal slopes equation for estimate of fatigue characteristics of metals", Journal of Engineering Materials and Technology, Vol. 110, PP. 55-58, (1988)

Nikic, M., and Z. Xia. "Alternative Selections of Delayed Coke Drum Materials Based on ASME Material Property Data." Proceedings of the ASME Pressure Vessels and Piping Conference (2012): PVP2012-78548

Nogami, S., Sato, Y., Tanaka, A., Hasegawa, A., Nishimura, A., and Tanigawa, H., "Effect of Specimen Shape on the Low Cycle Fatigue Life of Reduced Activation Ferritic/Martensitic Steel", Journal of Nuclear Science and Technology, 47(1), 2010, P. 47-52

Oka, M, et al. "Study On The Effects Of Switching Temperature On The Thermal Fatigue Life Of The Shell-To-Skirt Junction Of Coke Drum." Journal Of Pressure Vessel Technology-Transactions of ASME 133.6 (2011)

Oka, M., Ambarita, H., Kawashima, K. and Daimaruya, M., "Effect of hot feed injection time on thermal fatigue life of shell to skirt junction area of coke drums" Proceedings of ASME Pressure Vessels And Piping Conference (2010): PVP2010-25183

Oka, M., Himsar A., Masashi D., and Hiroyuki F., "Initiation of Bulges in a Coke Drum Subjected to Cyclic Heating and Cooling, also Cyclic Mechanical Loads" Journal of Thermal Stresses 33.10 (2010)

Ong, J. H., "An evaluation of existing methods for the prediction of axial fatigue life from tensile data", International Journal of Fatigue, Vol. 15 PP. 13-19, (1993)

Ong, J. H., "An improved technique for the prediction of axial fatigue life from tensile data", International Journal of Fatigue, Vol. 15-3 PP. 213-219, (1993)

Ono, Y., Yuri, T., Sumiyoshi, H., Matsuoka, S., and Ogata, T., "High-cycle fatigue properties and sub-surface crack initiation in Ti-5%Al-2.5%Sn ELI alloy", Journal of the Japan Institute of Metals, 69(8), 2003, 391-397

Panneerselvam, G. et al. "A study on the thermal expansion characteristics of Inconel-82 filler wire by high temperature X-ray diffraction", Materials Letters, 58 1-2 (2003) 216-221

Park, J. H., Song, J. H., "New estimation method of fatigue properties of aluminum alloys", Journal of Engineering Materials and Technology, Transactions of the ASME Vol. 125, PP. 208-214 (2003)

Park, J.H., Song, J.H. "Detailed evaluation of methods for estimation of fatigue properties" International Journal of Fatigue, 17:365 – 73, (1995)

Penso, J. A., Hazime, R., "Comparison of thermo-mechanical fatigue life assessment methods for coke drums", Proceeding of ASME 2010 Pressure Vessels and Piping Division conference, Washington, USA, (2010)

Penso, J. A., Lattarulo, Y. M., Seijas, A. J., Torres, J., Howden, D., and Tsai, C. L., "Understanding Failure Mechanisms to Improve Reliability of Coke Drum," PVP (Am. Soc. Mech. Eng.), 395, pp. 243–253. (1999)

Pieper, C.J., Shockley L.R. and Stewart, C.W., "Coke Drum Design-Longer Life through Innovation", AIChE 2000 Spring National Meeting, Atlanta, GA, March 5-9, 2000

Ramberg, W., & Osgood, W. R., "Description of stress-strain curves by three parameters" Technical Note No. 902, National Advisory Committee for Aeronautics, Washington DC, 1943

Ramos, A. J., Rios, C. and Vargas, J.A.R., "Fatigue Life Prediction of Delayed Coke Drums", Vision Techenologica, Vol.6, 93-100,(1999)

Ramos, A., Rios, C. and Vargas, J., "Mechanical Integrity Evaluation of Delayed Coke Drums", PVP-Vol.359, Fitness for Adverse Environments in Petroleum and Power Equipment, ASME (1997)

Ramos, A., Rios, C., Johnsen, E., Gonzalez, M., and Vargas, J., 1998, "Delayed Coke Drum Assessment Using Field Measurements and FEA," Analysis and Design of Composite, Process, and Power Piping and Vessels, ASME, New York, Vol. 368, pp. 231–237.

Ramos, A., Rios, C., Vargas, J., Tahara, T., and Hasegawa, T., 1997, "Mechanical Integrity Evaluation of Delayed Coke Drums," Fitness for Adverse Environments in Petroleum and Power Equipment, ASME, New York, Vol. 359, pp.291–298.

Raske, D. T. and Burke, W. F., "An extensometer for low cycle fatigue tests on anisotropic materials at elevated temperature", J. Phys. E. Sci. Instru., 1979, 12, 175

Richard Boswell, "Coke Drum Bulges", Stress Engineering Services, May, 2001

Roessle, M. L., Fatemi, A., "Strain-controlled fatigue properties of steels and some simple approximation", International Journal of Fatigue, Vol. 22 PP. 495-511, 2000

Rutt, D.K., Clark, R.D., "Stress Analysis Using Actual Coke Drum Bulge Profiles a Case Study", AIChE 2000 Spring National Meeting, Atlanta, GA, March 5-9, (2000)

Samman, M. and DuPlessis, P., "The Bulging Intensity Factor (BIF), A technique for assessing the bulging severity of coke drums", RMC-07-100 NPRA Reliability & Maintenance Conference, NPRA Houston, TX, (2007)

Sasaki, Y., and Niimoto, S., "Study on Skirt-to-Shell Attachment of Coke Drum by Evaluation of Fatigue Strength of Weld Metal" Proceedings of ASME Pressure Vessels and Piping Conference (2011): PVP2011-57314

Shargay, C., Singh, A., Munsterman, T., Antalffy, L., "Coke Drum Design and Fabrication Issues", Proceedings of ASME Pressure Vessels And Piping Conference (2010): PVP2010-25765

Shiozawa, K., and Lu, L., "Very high-cycle fatigue behaviour of shot-peened high-carbon-chromium bearing steel", Fatigue and Fracture of Engineering Materials and Structures, 25(8-9), 2002, P. 813-822

Shiozawa, K., Murai, M., Shimatani, Y., and Yoshimoto, T., "Transition of fatigue failure mode of Ni-Cr-Mo low-alloy steel in very high cycle regime", International Journal of Fatigue, 32(3), 2010, P. 541-550

Slot, T., Stentz, R. H. and Berling, J. T., "Controlled strain testing procedures", ASTM STP 465,1969, P.100

Socie, D. F., Mitchell, M. R. and Caulfield, E. M., "Fundamentals of Modern Fatigue Analysis", Fracture Control Program report No. 26, University of Illinois, USA, 1977

Sohel, M., Panwala, M., Srinviasan, K. N., Mehta, S. L., "Creep-fatigue interaction in coke drums: An approach based on API 579-1/ASME FFS-1 2007", Proceeding of the ASME 2009 Pressure Vessels and Piping Division conference 2009, Prague, Czech Republic

Stewart, C. W., Stryk, A. M., and Presley, L., "Coke drum design", Chicago Bridge & Iron, PTQ Q3, 2006

Stewart, C., "Vertical Plate Technology Extends the Life of Coke Drums" Welding Journal, 83, pp.34-36 (2004)

Sumner, G., "Techniques for high temperature fatigue testing", London: Elsevier Applied Science, c1985. print

Tao, G., Xia, Z., "A non-contact real-time strain measurement and control system for multiaxial cyclic fatigue tests of polymer materials by digital image correlation method", Polymer Testing, 24 (2005), 844-855

Walters, D. J. and Hales, R. "An extensometer for creep fatigue testing at elevated temperatures and low strain ranges", J. Strain Anal., 1981, 16, 145

Warren, J. R., Cowles, B. A., "A simplified thermal mechanical fatigue (TMF) test method", Journal of Engineering for Gas Turbines and Power, 108 (1986), 515-520

Weil, N.A. and Rapasky, F.S., "Experience with vessels of Delayed – Coking Units", API 23rd Midyear Meeting, (1958)

Wells, C. H., "Elevated temperature testing methods", ASTM 465, 1969, P. 87

Wood, D.S., Slattery, G.G., Wynn, J., Connaughton, M.D., and Lambert, M.E., "Preliminary results of the effect of environment on low cycle fatigue of type 316 and 9Cr1Mo steels", in: The influence of environment on fatigue, Inst. Mech. Engrs., London, P. 11-20, 1977

Xia, Z., Ju, F. and Plessis, P. D., "Heat Transfer and Stress Analysis of Coke Drum for a Complete Operating Cycle", Journal of Pressure vessel technology, 132 (2010)

Yamamoto, T., Arii, K. , Huhetaoli, S. Niimoto, S., Ohata, M., Tagawa, T., Minami, F., "Investigation of Bulging Behavior of Coke Drum -A practical analysis of bulging under complex quench conditions-", Proc. Pressure Vessels & Piping Division Conf., ASME PVP2011- 57428, (2011)

Yan, Z., Aumuller, J.J., Esaki, K., and Xia, Z. H., "Statistical Analysis of Shell Metal Temperature Data for a Coke Drum" Internal report (2014)

Zhang, Y. X., and Xia, Z. H., "Simplified Thermo-Elasto-Plastic Analysis Models for Determination of Global and Local Stresses in Coke Drums," ASME 2013 Pressure Vessels and Piping Conference (2013)

Appendix A Specimen Alignment Check

Based on ASTM E1012-05, Standard practice for verification of test frame and specimen alignment under tensile and compressive axial force application, the tubular specimen alignment was verified in the following way provided by this standard.

For a set of four gauges, in the same cross-sectional plane at under a given applied force, the average axial strain is:

$$\varepsilon_o = (\varepsilon_1 + \varepsilon_2 + \varepsilon_3 + \varepsilon_4)/4 \quad (1)$$

NOTE 2 Under zero axial force and in pure torsion, the average axial strain is zero.

The local bending strains are:

$$\varepsilon_{b1} = \varepsilon_1 - \varepsilon_o \quad (2)$$

$$\varepsilon_{b2} = \varepsilon_2 - \varepsilon_o \quad (3)$$

$$\varepsilon_{b3} = \varepsilon_3 - \varepsilon_o \quad (4)$$

$$\varepsilon_{b4} = \varepsilon_4 - \varepsilon_o \quad (5)$$

At the front of the machine where gauge 1 is initially located, the local bending strain component due to misalignment in the machine is:

$$\varepsilon_{b1.mc} = \frac{\varepsilon_{b1.0^o} - \varepsilon_{b1.180^o}}{2} \quad (6)$$

Where, $\varepsilon_{b1.0^o}$ and $\varepsilon_{b1.180^o}$ are the local bending strains measured by gauge 1 when located in orientation 0° and orientation 180°, respectively.

Equation (6) is applicable for the other gauge positions to determine $\varepsilon_{b2.mc}$, $\varepsilon_{b3.mc}$ and $\varepsilon_{b4.mc}$ respectively.

The maximum bending strain due to misalignment in the machine is:

$$\varepsilon_{b\,max\,.mc} = 1/2\sqrt{(\varepsilon_{b1.mc} - \varepsilon_{b3.mc})^2 + (\varepsilon_{b2.mc} - \varepsilon_{b4.mc})^2} \quad (7)$$

tension 235.4 MPa strain [10^{-6}]								
Gauge	0°	0° ε_b	90°	90° εb	180°	180° εb	270°	270° εb
1	1300	-21.5	1238	-17	1234	-4	1246	3.5
2	1330	8.5	1248	-7	1236	-2	1246	3.5
3	1326	4.5	1272	17	1238	0	1236	-6.5
4	1330	8.5	1262	7	1244	6	1242	-0.5
ε_o	1321.5		1255		1238		1242.5	
5	1428	15	1324	-1.75	1310	-25	1326	18.75
6	1407	-6	1326	0.25	1328	-7	1306	-1.25
7	1402	-11	1325	-0.75	1394	59	1290	-17.25
8	1415	2	1328	2.25	1308	-27	1307	-0.25
ε_o	1413		1325.75		1335		1307.25	

ε_b.mc	ε_b.mc	ε_b max.mc (0,180)	ε_b max.mc (90,270)
-8.75	-10.25	5.85	11.88
5.25	-5.25		
2.25	11.75	β_{mc} (%)	β_{mc} (%)
1.25	3.75	**0.44**	**0.95**
ε_b.mc	ε_b.mc	ε_b max.mc (0,180)	ε_b max.mc (90,270)
20	-10.25	28.38	9.25
0.5	0.75		
-35	8.25	β_{mc} (%)	β_{mc} (%)
14.5	1.25	**2.01**	**0.70**

The bending strain was calculated according to ASTM E1012-05 and found to be within 2% for repeated trials, which is less than the ASTM E606 required minimum value 5% for fatigue test.

Appendix B Derivation for Four Point Correlation Relation

$$\frac{\Delta\varepsilon}{2}=\frac{\tilde{\sigma}_f^{'}}{E}(2N_f)^{\tilde{b}}+\tilde{\varepsilon}_f^{'}(2N_f)^{\tilde{c}} \qquad \text{(A1)}$$

$$\frac{\Delta\varepsilon_e}{2}=\frac{\tilde{\sigma}_f^{'}}{E}(2N_f)^{\tilde{b}} \qquad \text{(A2)}$$

Two points (1/4, 2.5σ_f/E), (10^5, 0.9 σ_u/E) submit into equation A2

$$2.5\frac{\sigma_f}{E}=2\frac{\tilde{\sigma}_f^{'}}{E}(\frac{1}{2})^{\tilde{b}} \qquad \text{(A3)}$$

$$0.9\frac{\sigma_u}{E}=2\frac{\tilde{\sigma}_f^{'}}{E}(2\times10^5)^{\tilde{b}} \qquad \text{(A4)}$$

Put log on both side of equation A3 and A4

$$\log(2.5\frac{\sigma_f}{E})=\log(2\frac{\tilde{\sigma}_f^{'}}{E})+\tilde{b}\log(\frac{1}{2}) \qquad \text{(A5)}$$

$$\log(0.9\frac{\sigma_u}{E})=\log(2\frac{\tilde{\sigma}_f^{'}}{E})+\tilde{b}\log(2\times10^5) \qquad \text{(A6)}$$

Let A5 subtract A6 on both sides respectively, it becomes

$$\log(2.5\frac{\sigma_f}{E})-\log(0.9\frac{\sigma_u}{E})=\tilde{b}\log(\frac{1}{2})-\tilde{b}\log(2\times10^5) \qquad \text{(A7)}$$

Rearrange the equation

$$\tilde{b}=\frac{\log\left[2.5\sigma_f/0.9\sigma_u\right]}{\log\left[1/(4\times10^5)\right]} \qquad \text{(A8)}$$

Submit $\tilde{b}$ this into A3

$$\tilde{\sigma}_f^{'}=\frac{1}{2}E\times(2.5\frac{\sigma_f}{E})(2)^{\tilde{b}} \qquad \text{(A9)}$$

Or in the logarithmic form

$$\tilde{\sigma}_f^{'}=\frac{1}{2}E\times10^{\tilde{b}\log 2+\log\left(2.5\sigma_f/E\right)} \qquad \text{(A10)}$$

For plastic line

$$\frac{\Delta\varepsilon_p}{2}=\tilde{\varepsilon}_f^{'}(2N_f)^{\tilde{c}} \qquad \text{(A11)}$$

First $\Delta\varepsilon_e^{@}$ can be found from equation A2 and A9 at $N_f = 10^4$ cycles with ordinate of ¼ $D^{3/4}$.

$$\Delta\varepsilon_e^{@}=(2\times10^4)^{\tilde{b}}(2.5\frac{\sigma_f}{E})(2)^{\tilde{b}}=(2.5\frac{\sigma_f}{E})(4\times10^4)^{\tilde{b}} \qquad \text{(A12)}$$

Or in the logarithmic form

$$\Delta\varepsilon_e^{@} = 10^{\log(2.5\frac{\sigma_f}{E})+\tilde{b}\log(4\times10^4)} \qquad \text{(A13)}$$

Two points (10, ¼ $D^{3/4}$), (10^4, (0.0132 $-\Delta\varepsilon_e^{@}$)/1.91) submit into equation A11

$$\frac{1}{2}(\frac{1}{4}D^{3/4}) = \tilde{\varepsilon}_f^{'}(20)^{\tilde{c}} \qquad \text{(A14)}$$

$$\frac{1}{2}(\frac{0.0132-\Delta\varepsilon_e^{@}}{1.91}) = \tilde{\varepsilon}_f^{'}(2\times10^4)^{\tilde{c}} \qquad \text{(A15)}$$

Put log on both side of equation A14 and A15

$$\log[\frac{1}{2}(\frac{1}{4}D^{3/4})] = \log(\tilde{\varepsilon}_f^{'}) + \tilde{c}\log(20) \qquad \text{(A16)}$$

$$\log[\frac{1}{2}(\frac{0.0132-\Delta\varepsilon_e^{@}}{1.91})] = \log(\tilde{\varepsilon}_f^{'}) + \tilde{c}\log(2\times10^4) \qquad \text{(A17)}$$

Let A17 subtract A16 and rearrange, it gives

$$\tilde{c} = \frac{1}{3}\log\left[(0.0132-\Delta\varepsilon_e^{@})/1.91\right] - \frac{1}{3}\log\left\{\frac{1}{4}\left[\ln\left\{1/\left(1-RA\right)\right\}\right]^{3/4}\right\} \qquad \text{(A18)}$$

Use equation A14

$$\tilde{\varepsilon}_f^{'} = \frac{1}{2}10(\frac{1}{4}D^{3/4})(\frac{1}{20})^{\tilde{c}} \qquad \text{(A19)}$$

Or in the logarithmic form

$$\tilde{\varepsilon}_f^{'} = \frac{1}{2}\times10^{\tilde{c}\log\frac{1}{20}+\log\left[\frac{1}{4}\left[\ln\{1/(1-RA)\}\right]^{3/4}\right]} \qquad \text{(A20)}$$

Appendix C Experimental Setup CTE Test

Three thermocouples were installed, two on the top and bottom of the gauge length and one in the middle of the gauge length. An insulation disk was installed in between cooling cell and gripping flange to minimize the thermal gradient along the axial direction of the specimen. In addition, a band heater was installed on the gripping flange and adjusted to achieve the minimized thermal gradient. When temperature is stabilized at 20°C, the data was being recorded. The three TCs were closely and timely monitored. When the temperature between any of the TC exceeds ±1% of the temperature measured in the middle TC, the test will be stopped and restarted until this requirement satisfied. After successfully maintain the required temperatures, the temperature will heat up to 500°C, and the corresponding strain will also be recorded in time-basis.